Low-profile, Ultra Wideband and Dual Polarized Antennas and Feeding Systems

Mohammad Vahdani

Thèse

Présentée pour obtenir le grade de Docteur
de l'Ecole Nationale Supérieure des Télécommunications

Spécialité : **Electronique et Communications**

Mohammad VAHDANI

Low-profile, Ultra Wideband and Dual Polarized Antennas and Feeding Systems

Soutenue le 29 Octobre 2008 devant le jury composé de :

Adaildo GOMES D'ASSUNCAO	Rapporteur	Universidade Federal do Rio Grande do Norte
Ala SHARAIHA	Rapporteur	Université de Rennes I
Mahmoud KAMAREI	Examinateur	Université de Téhéran
Tan Phu VUONG	Examinateur	IMEP Grenoble
Alireza KAZEMIPOUR	Examinateur	Laboratoire National d'Essais
Bernard HUYART	Examinateur	Telecom ParisTech
Xavier BEGAUD	Directeur de thèse	Telecom ParisTech

For my wife Noushin

ACKNOWLEDGEMENTS

I appreciate every effort made by laboratory members throughout this research in ***Radio Frequency and Microwaves (RFM)*** Telecom ParisTech. Particularly I would like to thank my Director, Mr. Xavier BEGAUD for his guidance and support in my research. He didn't hesitate to give fruitful advices. Thanks to Professor Mahmoud KAMAREI and Dr. Alireza KAZEMIPOUR for their warm and creative concerns for this dissertation. I must also thank Professor Bernard HUYART, director of the group, for his sincere advice and support. Their comments on my research were so helpful for enhancing the dissertation quality.

I also thank to Mr. Professor B. HUYART for accepting the chairmanship of the jury, and Mr. Professors Adaildo GOMES D'ASSUNCAO and Ala SHARAIHA who have kindly agreed to report this dissertation and also for the attention they have brought.

I would like to give special thanks to my wife, Noushin, for her helps in building the baluns, antennas and measurements, and contribution for sharing ideas. She encouraged me through this research and without her support and prayer; I could not finish my dissertation at all.

I am grateful to my mother and father who prayed for me every day and patiently waited for this Ph.D. dissertation in IRAN. Thanks to my siblings, Farshid, Mahshid, and Maysam, and their families. I would like to thank my parents-in-law for their support and lovely care. I also thank my sister- and brother-in-law, Minoush and Sasha.

CONTENTS

LIST OF FIGURES

Chapter 1

Chapter 2

Chapter 3

Chapter 4

LIST OF TABLES

Chapter 2

Chapter 3

Chapter 4

Introduction

The main objective of this thesis is to obtain a wideband feeding system compatible with compact wideband antenna geometries with dual polarization properties. These feeding systems are designed according to the antenna performance and their structural nature.

Therefore we were encountered with two main problems: first of all investigating new balun configurations which can operate in wideband frequency. In other words, we had to achieve balun configurations presenting good impedance and fields matching in wide frequency bandwidth. Moreover, the aim of this balun design was to arrive to an integrated structure embracing these two properties-wideband characteristic and dual polarization properties.

The second problem was to propose and develop wideband antenna architectures with compact form and conformal design. Also it was desired to have dual polarization abilities.

In the designing procedure the main obstacle was that configurations embracing all these properties were rarely proposed in academic researches. In other words in the literature, it was presented rarely an integrated wideband balun connected to compact dual polarized antennas.

In this thesis two types of wideband feeding systems are proposed and developed:

- Tapered microstrip balun with wideband characteristics and simple geometry. This structure has two conductors whose strip width determines the impedance characteristics. This configuration has already existed as a classic balun and we have optimized it according to the applications needed.

- In early 2000's a compact form of microstrip-to-CPS (coplanar stripline) as a wideband feeding system attracted the attention of antenna designers. In this dissertation a developed 90° bended microstrip-to-CPS balun is proposed from which we obtained good performance results in field matching and impedance transformation.

Considering the performed investigation in wideband antenna categories, we have selected two antenna geometry types: sinuous and bow-tie antennas. In fact to verify the balun performance (field and impedance matching), we have employed these two antenna types which are fed by our proposed wideband balun.

Bow-tie antenna was utilized for many years in research activities and its ultra wideband impedance bandwidth and also its simple geometry make it compatible to be connected to our developed feeding system. In this thesis, we have proposed and developed a quasi bow-tie configuration integrated to coplanar stripline balun.

Our investigations show that the *sinuous antenna* is the best candidate for obtaining the three requested properties. The sinuous curve has a zigzag form and therefore has the ability to place two (or 4) antenna arms in a compact size. Despite its complicated geometry, the sinuous antenna provides ultra wideband characteristic and radiates in dual linear polarization modes in E- and H-planes.

We have developed two sinuous antenna models: the log-spiral configuration proposed by X. Begaud which is in slot antenna category and the other one a microstrip curved-log spiral. These two antenna types are placed in the subset of sinuous geometries.

During the years 2004-2008 my research activities were performed in ***R**adio **F**requency and **M**icrowaves (RFM)* Telecom ParisTech under the direction and support of Xavier Begaud and Bernard Huyart.

This dissertation consists of 4 chapters focusing on wideband feeding systems and presenting the two procedures of transformation gradually from single polarization to dual polarization and also from 3 dimensional to integrated structures:

Chapter 1. A Comprehensive Investigation of Compact Wideband Dual Polarization Antenna

Chapter 1 is a wide investigation of compact wideband antenna with dual polarization properties. First of all a historical feature of the wideband antenna is presented and we can get a brief sense of wideband antenna principles and geometries. Within this investigation, we'll select two antenna categories to modify and develop in next chapter. The bow-tie and sinuous are our antenna candidates.

Chapter 2. Feeding Systems for Ultra Wideband Single Polarization Antennas

The general concept of the planar balun (balanced-to-unbalanced circuits) will be presented in this chapter. Then the analysis and optimization of a tapered microstrip balun in standard form will be introduced and implemented on a slot sinuous antenna.

In next step the optimized balun connects to our desired antenna geometry (sinuous slot antenna) and the radiation characteristic of the antenna will be analyzed. Finally, we'll added a ground plane to achieve the directive property.

Chapter 3. Feeding Systems for Ultra Wideband Dual Polarized Antenna in 3-Dimensional Design

In chapter 3, a developed compact wideband feeding system will be presented. This chapter is an attempt to provide a wideband dual polarized structure in 3-dimentional configuration fed by our proposed wideband balun.

In order to verify the feeding system performance, a sinuous configuration antenna will be proposed consisting of two parallel antenna planes. For the feeding systems, two CPS baluns will be connected perpendicularly to two of the antenna planes.

Chapter 4. New Integrated Feeding System for Ultra Wideband Dual Polarized Antennas

The balun proposed in chapter 3 will be employed in 3-dimensional configuration with sinuous antenna, but the main application of such feeding systems is to achieve an integrated antenna structure. They can integrate simply with the planar balanced antennas because of microstrip-to-CPS geometry nature. The idea of this compact form balun comes from the microstrip-to-CPS balun configuration proposed in the early 2000's.

Chapter 4 is the heart of my thesis and consists of two main parts. Our proposed balun will be employed to be integrated with our antenna candidates in dual polarization modes: This balun type will be implemented on sinuous microstrip antenna and a quasi bow-tie antenna.

In this chapter for the first time an integrated coplanar stripline balun will be fed to two-arm sinuous antenna and as results good wideband radiation characteristics will be obtained. Also for the first time a so compact bow-tie configuration with dual polarized properties -implemented just on one small substrate- will be presented. In addition, it is for the first time that a bow-tie configuration with such compaction possessing will be proposed with dual polarization characteristic.

Therefore, in this thesis, we will traverse from a 3-dimensional wideband structure with single polarization (chapter 2) to integrated dual polarized architecture antennas (chapter 4).

Chapter 1

An Investigation of Compact Wideband Dual Polarization Antennas

1.1 Motivation

Ultra wideband (UWB) antennas have maintained their position for already a number of years as an interesting hot topic for such diverse applications as wireless communication systems, position and tracking, sensing and imaging, ground penetrating radars, wireless local area networks (WLAN), either civil or military communication systems, short pulse radar for automotive and robotics application and many others [1-2]. Also wideband antenna has been used recently for MIMO and diversity operations [3-5]. Although ultra-wideband is not an entirely new discovery, it is still considered an emerging field in the civil areas of data communication, imaging and radar [6].

The need to support capacity augmentation and to provide higher communication data rate explains the fundamentally increasing demand for wireless wideband communications. New researches show that wideband antennas are indispensable for providing wireless wideband communications [7]. In addition, many wireless wideband communication devices require low-profile structures in a compact size [8]. Another desirable feature is that of dual polarization to support polarization diversity [9-10].

Recently many research activities have indicated that UWB has a substantial effect on antenna design and explained how the UWB researches lead to progress in antenna design. In fact, in wideband systems design the antenna has been a fundamental challenge of the UWB radio system and simultaneous new challenges and opportunities are provided for antenna designers. The main challenge in UWB antenna design is the achievement to the wide impedance bandwidth while still maintaining high radiation efficiency especially for balanced antenna in dual polarization mode. Indeed, the requirements for wide bandwidths and dual polarization are associated with other crucial constraints such as small size and low cost because most promising ultra wideband applications will be in portable devices.

Moreover some of these antennas are balanced structure radiators. Therefore, they need a feeding system for field matching and also obtaining balanced fields in the input point of the antenna. Considering this as

the important problem in wideband antenna, the design of the feeding systems (in wideband and dual polarization) has become one of the hottest topics in this field.

Therefore in feeding systems subject, there are new demands for balun architecture with wideband and dual polarization nature with compact size which have the ability of easy integration into wideband balanced antenna configurations.

Certainly in antenna design, the demands exist for the antenna configurations with wideband and dual polarization in small size, conformal design, easy integration into other RF circuits and low cost. However many existing wideband antennas are electrically large and provide only one single polarization (linear or circular).

This dissertation presents the results of an investigation for feeding systems of such wideband antennas. Also the sinuous and bow-tie antennas are selected as the best candidates of the compact wideband antenna. The newly feeding system proposed can be integrated into planar wideband antennas and wideband array antennas to provide wide-scan, low-profile and dual-polarization features. Finally, I have to mention that all the antennas developed in this work are dedicated to frequency domain applications and not for time domain.

1.2 Literature Review

1.2.1 Wideband Antennas

1.2.1.1 The State of the Art of the UWB Antennas

Recent years have witnessed an increase of worldwide interest in ultra-wideband systems, in which the UWB radiator plays a decisive role. Academic and industrial researches on ultra wideband antenna subject are performed now in the civil areas of data communication and military investigation. Proper design of such antenna requires a deep understanding of the wideband antenna and their feeding systems. Hence, the aim of this thesis is to propose a developed antenna configuration with a new integrated feeding system design in order to arrive to a good performance in impedance matching, dual polarization radiation and compact form.

Ultra-wideband technology has been recently developed for wireless communications. Because UWB is a high data-rate, low-radiation leakage, less dispersion in comparison to a microstrip feed, easy integration with solid-state active devices, and short-range wireless technology and utilizing the unlicensed radio spectrum form 3.1 GHz ~ 10.6 GHz frequency band [6].

The IEEE (Institute of Electrical and Electronics Engineers) standard [11] defines the bandwidth of an antenna as "the range of frequencies within which the performance of the antenna, with respect to some characteristics, conforms to a specific standard." In this dissertation, the bandwidth is defined for impedance and radiation pattern separately. The impedance bandwidth is defined for a return loss better than 10 dB and VSWR (Voltage Standing Wave Ratio) less than 2. The radiation pattern bandwidth, however, is hard to define with a specific criterion, so it is simply taken to be the frequency range within which the patterns are acceptable for a specific application [12].

The bandwidth can be denoted as a percent of the center frequency B_p as follows:

$$B_p = \frac{f_U - f_L}{f_C} \times 100\% \tag{1}$$

where $f_c = \frac{f_L + f_U}{2}$, f_U and f_L are the upper and lower frequencies of operation for which satisfactory performance is obtained, respectively. Bandwidth may also be defined as a ratio B_r by [12]

$$B_r = \frac{f_U}{f_L} \quad (2)$$

Also when focusing on the communications area, ultra-wideband (UWB) is generally interpreted with reference to relative bandwidths (B_p) exceeding 20% or with absolute bandwidths of at least 500MHz.

Standing wave ratio (SWR) is the ratio of the amplitude of a partial standing wave at a maximum to the amplitude at an adjacent node (minimum), in an electrical transmission line. The SWR is usually defined as a voltage ratio called the VSWR, for voltage standing wave ratio. For example, the VSWR value 1.5:1 denotes a maximum standing wave amplitude that is 1.5 times greater than the minimum standing wave value.

The concept was further clarified in 2002, when the Federal Communications Commission (FCC) adopted a "First Report and Order" [13] that regulated the marketing and operation of UWB. FCC authorizes the unlicensed use of UWB in 3.1–10.6 GHz. The FCC power spectral density emission limit for UWB emitters operating in the UWB band is -41.3 dBm/MHz. This rule is modified in terms of national regulations. These different variations will be not presented in this manuscript.

The aim of this work is to realize compact ultra wide band antennas with dual polarization and not to analyze the different versions of UWB technology. Below we are summarized the terms and definition in this thesis:

- ***Terms and Definition:***

1. **UWB**: in this work, the term 'UWB' or wideband indicates on the frequency bandwidth in ratio (B_r) bigger than one octave. It means we propose the balun and antenna structures with $B_r = \frac{f_U}{f_L} \geq 2$. So in each part, the goal of designing an antenna or balun structure is to achieve a configuration with wideband characteristic and there are not any emphasis on the exact f_L and f_H. This is the reason why all frequency bandwidths are different all along the manuscript: our goal is to obtain more or less one octave bandwidth.

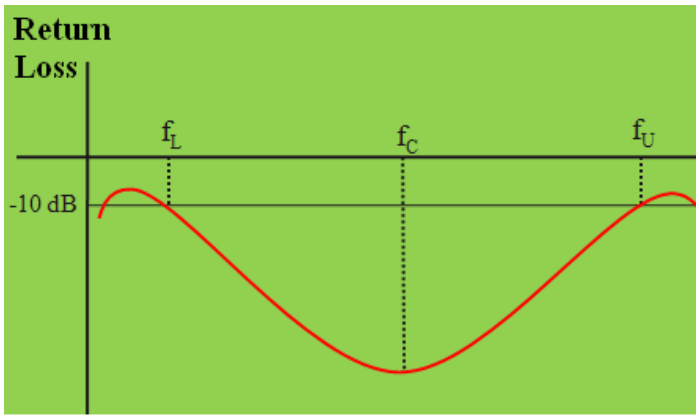

Fig.1.1. Return Loss and definitions.

2. **Return loss, Insertion loss**: return loss is the reflection of signal power resulting from the insertion of a device in an antenna structure or a transmission line. Also insertion loss is the loss of signal power resulting from the insertion of a device in that structure.

3. **Antenna Gain**: Antenna Gain is defined as the ratio of the radiation intensity of an antenna in a given direction to the intensity that would be produced by an isotropic antenna:

$$\text{Antenna Gain} = 4\pi \frac{\text{Radiation Intensity}}{\text{Antenna input power}}$$

That gain does not include losses arising from impedance mismatches and polarization mismatches.

The following part gives a brief survey and classification of existing UWB antennas. This historical consideration shows step by step a procedure to obtain developed configuration with wider frequency bandwidth and compact size for new commercial, industrial and academic research demands [14]:

- **Spheroidal antenna**

From the historical aspect, basic wideband antenna geometries have been investigated since the early 1940's. First of all Stratton and Chu [15] proposed the spheroidal antenna in 1941. They mentioned that zero reactance occurs when the antenna length is slightly less than a half wavelength for long thin wires. However, for fatter wires zero reactance may occur when the antenna length is greater than a half wavelength. For a spherical conductor there is no place at which input reactance is zero; there is always a capacitive component. It was evident that the fatter antenna makes the impedance curve broader, and thus provides wider bandwidth.

- **Biconical antenna**

The biconical antenna is formed with two infinite conical conducting surfaces end-to-end, but with a finite gap at the feed point. In 1943, Schelkunoff proposed an infinite biconical antenna which can be easily explained with Maxwell's equations [16]. The biconical antenna is still widely used for wideband antenna applications and its variations, including the discone antenna and the bow-tie antenna, are popular antennas for wideband applications. The input impedance of the infinite biconical antenna is real valued because there is only a pure traveling wave. In other words, the infinite structure has no discontinuities and does not cause reflections that, in turn, set up standing waves, which generate a reactive component in the impedance [11]. A practical biconical antenna is made by ending the two cones of the infinite bicone (Fig.1.1). The reactive part of the input impedance of finite biconical antenna can be held to minimum over a progressively wider bandwidth by increasing the angle θ_h . At the same time, the real part of the input impedance becomes less sensitive to changing frequency [11]. The new demands for planar antenna with low-profile properties cause biconical antenna become inapplicable to use although the biconical geometry idea obtained new quasi biconical-type configurations for low-profile antenna (such as bow-tie).

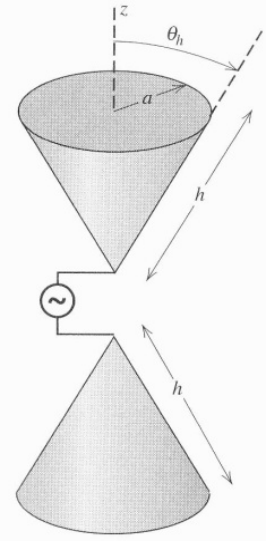

Fig.1.2. Biconical antenna geometry.

- **Bow-tie antenna**

The bow-tie antenna is a planar version of the finite biconical antenna and is a much simpler configuration (Fig.1.2). Although in comparison with infinite biconical antenna has a somewhat more frequency sensitive input impedance but it has conformal designs with less weight and less cost to build.

To know better, the bow-tie antenna can be simulated by a dipole geometry which has omnidirectional pattern with broad main beams perpendicular to the plane of the antenna. As it is indicated the bow-tie impedance frequency bandwidth is smaller than biconical because the surface currents are abruptly terminated at the discontinuities (the base of the triangular) and so the antenna bandwidth is limited [17]. The bow-tie antenna has been used in some applications like planar array for aircraft flight test and evaluation of an UHF radiometer system for many years [18] due to their many attractive advantages, such as simple design, planar structure, and broad bandwidth. Recently, much work has been done to enhance the impedance bandwidth and to obtain stable radiation patterns, such as resistive and capacitive (RC) loading [2] and different feeding technologies [19]. In chapter 3, we use the bow-tie configuration idea to obtain a new quasi bow-tie antenna architecture with wideband and dual polarization properties.

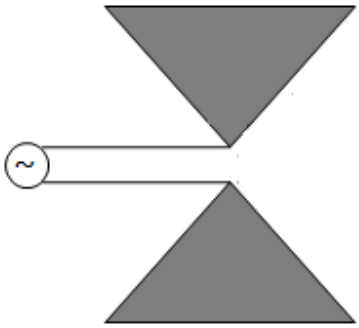

Fig.1.3. Bow-tie antenna geometry.

- **Teardrop antenna**

The staff of the U.S. Radio Research Laboratory at Harvard University has proposed new antenna geometry in 1941 with the idea of the transmission line that gradually diverges while keeping the inner and outer conductors ratio constant (Fig.1.3). This idea leads to several versions of geometry which is nominated teardrop antenna [20] with broadband frequency bandwidth. Several variations of this concept were developed, such as the teardrop antenna, sleeve antenna and inverted trapezoidal antenna, etc (Fig.1.3). For many years antennas with teardrop configuration were employed in television antenna of the Empire state building to obtain a relative wide bandwidth.

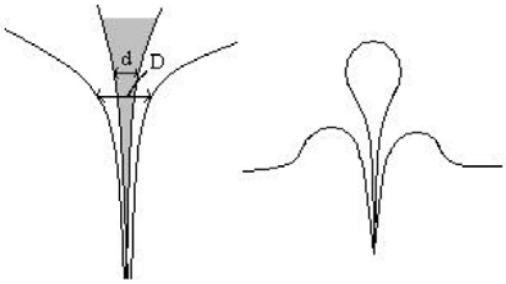

Fig.1.3. Two forms of teardrop antennas [14]

- **Frequency-independent antennas**

The frequency-independent antennas concept is the base of designing some wideband useful antennas. The main idea is: if by an arbitrary scaling the antenna is transformed into a structure identical to the original one, except for a possible rotation about the vertex, its properties will be independent of frequency. If the geometry of antenna has such property, the antenna will be a frequency-independent antenna and the antenna satisfies the angle condition, which means that its form can be specified entirely by angles only and not by particular dimension. R. C. Johnson in "*Antenna Engineering Handbook"* explains that there are two classes of antennas satisfying this condition [21]: conical antennas, made up of infinite cones of arbitrary cross section having a common vertex (we have studied in above section), and equiangular antennas, with surfaces generated by equiangular spirals having a common axis and the same defining parameter.

Since equiangular spirals are also called logarithmic spirals, the name "log-spiral antenna" is commonly used and will be used in the rest of this section [21].

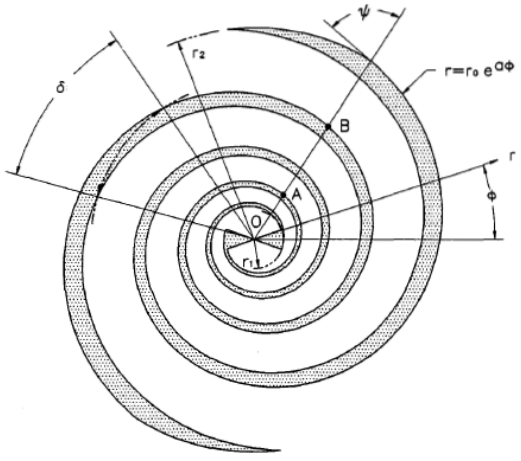

Fig.1.4. Two arms log-spiral antenna.

Planar log-spiral antennas are popular for the radiation of broadband circular polarization. These types of antennas are formed from a spiral two-wire transmission line that gradually transforms itself into a radiating structure (Fig.1.4). Typically the classic equation for a log-spiral curve is $r = r_0 e^{a\phi}$ and the geometry is defined by a (expansion coefficient) and the three angles ψ (pitch angle), δ and ϕ [21].

Spiral antennas have about 10:1 bandwidth, providing circular polarization in low-profile geometry [11]. The equiangular spiral and Archimedean spiral antennas are the most well known log-spiral antennas, but Archimedean spiral is not a truly frequency-independent antenna structure because the spacing between arms is specified by a constant, not an angle. Archimedean spiral antenna is generally well known for producing a broad main beams perpendicular to the plane of spiral [11].Also the input impedance for the equiangular spiral and Archimedean is about 120 Ω and is nearly real and the performance of the equiangular spiral is similar to that of the Archimedean [11].

- **Sinuous antenna**

Although log-spiral antennas have ultra wideband characteristics, in the early 1980's, some academic researches investigated a compact antenna geometry with dual polarization nature. In 1982, R. H. Duhamel invented the sinuous antenna, which provides dual-linear polarization and wide bandwidth in a compact, low-profile geometry [22]. The sinuous antenna geometry with multi-arc is more complicated than the log spiral antenna. The sinuous configuration concept is a self-complementary structure would lead to frequency independent input impedance (Fig.1.5).

Fig.1.5. The sinuous antenna geometry.

In 1996 Xavier Begaud presented a wideband sinuous slot antenna whose geometry looks like the sinuous antenna of R. H. Duhamel [23]. The major inconvenience of sinuous antenna (Duhamel) is high input impedance, close to 60π Ohms. The Duhamel's sinuous antenna has a four arm self-complementary structure that is fed in a balanced manner; and its diameter is about 0.4 wavelengths at lowest operating

frequency. Based on the self-complementary antenna theory (Babinet's principle), this antenna should have high input resistance close to 60π Ohms with an input reactance of zero over its bandwidth of operation in free space [22]. Considering the problem of designing a wideband balun who provides impedance transformation from 60π Ohms to 50 Ohms, he has presented a slot antenna geometry with low input impedance (close to 100 Ohms) [23] to have the simplicity in feeding system designing.
In chapter 2, 3 and 4 we have developed this configuration idea to obtain 3 versions of wideband antennas with dual polarization. In fact this idea is the basis of our dual polarized antennas and some integrated and compact feeding systems are presented.

1.2.1.2 Applications

The applications of UWB antennas change from wireless communications to radar imaging, and vehicular radar [6]-[7]:

1.2.1.2.1 Wideband Wireless Communication Systems

Over the last two decades wireless communication systems have been progressed. The explosive growth of the wireless communication market is expected to continue in the future, as the demand for all types of wireless services is increasing. The authors of "*Ultra Wideband Wireless Communication*" [6] claim that new generations of wireless mobile radio systems aim to provide flexible data rates (including high, medium, and low data rates) and a wide variety of applications (like video, data, ranging, etc.) to the mobile users while serving as many users as possible. In [6], it is shown how the wireless communication application, which is arguably the reason why UWB became part of the wireless world, including wireless home networking, high-density use in office buildings and business cores, UWB wireless mouse, keyboard, wireless speakers, wireless USB, high-speed WPAN/WBAN, wireless sensors networks, wireless telemetry and telemedicine.
Therefore, considering the limited bandwidth availability, accommodating the demand for higher capacity and data rates is a challenging task, requiring modern technologies that can coexist with devices operating at different frequency bands and operate in wider frequency bandwidth. In this point it is revealed that the antenna play one of the most important roles. The antenna must radiate well in wide frequency bandwidth with flexible geometry in UWB systems however the majority of the classic architecture has not the simultaneous ultra wide frequency bandwidth nature with compact size property.

1.2.1.2.2 Ground Penetration Radar (GPR)

After each war there is a real need for low-cost reliable detectors particularly for removing anti-personnel mines. Thus to detect such metal devices there is a demand for detectors which operate well over the widest possible bandwidth. Also such detectors must be as compact as possible) [24-25]. Ground penetration radar antennas are used in such applications and as it is indicated must operate over the widest possible bandwidth with flexible geometry. In [7] and [25] it is explained that the diverse wideband antenna designs such as TEM horns, bicones, bow ties, spirals and Vivaldi antennas are used in GPR antenna application.

1.2.1.2.3 Sensing and Imaging

Recently demands in in-body wireless communications bring into existence the compact wideband radiators for screening procedure [26-28]. As it is shown in [29], the transmitter in in-body wireless must have low-profile characteristic with low power and the wideband antennas with a small size play an important role in the in-body wireless communication.

In academic researches a number of groups worldwide are addressing this application and achieving a compact, wideband, reasonably efficient antenna design is one of the major difficulties. Various wideband antenna designs are employed in a human body, including horns, stacked-patches and resistively-loaded dipoles and monopoles [29-30].

1.2.1.2.4 Testing Systems

Academic activity and microwave technology in wideband antenna domain needs safe antenna parameters measurement within the electromagnetic compatibility community. For this reason, many researchers have indicated frequency- and time domain testing capability for wideband antennas and this topic is at the forefront of research and development in this area [31-32]. For example in reverberation chamber (RC), the presence of a wideband antenna can obtain the desired radiation in desired frequency band.

For this necessity some different types of antenna have been developed. In the laboratory (in chamber measurement setups) TEM horns can be normally used [31], [33]. Also for mobile testing, though, printed-circuit antennas are more appropriate. In the literature several different planar UWB antennas have been proposed covering a variety of frequency ranges such as the 1-6 GHz band [34], the 3.1-10.6 GHz band [35], the 5-20 GHz band [36] and even the 6-40 GHz band [37].

1.2.2 Wideband Dual Polarization Antennas

1.2.2.1 Applications

Having simultaneously wide bandwidth nature and dual polarization characteristic in many recent applications is desired. This section presents four of such widely applications:

1.2.2.1.1 Wideband Wireless Communication Systems

- **Base Station**

Recent years have seen an increased interest in using polarization diversity at the base station by the potential for reduced interference [38-39]. Also in previous section, it is shown the wideband characteristics demands in wireless communication system. For instance the authors of [40] shows that the dual polarization capability with levels of cross-polar radiation and isolation between orthogonally polarized channels better than -30 dB for GSM base station antenna arrays is desired.

In fact base stations for mobile services use vertical polarization because it is then simple to provide an omnidirectional antenna at both the mobile terminals and the base stations [21]. There is sometimes an advantage in using horizontal polarization for obstructed point-to-point links in hilly terrain, but the choice of polarization is often determined by the need to control cochannel interference. Orthogonal polarizations are chosen for antenna mounted close together in order to increase the isolation between them [21].

- **Antenna Design and Channel Characteristic**

The multipath fading channel has an important role in systems design and particularly in antenna design for a wideband wireless system. Our point-of-view in designing a wideband wireless system is that the antenna characteristics to satisfying the system demands and polarization diversity for the antenna arrays is one of the most important techniques. The authors of [41] show how polarization diversity antenna can mitigate the detrimental multipath fading.

Thus, with dual polarized antenna, it is possible to increase the performance of wireless communication system [42]. Moreover maximum performance occurs when the two polarizations are orthogonal (Co-polar/Cross-Polar) and the antenna features high isolation between the two ports.

1.2.2.1.2 MIMO Technology and Smart Antenna

In the literature, the so-called MIMO (Multiple Input Multiple Output) involves receiving or transmitting wireless network signals by means of multiple antennas and channels with enhanced transmission efficiency. In addition, [43] claims that MIMO is generally applied to current wireless network apparatuses where high speed long distance of transmission is desired.

MIMO and UWB technology have such fundamental benefits: greater coverage, highest data rate, interference rejection [6].

These benefits associate antenna wideband characteristics in the chain of UWB system. For instance in [43] it is described as a contemporary wireless router product with MIMO technology typically comprises three sets of half wave antennas, which are aligned in to a row or a triangle with , however, those antennas can only be arranged manually to an alternative polarization direction. They can radiate and receive single polarization. But Antenna arrays with dual polarization characteristic can significant increase such a system performance. The demands for dual polarized antenna are increased because of the necessity of such performance.

1.2.2.1.3 Direction of Arrival Estimation and ESM systems

In standard Electronic Support Measure (ESM) systems, the antennas and the other electronic devices are used to detect emitter signals and estimate several different parameters to provide situational awareness in an electronic warfare environment.

ESM systems are polarization sensitive. In such system, the single polarization antenna (for example vertical) can't receive the opposite polarization (horizontal polarization) and thus the receiver system misses the important data and the DOA algorithms do not operate well. However with dual polarized antenna the ESM system can receive two orthogonal and the system processing prepare suitable results [44]. In addition, ESM systems need radiators with wideband properties to obtain a better knowledge of environment.

1.2.2.1.4 Thickness Measurement

For the sea ice thickness measurement, the aircraft radar system requires two important characteristics: first of all the array antenna operate well in relative wideband antenna and moreover having dual polarization properties. This aircraft radar system must cover the frequency band to apply well the frequency interferometry technique. In addition, the system need detect two different vertical and horizontal characteristics because the radar system should detect the returns from the sea ice in two vertical and horizontal polarizations because it is not known the polarization of the reflected waves and

the receiver antennas must receive well the reflected signals. The authors of [45] claim that at least 20 dB of isolation between the two polarizations is required by the given radar system to clearly distinguish the returned signals of the two different characteristics of the sea ice [45].

1.2.3 Compact Wideband Dual Polarization Antennas

1.2.3.1 Compact and Low-profile UWB Antennas with Dual Polarization

As it is indicated in previous section, obtaining an antenna configuration with wideband and dual polarization characteristics is an important factor in the UWB systems. The wideband and dual polarization properties are discussed in previous sections but it remains another factor which plays an important role in antenna designing.

Recently compact and low-profile wideband antennas in several categories of the academic and military researches and new technology are demanded. In fact one of the critical issues in UWB system design is the size of the antenna for portable devices, because the size affects the bandwidth and gain greatly. Therefore, to miniaturize the antennas capable of providing broad bandwidth for impedance matching and acceptable gain will be a challenging task [46-47]. In the other hand there are some limitations to use the bulky size antenna even with good wideband performance and the demands for compact wideband antenna in portable devices such as (cell phone and laptop) are increasing [48-50]. Also in antenna array minimizing the antenna size is one of the so interesting subjects.

In such situation the planar antenna is so applicable because they exhibit a low profile, small size, light weight, low cost, and ease of fabrication and installation. Furthermore, they are readily adaptable to hybrid and monolithic microwave integrated circuits' fabrication techniques at RF and microwave frequencies [51-53]. However TEM horns, conical spiral, biconical and disk conical antennas too bulky for portable applications.

Also there are some theoretical limitations for frequency bandwidth of each antenna. In the following sections, the lower and upper frequencies of two important categories of wideband antennas are defined.

1.2.3.2 CPW-fed and CPS-fed Wideband Antenna with Dual Polarization

Some coplanar waveguide (CPW) antennas have been proposed for wide-band application because of their compact nature [54-55]. Also the CPS-fed (coplanar stripline) antennas are so interesting in integrated structures because of its architecture nature. In practical mobile UWB applications, antennas

which can be embedded or integrated into UWB devices are attractive to system designers. Antennas that can be directly printed onto PCBs are the most promising candidates for such applications. Because of some special advantages of the coplanar stripline antennas we use CPS-fed antennas to obtain an integrated wideband structures with dual polarization characteristic. In chapters 3 and 4, two main categories of CPS-fed antennas are presented.

1.3 Conclusion: Our Wideband Antenna Candidates

1.3.1. Introduction

The development of UWB systems are growing rapidly with the stringent requirements on impedance bandwidth, efficiency, gain, effective area, radiation pattern, polarization purity and linearly phase behavior. To satisfy these demands, new UWB antennas are needed.

Requirement for antennas vary with applications and systems. Accordingly, a need exists for an antenna that integrates the advantages of the discussed UWB technology and dual polarized antenna. Many applications such as wideband wireless communication, MIMO technology, direction-finding systems or reflector feeds require a compact wideband antenna element that provides orthogonal senses of polarization. Simultaneous polarization capability such as vertical and horizontal or right and left circular from a common aperture is of particular interest. It is one goal of the present thesis to provide some compact wideband antenna structure with dual polarized application.

To achieve the best antenna configuration, several different wideband antenna designs such as spheroidal, biconical, TEM horns, bow ties, spirals and Vivaldi and monopole disc antennas are used in wideband antenna application. This brief investigation shows that our fundamental requirement (compact wideband with dual characteristic) has been met with varying degrees of success by using elements such as crossed log periodic arrays of dipoles or by carefully configured and fed spiral antennas. This solution often failed, though, because they were either too large, their phase centers moved with frequency, their E- and H-plane radiation pattern beamwidth were not the same, or their radiation characteristics were not frequency-independent.

Among the frequency independent antennas, the sinuous antenna is one of the best candidates: it is planar, wideband, and dual polarized with a single aperture. The dual orthogonal linear polarizations can be used for polarization diversity, for transmit/receive operation or to produce simultaneous Left Hand Circular

Polarization (LHCP) and Right Hand Circular Polarization (RHCP). The sinuous antenna has been proposed as a solution to these requirements.

Also as we noted in 2.1.1, the bow-tie antennas bandwidths are not wide enough to meet the requirements for ultra short pulses exciting, and their radiation patterns are distorted at high frequencies. Recently, much work has been done to enhance the impedance bandwidth and to obtain stable radiation patterns.

We'll considerate the optimized developed quasi bow-tie antenna that has the wideband characteristics and it can be used for dual polarization application. It is planar, ultra wideband and actually compact. We consider this antenna design for two reasons: first of all the bow-tie geometry is less complicated than sinuous antenna.

Note that there is a main difference between the bow-tie and sinuous radiation pattern. The bow-tie has omnidirectional dipole-type radiation pattern, however the sinuous antenna provide a directive radiation pattern.

It is very easy to fabricate and integrate into UWB feeding systems. Also a good candidate to compare the bow-tie with other proposed configuration (sinuous antenna) that has more advantages than bow-tie structure is needed. We need a structure as a base UWB element to compare UWB radiation characteristics of the sinuous antenna.

In next section, state of the art of the sinuous antenna with more details is presented to provide a brief description on how it radiates with wideband properties. We need these parts to design and optimize sinuous antenna geometries in following chapters (2, 3 and 4) which will connect to developed wideband feeding system. In addition, the bow-tie antenna will employ in chapter 3 and the analysis of bow-tie antenna will be presented in that chapter.

1.4 The State of the Art of the Sinuous Antennas

1.4.1 Introduction

According to the results of the bibliography cited in section 1.2, among the frequency independent antennas, the sinuous antenna is one of the best candidates: it is planar, wideband, and dual polarized with a single aperture. The dual orthogonal linear polarizations can be used for polarization diversity, for transmit/receive operation or to produce simultaneous Left Hand Circular Polarization (LHCP) and Right Hand Circular Polarization (RHCP). As it was indicated in chapter 1, in the early 1980's, DuHamel has introduced an antenna configuration called the sinuous antenna which have the wideband characteristic with dual polarization nature. Moreover the antenna zigzag lines design as a compact form which obtain a low-profile and low cost structure.

Also Duhamel points that the American Heritage Dictionary defines the adjective sinuous as "characterized by many curves or turns; winding". The Archimedes spiral and log-spiral (also called equiangular spiral) antennas have been used for several decades to provide essentially frequency independent performance over extremely wide bandwidths. As discussed in the following pages, a special class of sinuous antenna is the log-periodic antennas. First of all, the section 1.4.2 describes a glance of the spiral antenna concept to have a deep sense of sinuous antenna.

1.4.2 Log-Spiral antennas [21]

Log-spiral antennas have wideband performance and commonly achieved over 10:1 bandwidths [21]. Fig.1.4 illustrates the planar log-spiral structure. The two-arm planar log-spiral strip antenna of Fig.1.4 is defined by the angles ψ and δ. The equation for a log-spiral curve is

$$r = r_0 e^{a\phi} \tag{3}$$

The other side of the strip may be defined by rotating the curve (3) by the angle δ to give

$$r = r_0 e^{a(\psi+\delta)} \tag{4}$$

and the second arm of the log-spiral structure is obtained by rotating the first arm by 180° around the origin *O*. The inner and outer radii of the finite log-spiral structures are given by r_1 and r_2, respectively.

The planar log-spiral antenna may be viewed and analyzed as a strip radiator with currents surface distribution along the arms or as a slot radiator with electric fields between the strips flowing along the slots. In fact the results should be the same. Johnson show that for $\delta = 90^\circ$, the planar structure is self-complementary, and Babinet's principle leads to the conclusion that the input impedance is $60\pi\ \Omega$ for free space (no dielectric loading) and independent of frequency [21].

1.4.3 DuHamel Sinuous Antenna [22]

A short definition of the Duhamel's sinuous antenna is summarized just to introduce the sinuous geometry conception that this idea will employ to design our new configuration in the following chapters. Although The Archimedes spiral and log-spiral antennas have been used for several decades to provide essentially frequency independent performance over extremely wide bandwidths, but Duhamel in his patent [30] has shown that the previous attempts to use four or more log-periodic elements placed on planar surface to provide two orthogonal senses of polarization with electrical properties and physical dimensions similar to the spiral antennas were unsuccessful.

The curves of Fig.1.6 show that the basic shape of a sinuous curve which, with a rotation, may be used to define an arm of a sinuous antenna.

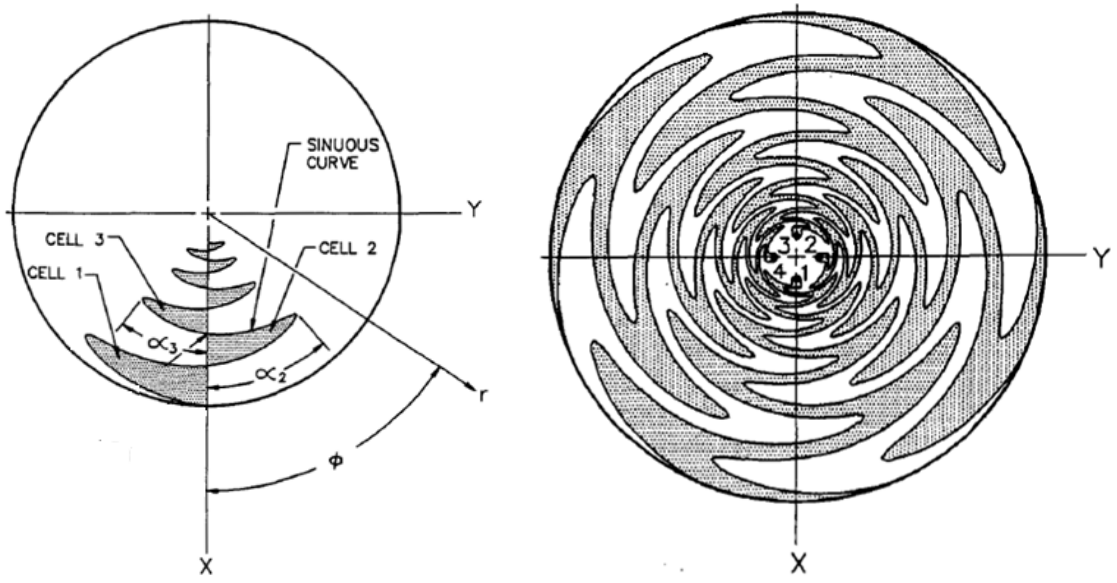

(a) (b)

Fig.1.6. (a) Basic sinuous curve and, (b) Four-arm sinuous antenna [21].

R. C. Johnson [28] presents an approximate equation to calculate the lowest operating frequency:

$$2r(\alpha_p + \delta) \approx \frac{\lambda}{2} \tag{5}$$

where the angles are expressed in radians. The lowest frequency is therefore limited by the antenna outer radius R_1, or $\lambda_L = 4R_1(\alpha_1 + \delta)$. The high-frequency limit is typically bounded by the feed-point design. For good performance at the high-frequency limit, the smallest segment should be somewhat smaller than

$\lambda_H / 4$ to provide a good transition from the feed-point area to the active region. A emprical formulation with acceptable approximation is presented by [21] and [22]:

$$2R_p(\alpha_p + \delta) \approx \frac{\lambda_H}{4} \tag{6}$$

The overall bandwidth may be increased by increasing R_1 and/or decreasing R_p. Dual circularly polarized bandwidths as 14:1 have been obtained, with the limitation for larger bandwidths being the feed circuitry. Feeding system of such an antenna is a critical component and this topic will be detailed in the following chapter.

1.4.4 The sinuous slot antenna

1.4.4.1 Introduction

Amplitude and/or phase comparison techniques with two-arm spirals may be used for one dimensional direction finding. For this type of applications and for beginning of the thesis we start with the simple polarization with two-arm sinuous antenna. Also this type of antenna is an element that we can use as a cell of the complicated dual polarization antenna in the future chapters. According to the state of the art in the previous section, we observed that the major inconvenience of Duhamel's sinuous antenna is high input impedance, close to 300 Ω. Considering the problem of design a wideband balun who provide impedance transformation from 270 Ω to 50 Ω, we decide to use a different antenna geometry with a low input impedance (50 or 100 Ω) [56]. In next section, we will study the optimization and develop a directive simple polarized sinuous slot antenna.

Most antenna applications require a ground plane in order to produce unidirectional beam. But the ground plane usually changes the antenna input impedance over the operating band. Thus, the performance of frequency independent antennas, such as the sinuous, is greatly altered when used with a ground plane. Another solution is to use an absorptive cavity, but this technique limits antenna efficiency to about 50% [57]. The major inconvenience of this antenna is high input impedance and a low efficiency, so we decide to use a different antenna geometry with a low input impedance and without the cavity back absorber.

1.4.4.2 Analysis and Optimization of a Simple Polarized Sinuous Slot Antenna

1.4.4.2.1 The Sinuous Slot Antenna Structure

The traditional sinuous antenna is a center-fed, broadband, self-complementary, four arm structure composed of arcs and bends. Like a traditional sinuous antenna, the proposed design is based on Duhamel's original geometry [22]. In 1996 the sinuous slot antenna was defined [23] by Xavier Begaud. The geometry of this antenna looks like the sinuous antenna of R. H. Duhamel (zigzag lines) [22] but the configuration of each arm is defined by the idea of log-spiral antenna. All the parameters are defined hereafter. Geometry of an *N*-arm equiangular spiral is defined by [56]

$$r_k = r_0 \exp(\phi - \frac{2\pi K}{N}) \tag{7}$$

where K is the arm considered, N the number of arm and a the spiral constant with $a = \sin\theta_0 / tg\mu$ (Fig.1.7).

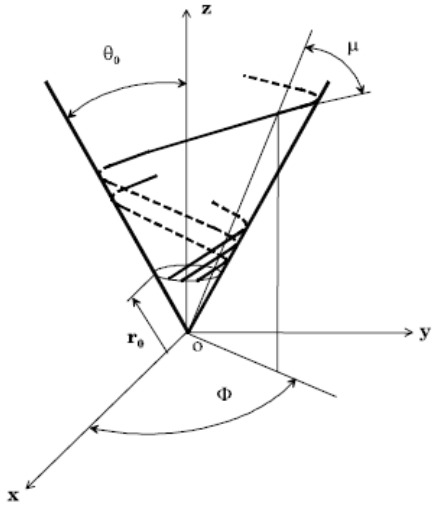

Fig.1.7. Geometry of a conical spiral antenna.

For a planar antenna $\theta_0 = \pi/2$ and so $a = \frac{1}{tg\mu}$. Excitation of *N*-arms is done on a circle of radius r_0, small compared to the wavelength and $d_0/\lambda < 0.1$ with $d_0 = 2r_0 \sin\theta_0 = 2r_0$. Length of one arm is $L = (r - r_0)\frac{1}{\cos\mu}$ and the last important parameter for a spiral antenna is angular width, defined as [99]

$$\delta = \frac{1}{a} Log\left(\frac{\sin\ \mu + \mathrm{C}}{\sin\ \mu - \mathrm{C}}\right) \tag{8}$$

Where C is a constant which can be determined at the centre of spiral $R = C\,r$ .The arm width is adjusted at the excitation by $R_0 = C\,r_0$ then one can determine *C*. When μ is defined, one can determine *a* and δ .

1.4.4.2.2 Sinuous Antenna Function

The frequency operation of this type of antenna limits is determined by its inner and outer diameters. However, it is different: This antenna structure is a two arm and is excited in a slot-mode. When excited with 180° phase progression between both input ports, the antenna demonstrates wideband behavior with maximum gain at broadside. For traditional printed/wire broadband sinuous antennas, an absorber-backed cavity is detrimental to the performance. As demonstrated, this two arm simple polarization antenna can be designed for applications needing wideband operation by finding the growth rate and radiating ring positions with circumference equal to the design wavelengths on individual arc of the antenna geometry [5].

Basically, in a sinuous antenna each arm is contained in an area defined by α_0. This is done, by rotating a single zigzag line clockwise and counterclockwise α_0 degrees about the origin (Fig.1.8). For a single polarized antenna, the parameter N is equal to two, and N is equal to four for a dual polarized antenna.

First calculations for a single polarization have shown that this antenna exhibits an input impedance that varies between 300 and 400 Ω. The idea is now to use the Babinet's principle: a complementary antenna has an input impedance equal to [5]

$$Z_c = (120\pi)^2 / (4Z) \qquad (9)$$

Where Z is the input impedance of the antenna and Z_C the input impedance of the complementary antenna. We optimized the antenna radiating characteristics for a normalized input impedance equal to 350 Ohms. This optimization is not a problem because the antenna is defined as a strip, which is easy to calculate with a modern analysis tool.

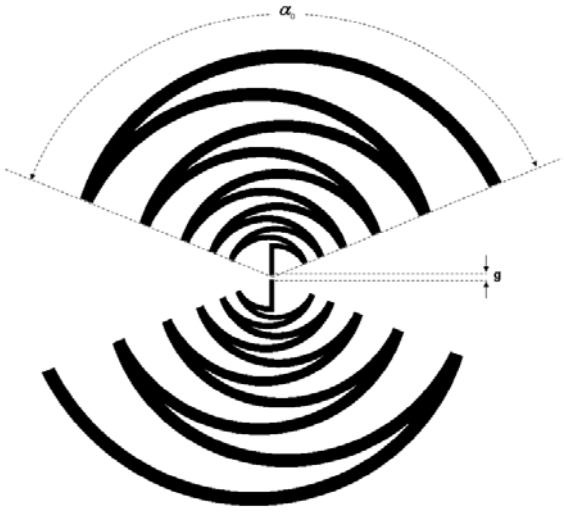

Fig.1.8. Geometry of single polarized sinuous strip antenna.

Then, the complementary antenna, the slot antenna, has a normalized input impedance equal to 100 Ω. This principle of slot sinuous antenna have been reused for others applications.

The developed antenna has three distinct regions. The feeding region is located from the physical center of the antenna. This region contains the balanced two-port feeding structure with slot width that transitions into the radiating slots of the antenna. The radiating region lies approximately between the feeding region and the termination region. The mid and high band antenna radiation occurs from the several arcs within this region. The handedness of the radiation is ultimately determined by the wrapping direction of the arcs. Therefore, active areas within this region will radiate in several continuous bands. The termination region consists of a final arc ending. Additionally, the antenna radiates (from this region) with lower efficiency but with otherwise good pattern and impedance performance.

1.5 References

[1] D.Tran, F.M. Tanyer-Tigrek, A. Vorobyov, I.E. Lager, L.P. Ligthart, "A Novel CPW-fed Optimized UWB Printed Antenna," *Proceedings of the 10th European Conference on Wireless Technology*, pp.40-43, Oct. 2007.

[2] G. Kumar and K. Ray, *Broadband Microstrip Antennas*, Artech House, 2003.

[3] C. Waldschmidt, W. Wiesbeck, "Compact wide-band multimode antennas for MIMO and diversity," *IEEE Transactions on Antennas and Propagation*, Vol. 52, Issue 8, pp.1963-1969, Aug. 2004.

[4] O. Klemp, H. Eul, "On the MIMO Capacity of Planar, Log.-Per. Four-Arm Antennas," *European Conference on Wireless Technology*, pp. 131-134. Oct. 3-4, 2005.

[5] M.Vahdani, X. Begaud, "A Directive Ultra Wideband Sinuous Slot Antenna," *Eucap*, Nice, France, Nov. 2006.

[6] H. Arslan, Z. N. Chen, M. G.Di Benedetto, *Ultra Wideband Wireless Communication*, John Wiley & Sons Inc., 2006.

[7] B. Allen, M. Dohler, E. Okon, W. Q. Malik, A. K. Brown, D. J. Edwards, Ultra-Wideband *Antennas and Propagation for Communications, Radar and Imaging*, John Wiley & Sons Inc., Chapter.7, pp. 111-121, 2007.

[8] Z. N. Chen, *Antennas for Portable Devices*, JOHN WILEY & SONS, Chapter 7, pp. 231-283, 2007.

[9] K. Hettak, G. Delisle, "Omnidirectional-dual Polarized Antenna for Wireless Indoor Applications at Millimeter Waves," *IEEE AP-S*. July 1999, pp.2054-2057.

[10] K. Hettak, G.Y. Delisle and M.G. Stubbs, "A Novel Variant of Dual Polarized CPW Fed Patch antenna for Broadband Wireless Communications," *IEEE AP-S. Int Symp.*, 16-21 July 2000, pp286-289.

[11] Antenna Standards Committee of the IEEE Antennas and Propagation Society, *IEEE Standard Definitions of Terms for Antennas, IEEE Std 145-1993*, The Institute of Electrical and Electronics Engineers, Inc, New York, pp.5, 1993.

[12] W. L. Stutzman and G.A. Thiele, *Antenna Theory and Design,* John Wiley & Sons Inc., *2nd edition*, New York, 1998.

[13] FCC report and order for part 15 acceptance of ultra wideband (UWB) systems from 3.1-10.6 GHz, Washington, DC, 2002.

[14] Seong-Youp Suh, "A Comprehensive Investigation of New Planar Wideband Antennas," Doctor of Philosophy in Virginia Polytechnic Institute and State University, pp. 6-36, 29 July 2002.

[15] Stratton and Chu, *Journal of Applied Physics*, March, 1941.

[16] C. Balanis, *Antenna Theory; Analysis and Design,* John Wiley & Sons Inc., Third edition, 2005.

[17] C. E. Smith, C. M. Butler, and K. R. Umashankar, "Characteristics of a Wire Biconical Antenna," Microwave J., pp. 37-40, September 1979.

[18] M. C. Bailey, "Broad-Band Half-Wave Dipole," *IEEE Transactions on Antennas and Propagation*, Vol. AP-32, No. 4, pp. 410-412, April 1984.

[19] K. Kiminami, A. Hirata, and T. Shiozawa, "Planar Bow-tie Antenna Embedded in Circular Aperture Within Conductive Frame," *IEEE Antennas and Wireless Propag. Lett.*, vol. 5, pp. 399-401, 2006.

[20] Radio Research Laboratory (U.S.), "*Very High-frequency Techniques*," McGraw Hill, New York, 1947, pp.1-25, Chap 1.

[21] R. C. Johnson, *Antenna Engineering Handbook*, Third Ed., McGraw Hill, 1993.

[22] R. H. Duhamel, "Dual Polarized Sinuous Antennas," *U.S. Patent 4,658,262*, April 14, 1987.

[23] X. Begaud: "Analyse d'Antennes et de Réseaux d'Antennes Large Bande et Bipolarisation par une Méthode d'Eléments Finis de Surface". Thesis - University of Rennes 1, December 19, 1996.

[24] D. Daniels, Ground-Penetrating Radar, Institution of Electrical Engineering, 2004.

[25] J.S. Lee, C. Nguyen and T. Scullion, "A Novel, Compact, Low-cost, Impulse Ground-penetrating Radar for Nondestructive Evaluation of Pavements," *IEEE Transactions on Instrumentation and Measurement*, 53, 1502–9, 2004.

[26] M. El-Shenawee, "Resonant Spectra of Malignant Breast Cancer Tumors Using the Three-Dimensional Electromagnetic Fast Multipole Model, *IEEE Transactions on Biomedical Engineering*, 51, 35–44, 2004.

[27] S.K.S. Gupta, S. Lalwani, Y. Prakash, E. Elsharawy and L. Schwiebert, "Towards a Propagation Model for Wireless Biomedical Applications," *IEEE Int. Conf. on Commun.*, pp.1993-1996, May, 2003.

[28] M. Ghavami, L.B. Michael and R. Kohno, "Ultra Wideband Signals and Systems in Communication Engineering," John Wiley & Sons, England, 2004

[29] A. Fort, C. Desset, P. De Doncker, P. Wambacq and L. Van Biesen, "An Ultra-wideband Body Area Propagation Channel Model – From Statistics to Implementation," *IEEE Trans. Microwave Theory Tech.*, vol.54, pp.1820-1826, April 2006.

[30] S. Matsuda, H. Harada and R. Kohno, "A Study on Stochastic Radiowave Propagation Model Inside a Human Body," *IEICE Tech. Report*, WBS2005-59, Dec., 2005.

[31] R.T. Johnk, D.r. Novotny, C.M. Weil, M. Taylor and T.J. O"Hara, "Efficient and Accurate Testing of an EMC Compliance Chamber Using an Ultrawideband Measurement System", *IEEE EMC-S Int.* Dig., vol. 1, pp. 302-307, Aug. 2001.

[32] J.D. Brunett, R.M. Ringler and V.V. Liepa, "On Measurements for EIRP Compliance of UWB Devices", *IEEE EMC-S Int,*Dig., vol. 2. pp. 473-476, Aug. 2005.

[33] K. Chung, S. Pyun and J. Choi, "Design of an Ultrawide-band TEM Horn Antenna with a Microstrip-type Balun", *IEEE Trans. Antennas Propogat*, Vol. 53, pp. 3410-3413, Oct. 2005.

[34] Z. Ying and J. Andersson, "An Ultra Wideband "Cobra" Patch Antenna", *IEE Proc.-Microw. Antennas Propag.*, Vol. 151, pp. 486-490, Dec. 2004.

[35] H.R Chuang, C.C. Lin and Y.C. Kan, "A Printed UWB Triangular Monopole Antenna", *Microwave J.*, Vol. 49, pp. 108-120, Jan. 2006.

[36] M. A. Peyrot-Solis, G.M. Galvan-Tejada and H. Jardon-Aguilar, "Directional UWB Planar Antenna for Operation in the 5-20 GHz Band", *Proc. 17th Int. Zurich Symp. EMC*, pp.277-280, Feb./Mar. 2006.

[37] K. Rambabu, H.A. Thiart, J. Bornemann and S.Y. Yu, "Ultra-wideband Printed-circuit Antenna", *IEEE Trans. Antennas Propagat.,* Vol. 54, pp. 3908-3911, Dec. 2006.

[38] B. Glance and L. J. Greenstein, "Frequency Selective Fading Effects in Digital Mobile Radio with Diversity Combining," *IEEE Trans. Commun., V*ol. COM-31, No. 9, pp. 1085-1094, 1983.

[39] R.G. Vaughan, "Polarization Diversity in Mobile Communications," *IEEE Trans. Vehicular Technol*. 39, pp.177-186, August 1990.

[40] Fedir F. Dubrovka, Sergiy Y. Martynyuk, "Wideband Dual Polarized Planar Antenna Arrays," *Antenna Theory and Techniques*, Vol.1, pp. 91-96, Sept. 2003.

[41] K. Hettak, G. Y. Delisle, M. G. Stubbs, "A Novel Variant of Dual Polarized CPW Fed Patch Antenna for Broadband Wireless Communications," vol.1, pp. 2000.

[42] C.C.Y. Lee, "Polarization Diversity System for Mobile Radio", *IEEE Trans. Communications*, pp.912-923, Oct. 1972.

[43] Nan Lin Li, "Dual polarized antenna," *U.S. Patent 7310066*, December 18, 2007.

[44] Tommy H. Lam, "Integrated feed broadband dual polarized antenna," *U.S. Patent* 6621463, December 16, 2003.

[45] J. Huang, Z. A. Hussein, and A. Petros, "A VHF Microstrip Antenna with Wide-Bandwidth and Dual-Polarization for Sea Ice Thickness Measurement," *IEEE Trans. On Antennas and Propag*., Vol. 55, No. 10, Oct. 2007.

[46] S. W. Su, K. L. Wong, and C. L. Tang, "Ultra-Wideband Square Planar Monopole Antenna for IEEE 802.16a Operation in the 2-11 GHz Band," *Microwave and Optical Technology Letters*, vol. 42, no.6, pp. 463–466, Sep. 2004.

[47] J.D. Kraus, *Antennas,* 2nd edition, pp. 340–358. New York: McGraw-Hill, 1988.

[48] S. Honda, M. Ito, H. Seki, and Y. Jinbo, A Disk Monopole Antenna with 1:8 Impedance Bandwidth and Omnidirectional Radiation Pattern. *Proceedings of the International Symposium of Antennas and Propagation*, Sapporo, Japan, pp. 1145–1148, 1992.

[49] M. Hammoud, P. Poey, and F. Colombel, "Matching the Input Impedance of a Broadband Disc Monopole," *Electronics Letters*, 29 (1993), 406–407.

[50] Z.N. Chen and M.Y.W. Chia, *Broadband Planar Antennas: Design and Applications*. Chichester: John Wiley & Sons, Ltd, 2006.

[51] S.S. Sandler and R.W.P. King, "Compact Conical Antennas for Wide-band Coverage," *IEEE Trans. Antennas Propagat.,* 42(3), 436–9, 1994.

[52] T.W. Hertel and G.S. Smith, "On the Dispersive Properties of the Conical Spiral Antenna and Its Use for Pulsed Radiation," *IEEE Trans. Antennas Propagat*., 51(7), 1426–33, 2003.

[53] D.L. Senguta and Y.P. Liu, "Analytical Investigation of Waveforms Radiated by a Resistively Loaded Linear Antenna Excited by a Gaussian Pulse," *Radio Science*, 9, 621–30, 1974.

[54] T. G. Ma, and S. K. Jeng, "Planar Miniature Tapered-Slot-Fed Annular Slot Antennas for Ultrawide-Band Radios," *IEEE Transactions on Antennas and Propagation*, vol. 53, no.3, pp. 1194–1202, Mar. 2005.

[55] P. Li, J. Liang, and X. Chen, "Study of Printed Elliptical/Circular Slot Antennas for Ultra Wideband Applications," *IEEE Transactions on Antennas and Propagation Society International Symposium*, vol. 54, No. 6, pp. 1670-1675, Jun. 2006.

[56] X. Begaud, P. Poey, J. P. Daniel and G. Dubost, "Design of wideband dual polarized slot antenna," AP2000 Millennium Conf. Antennas and Propagation, Davos, Apr. 2000.

[57] M. C. Buck, J. Burford, D. S. Filipovic, "Multiband Two Arm Slot Sinuous Antenna," *Antennas and Propagation Society International Symposium*, IEEE, Vol. 1, pp. 165-168, Jun. 2004.

Chapter 2
Feeding Systems for Ultra Wideband Antennas

2.1 The state of the art of Feeding Systems for Ultra wideband Antennas

2.1.1 Introduction

Baluns are required for balanced mixers, push-pull amplifiers, balanced frequency multipliers, phase shifters, balanced modulators, feeding systems for antennas, and numerous other applications. Whenever a balanced antenna (i.e., dipole, loop or spiral) is used, the issue of how to feed the antenna becomes relevant. Because a balanced antenna requires a balanced feed, a balun is needed.

A balanced antenna fed by a two-wire transmission line is a balanced system with respect to the lines, provided that the two feed points on the balanced antenna have the same orientation and placement with respect to the lines. If the balanced (symmetrical) antenna is connected to a coaxial transmission line, the transition from the feed line to the balanced antenna is an unbalanced (asymmetrical) driven system.

The balun is inserted between the feed line and the antenna in order to provide a transition between the coaxial cable and balun output port (Fig.2.1). If the balun operates well in field matching and obtain a balanced feed in the antenna input port, the balun will produces a symmetrical radiation pattern for our desired antenna.

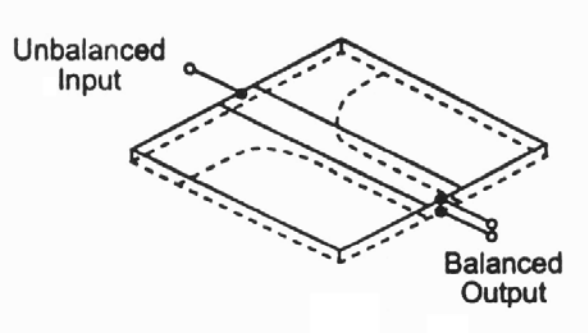

Fig.2.1. A typical schematic for a balanced to unbalanced structure [1].

In this and the following chapters, it will show how a certain wideband balun it works and how it can obtain the symmetrical surface current distribution on the antenna plane to have a suitable radiation performance.

This transition from a balanced medium to an unbalanced one requires special techniques, which are described in this section. Because the focus of this thesis is on wideband planar structures, only scheme based on the latter concept are discussed.

2.1.2. The State of the Art of the Feeding Systems for Ultra Wideband Antennas

2.1.2.1 Balanced-to-Unbalanced Transformation

A balun (balanced-to-unbalanced) is a transformer used to connect balanced transmission line circuits to unbalanced transmission line circuits. Fig.2.1-3 show examples of balanced and unbalanced transmission lines, respectively. Two conductors having equal potential with 180-degrees phase difference constitute a balanced line. In this case, no current flows through a grounded shield (i.e. $I_1 = I_2$ and $I_s = I_g = 0$). When this condition is not satisfied, as shown in Fig.2.2, where I_s is finite, the transmission line is termed as unbalanced. In addition, to provide a matched transmission between a balanced and an unbalanced line, baluns operate as center-tap transformers for push-pull applications used in radio frequency applications [1].

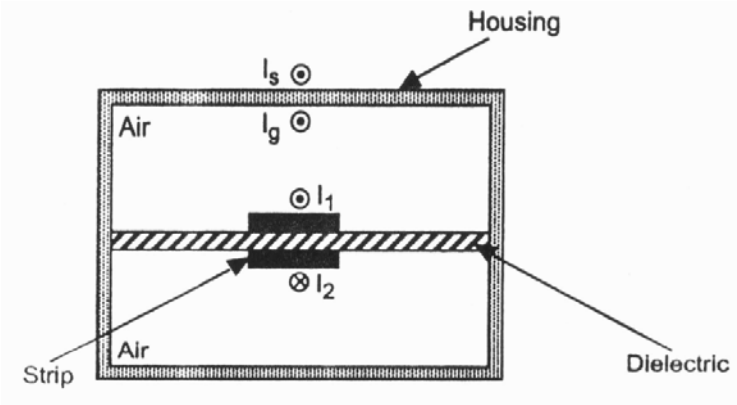

Fig.2.2. Shielded parallel strip balanced transmission line [1].

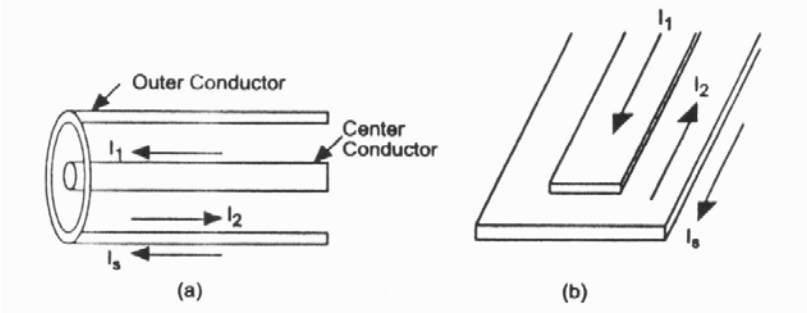

Fig.2.3. Unbalanced transmission line (a) coaxial and (b) microstrip [1].

Over the past half-century, several different kinds of balun have been developed [2]-[6]. Early coaxial baluns were used exclusively for feeding dipole antennas. Later, planar baluns using stripline techniques were developed for balanced mixers and printed antennas feeds. Current interest in balun structures is focused toward making it planar, compact and more suitable as antenna feeding system.

For the beginning of wideband balun study, it is proposed analysis and synthesis of a tapered microstrip transmission line as the basis structure of wideband microstrip balun. Also it is presented many ideas to geometry design of the microstrip-to-balanced stripline balun.

In addition in some applications, it is necessary to connect the feed terminals on the balanced antennas to an unbalanced coaxial cable that requires not only a balanced-to-unbalanced transformation circuit, but also an impedance match due to the different characteristic impedances of the antenna and the cable.

2.1.2.2 Exponential Tapered Microstrip Structure

In this part it is summarized the analysis of an exponential tapered microstrip structure. This analysis helps us to design and develop our desired tapered microstrip geometry.

Tapered microstrip line consists of a tapered strip printed on the substrate and an infinite ground plane on the other side of the substrate. This structure widely use as a balun for wideband antennas especially for impedance matching, couplers, filters, and interconnections in microwave integrated circuits (MICs). It is desired to optimize a tapered microstrip balun which use as an impedance transformer to match a line of impedance Z_1 to a load of impedance Z_2 (Fig.2.4).

The most tapered microstrip analysis [7]-[9] are based on the Riccati differential equation. In this way, the reflection coefficient can be obtained by a simple Fourier transform of a function of characteristic impedance [10].

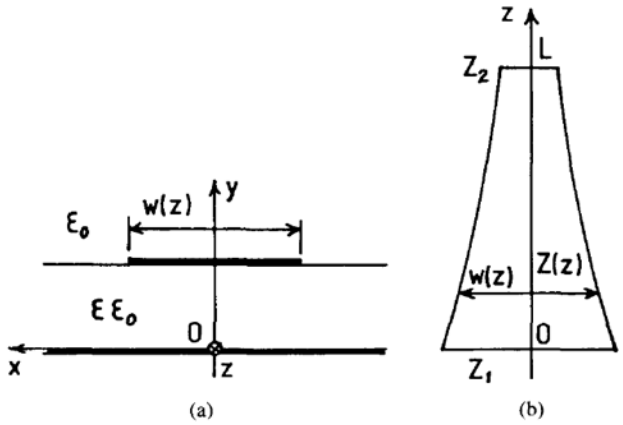

Fig.2.4. Tapered microstrip transmission line. (a) Cross-section and (b) z -dependent configuration of strip conductor [10].

According to [10], the characteristic impedance of the tapered microstrip configuration can be calculated by the equation (1):

$$Z = \eta / \left\{ (C_0(w/h)/\varepsilon_0)\sqrt{\varepsilon_{eff}(w/h,0)} \right\} \tag{1}$$

where

$\eta = \sqrt{\mu_0/\varepsilon_0}$ denotes the intrinsic impedance of free space,

$\varepsilon_{eff}(z,\omega)$ denotes the effective permittivity,

and $C_0(w/h)$ is the line capacitance per unit length for the case of $\varepsilon_r = 1$ and shape ratio w/h .

In ref. [8] an approximate formula for $C_0(w/h)/\varepsilon_0$ has been presented in the case of $0.1 \le w/h \le 0.7$

$$C_0(w/h)/\varepsilon_0 = 0.4109 + \sqrt{5.940w/h + 0.4631} \tag{2}$$

And an approximate formula for $\varepsilon_{eff}(w/h,0)$ [8]

$$\begin{aligned} \varepsilon_{eff}(w/h,0) = 4.5 + 1.832 \{ & \exp 0.9282 \log_{10} \mathrm{A} \\ & -0.3367 \{\log_{10} \mathrm{A}\}^2 - 0.3189 \{\log_{10} A\}^3 \\ & -0.0615 \{\log_{10} \mathrm{A}\} \} \end{aligned} \tag{3}$$

where

$$A = \log_{10}(w/h/4.4) \tag{4}$$

The characteristic impedance of the tapered microstrip is the function of relative permittivity and the curve of the characteristic impedance will vary respect to ε_r. In the [10] has presented an example of the case $\varepsilon_r = 8$, $Z_1 = 63.58\ \Omega$ ($w/h = 0.7$ at $z = 0$), $Z_2 = 117.99\ \Omega$ ($w/h = 0.1$ at $z = L$). Note that the resulting relation between w/h and z/L is shown by the dashed line in Fig.2.5.

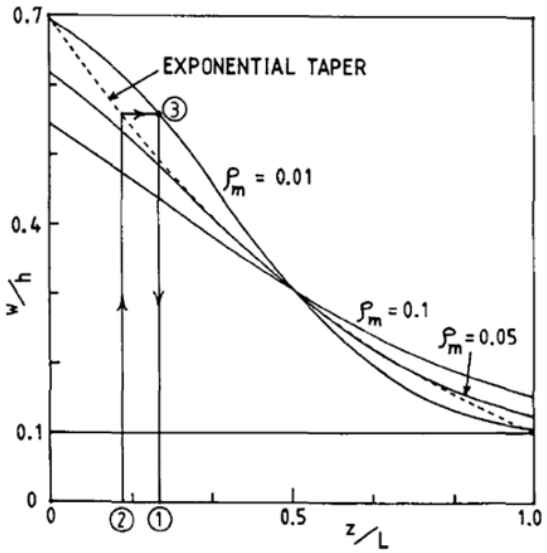

Fig.2.5. The z -dependent configuration of microstrip exponential taper and Tchebycheff tapers (ε_r =8) [10].

Now it is possible to design and optimize the dimension parameters of a microstrip exponential taper with Fig.2.5 for certain Z_1, Z_2. In the following chapters we utilize the substrate with $\varepsilon_r = 2.17$ and it must involve $\varepsilon_r = 2.17$ in equation (1) to calculate characteristic impedance respect to the L/λ_0 for any point of the microstrip line. In section 2.2, we optimize a microstrip-to-balanced stripline with our fabrication parameters.

2.1.2.3 Microstrip-to-Balanced Stripline Balun

In this part, a microstrip-to-balanced stripline balun is presented. First of all a smooth transition from a microstrip line to a balanced stripline as shown in Fig.1 operates as a balanced balun. This figure shows a tapered Microstrip-to-balanced Stripline Balun. When a microstrip is joined to a balanced stripline, a step discontinuity between the ground plane of the microstrip line and the bottom conductor of the balanced stripline exists. A step discontinuity also exists between the top strip conductors of these two lines. Transmission-line tapers are generally employed to achieve a good match between the two lines [1].

An example of a transition from microstrip to balanced stripline when connected back-to-back, to simplify measurements, is shown in Fig.2.6. For the characteristic impedance, for example $50\ \Omega$, the stripwidth for the microstrip, W_m, is smaller than the stripwidth for the balanced stripline W_b. When these two lines are connected, both the stripline conductor and the ground plane are tapered to match the

dimensions. Several tapering techniques are available (such as Chebyshev tapering contour along the balun's length [11]) and always are selected a specific taper shape based on the bandwidth requirement.

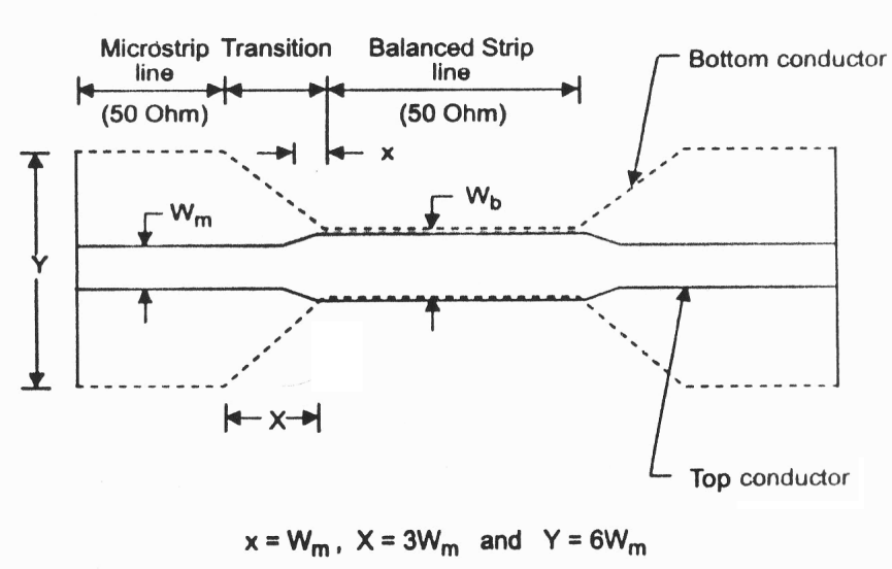

Fig.2.6. Unbalanced-to-balanced transitions connected back-to-back [1].

A simple linear taper, such as shown in Fig.2.6, can easily achieve an octave bandwidth. For the fabricated example shown in the figure, $x = W_m$, $X = 3W_m$, and $Y = 6W_m$ and the transitions were characterized on 62.5-mil-thick polystyrene substrate ($\varepsilon_r = 2.55$) and on 50-mil-thick alumina substrate ($\varepsilon_r = 9.7$). The complete assembly was 2.54 cm long and the connectors used were of OSM-stripline-type, which have about 0.1-dB insertion loss per connector at S-band [1].

Fig.2.7 shows typical measured VSWR for two transitions as well as for the through line. For the polystyrene transition the maximum VSWR over 2.4 to 4.5 GHz was 1.2, whereas for the alumina case the VSWR was less than 1.2 over the 1.7 to 3.2 GHz frequency range. Typical measured insertion loss was less 0.6 dB and 0.4 dB, respectively, for these two transitions [1].

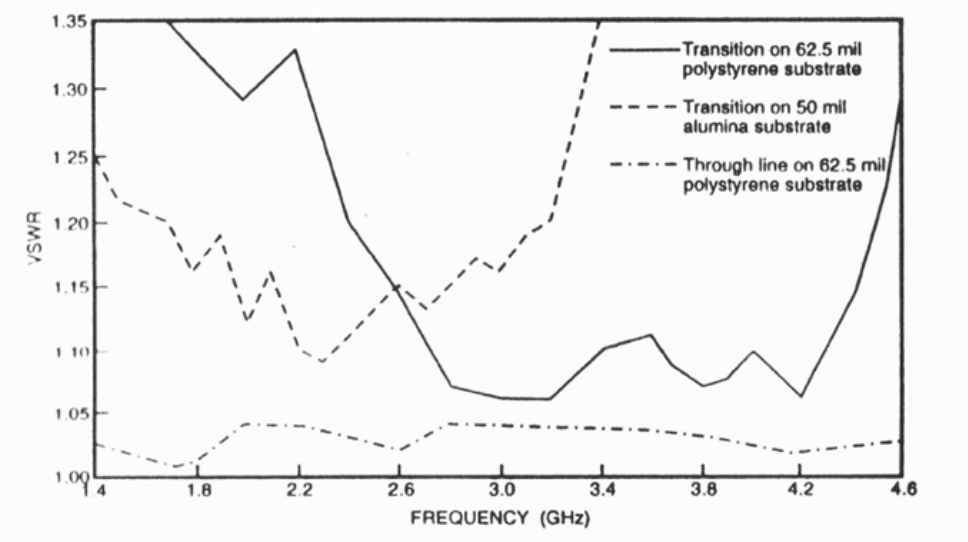

Fig.2.7. Measured performance of transitions fabricated on polystyrene and alumina substrates [1].

2.1.2.4 Variation of Microstrip-to-Balanced Stripline Baluns

Also in 1996 X. Begaud has used the microstrip-to balanced stripline geometry in his thesis (chapter 2) [12]. He has optimized this architecture and has presented a new balun configuration with a bend to feed a Star ("étoile") antenna. The results show VSWR is better than 2.5 between 2 to 4 GHz.

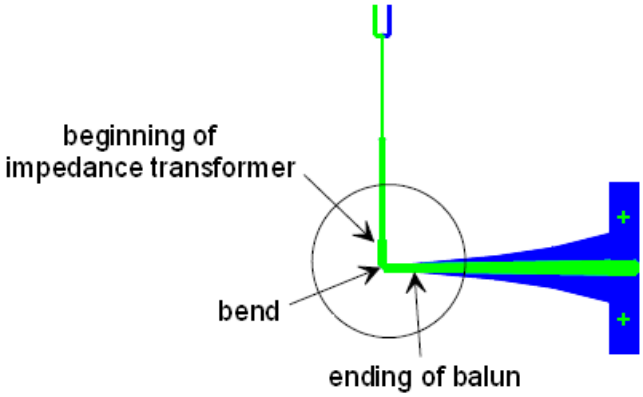

Fig.2.8. Unbalanced-to-balanced transitions configuration [12].

In Laboratoire Antennes & Télécommunications (Université de Rennes), Ph. Gonnet et al. have presented two experimental versions of wideband baluns with the idea of microstrip-to-Balanced Stripline configuration [13]. In 1999, they have proposed two developed category of feeding systems: Tapered transmission lines and the conventional type of baluns. They implemented them to feed a four-arm

sinuous antenna and the results show good impedance matching and electrical characteristics over more than one octave frequency bandwidth.

Moreover A. Kazemipour in 2002 has presented another variation of balun which operates well in high frequency (300 MHz to 1 GHz) and they are employed for calculation of coupling between the dipole (chapter 2) and star antennas (chapter 4) [14]. Also in recent years, a dual polarized feed for reflector-based searching systems is proposed [15] and also the feeding system is realized by the conception of microstrip tapered baluns.
Finally I have optimized this type of balun to feed a directive sinuous slot antenna with simple polarization in 2006 [16]. This optimized microstrip balun operates well in ultra wideband (from 10 MHz to 9.75 GHz) which is presented in next section.

2.1.3 Conclusion

In this section, the taper microstrip-to-balanced stripline balun has been introduced as a wideband balun for balanced planar antennas. Also a brief history of wideband microstrip-to-balanced stripline is presented. Furthermore, the formula of characteristic impedance of a typical tapered microstrip structure is calculated.
Apart from microstrip baluns, coplanar waveguide (CPW) and coplanar stripline (CPS) baluns have also been reported. We will study these types of baluns in chapter 3. In next section, it is used the microstrip-to-balanced stripline balun because of its simple planar structure and its compatibility with our antenna geometry.

2.2 Optimization and Fabrication of a Feeding System for a Simple Polarized Sinuous Slot Antenna

2.2.1 Introduction

In this section, a microstrip-to-balanced stripline is developed to feed a simple polarized sinuous antenna. First of all it is presented the optimization of slot sinuous antenna to connect to our feeding system and to verify the balun performance in ultra wideband frequency.

2.2.2 Optimization of a Simple Polarized Sinuous Slot Antenna

2.2.2.1 Optimization of the Antenna and consideration of the Parameters Variations μ, α_0

In chapter 1, it has been explained how operates a slot sinuous antenna (Fig.2.9). For an improved matching, we have optimized the antenna parameters. To design an optimized slot sinuous configuration, we have considered a wideband frequency between 2 and 10 GHz for antenna. It means f_L=2 GHz and f_H=10 GHz. In the other hand, the frequency bandwidth of sinuous antenna configuration has been used by below equation [4]:

$$R_{ex}.\alpha > \lambda_B/2$$

$$R_{in} < 0.1\ \lambda_H$$

Thus, we arrive to α=135° with R_{in}=3 mm and R_{ex}=32.3 mm in optimization procedure. Optimized characteristics have been obtain with $\mu = 85^\circ$, $\alpha = 135^\circ$ and an expansion rate $\tau = r_n / r_{n+1} = 0.0875$. It's important to note that this slot antenna is not rigorously the complementary antenna of the strip antenna, because the metal around the slot hasn't infinite dimensions.

In the first steps of this work, the radiating part of the antenna was only metallic and the normalized impedance was closed to $82\,\Omega$. So first we optimized a balun for wideband impedance transformation from 50 Ω to $82\,\Omega$.

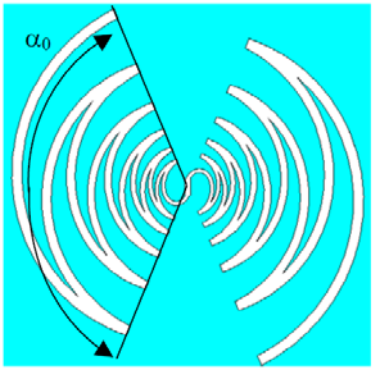

Fig.2.9. Geometry of single polarized sinuous slot antenna.

2.2.2.2 Consideration of the Substrate Permittivity's Effect on the Antenna Input Impedance

In fact, the radiation characteristics and especially the input impedance of the sinuous slot antenna change with the substrate permittivity. In Fig.2.10 we present the Input Return Loss for three supports: DiClad880 (thickness=0.762 mm, ε_r=2.17, tanδ=0.0009), FR4 (thickness=0.8 mm, ε_r=4.3, tanδ=0.002) and without support (air). The widest –10 dB bandwidth is obtained by simulator CST Studio Suite 2008 [17] for Diclad880. The –10 dB simulated bandwidth is between 3 GHz to 10 GHz for the return loss.

For the realization of the antenna, it is necessary to have a lightweight support and a normalized impedance not so low, to be sure to connect the bifilar line at the center of the sinuous antenna, so we choose the DiClad880 for the substrate of the radiating part of the sinuous slot antenna.

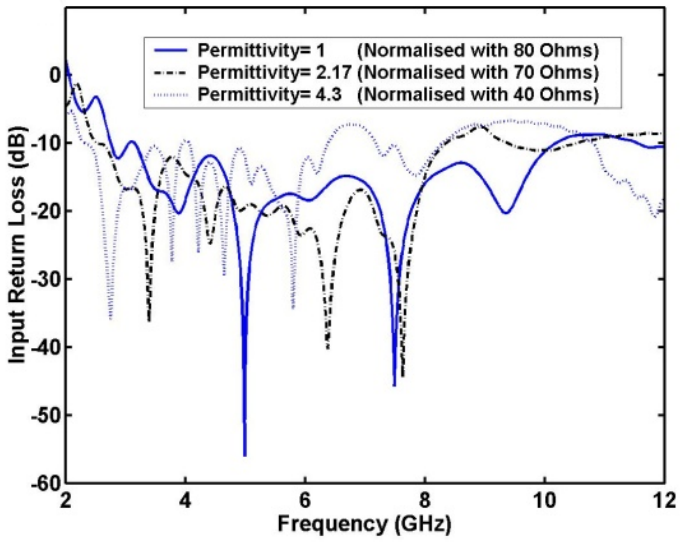

Fig.2.10. Simulated Return Loss of sinuous slot antenna with three different substrates.

2.2.3 Analysis, optimization and realization of a UWB Feeding System [15]

2.2.3.1 Analysis and realization of a UWB Microstrip-to-balanced stripline balun

In subsection 2.1.2.3, it is proposed microstrip-to-balanced stripline (microstrip to parallel strip) as a wideband balun that it has good performance to balanced-to-unbalanced transformation. Also it is suitable as an impedance transformer to connect to our sinuous antenna.

As it is shown in Fig.2.11 both conductors width (strip and ground plane) gradually change. The top strip width changes linearly from 2.4 mm at the microstrip to 2 mm at the parallel strip. The ground plane conductor width changes from 12 mm to 2 mm in such a way that, and the cross-sectional point along balun length (50 mm), the characteristic impedance gradually changes from 50 to $70\,\Omega$. For various top conductor widths, simulations of continuous transmission lines were performed with different ground plane widths for obtain balun good performance. In addition various values for structure length, from 20 mm to 60 mm, were evaluated and 50 mm was found to be the best.

Finally a microstrip taper balun for wideband applications has been optimized to ultra wideband bandwidth. The geometry is presented on Fig.2.11 and the dimensions of the different parts of the balun are listed in Tab 1. h is the thickness of the substrate (DiClad 880), the permittivity is 2.17 and $\tan\delta = 0.0009$.

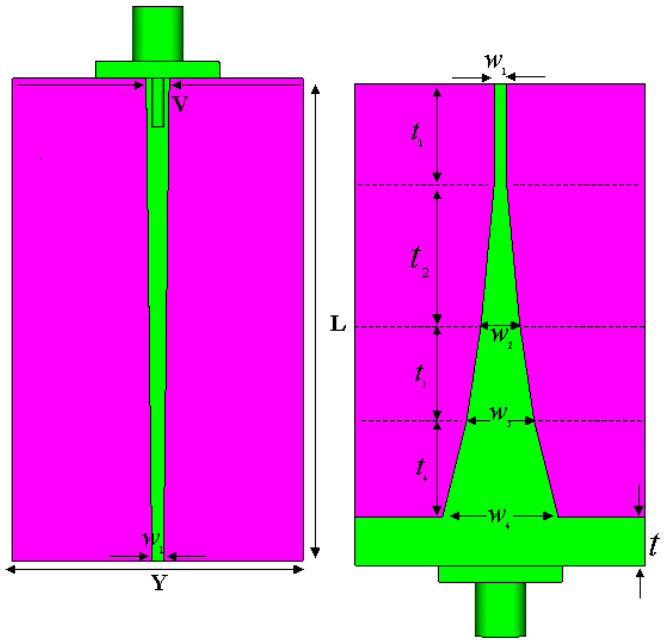

Fig.2.11. Configuration of the microstip taper balun with SMA connector.

Table 1.1. DIMENSIONS OF THE TRANSITIONS (Unit: Millimeters)

h	L	Y	V	w	w_1	W_2	W_3	t	t_1	t_2	t_3	t_4
0.762	*50*	*3*	*2.4*	*2*	*4*	*7*	*12*	*5*	*10*	*15*	*10*	*10*

2.2.3.2 Insertion Loss, Return Loss and Phase Difference

This balun has been realized and measured with a CMS load of 70 Ohms connected to the lecher line (parallel strips) port, the other port is a 50 Ohms SMA connector. The –10 dB measured bandwidth is between 10 MHz and 9.75 GHz and the –15 dB measured bandwidth is between 10 MHz and 7.3 GHz (Fig.2.12).

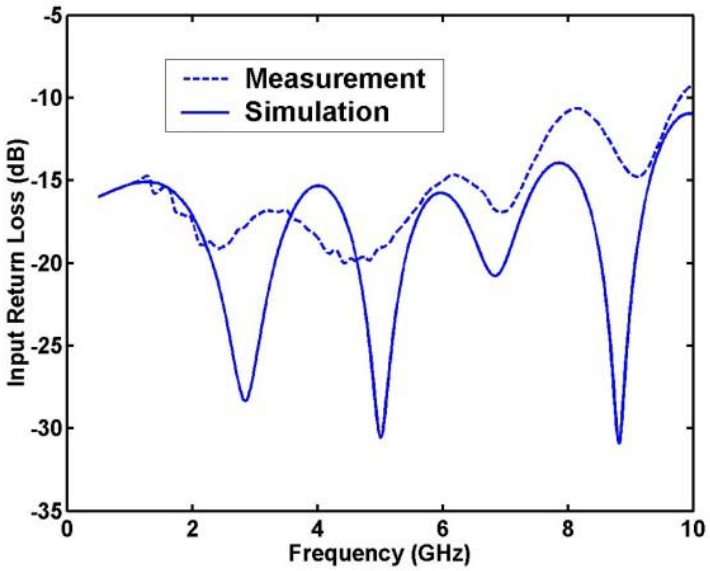

Fig.2.12. Measured and simulated Return Loss of microstip taper balun with a load of 70 Ω.

A good agreement is observed between simulation and measurement. The difference between simulation and measurement is due to the difficulty to obtain a perfect alignment of the two sides of the balun printed on the same substrate

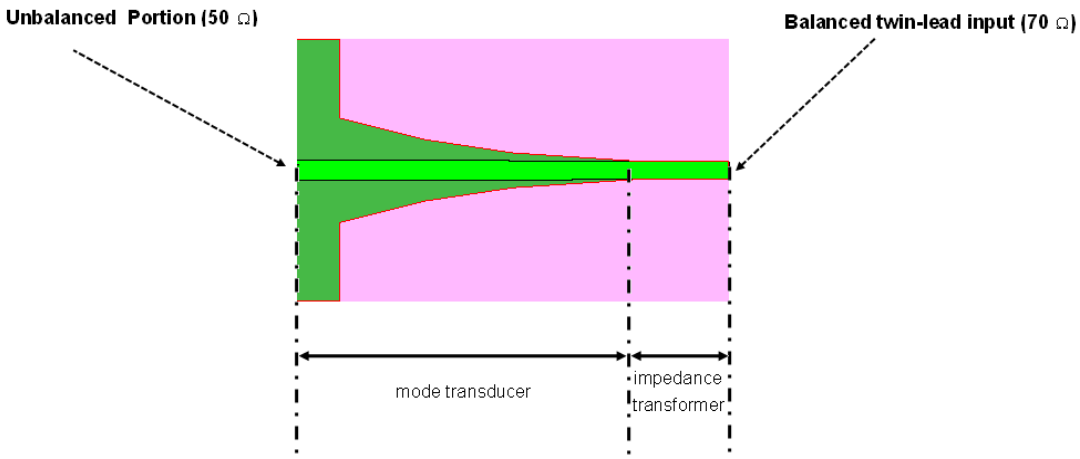

Fig.2.13. Drawing of the balun.

To validate the balun performance it is joined two structures back-to-back. This was done at the parallel strip outputs with the orientation such that the ground planes were connected electrically. Two SMA connectors were soldered on. As shown in Fig.2.13, this taper-line balun has two sections: the balanced line portion which matches the antenna impedance to ~70 Ω and a portion which actually performs the mode transduction. One method to confirm the proper function of this balun design is to connect two baluns back-to-back (end-to-end) at the balanced port (Fig.2.14). Clearly, the center of this circuit arrangement is a balanced twin lead, while the ends, which are microstrip-to-coax transitions, are unbalanced.

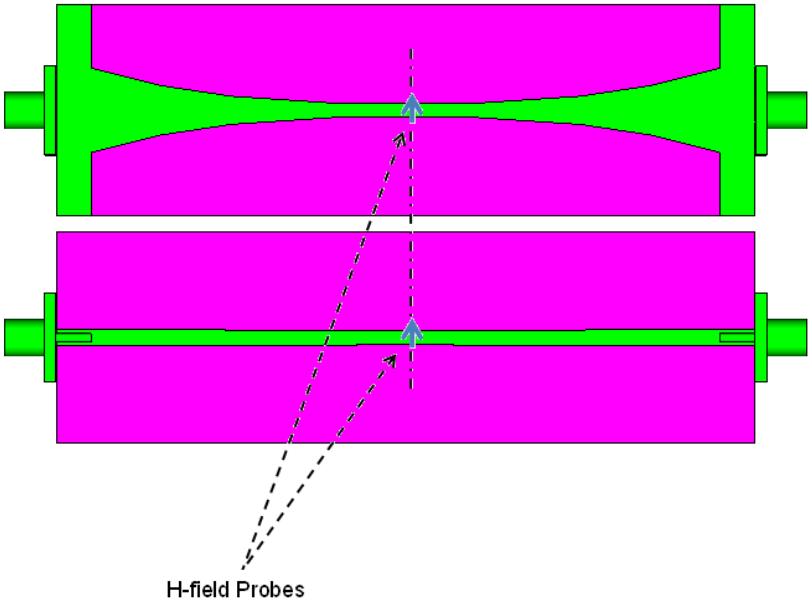

Fig.2.14. Back-to-back connection of the balun with two H-field probes.

Simulated S_{11} and S_{21} for the back-to-back balun is shown in Fig.2.15. This Figure shows that the transmission property of this circuit is $S_{21} \geq -1$ dB for frequencies from 2 GHz to 11.8 GHz. The return loss is $S_{11} \leq -10$ dB for frequencies from 2 GHz to above 12 GHz and $S_{11} \leq -15$ dB for frequencies before 2 GHz to 6.6 GHz (Fig.2.15).

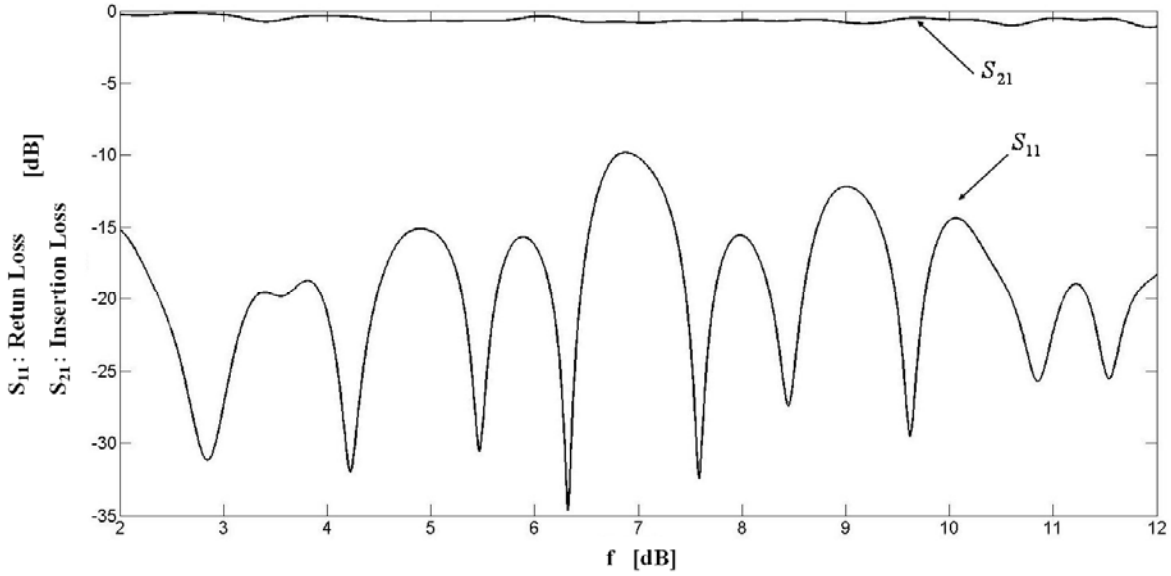

Fig.2.15. Simulated Return Loss and Insertion Loss of back-to-back balun.

To check the balun's current balance, two H-field probes were placed at the center of parallel strip outputs (on top and bottom conductors respectively) with simulator CST Studio Suite 2008 (Fig.2.16).

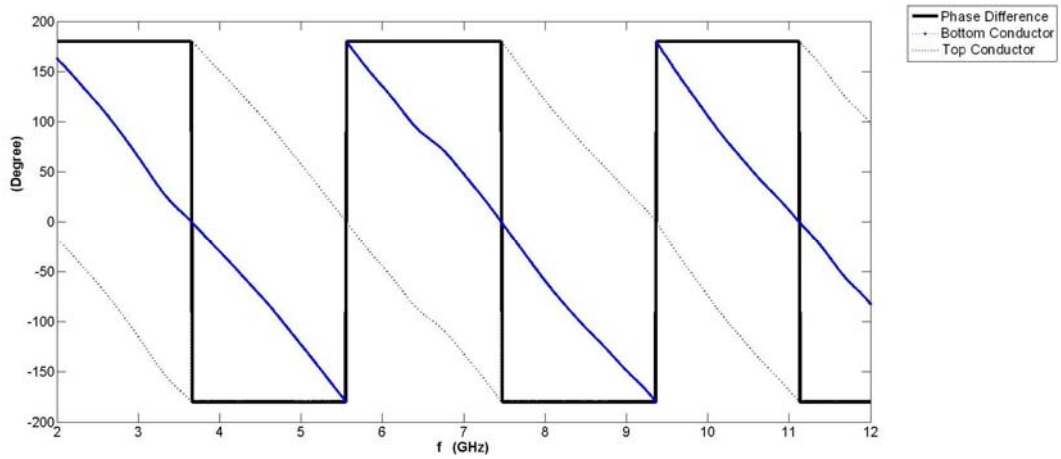

Fig.2.16. H-field probe phase for two points are shown in Fig.2.14 to check the balun's current surface balance.

- ***Results Interpretation :***

1. A comparison of the two H-field in this point shows a 180° phase difference over the bandwidth (180° phase difference from 2 to 12 GHz).
2. The balun can operate well to field matching between a unbalanced field (coaxial cable) and a balanced stripline.
3. This fact shows that this optimized balun can be used to feed a balanced antenna as a sinuous antenna in wideband frequency bandwidth (from 2 to 12 GHz).

In this point, we have obtained a balun with wideband characteristic which can transform the impedance 50 to 70 Ω. In next section the optimized sinuous slot antenna connected to the proposed feeding system to validate good field matching and impedance transformation of the balun in wideband frequency.

2.2.4 Realization and Measurement of the Antenna Connected to the Balun

The geometry of the proposed sinuous slot antenna fed by the tapered balun transition connected to a SMA connector is presented in Fig.2.17. The dimensions of the structure are inside a 5.3×5.3×5 cm^3 volume.

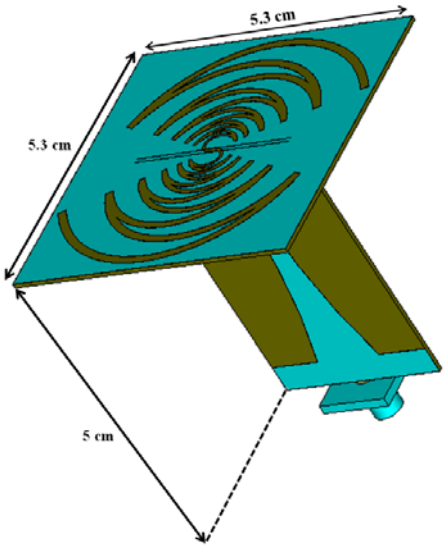

Fig.2.17. The geometry of the UWB sinuous slot antenna.

The simulated and measured return losses of the proposed geometry are presented on Fig.2.18. A good agreement is achieved between measurement and simulation. The measured return loss of the sinuous slot antenna is lower than -10 dB between 3.15 GHz and 10 GHz. The difference between simulation and

measurement is due the difficulty to obtain a perfect alignment of the two sides of the balun printed on the same substrate.

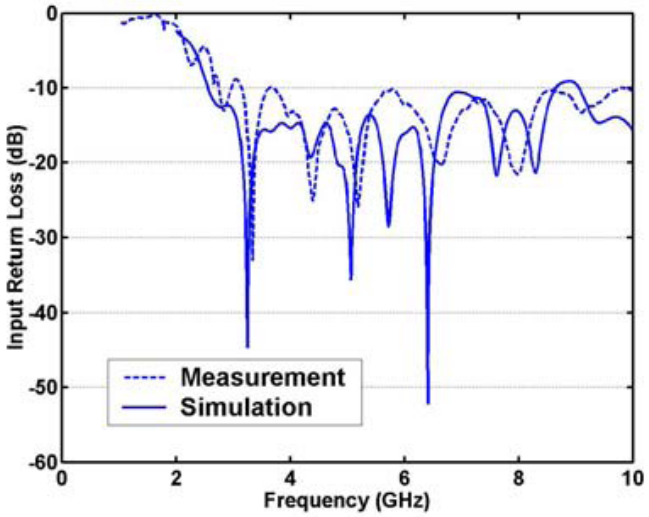

Fig.2.18. Simulated and measured return loss of the proposed geometry of the sinuous slot antenna.

As it was shown, the –10 dB simulated bandwidth for the return loss of the sinuous slot antenna without any balun was 3 GHz to 10 GHz (Fig.2.12). These simulated results have calculated in CST simulator with a discrete port in central region of the antenna. The comparison of the return losses (Fig.2.10 and 2.18, antenna with and without balun) shows that the balun operates well in this wideband frequency to field matching and impedance transformation.

2.2.5 Directive Ultra Wideband Sinuous Slot Antenna

The objective of this part is to increase the radiation performance of previous sinuous antenna in wideband frequency and to verify that the balun can be used in this configuration. To obtain a directive antenna, we have added a limited ground plane to this ultra wideband antenna (Fig.2.19). It is possible to increase the antenna gain without changing the antenna volume by a reflector plane that protect the circuit to be behind the plane.

The size of the ground plane is 5 cm by 5 cm. The influence of the distance between this limited ground plane and the radiating part has investigated and the optimized distance between the limited ground plane and the radiating part has been chosen equal to 3.75 cm. In fact, if the ground plane is closed to the radiating part, the bandwidth of the antenna is limited to less than one octave by images principle. We chose a distance that is closed to a quarter wavelength at the lowest frequency, to use the images

principles, and for the highest frequency the antenna is "far" from the ground plane, so its effect is limited.

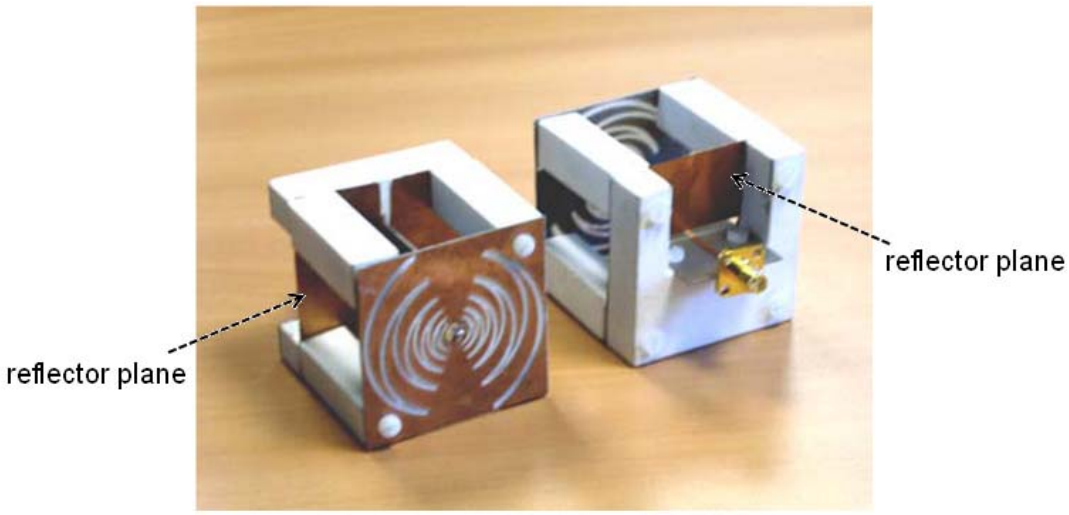

Fig.2.19. Two compact directive UWB slot sinuous antennas with support.

The antenna in Fig.2.19 was fabricated and fixed on a dielectric support (Eccostock-LoK) with low permittivity ($\varepsilon_r = 1.7$). The measured return loss of the UWB sinuous slot antenna is shown in Fig.2.20.

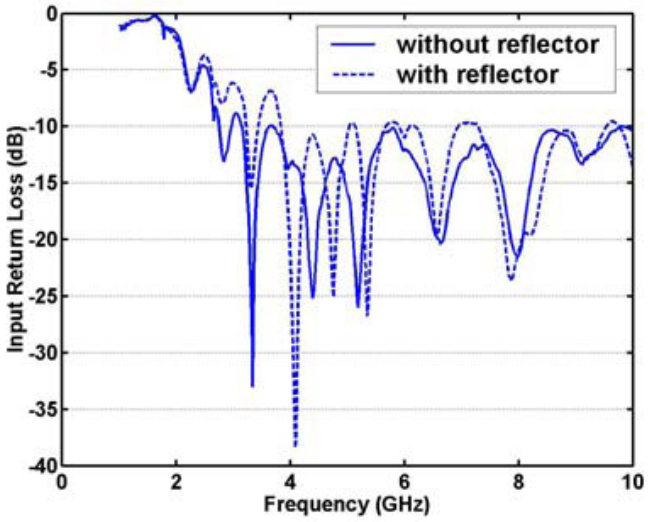

Fig.2.20. Measured Return Loss of the ultra wideband sinuous slot antenna with and without reflector.

The measured bandwidth of the directive antenna is between 3.9 and 9.6 GHz.

This bandwidth is smaller than the one obtained without reflector. It's essentially due to the presence of the ground plane. The gain of the antenna has been calculated with and without reflector (Fig.2.21).

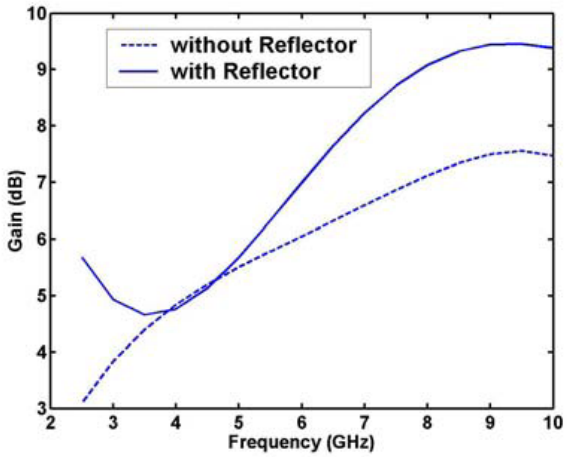

Fig.2.21. Gain of the sinuous slot antenna with and without reflector

- ***Results Interpretation:***

1. The gain is increased with reflector from 4.6 to 9.5 dB between 4 GHz and 9.6 GHz.
2. Between 2.5 and 3.9 GHz the antenna is not matched, so the gain is not significant.
3. The figure shows an important advantage of this antenna radiation: the antenna gain increases significantly in high frequencies (> 5 GHz) by using reflector about 2 dB.
4. At 4 GHz the distance between antenna and ground plane is equal to a half of wavelength, it's the reason of the minimum of gain.

2.2.6 Radiation Pattern of the Antenna

To verify how really radiates the directive sinuous slot antenna, we present the simulated directivity radiation patterns at different frequencies in E and H-planes (Fig.2.23 and 2.24). Also the definition of E-plane (x-z) and H-plane (y-z) is shown in Fig.2.22.

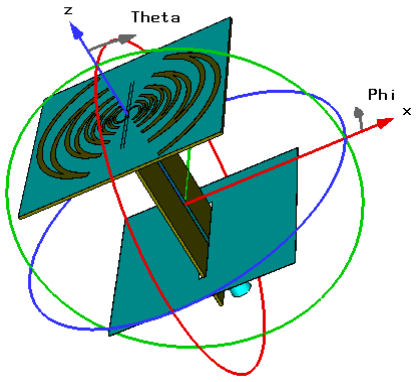

Fig.2.22. Definition of E-Plane (Phi=0°) and H-Plane (Phi=90°).

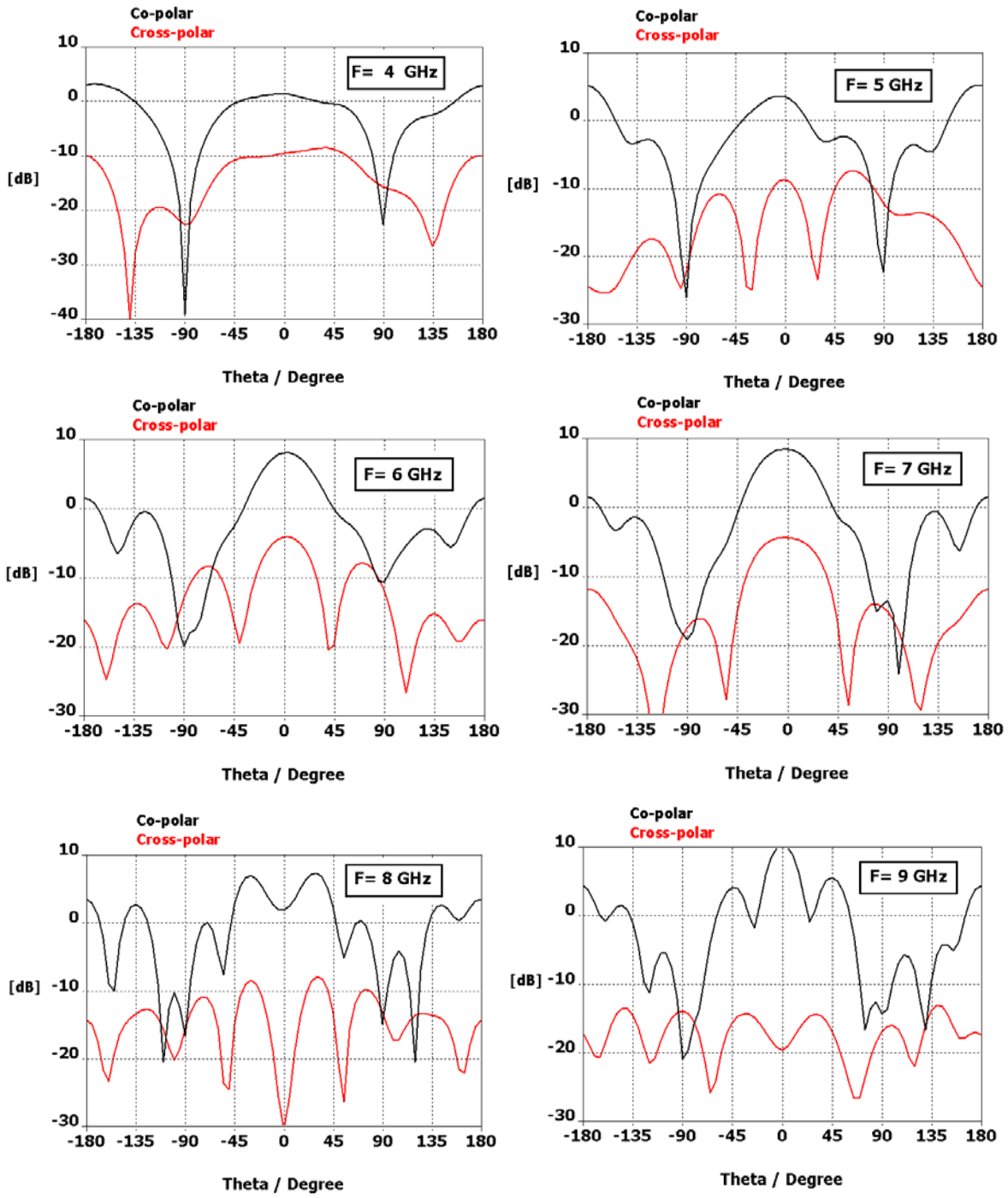

Fig.2.23. Simulated Directivity radiation patterns of the UWB directive sinuous slot antenna for F= 4, 5, 6, 7, 8 and 9 GHz: E-plane (Phi=0°).

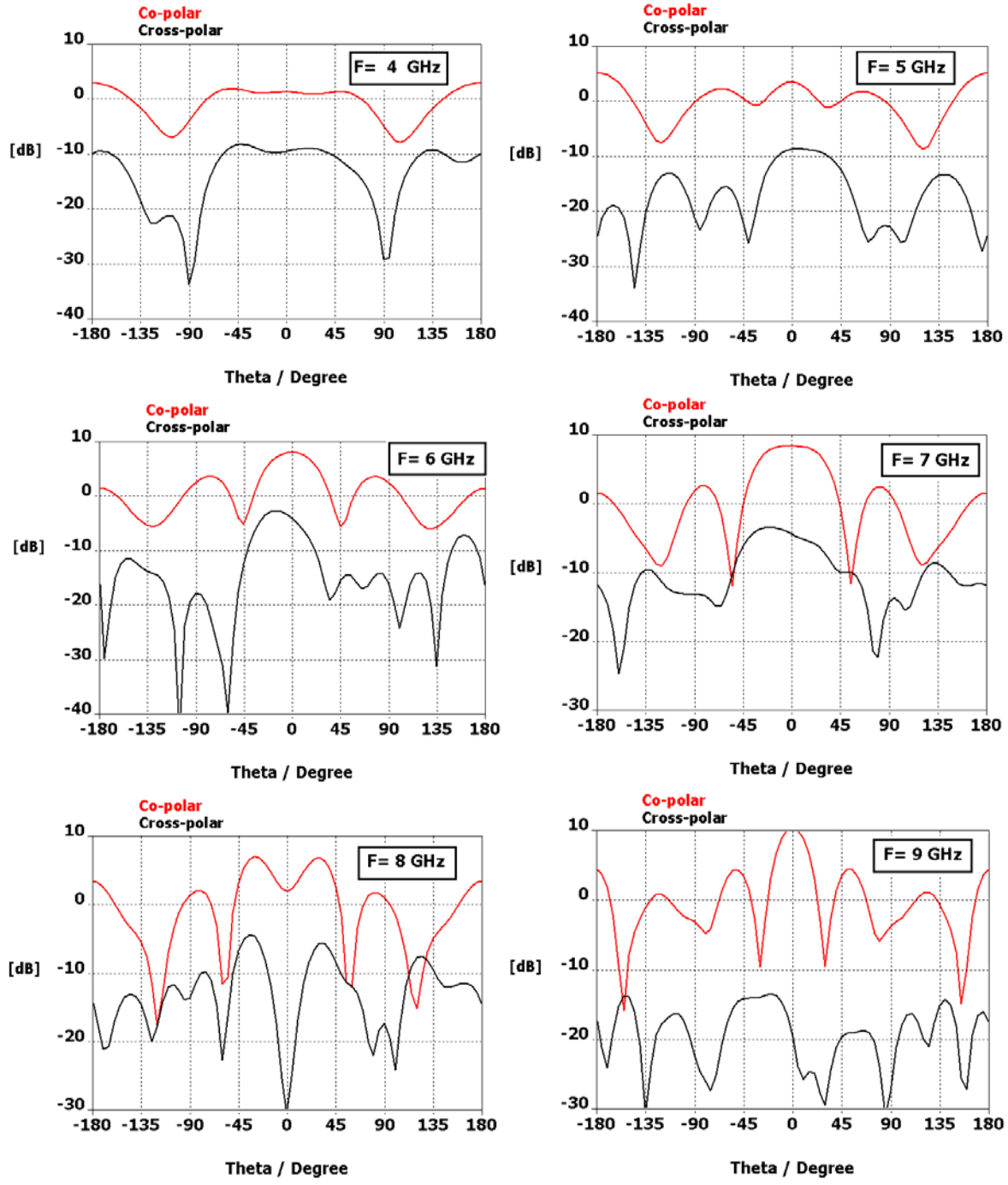

Fig.2.24. Simulated Directivity radiation patterns of the UWB directive sinuous slot antenna for F= 4, 5, 6, 7, 8 and 9 GHz: H- plane (Phi= 90°).

All the radiation patterns present a directive behavior. The balun is well match to the radiating part because almost all the radiation patterns are symmetric. At the lowest frequencies the ground plane is small, so the antenna has a bidirective radiation. Oscillations observed at the highest frequencies are also due to the limited size of the ground plane. At 9 GHz, it's the central part ("S" shape) of the sinuous antenna that radiates, not the sinuous part. The cross polarization level is better than -10 dB approximately in the entire band. Another conclusion is that the balun can be used to feed a directive wideband antenna.

2.3 Conclusion

In this chapter the analysis and optimization of the microstrip-to-balanced stripline balun has been done and a measured bandwidth from 100 MHz to 9.75 GHz has been obtained. The radiation characteristics of an ultra wideband sinuous slot antenna fed by balun have been analyzed and the antenna has a measured bandwidth from 3.15 to 10 GHz for a return loss better than –10 dB. To obtain a directive antenna we have added a ground plane and the effect of the limited ground plane have been studied. The directive antenna has a measured bandwidth from 3.9 to 9.6 GHz for a return loss better than –10 dB. The behavior of radiation patterns and gain has been presented.

Generally, the unidirectional radiation pattern is achieved by employing a ground plane below the radiating element; however, this introduces the risk of degrading characteristics of the antenna. Finally we fabricated a compact directive UWB slot sinuous antenna that is included in a 5 cm^3 volume (approximately) and the gain of the sinuous slot antenna with reflector is increased from 4.6 to 9.5 dB between 4 GHz and 9.6 GHz.

This category of wideband baluns contains two metal layers. This structural nature hardens utilization of this type of balun in dual polarization form for planar antennas (such as sinuous antenna). Also it is usually very difficult to simply integrate these baluns with planar antennas in two dimensional form (for example our voluminous sinuous antenna in this chapter). However the integrated wideband antenna geometries are desired.

In the following chapters we investigate other types of wideband feeding systems to provide balun with integration ability and simple structure in dual polarization modes.

2.4 References

[1] R. Mongia, I. Bahl, and P. Bhartia, *RF and Microwave Coupled-Line Circuits*, Norwood, MA: Artech House, 1999, ch.11.

[2] N. Marchand, "Transmission-Line Conversion transformers", *Electronics*, Vol. 17, December 1944, pp 142-145.

[3] W. K. Roberts, "A new wide-band balun," *Proc. IRE,* vol. 45, pp.1629–1631, Dec. 1957.

[4] H. R. Phelan, "A Wide-Band Parallel-Connected balun," *IEEE Trans. Microwave Theory Tech.*, Vol. MTT-18, May 1970, pp.259-263.

[5] M. Engels and R. H. Jansen, "Design of Integrated Compensated Baluns," *Microwave Optical Tech. Lett.,* vol. 14, no. 2, pp. 75–81, Feb. 1997.

[6] J.S. Sun, G.Y. Chen and Y.D. Chen, "The Wideband Marchand Balun Transition Design," *7th International Symposium on Antennas and Propagation*, pp.796-799, Guilin, China, Oct. 2006.

[7] P. Pramanick and P. Bhartia, "Tapered Microstrip Transmission Line," *IEEE MTT-S Int. Microwave Symp. Dig.,* June 1983, pp. 242-244.

[8] P. Pramanick and P. Bhartia, "A Generalized Theory of Tapered Transmission Line Matching Transformers and Asymmetric Couplers Upporting Non-TEM Modes," *IEEE Trans. Microwave Theory Tech.,* Volume 87, Issue 1, pp. 361 – 364, Jun. 1987.

[9] L. R. Walker and N. Wax, "Non-uniform Transmission Lines and Reflection Coefficients," *J. Appl. Phys.,* vol. 17, pp. 1043-1045, Dec. 1946.

[10] M. Kobayashi and N. Sawada, "Analysis and Synthesis of Tapered Microstrip Transmission Lines," *IEEE Trans. Microwave Theory Tech.*, Vol.40, No.8, pp.1642–1646, Aug. 1992.

[11] G.D. Vendelin, A.M. Pavio, U.L. Rohde, *Microwave Circuit Design Using Linear and Nonlinear Techniques*, New York NY: Wiley & Sons, 1990.

[12] X. Begaud, *Analyse d'Antennes et de Réseaux d'Antennes Large Bande et Bipolarisation par une Méthode d'Eléments Finis de Surface,* Thesis - University of Rennes 1, December 19, 1996.

[13] Ph. Gonnet, A. Sharaiha, C. Terret, A. Skrivervik, "Feeding Networks for Sinuous Antennas," Microwave and Optical Technology Letters, vol. 20, num. 3, pp. 195-200, 1999.

[14] A. Kazemipour, *Contribution à l'étude du couplage entre antennes application à la compatibilité électromagnétique et à la conception d'antennes et de réseaux d'antennes,* Thèses – Ecole nationale supérieure des télécommunications, Décembre 12, 2002.

[15] K. M. Pour-Aghdam, R. Faraji-Dana, J. Rashed-Mohassel, 'The sinuous antenna-A dual polarized feed for reflector-based searching systems,' AEU, vol 59 , pp.392-400, 2005.

[16] M. Vahdani, X. Begaud, "A Directive Ultra Wideband Sinuous Slot Antenna," *European Conference on Antennas and Propagation (EuCAP)*, November 2006.

[17] CST Studio Suite Software, version 2006B and 2008.

Chapter 3
Feeding Systems for Ultra Wideband Dual Polarized Antenna in 3 Dimensional Design

3.1 Introduction

In chapter 2, a wideband sinuous antenna with simple polarization was developed but the objective of this thesis is to arrive to a wideband structure with dual polarization characteristic. In fact that feeding system for sinuous slot antenna was an intermediate idea to obtain a suitable configuration for a dual polarized architecture. However, the two layer geometry of microstrip-to-balanced balun does not bring into existence the chance of having proper dual polarized feeding system for a sinuous antenna. In the other hand this type of balun makes the achievement of dual polarization feeding sinuous antenna impossible. The sinuous antenna is a center-fed structure and two balun with 90° should connect to the antenna structure. This structural problem hardens each proper connection between the two baluns and the dual polarized sinuous antenna.

Undoubtedly which is indicated above is not the only problem. Another problem is that this balun should transform SMA impedance ($50\,\Omega$) to input impedance of dual polarized structure (in this chapter we will see it is about $160\,\Omega$). In chapter 2 we have seen that in order to have an impedance transformation between 50 to 70 Ω, we should have a balun with parallel stripwidth of about 1 mm. When the input impedance increases (to 160 Ω) the balun width should decrease (about 0.15 mm). This is a technical problem and limitation in fabrication and welding.

Therefore, in this chapter we investigate another wideband balun whose characteristic impedance can be controlled by its dimensions (especially for large impedances). In addition, it is desired to have a simple configuration to be designed in dual polarization structures.

Coplanar baluns are good candidates to achieve these advantages and also they give us an excellent conception to arrive to an integrated wideband structure (We will present it in chapter 4). In this chapter we present a new microstrip-to-coplanar stripline balun which operates well in wideband frequency. In next stage, to verify the wideband balun performance in dual polarization, we will employ the balun with sinuous antenna.

3.2 The state of the art of Coplanar Baluns for UWB Antennas

3.2.1 Introduction

In chapter 2, we have presented a wide category of wideband feeding systems. In this section we continue our investigation on the wideband feeding system subject for dual polarized antennas. In recent years, there is an increasing demand to integrate planar antennas into three-dimensional packages as well as designing antennas on multilayer laminates, which pose as a challenge, especially to ultra-wideband (UWB) antenna design.

The main challenge in feeding systems is bandwidth enhancement with the ability of integration with other recent wideband antenna structures. In this field a number of efforts have reported. Among the baluns, planar baluns usually are one of the most desired configurations because of their ease of implementation. The microstrip antenna fed by a coplanar waveguide (CPW) and coplanar stripline (CPS) has the advantages of easy mass production and lower antenna assembling cost.

Moreover, the use of coplanar feeding is more suitable for integration with circuit devices and design of antenna array compared to other exciting feeding structures [1]-[2]. CPW-fed and CPS-fed microstrip antennas have been widely used for various applications because they are compatible with monolithic microwave integrated circuits (MMICs) and active devices. In addition, the bandwidth of CPW-fed and CPS-fed microstrip antennas are larger than these of conventional microstrip antennas [3].

We can find two different balun functions:

- Converting fields between unbalanced circuits and balanced structures: the antenna has balanced structure. Thus, there are two signal components with the same magnitude but with 180-degree phase difference at the feed point of the antenna. Also the SMA connector is an unbalanced circuit.

- Impedance transformer: between SMA ($50\,\Omega$) and antenna input impedance.

Whenever a balanced antenna is used, the issue of how to feed the antenna becomes relevant. Considering that a balanced antenna requires a balanced feed, a balun is needed. If the balanced (symmetrical) antenna is connected to a coaxial transmission line, the transition from the feed line to the balanced antenna is an unbalanced (asymmetrical) driven system. The balun is inserted between the feed line and the antenna in

order to provide a transition between the unbalanced and balanced parts. Thus, the balun produces a symmetrical radiation pattern from the desired antenna.

In some applications, it is necessary to connect the feed terminals on the balanced antennas to an unbalanced coaxial cable that requires not only a balanced-to-unbalanced transformation circuit, but also an impedance match due to the different characteristic impedances of the antenna and the cable.

Traditional feeding techniques include the use of direct feed [4], electromagnetically coupled [5, 6], aperture coupled microstrip line [7]-[9], coaxial probes [10], coplanar waveguides (CPW) and coplanar stripline (CPS) [11-13]. The planar antennas for UWB applications fed by CPW and CPS can be easily integrated with the multilayer circuit devices.

In this chapter we have used a wideband microstrip-to-coplanar stripline that offers the advantages of easy integration with wideband planar antenna, compact size eliminating the need for via-hole.

In next section we introduce the analytical formulae of coplanar waveguide structure as a brief introduction of coplanar stripline baluns study.

To aid the balun design and characterization, the electromagnetic simulation program CST Studio Suite Version 2008, was used to predict the performance of the balun structure. The measured results of the constructed balun structure were then compared to the simulated results.

3.2.2 Coplanar Waveguide (CPW)

Recent reported efforts show the popularity of coplanar waveguide balun antenna feeding in wideband domain. They operate well in wideband frequency to field matching and impedance transforming and also they can be printed on a single side of the substrate. References [12]-[13] offer the CPW as wideband balun for quasi-monopole antenna architectures. This is due to the configuration, the ability of providing the omnidirection pattern and broad bandwidth required for UWB communications and also the easy integration with microwave circuits [14]-[15]. Because both the center and the ground conductors of a CPW lie in the same plane, active devices can be easily placed in series or shunt across the transmission line without requiring a via hole geometry.

Fig.3.1 to Fig.3.3 show several variations of coplanar waveguide architectures. The SMA connectors are employed between the center conductor (strip with formal positive potential) and two outer conductors as a ground plane (with the same formal negative potential). The references [16]-[17] claim that the mode of propagation along a coplanar line can be considered quasi TEM.

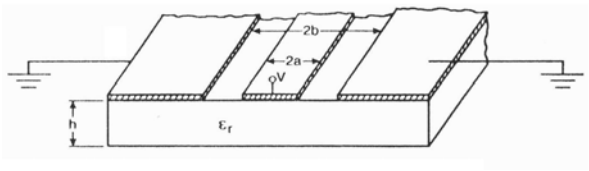

Fig.3.1. Coplanar waveguide on a finite thickness dielectric substrate.

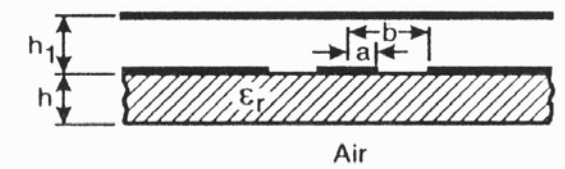

Fig.3.2. Cross section of a coplanar waveguide with upper shielding [18].

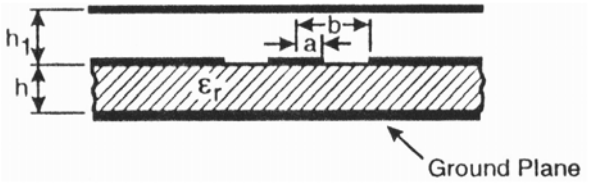

Fig.3.3. Cross section of a conductor-backed coplanar waveguide with upper shielding [18].

3.2.2.1 Analytical Formulae [18]

Wen in 1969 has proposed a typical CPW structure which the fundamental idea is to design variations of coplanar waveguide configurations (Fig.3.1). Wen has assumed that the signals propagate in TEM mode on metal conductors and also he has considered that conductors lie on substrates with finite thickness (h) and relative permittivity (ε_r). The authors [18] have presented a closed form analytical formula for the characteristic impedance of a typical CPW: (assumption: thickness of the metal $t \approx 0$)

$$Z_0 = \frac{30\pi}{\sqrt{\varepsilon_{re}}} \frac{K(k')}{K(k)} \tag{1}$$

$$\varepsilon_{re} = 1 + \frac{\varepsilon_r - 1}{2} \frac{K(k')K(k_1)}{K(k)K(k_1')} \tag{2}$$

where

$k = a/b$; $\quad k' = \sqrt{1-k^2}$

$k_1 = \sinh(\pi a/2h)/\sinh(\pi b/2h)$; $\quad k_1' = \sqrt{1-k_1^2}$

ε_{re} : relative effective permittivity,

K : is the complete elliptic integral of the first kind and $K(k)/K(k')$ is given with an acceptable approximate expression: [18]

$$\frac{K(k)}{K(k')} = \frac{K(k)}{K'(k)} = \begin{cases} \frac{1}{\pi}\ln\left(2\frac{1+\sqrt{k}}{1-\sqrt{k}}\right), & 0.5 \le k^2 \le 1 \\ \frac{\pi}{\ln\left(2\frac{1+\sqrt{k'}}{1-\sqrt{k'}}\right)}, & 0 \le k^2 \le 0.5 \end{cases} \tag{3}$$

The effective dielectric constant and characteristic impedance of CPW are shown in Fig.4 for our substrate (DiClad880) $\varepsilon_r = 2.17$ which is employed in several layouts in next sections.

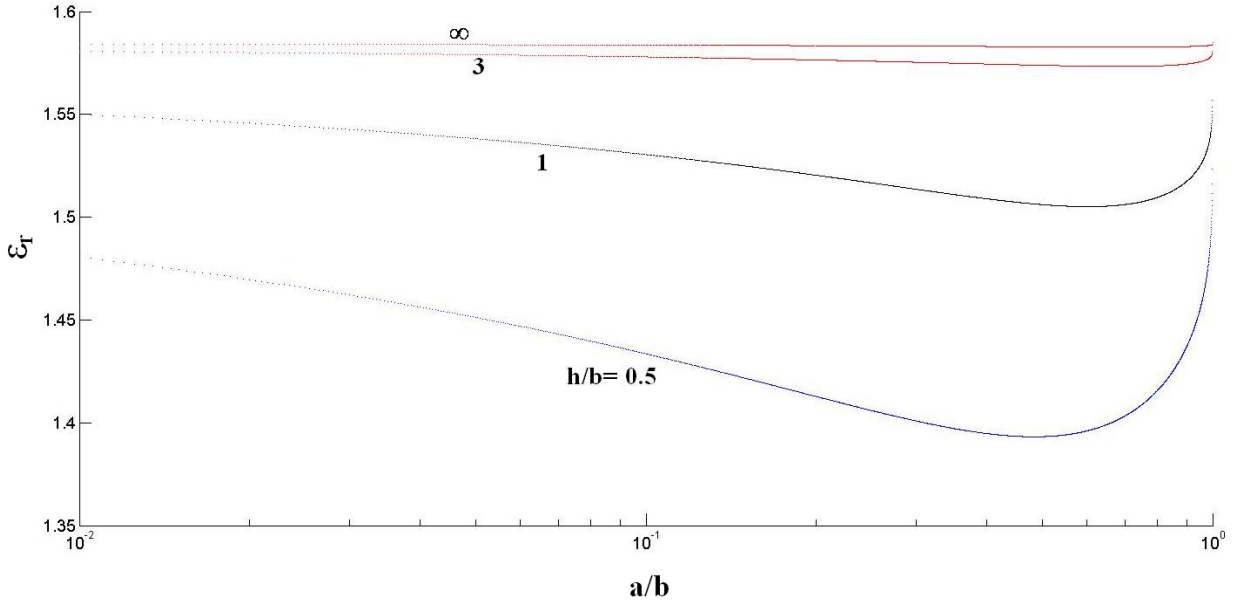

(a)

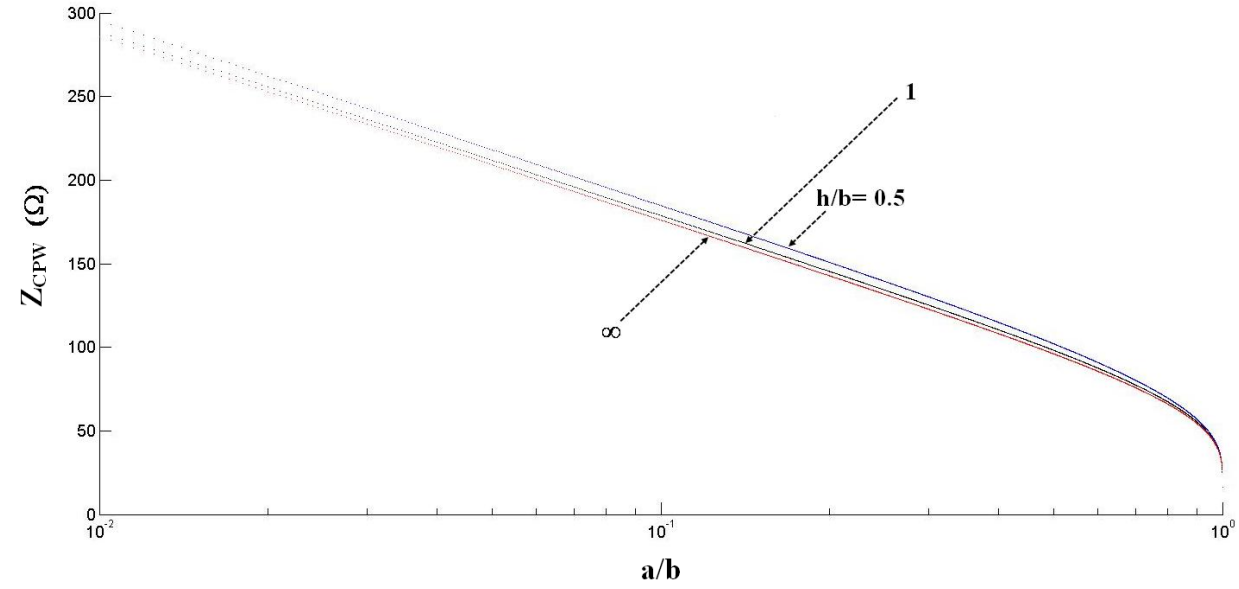

(b)

Fig.3.4. (a) Relative effective permittivity, and (b) characteristic impedance of CPW as a function of aspect ratio a/b for values of h/b, $\varepsilon_r = 2.17$.

3.2.2.2 Conclusion

In this section the standard topology of a coplanar waveguide (CPW) transition was introduced which addresses the requirements for wideband fed application.

Although coplanar waveguide has several advantages, but it is not our main choice to be used in the antenna structure considering that a balun configuration with two balanced strips to feed the antenna is desired. It is considered a brief study of CPW characteristic because CPW geometry is the basis conception of another topology which is coplanar stripline.

In the following section, we will show that coplanar stripline (CPS) has the same advantages of a coplanar waveguide (CPW). Moreover, as it is indicated, our objective in this chapter is to arrive to a balun configuration with high characteristic impedances to feed antenna structures with bigger impedances. This is the important difference between CPW and CPS. Also, CPS is a balanced transmission line which is useful for balanced architecture such as symmetrical antenna. Thus in the next section we will introduce and develop a coplanar stripline balun as a wideband antenna feeding system.

3.2.3 Microstrip-to-Coplanar Stripline Balun

3.2.3.1 Analysis and Optimization of a UWB Microstrip-to-CPS Balun

In this section, we have studied a high performance balun in wideband frequency with a new configuration which was presented for the first time by Y.-H. Suh and K. Chang in 2001 [20]. They have employed a connection between microstrip line to coplanar stripline that helped them achieve a wideband balanced planar transmission line with several structural advantages:

- Ability of integrated connection with other circuits
- Compact and low-profile structure
- Elimination of the need for a via-hole (which leads to technical problem and parasitic effects)

Considering these advantages, the microstrip-to-CPS balun is a good candidate for our objective in this chapter to feed a dual polarized sinuous antenna in three dimensional form and it is desired for next chapter (4) to obtain an integrated configuration to feed sinuous and bow-tie antennas.

From 1995 several microstrip-to-CPS transitions have been reported. First of all, we can mention a coplanar stripline reported by Wen-Hua Tu and Kai Chang [20]. They have presented a new uniplanar transition for circuit and antenna feeding applications with a 3-dB back-to-back insertion loss bandwidth of 59%. Later in 1997, Y. Qian and T. Itoh have introduced a broadband uniplanar microstrip-to-CPS transition with a 3-dB back-to-back insertion loss bandwidth of 68%.

Although these configurations had a broadband bandwidth, a balun structure with wider frequency band is desired. In these reported efforts there is another inconvenience. These structures are not suitable for our impedance transformation because they are all built on high dielectric substrates. In next section, we show how using substrate with high permittivity lead to a low characteristic impedance for the coplanar stripline. However as it is indicated in the introduction of this chapter, we investigate a wideband balun to feed our dual polarized antennas with high input impedance.

Recently Wen-Hua Tu and Kai Chang have presented (as it is considered above) a microstrip-to-CPS transitions on low dielectric-constant substrate ($\varepsilon_r = 2.33$). With this low permittivity they have arrived to a coplanar with 184 Ω with a 3-dB back-to back insertion loss bandwidth from 1.3 to 13.3 GHz [19]. This impedance transformation (50 to 184 Ω) with wideband frequency is very interesting to feed our antenna structure in this and next chapter.

The proposed transition consists of a microstrip matching transformer and a radial stub with a coplanar stripline. We use this concept to design our wideband balun for two types of wideband antennas, Sinuous and quasi-Bow-Tie. As it was indicated, in this chapter we present a 3-dimensional form sinuous antenna and in next chapter, our objective will be the an integrated antenna structure.

3.2.3.1.1 Impedance and Field Matching ([19] and [21])

Fig.3.5 shows the configurations of the proposed transitions. To design a transition, field matching and impedance transforming are required. The reason of using radial stub can be explained by the need of 90° field rotation. As it is shown in Fig.3.5, we have three parts in this microstrip-to-stripline structure:

- Microstrip line
- Coplanar stripline
- Transition part containing radial stub

The electric field in the microstrip line part is parallel to the y-axis between the strip and ground plane and the electric field in the CPS is parallel to the x-axis between two striplines. Therefore, we need an element to rotate 90° in transition part for wideband frequencies. This element is a quarter wavelength radial stub and the resonant frequency of the radial stub depends on its radius and angle θ. At resonance frequency, the radial stub equals a short circuit. Thus, RF signals continue between the coplanar stripline and the microstrip ground plane.

In the next section, we will study the analytical formulae of the characteristics of coplanar stripline to obtain the desired characteristic impedance of the line.

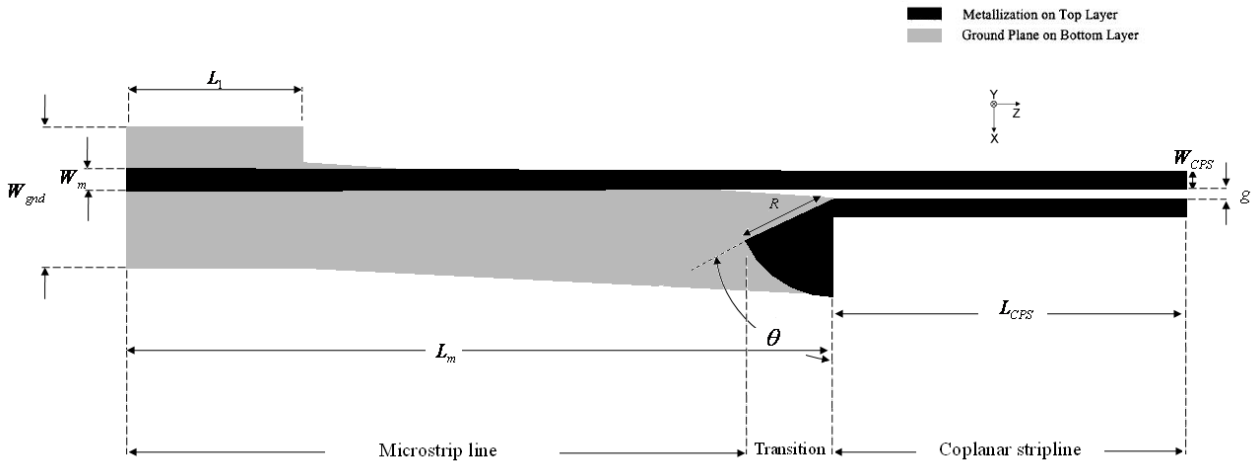

Fig.3.5. The microstrip-to-CPS configuration [19].

3.2.3.1.2 Analytical formulae of a Coplanar Stripline (CPS)

The topology of the coplanar stripline is complementary to that of the coplanar waveguide:

$$Z_{CPW}\, Z_{CPS} = \frac{\eta_0^{\,2}}{4\varepsilon_{re}} \tag{4}$$

It consists of two metallic strips placed on the same side of a dielectric (Fig.3.6).

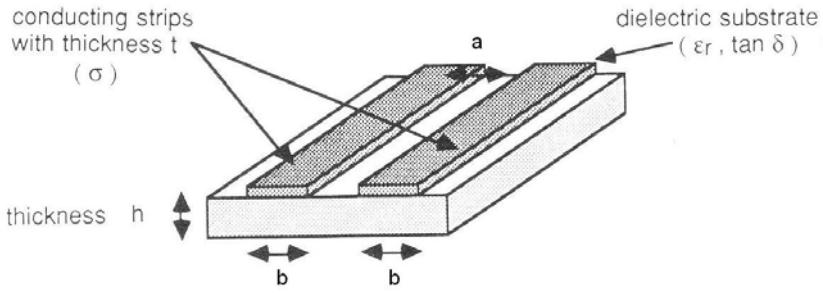

Fig.3.6. Coplanar stripline.

As for the coplanar waveguide, an approach based on the quasi-TEM approximation can be used. This leads to the following expression of characteristic impedance Z_0 (assuming that the thickness t of the conductor is negligible):

$$Z_0 = \frac{120\pi}{\sqrt{\varepsilon_{re}}} \frac{K(k)}{K(k')} \tag{5}$$

where the function $K(k)$ and $K'(k)$ are as defined in section 3.2.2.1. The expression of the relative effective permittivity ε_{re} is equivalent to that of the coplanar waveguide in which W is now the width of the ribbon and S is the space between the strips. Fig.3.7 shows the characteristic impedance of CPS (equation 5) as a function of aspect ratio a/b for values of h/b and $\varepsilon_r = 2.17$.

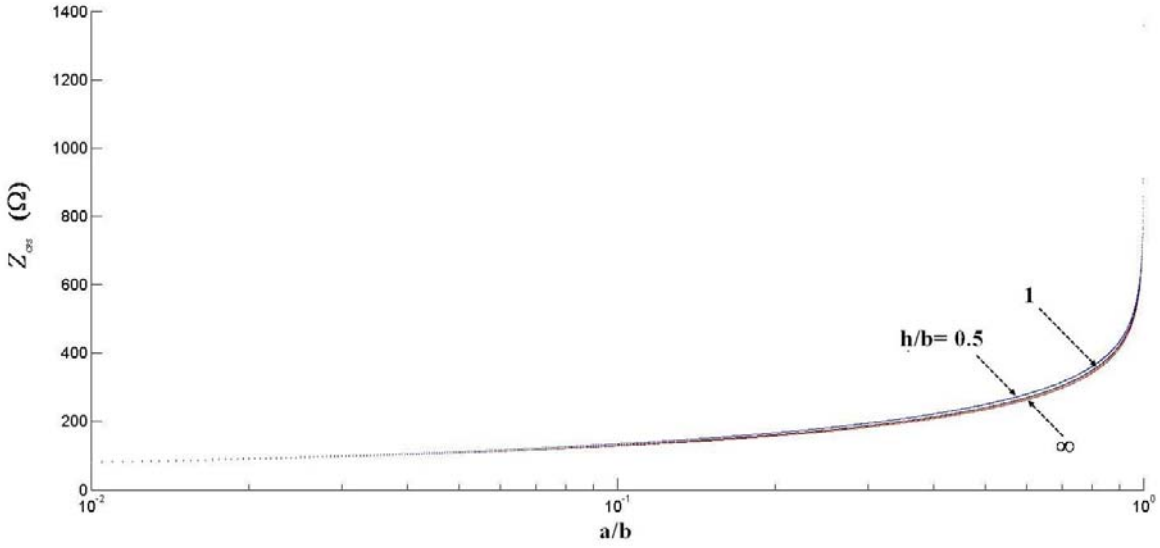

Fig.3.7. Characteristic impedance of CPS as a function of aspect ratio a/b for values of h/b, $\varepsilon_r = 2.17$.

3.2.3.1.3 Parametric Studies of Microstrip-to-CPS Balun

In order to study balun function, it is desired to have a parametric study of the three parts of the balun containing the microstrip length and width, dimensions and the angle of the radial stub, and the configuration of the coplanar stripline part (Fig.3.5). First of all, the input impedance of the antenna connected to balun must be selected. In the other hand at the beginning we should know the input impedance of the block connected to the balun at the end of the CPS. In order to find it, the input impedance of the desired antenna must be determined. In next section, before the optimizing of the balun we will calculate the input impedance of the dual polarized sinuous antenna. But in this section we suppose $Z_{in-antenna} = Z_{out-CPS} = 174\ \Omega$. Also the center frequency of the transition is designed at 9 GHz. The dimensions of the radial stub are $R \approx 5.5$ mm, and $\theta = 65^{\circ}$, where $R = \lambda_g / 4$, and λ_g is the guided wavelength at 9 GHz.

The impedance-matching transformer is optimized for impedance matching between SMA ($50\ \Omega$) and CPS ($174\ \Omega$). Since the characteristic impedance of the CPS (Z_{CPS}) is higher than $50\ \Omega$ of the microstrip line (Z_m), a linear tapered matching transformer in part of microstrip line is used.

The optimized dimensions of the transitions are listed in Table.1. The transition is built on DiClad 880 substrate with a thickness of $h = 0.762$ mm and a relative dielectric constant $\varepsilon_r = 2.17$. To simulate the balun structure by the CST software, a load with R=$174\ \Omega$ between the coplanar striplines is considered.

Table I. DIMENSIONS OF THE TRANSITIONS (Units: Millimeters)

L_1	L_m	L_{CPS}	W_m	W_{gnd}	W_{CPS}	g	θ	R	h	ε_r
10	40	20	1.3	8	1	0.6	65°	5.5	0.762	2.17

Fig.8 shows the simulation results of return loss for the microstrip-to-CPS. It shows a return loss better than -10 dB from 2 to 14.9 GHz.

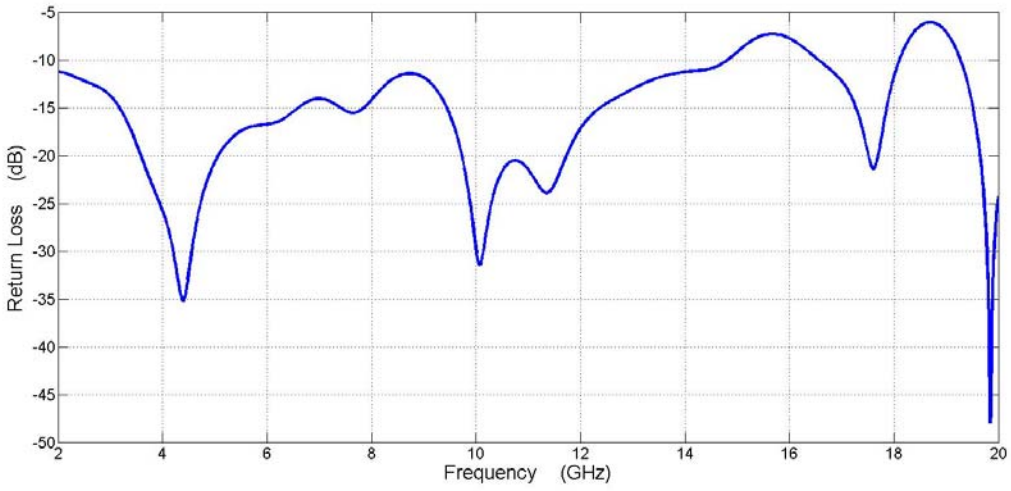

(a)

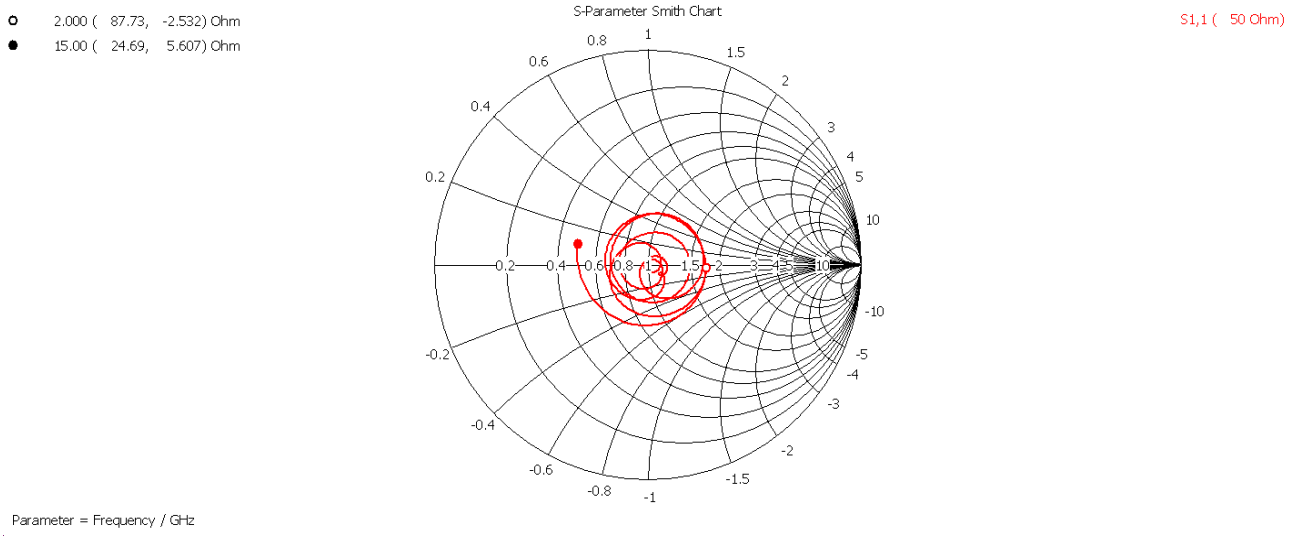

(b)

Fig.3.8. Simulated (a) return loss and (b) input impedance (normalized at 50 Ω).

3.2.3.1.4 Transition Performance

The balun designers are commonly interested in the study of back-to-back configurations because of several reasons: They can easily fabricate the balun and measure the return loss and insertion loss without the necessity of loads. Also it is possible to validate the convenience of the 180-degree phase difference.

The structure of back-to-back CPS-to-microstrip transition is illustrated in Fig.3.9. The circuit simulation was accomplished with the aid of CST software. The CPS characteristic impedance is selected $174\,\Omega$ (as it is mentioned above), as was calculated by Equation (5) and simulated with CST. The gap between CPS strips is 0.6 mm and the strip width is 1 mm with CPS optimized length of $L_{CPS} = 14$ mm. The microstrip line's width and length are 1.3 mm and 40 mm, respectively. Since the transition with radial stub can provide a wider bandwidth, the angles of the radial stub should also be investigated and optimized and the rotation angle, ϕ, is optimized at 25°. Transitions with the radial stubs of different angles are compared. This suggests that the transition with a 65° radial stub can provide a wider bandwidth.

Also DiClad 880 is used as the substrate with a dielectric constant 2.17 and the thickness of 0.762 mm.

Fig.3.9. Balun back-to-back configuration.

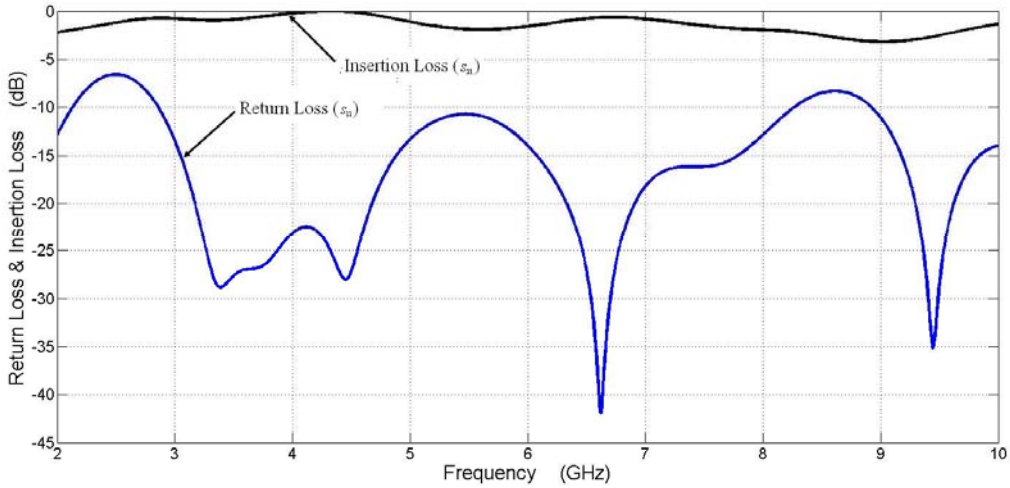

(a)

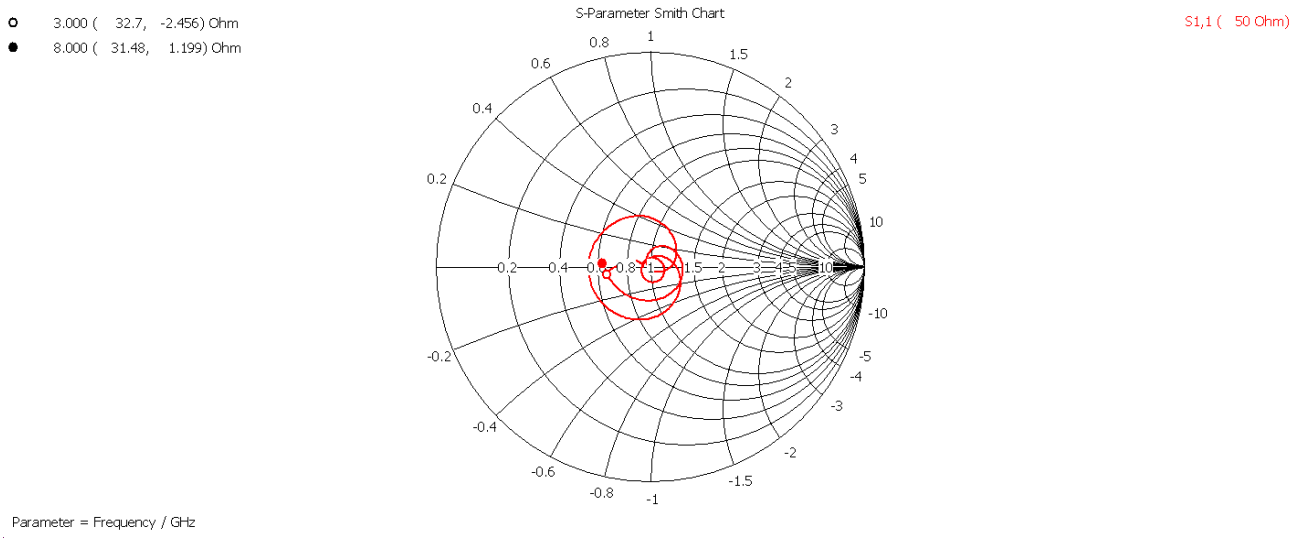

(b)

Fig.3.10. Simulated (a) return loss and (b) input impedance (normalized at 50 Ω).

Fig.3.10. shows that the optimal transition microstrip-to-CPS has a return loss better than -10 dB from 2.8 to 8.3 GHz. Also as it is shown in Fig.3.10, the 2-dB back-to-back insertion loss is achieved from 2 to 8 GHz. Also for the convenience of the 180-degree phase difference function of the balun, the back-to-back transition configuration with the microstrip-line is studied. We placed two probes on the center of two coplanar striplines and we calculated the magnetic fields phase difference ($\vec{H}_1 - \vec{H}_2$) of these two points (Fig.3.11).

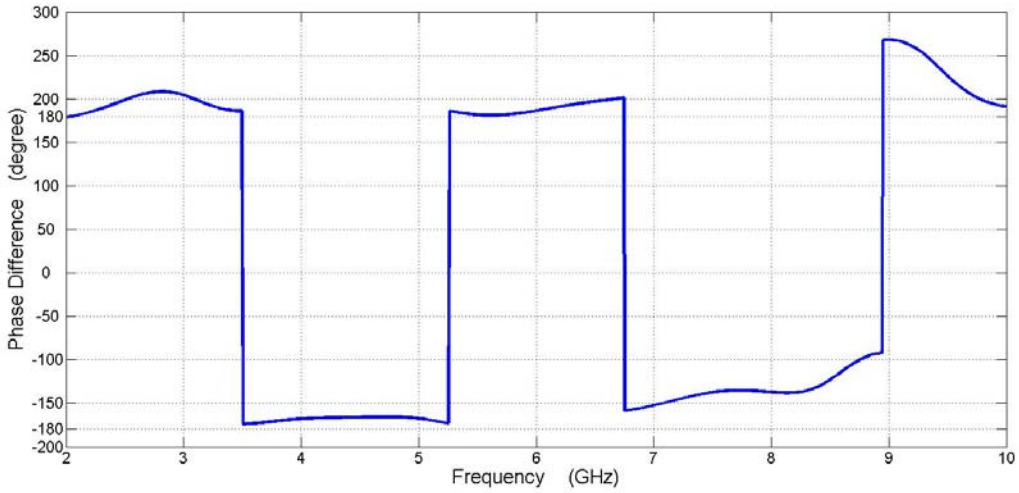

Fig.3.11. Phase difference of the central points of coplanar striplines in Fig.3.9.

Fig.3.11 validates a 180-degree phase difference between these two points from 2 to 7.5 GHz with a 20 degree tolerance and thus it is shown that the balun operates properly in field matching in this wideband frequency.

3.2.4 Conclusion

In this section a microstrip-to-coplanar stripline balun topology is developed which provides wideband transition characteristics, requires much less real estate and gives an on-axis input/output geometry. In addition, this transition operates without the need of via-holes in contrast to the transition given in [9] where grounding pins were used to ensure a good electric short at the end of the slotline radial stub. Because of these properties, this transition can easily be used as feeds for balanced antennas in UWB applications.

In summary, the design procedure for balun is summarized as following:

1) Given the output impedance of the balun (input impedance of the desired UWB antenna), calculate the dimensions of coplanar stripline.

2) Given the transition center frequency and substrate parameters, calculate the radius of the radial stub. The radius is $\lambda_g / 4$, where λ_g is the guided wavelength at the center frequency.

3) Given the dimensions of CPS and required transition bandwidth, calculate and determine the characteristic impedance of the matching transformer and its dimension.

4) With the initial parameters obtained from above, using, for example, the simulator CST Studio Suite to take all parasitic effects into account and optimize the design.

Finally a simple and low cost CPS-to-microstrip transition was designed and simulated. Performance results for the balun geometry and back-to-back configuration show return losses better than 10 dB from 2 to 14.9 and 2.8 to 8.3 GHz respectively. Also this wideband transition has many applications in feeding printed dipole antennas, and in integration with MIC or MMIC passive or active devices.

To validate the simulation results presented in this section, the simulated return loss and insertion loss of a developed compact microstrip-to-CPS balun are compared with measured results (in section 3.3).

3.3 New Developed Compact Microstrip-to-CPS Balun: Design and Fabrication of a Bended Microstrip-to-CPS Balun

3.3.1 Introduction

In order to reduce the antenna size a 90° bended balun is developed. Indeed for realizing a reduced layout size of a wideband antenna, a 90° bended balun is proposed with saving the balun impedance and field matching. By 90° bending of balun, the length of the whole geometry of antenna can be reduced to less than half of the original length, thereby saving the overall layout area of the antenna.

In this study, a 90° bended balun is proposed and designed to feed our balanced antenna. It is a recent approach to reduce the size while maintaining the balun performance.

3.3.2 Modeling of 90° Bended Microstrip-to-CPS and Transition Design

In this section, a modified compact ultra-wideband transition structure between a microstrip line and a CPS is proposed. This transition design is the developed form of the standard microstrip-to-CPS introduced in section 3.2 (Fig.3.5) and can be applicable to reduce the layout size of the antenna with feeding system structure.

As it is shown in Fig.3.12, the strip and the ground is turned 90 degrees in microstrip region. The rotation is performed in a specific point that inhibits any interference in the balun performance. With the help of simulation, the position of this point to bend the strip and ground is found and thus this discontinuity in balun geometry doesn't lead to impedance mismatch or any changes in balun characteristics. w_m, w_{cps}, w_1, w_2 are width of microstrip in region A-A', with of coplanar striplines in region C-C' and the width of two strips in Region B-B' and w_g is the variant width of the ground plane in region B-B'.

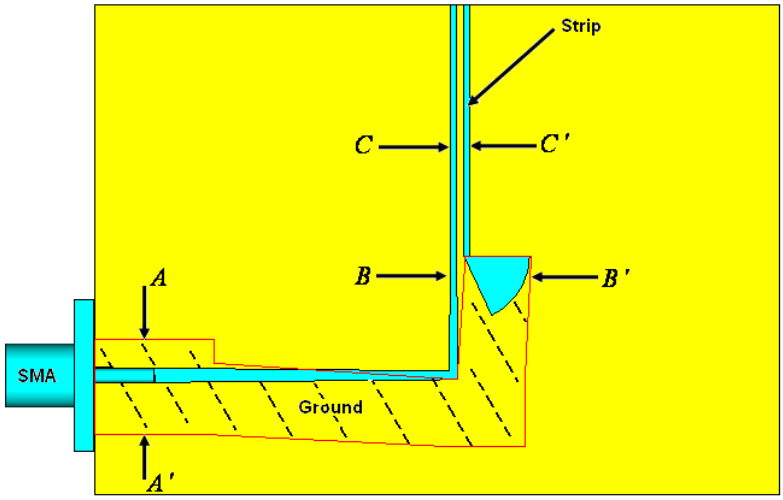

Fig.3.12. Proposed structure of the developed microstrip-to-CPS transition.

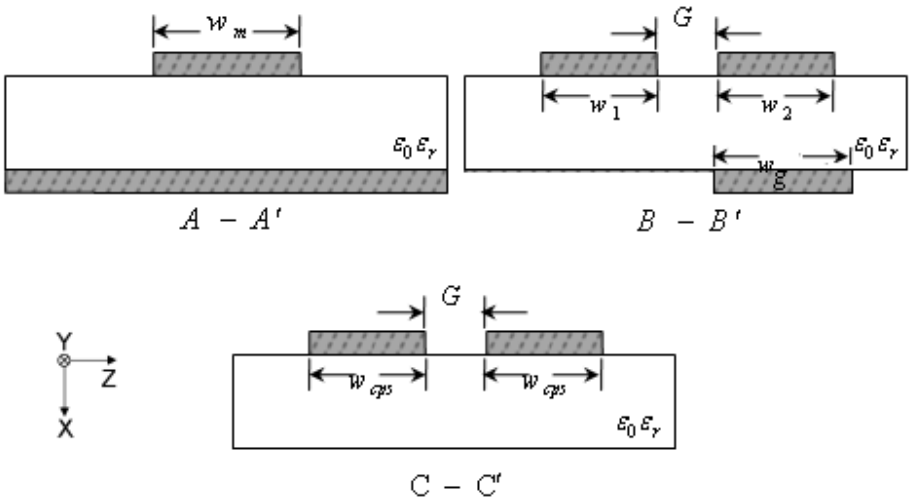

Fig.3.13. side view of each balun section.

Fig.3.12 shows the proposed structure of the microstrip-to-CPS transition. Also Fig.3.13 presents a side view of each part of the balun with its parameters.

We want to explain how the electric field continues along the balun to perform our desired field matching and impedance transformation. As Fig.3.13 shows there are three parts in this balun configuration:

- *Microstrip line (A-A'):* the electric fields are parallel to the x-axis between the strip and ground plane.

- *Coplanar stripline (C-C'):* the electric fields are parallel to the z-axis across two striplines.

- *Transition (B-B'):* the electric fields gradually rotate 90° from the microstrip line to coplanar striplines because of the presence of radial stub.

Fig.3.14 shows the electric field distribution along the three mentioned parts. The transition part contains a strip with a lateral ground plane. The reference [21] claims that by using the radial stub and gradually shaping of the ground plane between sections B-B' and C-C', the electric field rotates 90° in wideband frequency and thus at the CPS part we observe the balanced electric field. Therefore this microstrip-to-CPS configuration can obtain our desired field matching.

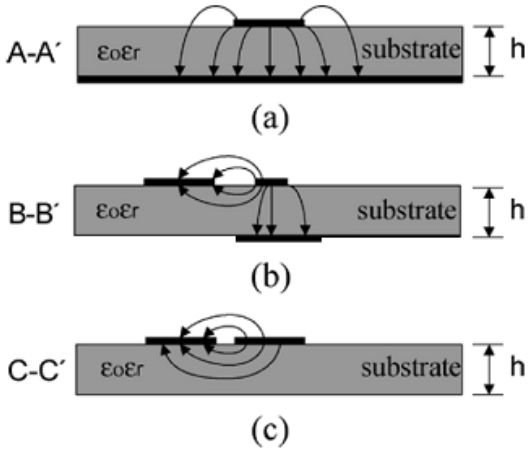

Fig.3.14. Cross-sectional view of the electric distributions: (a) microstrip line, (b) transition, and (c) coplanar striplines [21].

Another desired characteristic of this balun structure is the good impedance transformation between the SMA connector and the antenna feed point. Therefore our balun should prepare a good impedance transition between its input point (microstrip line) and output point (coplanar stripline).

The design and fabrication of the balun was performed on DiClad 880 with relative dielectric constant of 2.17 and thickness of 0.762 mm.

Analytical formulation of the characteristic impedance of the microstrip line shows that the stripwidth of 1.3 mm has characteristic impedance of $50\,\Omega$. The impedance characteristic of the CPS should be considered equal to input antenna impedance (in this study it is supposed equal to $145\,\Omega$).

Therefore, we defined $Z_{CPS} = Z_{in-antenna} = 145\ \Omega$ and then we achieve to $w_{cps} = 0.52461$ mm and $G = 0.6$ mm. For calculation of the characteristic impedance of CPS, the analytical formula (Equation (5)) were used and 3-D EM simulations were performed with the CST Microwave Studio. To achieve wideband impedance matching between these transmission lines, the impedance of the transition is linearly tapered.

To study the characteristic impedance of the transition region (B-B'), it has two major parameters of conductors: strip width and the ground-shaped. The strip transition is designed by linear connection between the microstrip width (w_m) and CPS width (w_{CPS}) to optimally match between A-A' and B-B'. In B-B', the strip is formed gradually as a trapezoid. Also the ground plane is modeled as shown in Fig.3.12 to achieve a better impedance match between microstrip and coplanar stripline parts. The microstrip impedance characteristic is 50 Ohms and the CPS impedance characteristic is 145 Ohms. On the other hand, the ground plane width becomes smaller (toward CPS) to result in higher characteristic impedance [21]. Therefore, the characteristic impedance of the transition at this point becomes very close to that of the CPS.

- **Why a microstrip-to-CPS structure has wideband characteristics?**

Fig.3.12 illustrates the configurations of the proposed transitions. We have claimed in our manuscript this transition can operate well in field matching and impedance transforming between the SMA connector and the antenna structure. Fig.3.12 shows that the balun have three parts: microstrip line (A-A$^{'}$), coplanar stripline (C-C$^{'}$) and transition part (B-B$^{'}$) [19]. It is clear the wideband characteristics of microstrip line and CPS structures. Now we want to explain how the transition part can provide a wideband characteristic to field matching between two other parts.

To achieve a transition function in middle region of the balun, a radial stub has been employed. The radial stub has three properties:

A. **Field Rotation:** The Radial stub is in common use in both hybrid and monolithic microstrip circuits and can be used for the field rotation. Fig.3.13 shows the three cross-sectional views of the electric-field distributions at three locations. The electric field in the microstrip line part is parallel to the x-axis between the strip and ground plane and the electric field in the CPS is parallel to the z-axis between two striplines. Therefore, we need an element to rotate 90° in transition part (B-B$^{'}$). This element is a radial stub.

B. **Virtual Short Function:** The resonance frequency of the radial stub depends on its radius and angle θ. At resonance frequency, the radial stub equals a short circuit, thus the radial stub introduces the virtual short near the edge of the mode and regions at the center frequency. Since the virtual short is equal potential with the ground plane, some fields of the microstrip line couple to the edge of the virtual short, and the transition mode is formed. After the ground plane is removed, the CPS mode is obtained.

C. **Wideband Characteristics::** The dimensions of the radial stub has been considered $R \approx 5.5$ mm, and $\theta = 65^{\circ}$ in chapter 3, where $R = \lambda_g / 4$, and λ_g is the guided wavelength at 9 GHz. In fact the radial stub has been considered and optimized as a quarter –wavelength rectangular open stub.

   When a constant impedance levels in wideband frequency are required, the behavior of the conventional stub (like quarter-wavelength rectangular stub) degrades as a result of the excitation of higher order modes. The Radial stub on the contrary provides an almost constant impedance level at a well specified insertion point in a wide frequency band [22]. Therefore, the radial stub can provide a wider bandwidth due to the wide-band virtual short characteristic and the smoother field rotation by the radial stub in the coupling region.

Therefore this microstrip-to-CPS configuration can obtain our desired field matching in wideband frequency.

3.3.3 Balun Performance

To perform a suitable structure for the measurement and to calculate balun return loss and insertion loss, it is necessary to design and fabricate an optimized configuration. The configuration of a 90° bended microstrip-to-CPS is illustrated in Fig.3.15. Characteristic impedance of the CPS is 160 Ohms and the microstrip feed line has the input impedance of 50 Ohms. The microstrip-to-CPS transition was designed with the design guidelines in section 3.2. The dimension of the structure is as follows in table.2. The return loss of the transition is simulated by using the CST 2008 and it is shown in Fig.3.16.

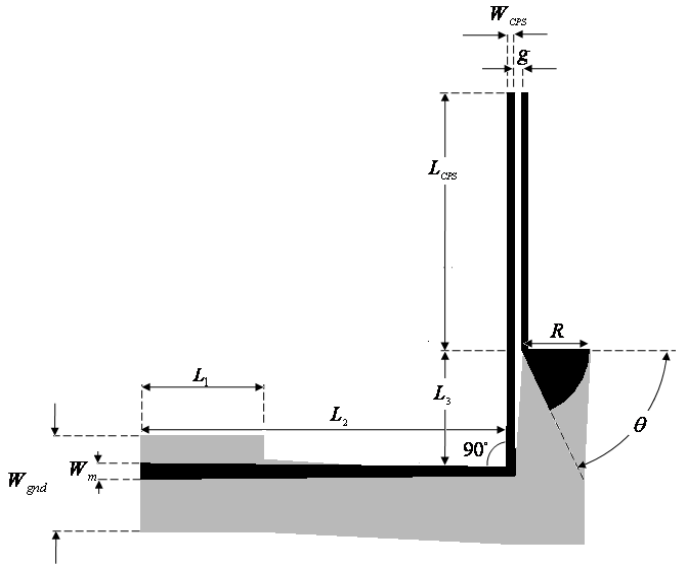

Fig.3.15. 90° bended balun parameters.

Table II. DIMENSIONS OF THE TRANSITIONS (Unit : Millimeters)

L_1	L_2	L_3	L_{CPS}	W_{gnd}	W_m	W_{CPS}	g	R	θ
10	27.46	11.45	20	8	1.3	1	0.6	5.5	65°

The CPS-to-microstrip transition exhibits wideband performance from 2.5 GHz to 18.4 GHz with a return loss of better than 10 dB.

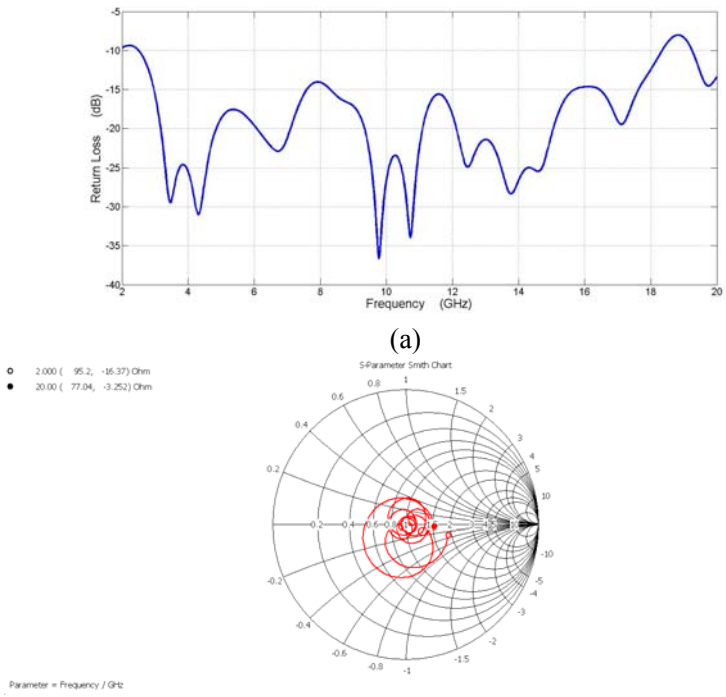

(a)

(b)

Fig.3.16. Simulated (a) return loss and (b) input impedance (normalized at 50 Ω).

3.3.3.1 Balun Performance in back-to-back configuration

The configuration of back-to-back is illustrated in Fig.3.17. As it is mentioned above, characteristic impedance of the CPS is 160 Ohms and the microstrip feed line has the input impedance of 50 Ohms. The structural parameters of the back-to-back transition are the same with balun geometry (Table.II) and this structure is fabricated with these parameters. The top and bottom views of the fabricated transition are shown in Fig.3.18. The return loss and insertion loss of the back-to-back transition are simulated using the CST 2008.

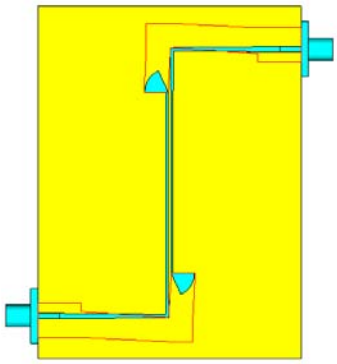

Fig.3.17. Back-to-back configuration of the balun.

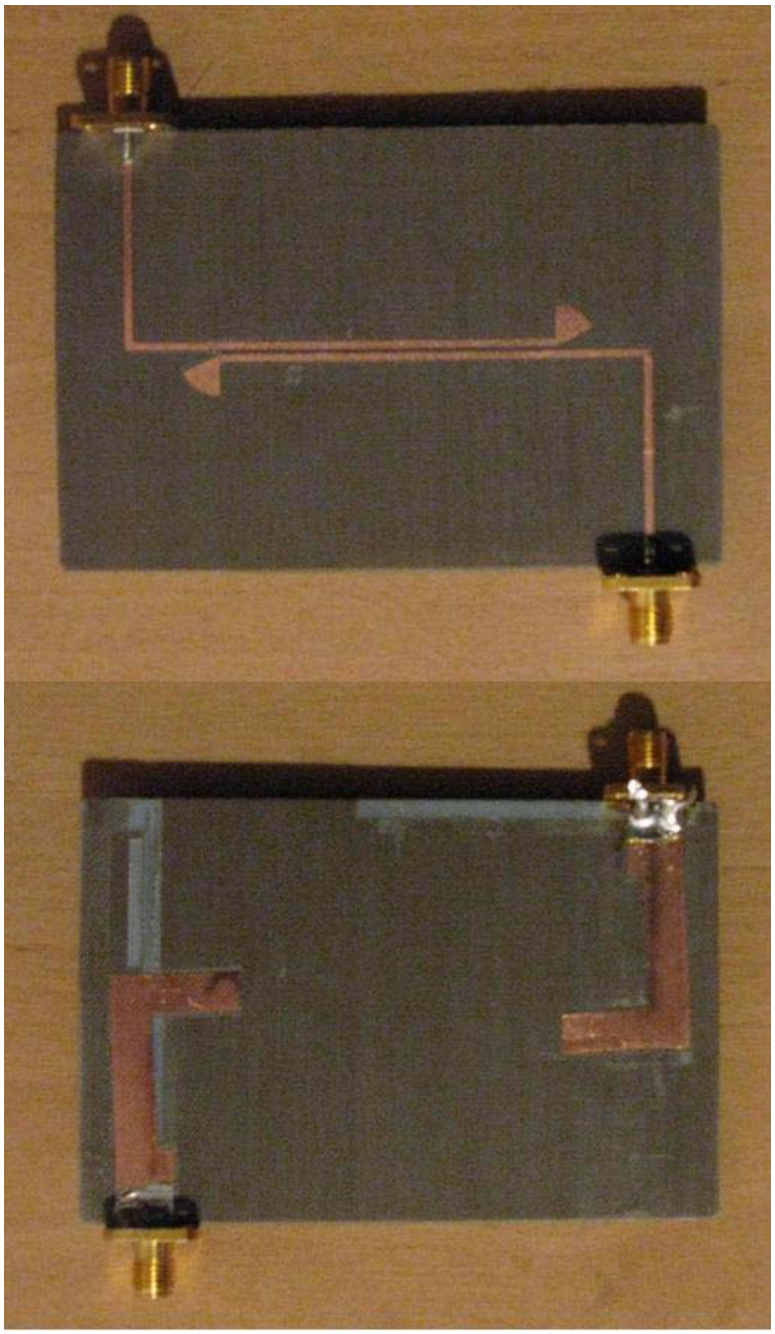

Fig.3.18. Fabrication of the back-to-back configuration.

The measurement and simulation results of the back-to-back configuration of the CPS-to-microstrip transition are presented in Fig.3.19. The CPS-to-microstrip transition exhibits wideband performance from 3 GHz to 10 GHz with an insertion loss of less than 3 dB and a return loss of better than 10 dB for the back-to-back transition. Insertion losses are measured in back to back configuration, so in use (connected to antenna) the balun have a half of these insertion losses.

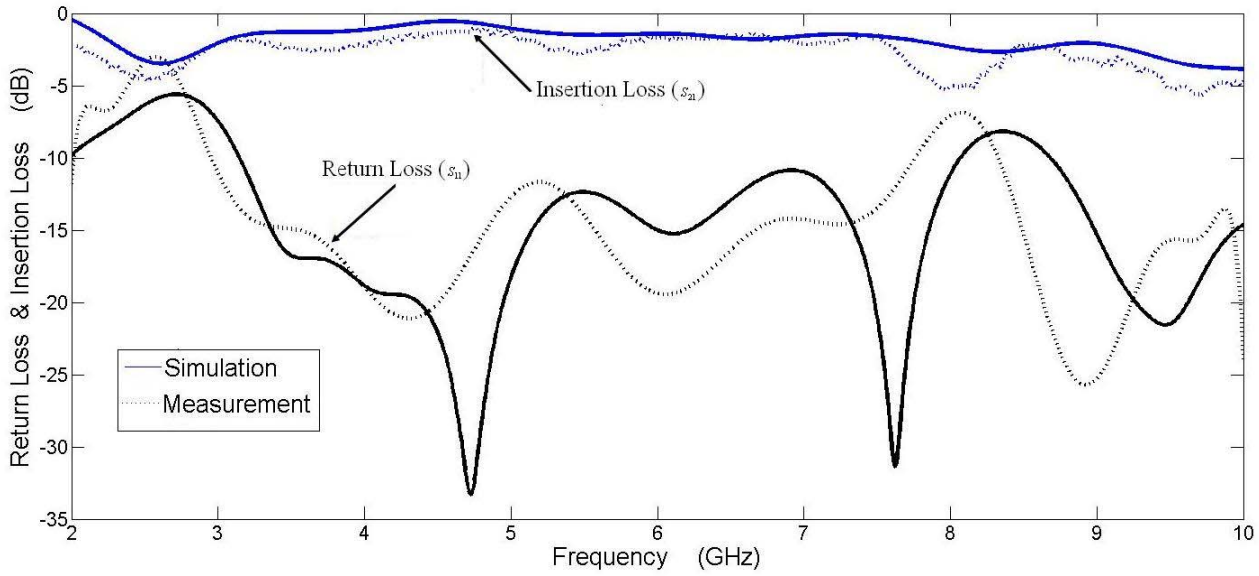

Fig.3.19. Measured and simulated (a) return loss and (b) input impedance (normalized at 50 Ω).

As we had performed for classic microstrip-to-CPS in section 3.2, for the convenience of the 180-degree phase difference function of the balun, the back-to-back transition configuration with the microstrip-line is studied. We have simulated the back-to-back geometry and placed two probes on the center of two coplanar striplines and we calculated the magnetic fields phase difference ($\vec{H}_1 - \vec{H}_2$) of the these two points.

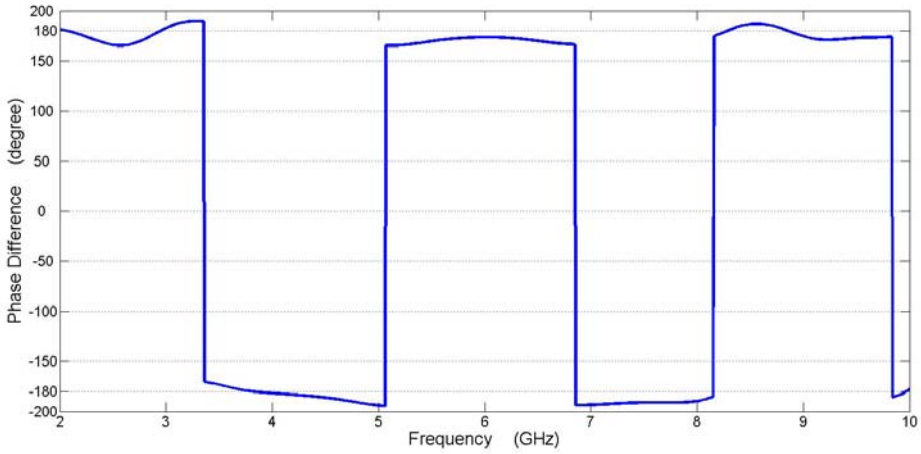

Fig.3.20. Phase difference of the central points of coplanar striplines shown in Fig.3.17.

Fig.3.20 validates a 180-degree phase difference between these two points from 2 to 10 GHz with a 10 degree tolerance and thus it shows that the balun operates properly in field matching in its whole wideband frequency.

The simulated results shows the surface current distribution for f= 3, 4, 5, 6 and 7 GHz of the bended microstrip-to-CPS balun (Fig.3.21) that the balun is fed by one of the SMA (the left port).

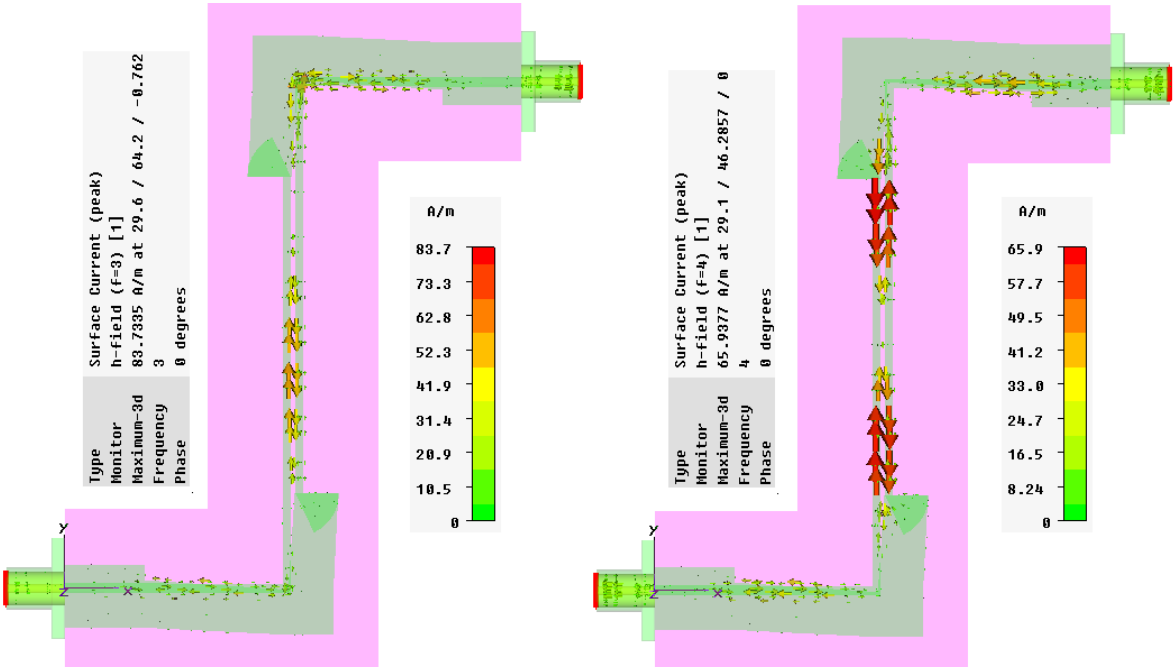

Fig.3.21. Surface Current distribution at 3, 4, 5, 6 and 7 GHz of the bended microstrip-to-CPS balun.

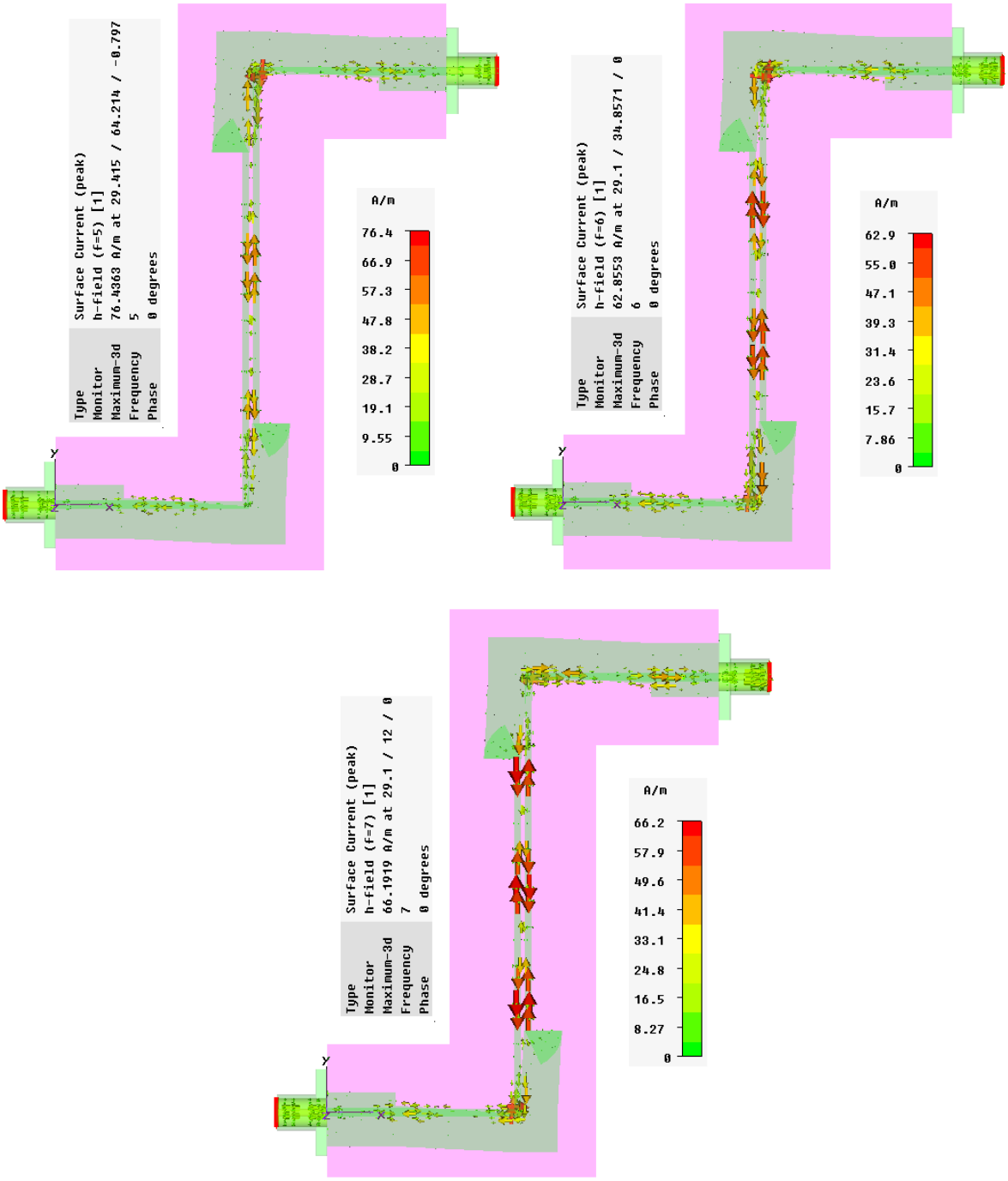

Fig.3.21. (continued) Surface Current distribution at 3, 4, 5, 6 and 7 GHz of the bended microstrip-to-CPS balun.

- ***Interpretation of the results:***

1. The distributions of surface current on CPS regions (coplanar stripline) are symmetrical for the balun frequency bandwidth.
2. The current distributions show the balun operates well in field matching between the coaxial transmission line (unbalanced current distribution) and a balanced striplines. Figure.20.bis illustrates the CPS balun can provide the two symmetrical feed points at the end of balance striplines. So these balanced lines are suitable for feeding balanced antennas such sinuous or bow-tie.

3.3.4 Conclusion

In this section a wideband compact balun (microstrip-to-coplanar stripline) is studied which is applicable as a balanced antenna feeding in UWB systems. This wideband transition design consists of three parts: Microstrip line, transition and coplanar stripline. The design idea comes from a microstrip-to-CPS geometry which was proposed by Y-H Suh and K. Chang [19]. In the past, the microstrip line and the coplanar waveguide (CPW) were the two preferred transmission structures for realizing MIC's but the CPS has more advantages than conventional microstrip line which are explained in this chapter. Also CPS baluns has all the advantages of coplanar waveguide balun.

This bended microstrip fed CPS does not require any bonding wire and reduces the layout size and thus its application extends in compact wideband systems. This balun demonstrated a 3dB insertion loss (in back to back configuration) for the frequency range of 3 GHz to 10 GHz and the return loss better 10 dB for the frequency range of 3 GHz to 10 GHz. Finally, the balun with 180-degree phase deference function (converting signals between an unbalanced structure and a balanced circuit structure) in the desired frequency bandwidth is validated.

In next section, two bended microstrip-to-CPS will be employed to feed a dual polarized sinuous antenna to verify the balun performance in ultra wideband frequency.

3.4 Dual Polarized Sinuous Antenna Design

3.4.1 Introduction

In chapter 2, a wideband feeding system is employed to feed a simple polarized sinuous antenna. Now we want to present a three dimensional developed structure to feed a dual polarized sinuous antenna. In this chapter we investigate a dual polarized sinuous antenna structure to achieve a dual polarized characteristic with a good operation in wideband frequency.

3.4.2 Optimization of a Microstrip Sinuous Antenna

The geometry of the microstrip sinuous antenna is shown in Fig.3.22 where each arm of sinuous antenna is limited in an area defined by α_0. As it is indicated in chapter 2, it is done by rotating a single zigzag line clockwise and counterclockwise α_0 degrees about the origin and for a single polarized antenna there are only two arms. The feeding region is constructed by two strips as it is shown in Fig.3.22. To design an optimized microstrip sinuous configuration, we have considered a wideband frequency between 2 and 10 GHz for antenna. It means f_L=2 GHz and f_H=10 GHz. In the other hand, the frequency bandwidth of sinuous antenna configuration has been used by below equation [23]:

$$R_{ex}.\alpha > \lambda_B/2 \quad (6)$$

$$R_{in} < 0.1\ \lambda_H \quad (7)$$

Thus, we arrive to α=135° with R_{in}=3 mm and R_{ex}=32.3 mm in optimization procedure. The antenna geometry is optimized to obtain the best impedance matching. The antenna geometry parameters are the same as proposed in chapter 2 except the parameter g which is equal to 0.6 mm. (It should be mentioned again that our structure is a microstrip sinuous antenna and not a slot sinuous.)

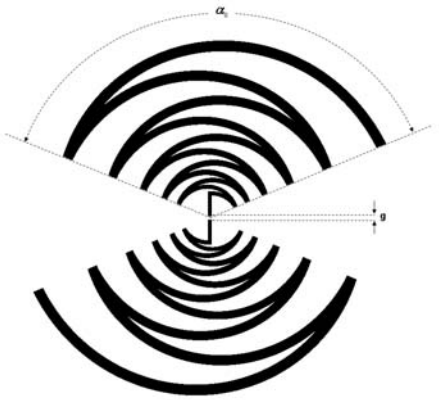

Fig.3.22. Microstrip Sinuous antenna geometry.

For the simulation of the antenna structure, it is considered a delta gap voltage source (discrete port in CST Studio suite) between two strips in antenna center. The simulated results of the return loss are illustrated in Fig.3.23. As it is shown, a 10 dB return loss bandwidth from 2.2 GHz to 8.5 GHz is obtained. The return loss is normalized by R=160 Ohms and it means that the input impedance is considered close to R=160 Ω in the antenna frequency bandwidth.

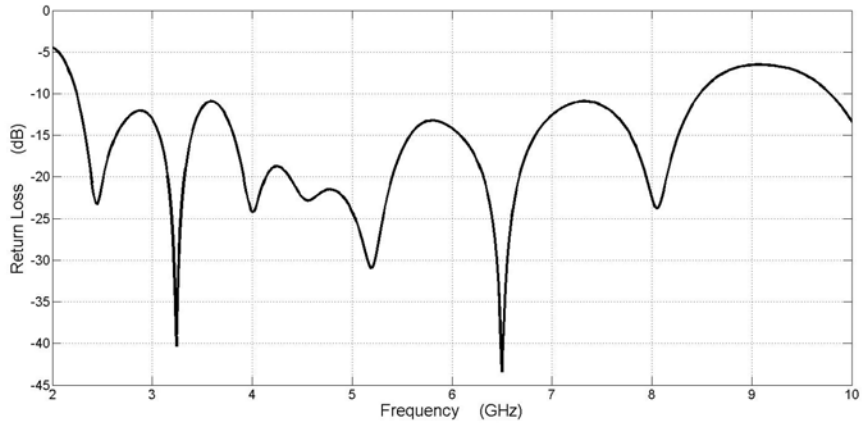

(a)

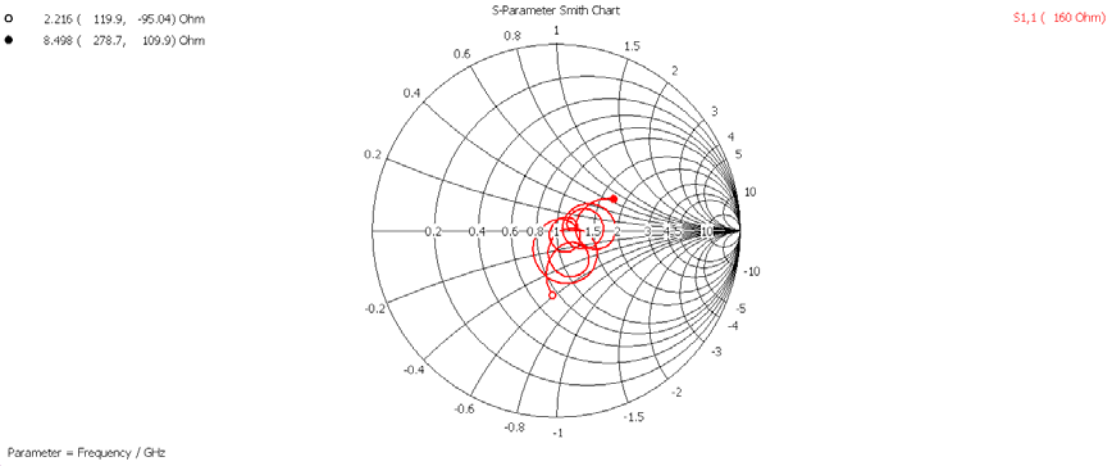

(b)

Fig.3.23. Simulated (a) return loss and (b) input impedance (normalized at 50 Ω).

Therefore in the next step, we will connect our developed balun to this sinuous structure to verify the wideband feeding system performance.

3.4.3 Implementation of the Balun on the Sinuous Antenna in Dual Polarized Configuration (3-Dimensional Design)

3.4.3.1 Modeling of Balun-Sinuous Antenna Connection: Single Polarization

To minimize the coupling between antenna and balun planes especially in antenna's central region, a voluminous design with antenna and balun planes orthogonal to each other is proposed. Fig.3.24 shows this connection between antenna and balun. Also in Fig.3.25 illustrates the fabrication of the 3-D configuration of the antenna.

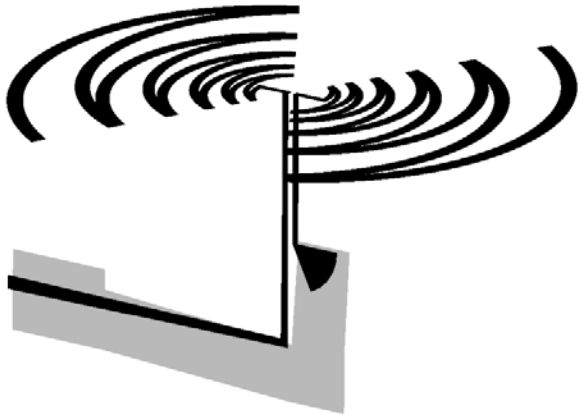

Fig.3.24. Sinuous antenna connected to the balun geometry in first form.

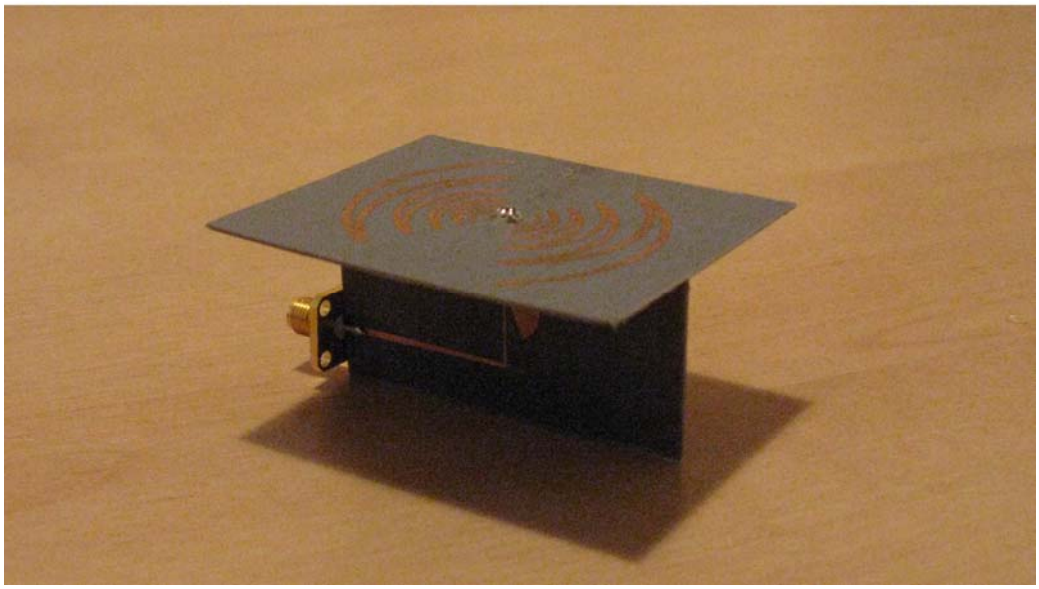

Fig.3.25. Fabrication of the 3-D configuration of single polarized sinuous antenna.

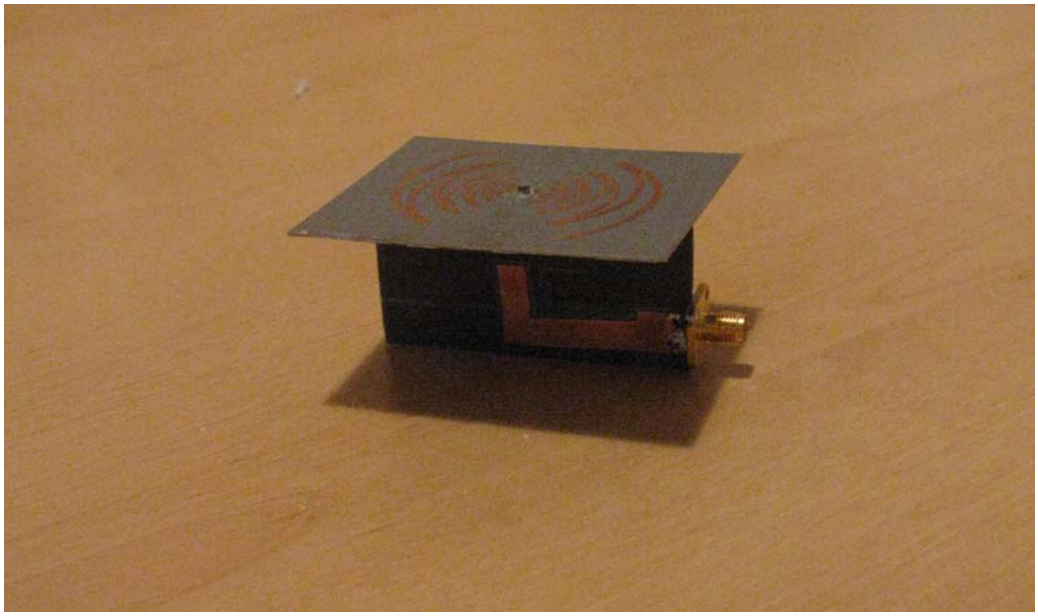

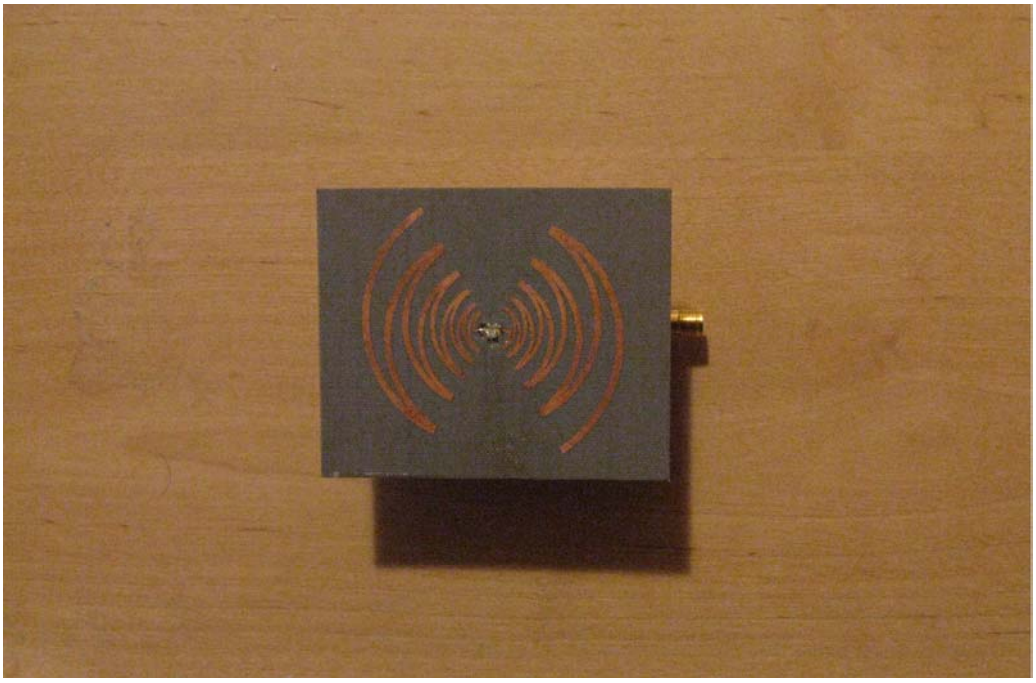

Fig.3.25. (continue) Fabrication of the 3-D configuration of single polarized sinuous antenna.

Simulated results of this CPS-fed sinuous antenna are performed. The antenna and balun are fabricated on DiClad 880 substrate (ε_r=2.17, h=0.762 mm). In addition, the microstrip part of the balun has connected to a 50 Ω SMA connector. Fig.3.6 shows the simulated results of the return loss normalized at 50 Ω.

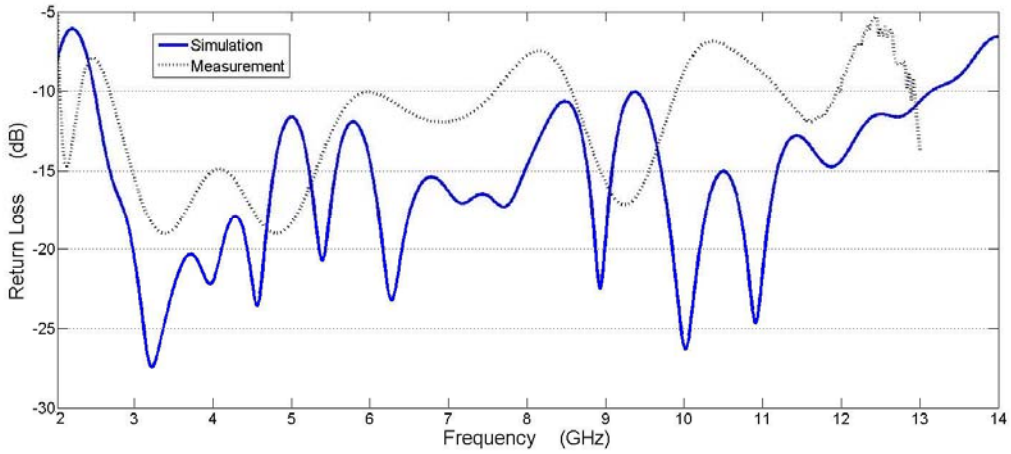

(a)

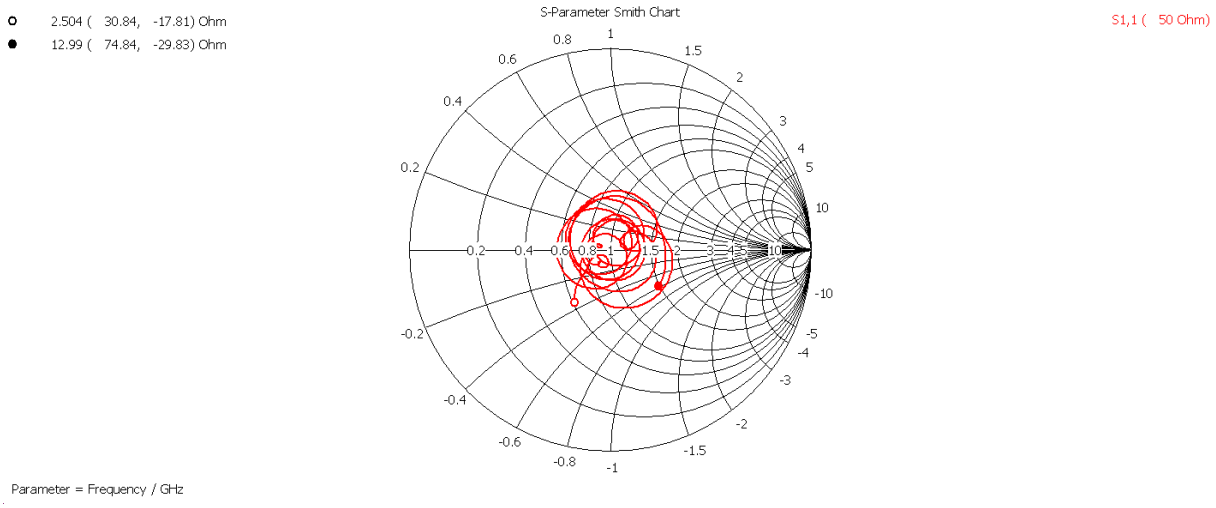

(b)

Fig.3.26. (a) Measured and simulated return loss and (b) simulated input impedance (normalized at 50 Ω).

Fig.25 illustrates that the antenna has achieved a measured 10 dB bandwidth of 2.68 to 7.6 GHz. The comparison between measured and simulation return losses shows:

- An approximate agreement between 2.7 to 7.6 GHz.
- Although for f > 7.6 GHz there are level differences between measurement and simulation return losses, measurement curve pursues the simulation curve up to 10 GHz.

- It seems that the welding between the balun and antenna in central region causes the differences between the return loss in high frequency. In fact the gap between the stripline is so tiny (g=0.6 mm) and the welding in this region changes the CPS part in high frequency.
- The problems of welding in connection region leads toward the integrated structure without the necessity of any welding.

The radiation patterns (antenna directivity) are simulated at frequencies of 3, 4, 5, 6, and 7 GHz in E- and H-plane (Fig.3.27 to 3.29). The definition of E-plane (x-z) and H-plane (y-z) is shown in Fig.3.27.

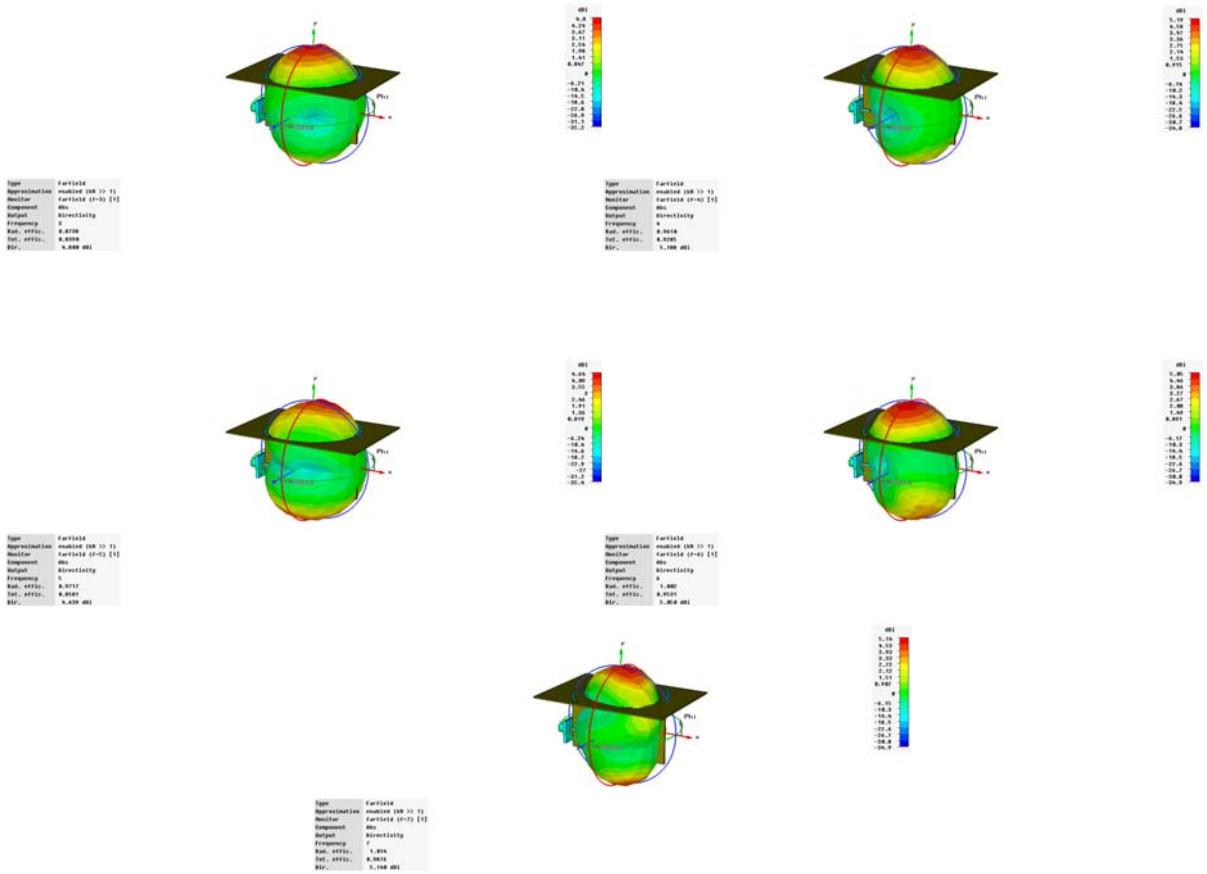

Fig.3.27.Directivity radiation patterns at 3, 4, 5, 6, and 7 GHz of the sinuous antenna geometry.

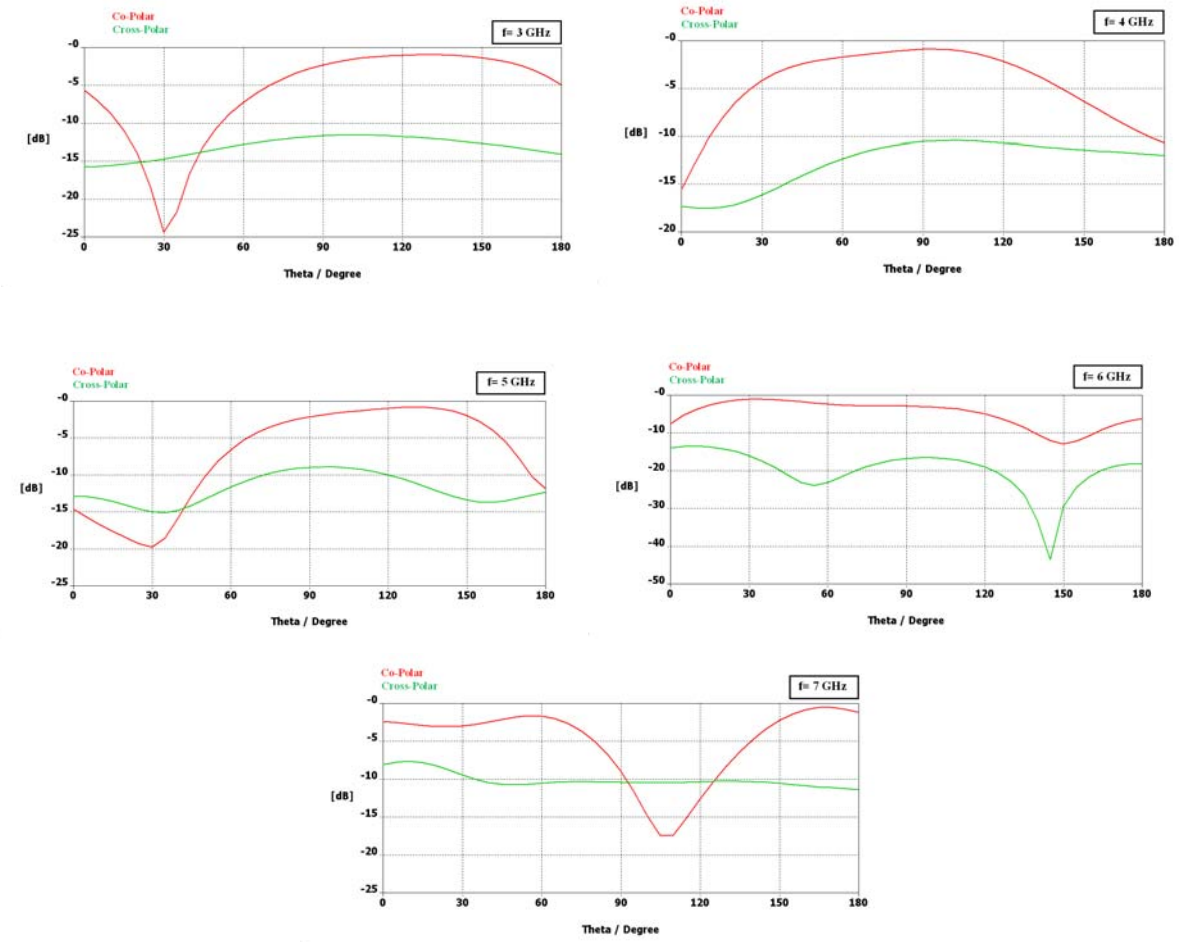

Fig.3.28. E-plane ($\phi = 0^{\circ}$) directivity radiation patterns at 3, 4, 5, 6, and 7 GHz of the sinuous antenna geometry.

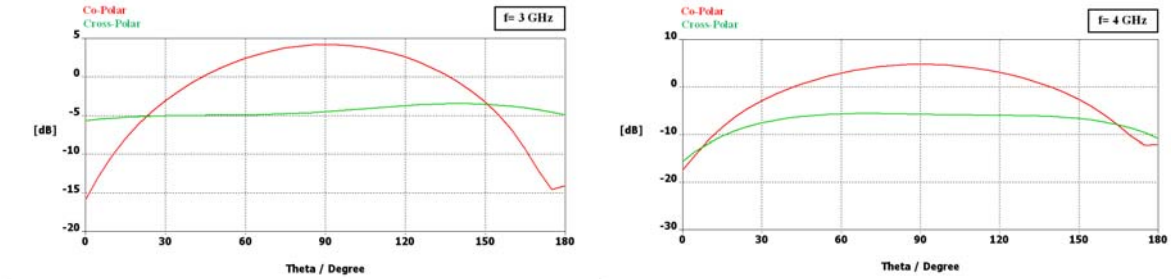

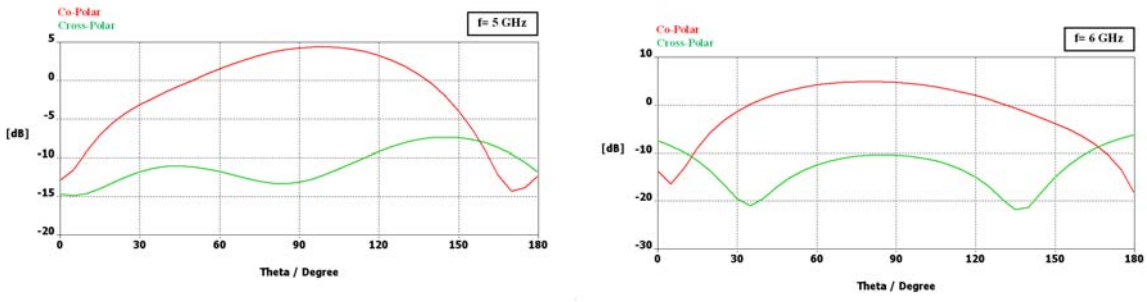

Fig.3.29. H-plane ($\phi = 90^{\circ}$) directivity radiation patterns at 3, 4, 5, 6, and 7 GHz of the sinuous antenna geometry.

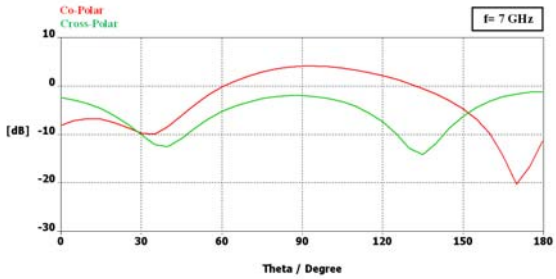

Fig.3.29. (continued) H-plane ($\phi = 90^{\circ}$) directivity radiation patterns at 3, 4, 5, 6, and 7 GHz of the sinuous antenna geometry.

Fig.3.27 to Fig.3.29 shows that H-plane radiation patterns are symmetric and also that the balun system performs a balance field in the antenna's feeding point. The E-plane radiation patterns are not symmetrical in whole wideband frequency. In fact, the 90° bended balun is located in the E- plane and it modifies the symmetry of antenna, and consequently leads to have a symmetrical radiation pattern.

In addition, there are minimum differences of about 10 dB between co-polar and cross polar components in this frequency bandwidth. This point demonstrates the antenna's linear polarization characteristic.

To study the radiation pattern, the HPBW (Half-Power Beamwidth) is presented in E- and H-planes in Table III. Also Fig.3.30 shows how we calculated HPBW at 4 GHz for directivity radiation pattern in H-plane.

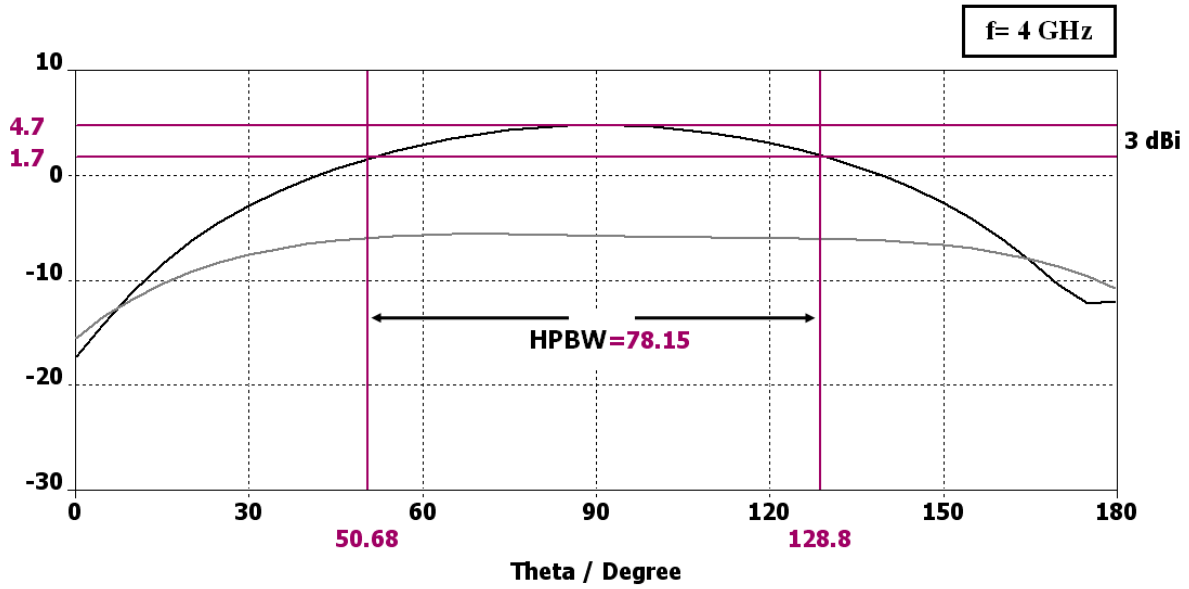

Fig.3.30. HPBW calculation of a single polarization sinuous antenna in H-plane for f=4 GHz.

Table.III. HPBW in E- and H-planes for a single polarization sinuous antenna.

Frequency (GHz)	HPBW E-Plane (°)	HPBW H-Plane (°)
3	99.5	80
4	102	78
5	87	72
6	100.5	76.5
7	79	62

Table.III shows that HPBW in E- and H-plane has small variations from 3 to 7 GHz particularly for H-plane.

The simulated gain of the antenna is shown in Fig.3.31. It shows that the gain of the sinuous antenna oscillates from 4.2 to 5.3 dB between 3 GHz and 8 GHz. Note that the antenna is matched from 2.68 and 7.6 GHz, so the gain is not significant out of this range.

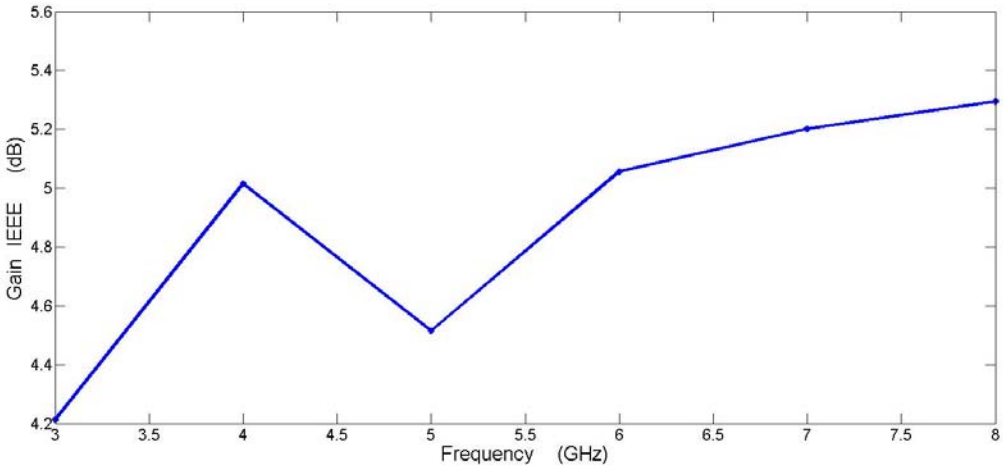

Fig.3.31. Simulated gain of the sinuous antenna.

3.4.3.2 The Sinuous Antenna in Dual Polarized Configuration

The dual polarized antenna structures need two antenna planes with two different baluns for each antenna with a 90 degree rotation. The idea is to have two parallel substrates with a small distance between them. Therefore, the dual polarized antenna structure consists of two identical cells and each cell is the sinuous antenna proposed above. However there is an overlap between two coplanar striplines of the two balun. This idea leads to balun connection together. One solution to overcome this drawback is to turn ϕ degree the second balun plane as it is shown in Fig.3.32.

Fig.3.32 illustrates the second cell of the dual polarized antenna configuration.

(a)

Fig.3.32. (a) Sinuous antenna connected to the balun geometry in second form.

(b) (c)

Fig.3.32. (Continued) (b), (c) Sinuous antenna connected to the balun geometry in second form.

Note that the antenna and balun geometries for the two cells are the same. Also the optimized ϕ is investigated to obtain the best return loss for the sinuous antenna radiation and we arrived to $\phi = 55^{\circ}$.

As it was mentioned, in the first cell the antenna and balun are orthogonal and in the other one, the angle between the antenna and balun was 55 degree. The optimized distance between two antenna planes has obtained with 4.2 mm to arrive the widest bandwidth impedance matching. In Fig.3.33 the sinuous antenna in dual polarized configuration with coplanar balun is presented.

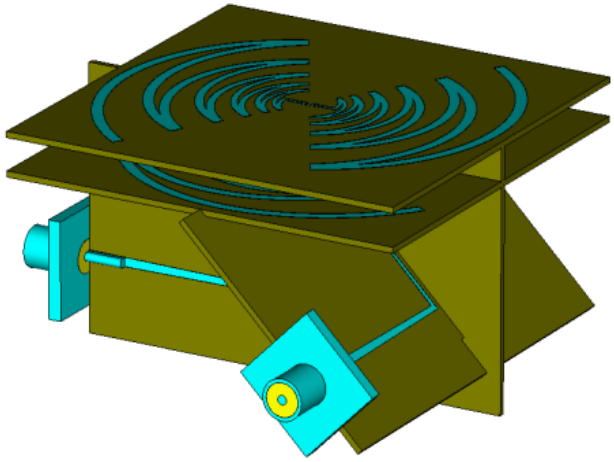

(a)

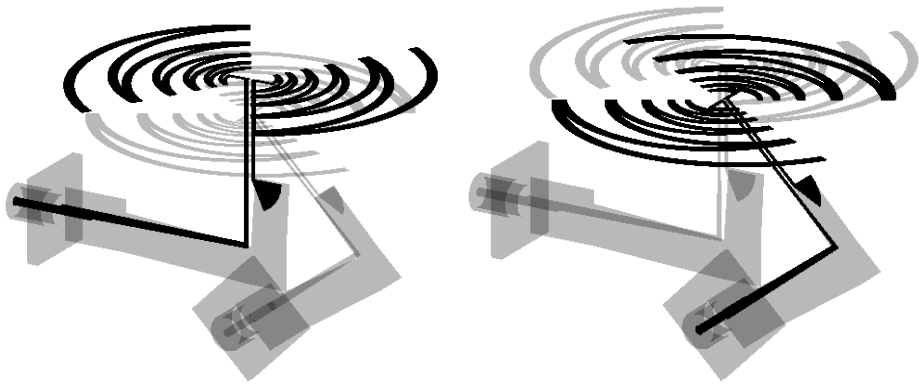

(b) (c)

Fig.3.33. Sinuous antenna connected to the balun geometry in dual polarized form.

Fig.3.34 and 3.35 illustrate the return loss and insertion loss of the first and second ports of dual polarized antenna. The return loss is better than -10b from 2.8 GHz to 9.2 GHz (bandwidth ≈ 6.4 GHz) for polarization 1 (port 1) and from 2.6 GHz to 8.3 GHz (bandwidth ≈ 5.7 GHz) for polarization 2 (port 2). Also the insertion losses show that the transmission property of this structure is almost in the impedance frequency band.

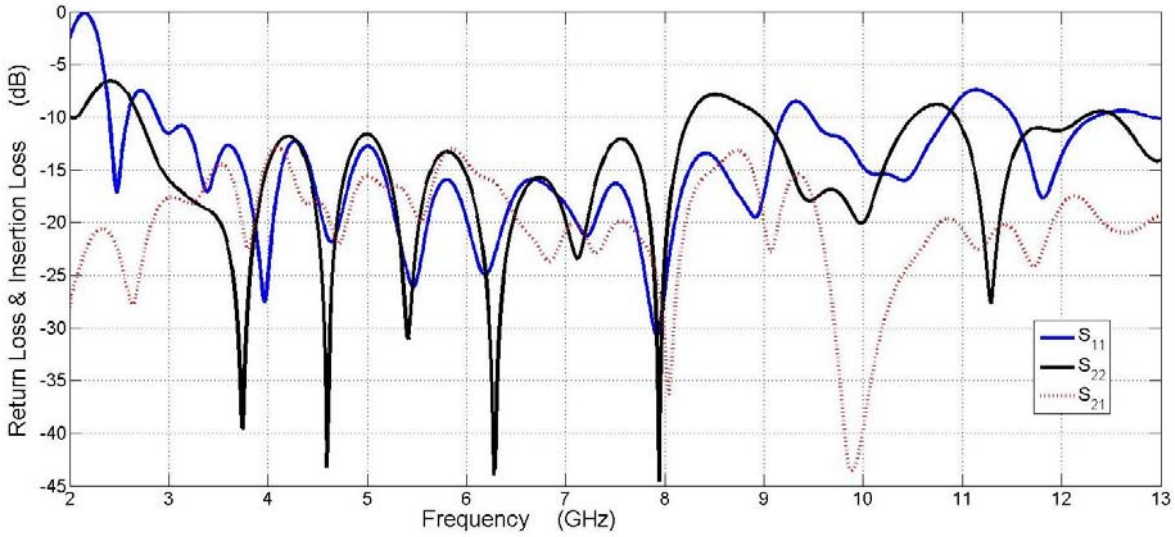

Fig.3.34. Simulated return loss and Insertion Loss (The input impedance is normalized at 50 Ω).

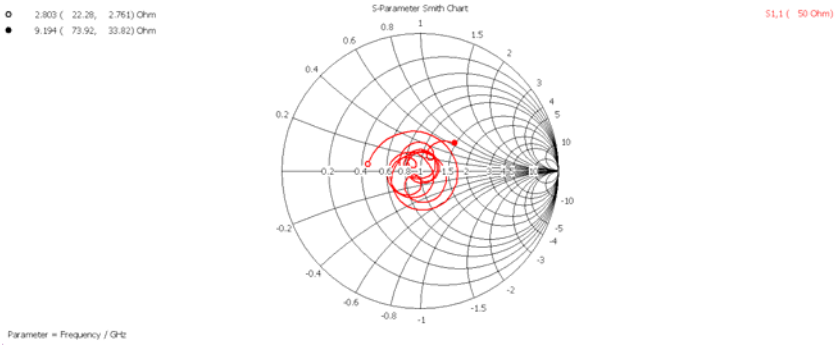

(a)

Fig.3.35. Simulated Input Impedance (a) port 1 (b) port 2 (normalized at 50 Ω)

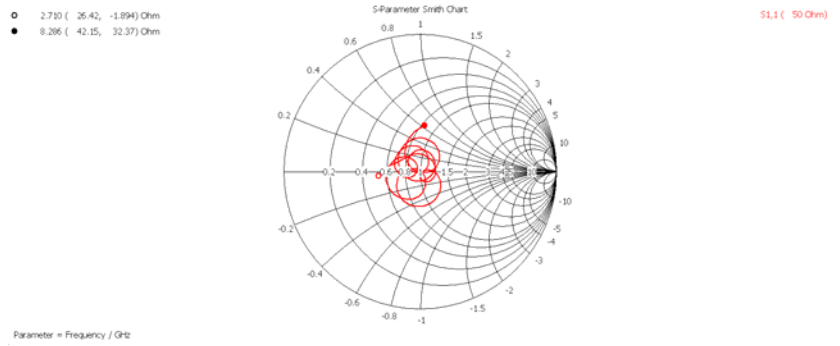

(b)

Fig.3.35. (continued) Simulated input impedance (a) port 1 (b) port 2 (normalized at 50 Ω).

The comparison of the impedance matching between two cells of the dual polarized antenna shows that when the angle between the antenna and balun is 90 degree, the destructive coupling is minimum (for example in comparison with $\phi = 55^{\circ}$). In Fig.3.36 to 3.40 the directivity radiation patterns of two ports in E- and H-planes are presented in 3D Cartesian forms (at different frequencies: 3, 4, 5, 6, 7 and 8 GHz).

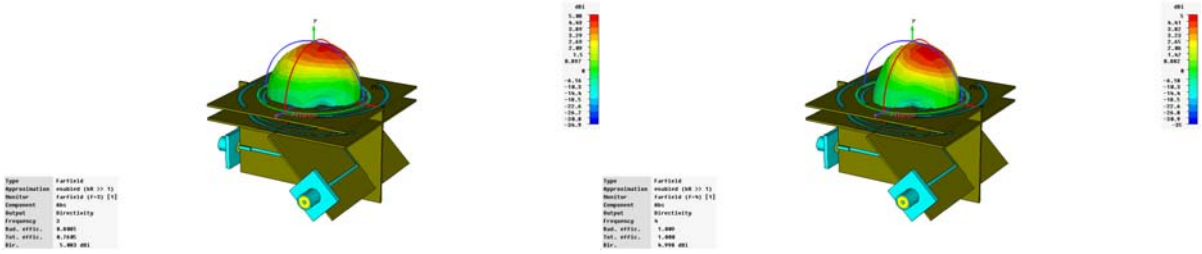

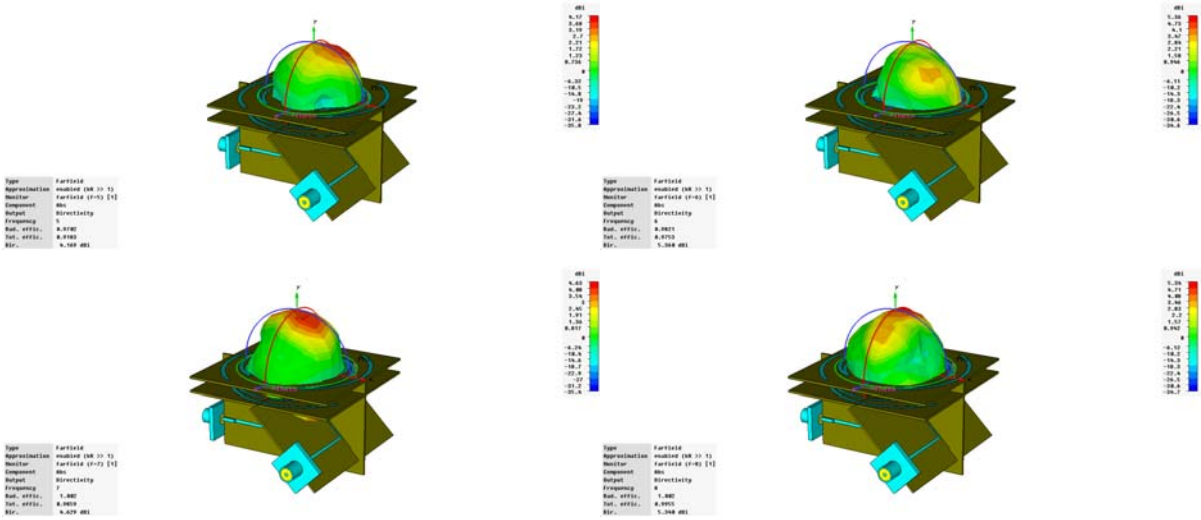

Fig.3.36. Directivity radiation patterns at 3, 4, 5, 6, 7 and 8 GHz of the dual polarized sinuous antenna geometry (Polarization 1).

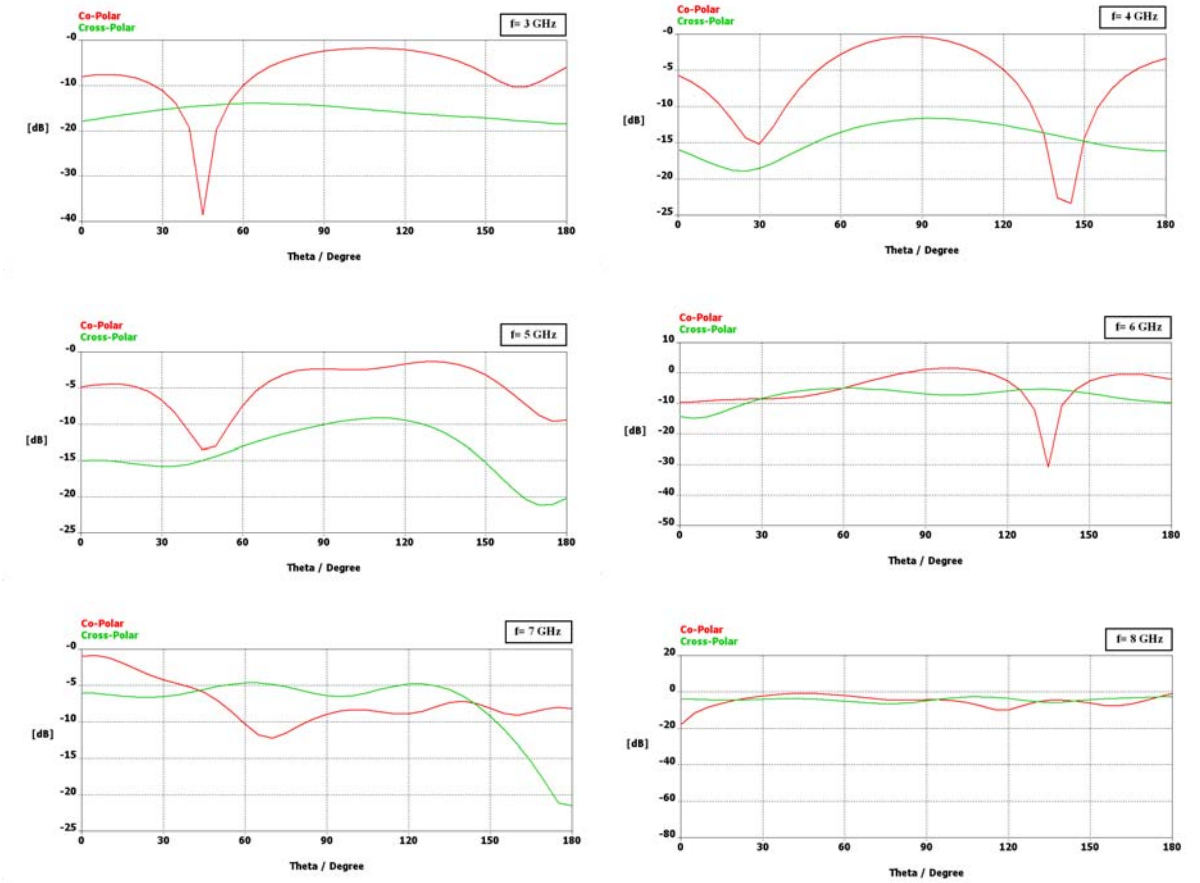

Fig.3.37. E-plane ($\phi = 0^{\circ}$) directivity radiation patterns at 3, 4, 5, 6, 7 and 8 GHz of the dual polarized sinuous antenna geometry (Polarization 1).

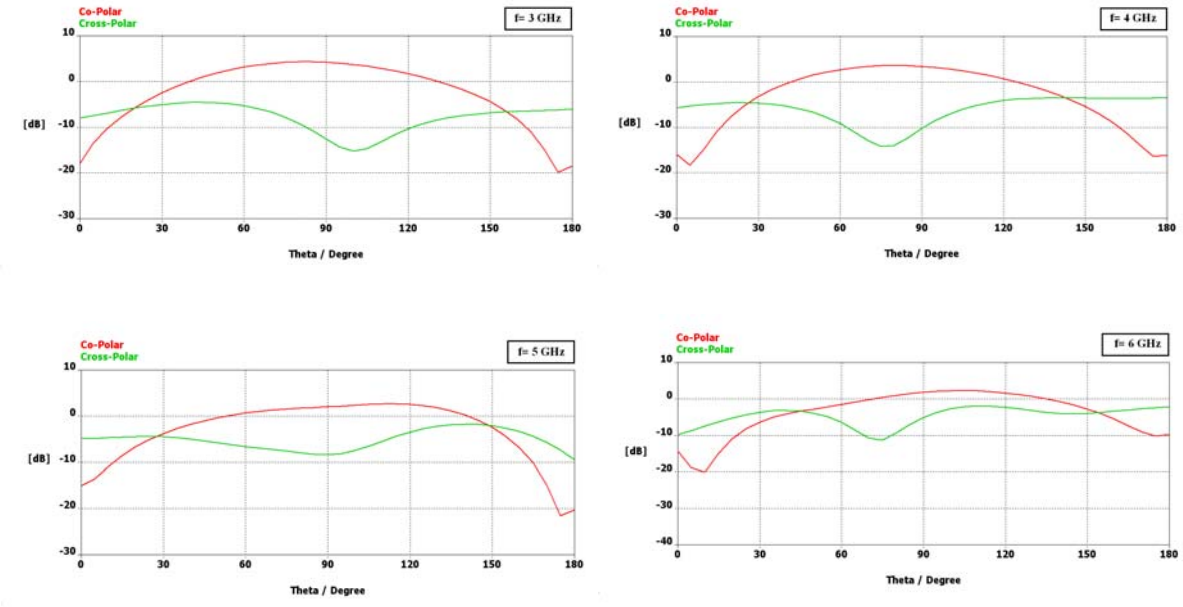

Fig.3.38. H-plane ($\phi = 90^{\circ}$) directivity radiation patterns at 3, 4, 5, 6, 7 and 8 GHz of the dual polarized sinuous antenna geometry (Polarization 1).

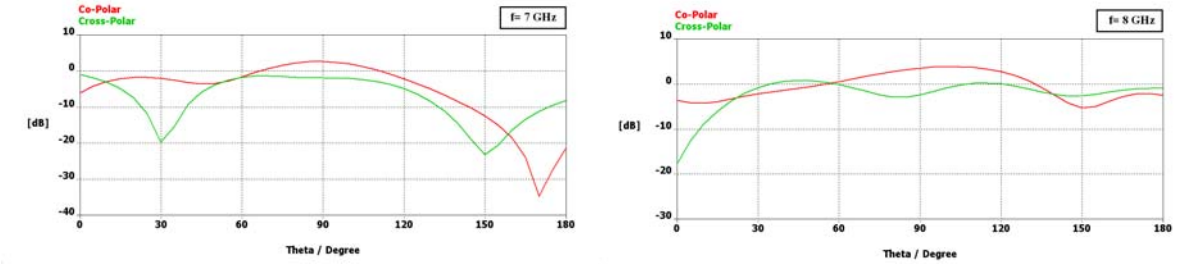

Fig.3.38. (continued) H-plane ($\phi = 90^{\circ}$) directivity radiation patterns at 3, 4, 5, 6, 7 and 8 GHz of the dual polarized sinuous antenna geometry (Polarization 1).

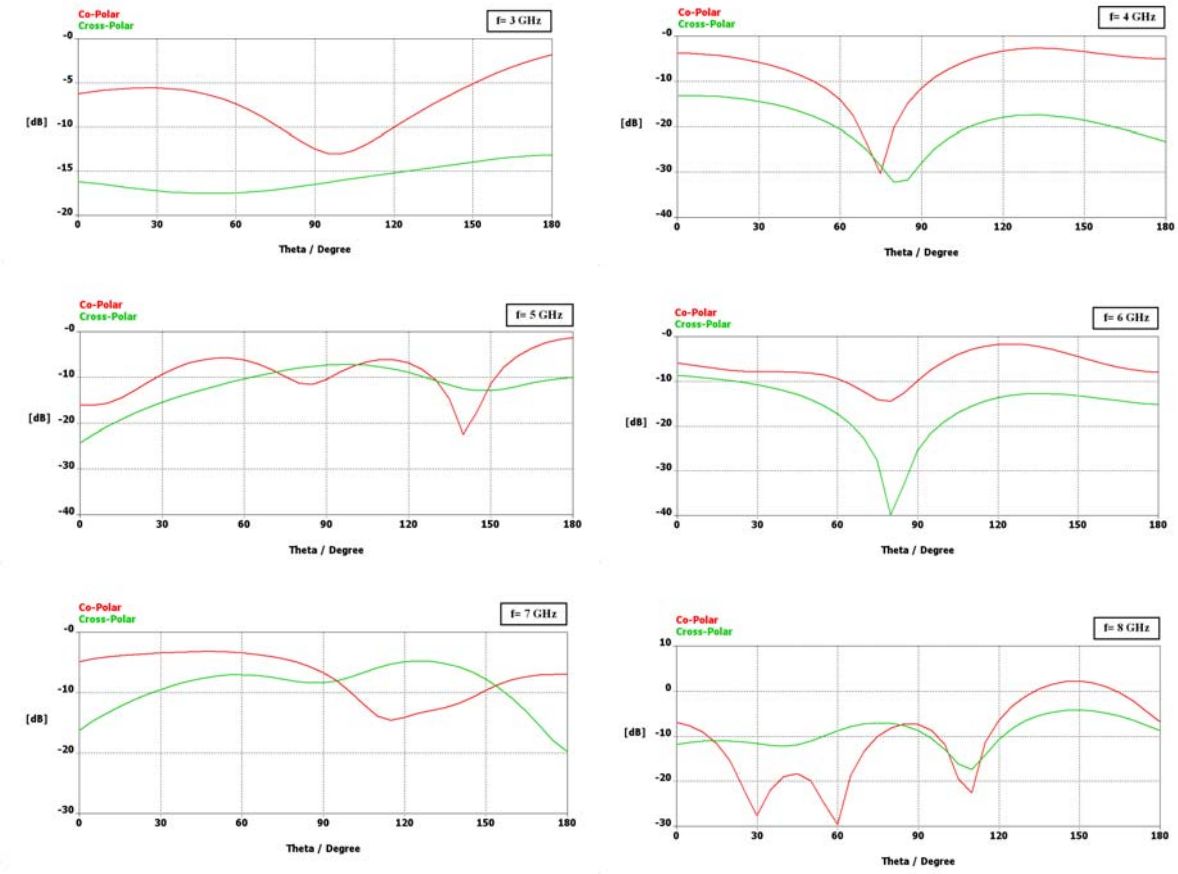

Fig.3.39. E-plane ($\phi = 0^{\circ}$) directivity radiation patterns at 3, 4, 5, 6, 7 and 8 GHz of the dual polarized sinuous antenna geometry (Polarization 2).

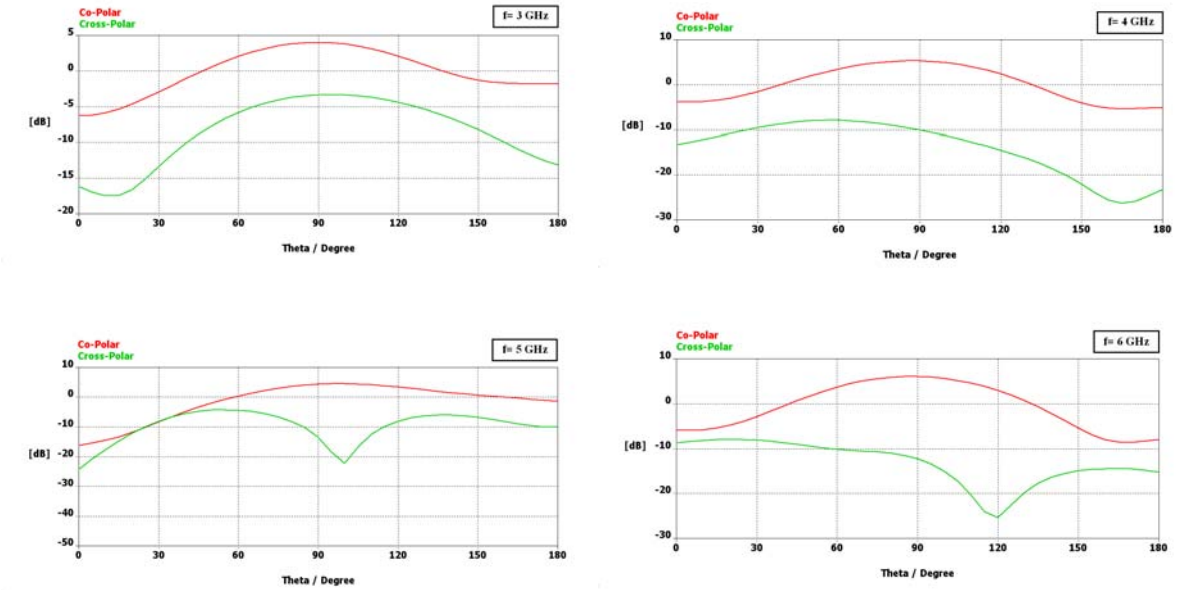

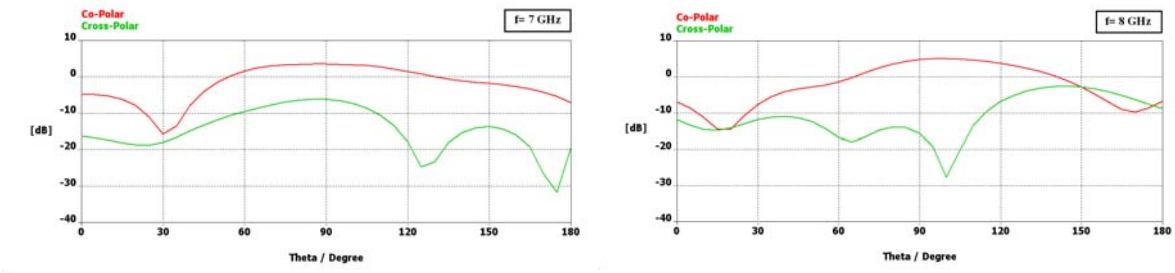

Fig.3.40. H-plane ($\phi = 90^{\circ}$) directivity radiation patterns at 3, 4, 5, 6, 7 and 8 GHz of the dual polarized sinuous antenna geometry (Polarization 2).

The radiation patterns in E- and H-plane for two polarizations (first and second ports) show:

- All the radiation patterns in H-plane present an approximately symmetric behavior around $\theta = 90^{\circ}$ unlike the E-plane which shows some asymmetry.
- The cross polarization level is not always better than -10 dB in the entire frequency bandwidth. The comparison between the dual polarization mode relative to single polarization shows that when two antenna structures are used together with their baluns the linear polarization nature decreases when f > 7 GHz.

HPBW (Half-Power Beamwidth) is presented below (Table.IV) in E- and H-planes for vertical and horizontal polarizations:

Table.IV. HPBW in E- and H-planes for a single polarization sinuous antenna.

Frequency (GHz)	HPBW (Polarization 1) E-Plane (°)	HPBW (Polarization 1) H-Plane (°)	HPBW (Polarization 2) E-Plane (°)	HPBW (Polarization 2) H-Plane (°)
3	67	73	68	77
4	56	76	74	68
5	81.5	88	41	76
6	42.5	73.5	60	62.5
7	96	51	88.5	70

8	49	67	34	58

Table.IV shows small variations in H-plane from 3 to 7 GHz for two polarizations but in E-plane it is observed a variation about 45°. Also Table.V illustrates HPBW difference between E-plane and H-plane diagrams as the HPBW average for E- and H-plane are about 65° and 71.5° respectively for polarization 1 and 61° and 68.5° respectively for polarization 2.

The simulated gain of the antenna is shown in Fig.3.41 for two vertical and horizontal polarizations. The gain of the sinuous antenna oscillates from 4 to 5.3 dB for polarization 1 (port 1) and from 3.8 to 6.2 dB for polarization 2 (between 3 GHz and 8 GHz). Note that the antennas are matched from 2.8 GHz to 9.2 GHz (polarization 1) and from 2.6 GHz to 8.3 GHz (polarization 2), so the gain is not significant out of this range.

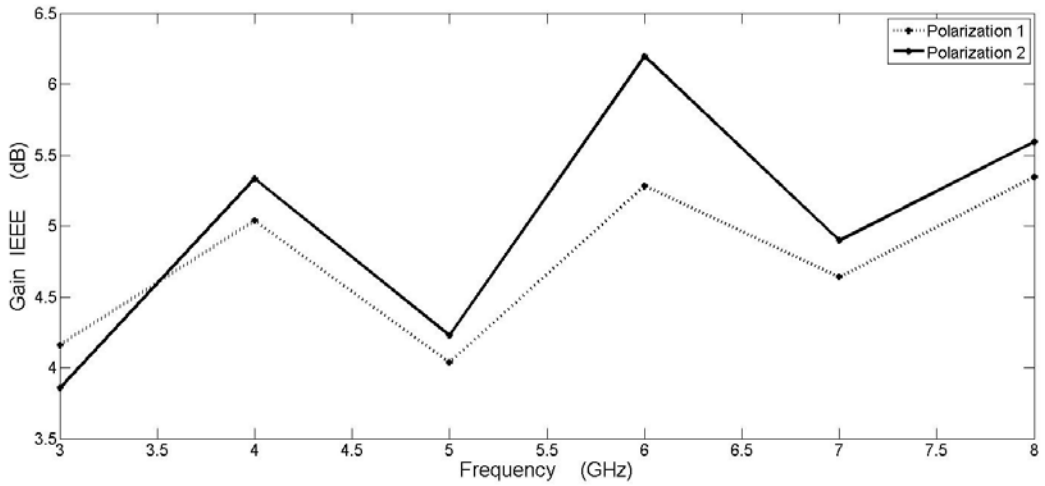

Fig.3.41. The simulated gain of the sinuous antenna.

3.5 Conclusion

In some wideband applications, the priority is not with compact and integrated configurations. In these applications, the designers try to have wider impedance frequency bandwidth.

In this chapter we tried to obtain a 3 dimensional antenna configuration with wideband frequency in dual polarization mode. A microstrip-to-CPS balun orthogonal to the antenna plane was presented. The return loss is better than 10 dB from 2.8 GHz to 9.2 GHz for polarization 1 and from 2.6 GHz to 8.3 GHz for polarization 2.

The simulation results for single polarization were validated by measured return loss and insertion loss. Therefore, we can also assume that the simulation results for dual polarized sinuous antenna will be in good agreement with the measurements in its wideband frequency. Finally the antenna in dual polarization mode can radiate well from 2.6 GHz to 8.3 GHz.

The directivity radiation patterns in H-plane present an approximately symmetrical form around $\theta = 90^{\circ}$ but the E-plane shows some asymmetry in high frequency.

The gain of the dual polarized sinuous antenna oscillates from 4 to 5.3 dB between 3 GHz and 8 GHz for polarization 1 and from 3.8 to 6.2 dB for polarization 2 (between 3 GHz and 8 GHz).

In conclusion these 3D configurations give some matched wideband antenna but impaction of 3-dimentionnal feeding system is important on radiation pattern.

3.6 References

[1] Nasimuddin and Zhi Ning Chen, "Wideband Directional Microstrip Antennas fed by CPW-loop Combination," ICUWB 2007. IEEE International Conference**,** pp. 700-702, 24-26 Sep. 2007.

[2] X. H. Yang and W. X. Zhang, "Coplanar waveguide antenna arrays for MIC/MMIC at millimeter wave frequencies," Electronics Letters, vol. 26, pp. 1464-1465, 1990.

[3] X. Ding and A. F. Jacob, "CPW-fed slot antenna with wide radiating apertures," IEE Proc. Microwaves, Antennas and Propagation, vol. 145, pp. 104-108, 2003.

[4] M. A. Saed, " Reconfigurable Broadband Microstrip Antenna Fed by a Coplanar Waveguide," Progress In Electromagnetics Research, Vol. 55, pp. 227–239, 2005.

[5] Benalla, A. and K. C. Gupta, "Transmission line model for two-port rectangular microstrip patches with ports at the nonradiating edges," *Electronics Letters*, Vol. 23, 882–884, 1987.

[6] Pozar, D. M. and B. Kaufmann, "Increasing the bandwidth of a microstrip antenna by proximity coupling," *Electronics Letters*, Vol. 23, 368–369, 1987.

[7] Katehi, P. B. and N. G. Alexopoulos, "On the modeling of electromagnetically coupled microstrip antennas — The printed strip dipole," *IEEE Trans. on Antennas and Propagation*, Vol. AP-32, 1179–1186, 1984.

[8] Pozar, D. M., "Microstrip antennas," *Proc. IEEE*, Vol. 80, 79–91, 1992.

[9] Pozar, D. M., "A microstrip antenna aperture — Coupled to a microstrip line," *Electronics Letters*, Vol. 22, 49–50, 1985.

[10] Gronau, G. and I. Wolff, "Aperture-coupling of a rectangular microstrip resonator," *Electronics Letters*, Vol. 22, 554–556, 1986.

[11] Y. Qian and T. Itoh, "A Broad-band Uniplanar Microstrip-to-CPS transition," in *Proc. Asia–Pacific Microw. Conf.*, vol. 2, pp. 609–612, 1997.

[12] S.-Y., Suh, W, Stutzman, W., Davis and J. Waltho 'A novel CPW-fed disk antenna'. IEEE Antennas and Propagation Society Int. Symp., June 2004, Vol. 3, pp. 2919–2922.

[13] Liang, X.-L., Zhong, S.S., and Wang, W. 'Elliptical planar monopole antenna with extremely wide bandwidth', Electron. Lett., 2006, 42, (8), pp. 441–442.

[14] Kwon, D.-H., and Kim, Y. 'CPW-fed planar ultra-wideband antenna with hexagonal radiating elements'. IEEE Antennas and Propagation Society Int. Symp., June 2004, Vol. 3, pp. 2947–2950.

[15] Lee, S.H., Park, J.K., and Lee, J.N. 'A novel CPW-fed ultra-wideband antenna design', Microw. Opt. Technol. Lett., 2005, 44, (5), pp. 393–396.

[16] Wen, C. P., "Coplanar Waveguide: A Surface Strip Transmission Line Suitable for non-Reciprocal

Gyromagnetic Device Applications," *IEEE Trans*., Vol. MTT17, Dec. 1969, pp. 1087-1090.

[17] Wen, C. P., "Coplanar Waveguide Directional Couplers," *IEEE Trans*., Vol. MTT-18, June 1977, pp.318-322.

[18] R. Mongia, I. Bahl, and P. Bhartia, *RF and Microwave Coupled-Line Circuits*, Norwood, MA: Artech House, 1999, ch.11.

[19] Y.-H. Suh and K. Chang, "A wideband coplanar stripline to microstrip transition," *IEEE Microw. Wireless Compon. Lett.*, vol. 11, no. 1, pp. 28–29, Jan. 2001.

[20] N. I. Dib, R. N. Simons, and L. P. B. Katehi, "New uniplanar transitions for circuit and antenna applications," *IEEE Trans. Microw. Theory Tech.*,vol. 43, no. 12, pp. 2868–2872, Dec. 1995.

[21] Wen-Hua Tu and Kai Chang, "Wide-band Microstrip-to-Coplanar Stripline/Slotline Transitions," *IEEE Trans. Microw. Theory Tech.*,vol. 54, no. 3, pp. 1084–1089, March. 2006.

[22] R. Sorrentino, L. Roselli, 'A New Simde and Accurate Formula for Microstrip Radial Stub,' IEEE MICROWAVE AND GUIDED WAVE LE'ITERS, VOL. 2, NO. 12, DECEMBER 1992.

[23] R. C. Johnson, *Antenna Engineering Handbook*, Third Ed., McGraw Hill, 1993.

Chapter 4
New Integrated Feeding System for Ultra Wideband Dual Polarized Antennas

4.1 Introduction

There is an increasing demand for integrated and low-profile antenna configurations in ultra wideband domain in several categories of the academic and military researches and new technology [1]-[3]. The size and compactness of antenna structure is one of the critical issues for portable devices, because the size affects the bandwidth and gain of antenna. Therefore, to miniaturize the antennas capable of providing wide bandwidth for impedance matching and acceptable gain will be a challenging task [2]. In the other hand, as it was mentioned in chapter one, there are some limitations to use the bulky size antenna even with good wideband performance and the demands for compact wideband antenna in portable devices such as (cell phone and laptop) are increasing [1].

Also in antenna array minimizing the antenna size is one of the so interesting subjects. Recent years have seen an increased interest in using polarization diversity at the base station by the potential for reduced interference [4]. The authors of [5] show how polarization diversity antenna can mitigate the detrimental multipath fading and with dual polarized antenna, it is possible to increase the performance of wireless communication system [6]. Moreover in such systems, as it was indicated in chapter one, maximum performance occurs when the two polarizations are orthogonal (co-polar and cross-polar) and the antenna features high isolation between the two polarization.

The objective of this chapter article is the achievement of integrated geometry to obtain a wideband compact antenna with dual polarized characteristics. Moreover, to design such antenna, it is necessary to have a balun with wideband characteristic in field and impedance matching.

In chapter 3, a microstrip-to-CPS wideband balun has proposed and for its performance validation, a 3-dimensional connection with a dual polarized sinuous antenna was presented. The result was a voluminous structure with wideband characteristic and dual polarization property.

Our final objective is to achieve to an integrated antenna structure. We have explained (chapter 3) that the coplanar baluns are very suitable to achieve this objective because of their geometry and performance. Now, in this chapter we want to propose two different developed wideband antenna configurations with dual polarized characteristic. Our integrated balun configurations have been employed with sinuous and quasi bow-tie antennas and their performances have been validated.

4.2 A New UWB CPS-fed Dual Polarized Quasi Bow-Tie Antenna

4.2.1 Introduction

In recent years, considerable efforts have been dedicated to wideband compact planar antenna with low-profile configuration. One of such antennas is the "Bow-Tie". Due to their light weight and thin profile configurations, low cost of fabrication, reliability, conformal structure and ease of fabrication, microstrip bow-tie type antennas have been widely used in both theoretical researches and engineering applications [7]. Also, their simple geometries make it compatible to be connected to the planar feeding system.

The main challenge in wideband antenna feeding systems is bandwidth enhancement with the ability of integration with other recent wideband antenna structures. In this field, a number of wideband microstrip antennas which have been fed by coplanar waveguide (CPW) have been reported [8]-[10] but they have not dual polarized nature. The design objective is to obtain a compact UWB antenna just on one substrate in dual polarized application.
The coplanar stripline (CPS) baluns not only have the same advantages of a coplanar waveguide (CPW) but also CPS has two balanced striplines which is useful to feed balanced architecture such as symmetrical antennas. Also the CPS configuration can obtain the high characteristic impedances to feed antenna structures with bigger impedances such as a bow-tie antenna [11]-[13].

Recently Wen-Hua Tu and Kai Chang have presented a microstrip-to-CPS transitions that they have arrived to a CPS with 184 Ω impedance characteristic and with a -3dB back-to back insertion loss bandwidth from 1.3 to 13.3 GHz [11]. This impedance transformation (50 to 184Ω) with wideband frequency is very interesting to feed wideband microstrip antenna structures.

In following sections, first of all a summary concept of wideband bow-tie antenna is presented. Then, a quasi bow-tie geometry with wideband characteristic is proposed in next section. Moreover an optimized microstrip-to-CPS balun type in wideband frequency to obtain several structural advantages is presented: providing wideband transition characteristics, ability of integrated connection with other circuits, its compact and low-profile structure and finally elimination of the need for a via-hole which leads to technical problem and parasitic effects. In addition, an investigation on the relations between the antennas planes for dual polarized configuration is performed. Finally the complete structure of dual polarized integrated bow-tie configuration with the simulation and measurement results is carried out.

4.2.2 The Quasi Bow-Tie Antenna Structure

4.2.2.1 Principle of Bow-Tie antenna design

As it was cited in chapter 1, the bow-tie antenna has been used in some applications like planar array for aircraft flight test and evaluation of an UHF radiometer system for many years [14-15] due to their many attractive advantages, such as simple design, planar structure, and broad bandwidth [16]–[18]. Also, we have mentioned that many efforts have been reported to enhance the impedance bandwidth and to obtain stable radiation patterns, such as resistive and capacitive (RC) loading [19], [20] and different feeding technologies [17]-[18] and [21]-[22].

To design and to have an applicable sense of the planar bow-tie antenna, it is necessary to know the concept of the biconical antenna. In fact the wideband bow-tie antenna structure idea comes from the biconical antenna geometry in planar form. When we talk about broadband antenna, it will be observed that the frequency bandwidth of a simple dipole antenna can be increased by using thicker wire as indicated in Fig.4.1 [23]. With this idea it is possible to increase the antenna bandwidth if the conductors are flared to form a biconical structure. With the attention to Rumsey considerations in independent-frequency antenna subject [23], it is observed that frequency independent antennas are designed to minimize finite lengths and maximize angular dependence and that the biconical antenna is an example of frequency-independent antenna. Also the bow-tie antenna has wideband nature because its geometry concept comes from the biconical antenna.

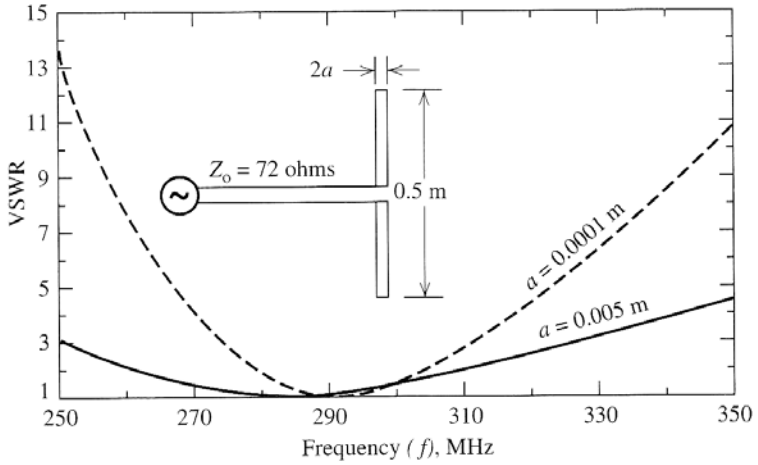

Fig.4.1. VSWR as a function of frequency for dipoles of different wire diameters [7].

Therefore, the infinite biconical antenna will be studied, followed by the practical forms of planar bow-tie antenna. Then, a new dual polarized quasi bow-tie connected to an optimized bended microstrip-to-CPS balun (that was introduced in previous section) is proposed. The proposed design is applicable as a

compact, wideband and dual polarized antenna just on one substrate in the UWB systems. The ever increasing demand for compact wideband wireless communication equipment explicitly needs research in such wideband low profile configuration topics.

4.2.2.2 The Bow-Tie Antenna Structure and Wideband Characteristic

Limiting the two cones of the infinite bicone will produce a practical finite biconical antenna which is shown in Fig.4.2. W. L. Stutzman and G. A. Thiele explain that for a finite biconical antenna, TEM waves exist together with higher-order modes created at the ends of the cones [7]. These higher-order modes are the major contributors to the antenna reactance [24]. In the other hand when we cut the end of the cones of an ideal biconical antenna, the ends cause reflections that set up standing waves. These standing waves produce input impedance with the reactance part. The consideration of the biconical antenna shows that the reactance part of the input impedance is sensitive to θ_h and it is possible to control it by changing the θ_h parameter and can be hold to minimum by increasing the θ_h .

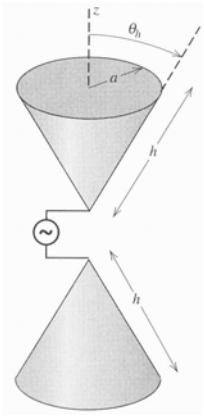

Fig.4.2. Finite biconical antenna geometry.

To achieve wideband characteristic, it should be held constant the real part of the input impedance over the frequency bandwidth. Fortunately with increasing the θ_h, the real part of the input impedance becomes less sensitive to changing frequency. Fig.4.3 shows these two facts involved in controlling the two parts of complex input impedance by plotting the real and reactance part versus the height of the L_h for a conical monopole [25].

In recent years, considerable efforts have been dedicated to wideband compact planar antenna with simple fabrication. One of such antennas is the “bow-tie” (Fig.4.4). In Fig.4.4, h is the side length of the bow-tie

strip, θ_h is the angle of equilateral triangular and g is the gap between the triangles. Bow-tie antenna is the planar form of finite biconical antenna.

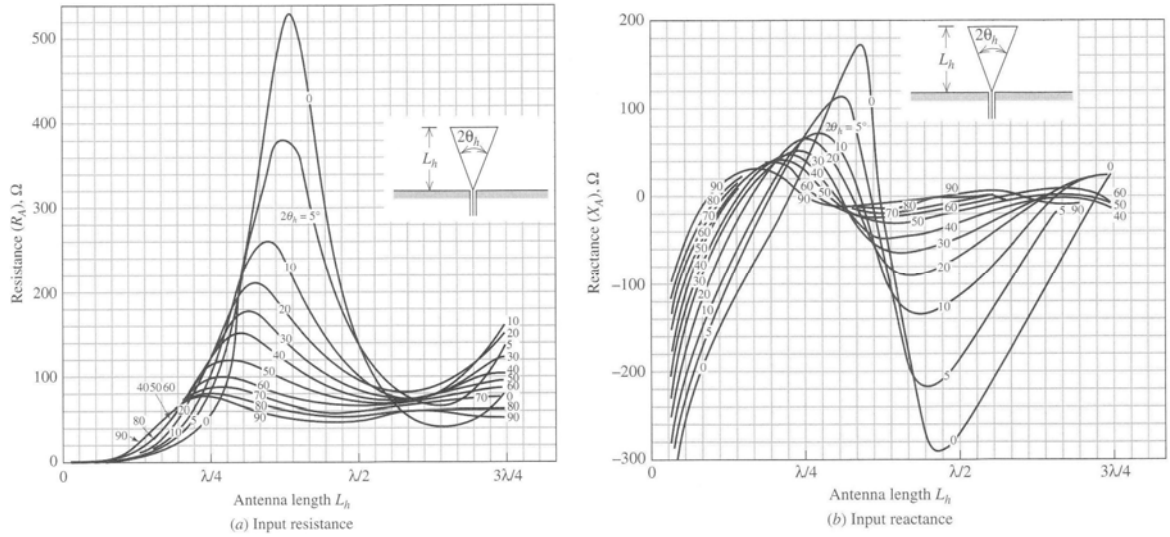

Fig.4.3. Input impedance of a conical monopole versus monopole height L_h [23].

The bow-tie consists of two triangular flat metal plates arranged in the configuration of a bow-tie, with a feeding point at the gap between the apexes of the triangles. Due to their light weight and thin profile configurations, low cost of fabrication, reliability, conformal structure and ease of fabrication, microstrip bow-tie type antennas have been widely used in both theoretical researches and engineering applications [7].

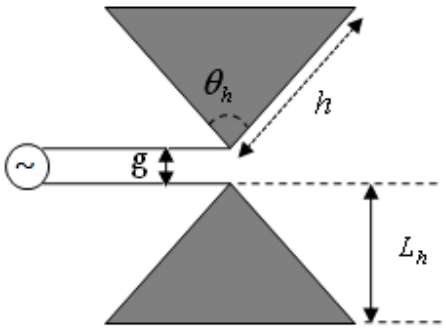

Fig.4.4. Bow-tie antenna geometry.

Stutzman and Thiele claim that the bow-tie type antenna has somewhat more sensitive input impedance to changing frequency than the finite biconical. In addition, in all following bow-tie designs, it is considered that $\theta_h = 90^\circ$ because of nature of the real part of input impedance. λ_L

4.2.2.3 Design Consideration of a Quasi Bow-Tie Antenna

4.2.2.3.1 Optimization of Bow-Tie antenna without balun

At the first stage, a bow-tie antenna geometry is designed with $L_h = 38\ mm$, h=53.74 mm, g=0.6 mm and $\theta_h = 90^\circ$. The geometry of the proposed antenna is depicted in Fig.4.4. The antenna lies on DiClad 880 substrate with thickness $h = 0.762$ mm and ε_r=2.17. The dimensions of the bow-tie antenna are chosen in order to achieve the minimum return loss. The dimensions of the antenna are optimized to obtain the smith chart curve with minimum radius. In CST simulator, a voltage delta gap source (discrete port) between the two heads of the triangles as an antenna feeding is assumed.

The simulation result concerning the return loss of this geometry at the feeding point is illustrated in Fig.4.5. The simulation results show that the antenna has a good wideband property from 2.5 GHz to frequencies higher than 20 GHz. Note that the return loss is normalized at $R = 165\ \Omega$ and thus for design a balun, it should have an impedance matching between $50\ \Omega$ and $165\ \Omega$.

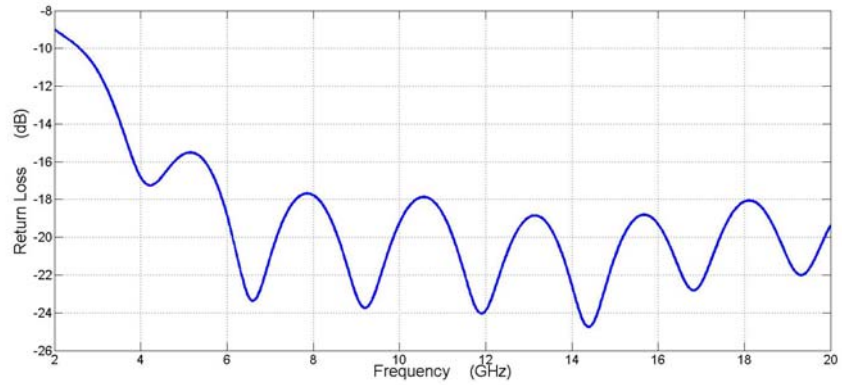

(a)

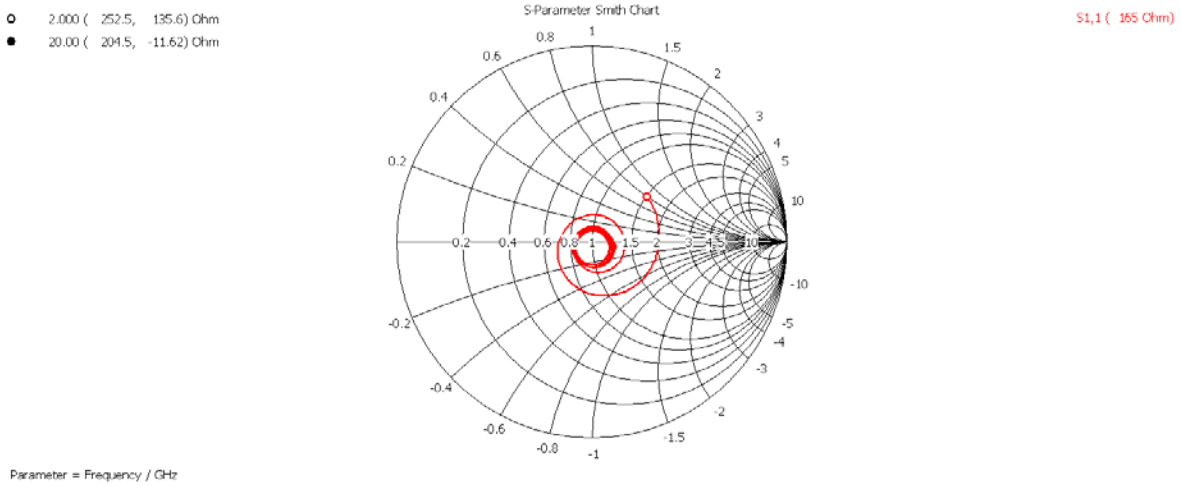

(b)

Fig.4.5. Simulated (a) return loss and (b) input impedance (normalized at 165 Ω).

In the next section, an integrated balun feeds our optimized geometry in its impedance frequency bandwidth.

4.2.2.3.2 Bow-Tie antenna with balun (Single polarization)

The bow-tie antenna is a balanced antenna with two symmetric metal parts with wideband characteristic. Therefore as a feeding system it is necessary to use a balun with wideband characteristic and two symmetric striplines. In section 3.3 a new compact wideband balun which has suitable geometry for implementation on the optimized bow-tie as a feeding system was proposed. First of all a microstrip-to-CPS is optimized to impedance matching between 50 Ω and 165 Ω. As it was indicated in previous sub-section R=165 Ω is the input impedance of bow-tie antenna. Fig.4.6 illustrates a balun integrated to our optimized bow-tie. Table.1 summarizes the balun dimensions for the bow-tie antenna schemes proposed in previous sub-section.

Table I. Dimensions of the bow-tie antenna in single polarization. (Unit: Millimeters)

L_1	L_m	L_{CPS}	L_h	W_{gnd}	W_{CPS}	W_m	h	R	θ_h	θ
10	40	14.6	38	8	1	1.3	53.74	5.5	90°	65°

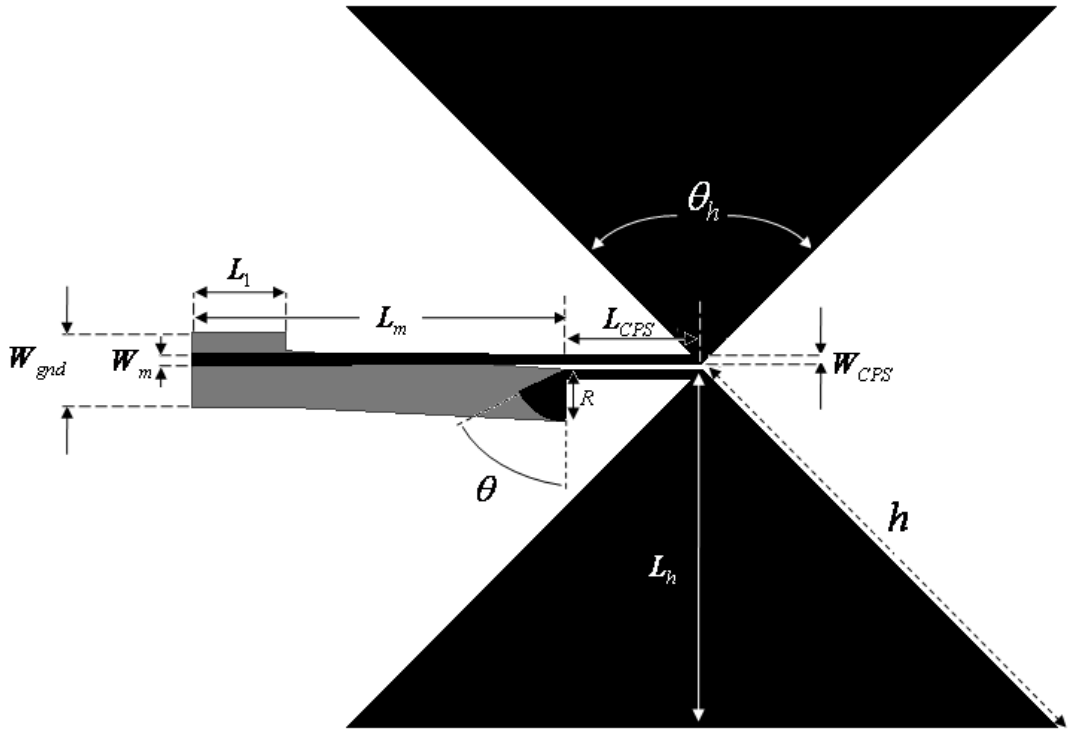

Fig.4.6. Bow-tie antenna connected to the wideband balun configuration.

Also the gap between two coplanar striplines is equal to 0.6 mm and DiClad 880 is used as the substrate with a dielectric constant of 2.17 and thickness equal to 0.762 mm. The simulated return loss of the proposed structure is shown in Fig.4.7. The overall dimension of the proposed design is $9.2\,\mathbf{cm} \times 7.5\,\mathbf{cm}$ or $0.8\lambda_L \times 0.7\lambda_L$ where λ_L is the wavelength at low frequency (f_L=2.75 GHz).

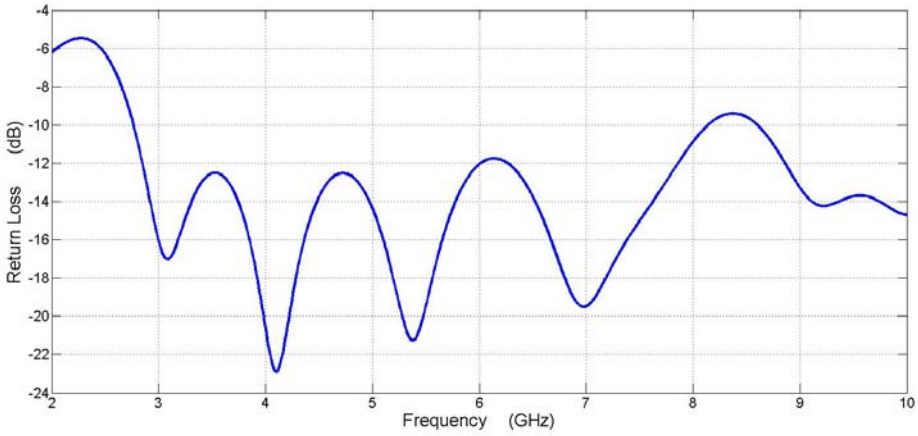

(a)

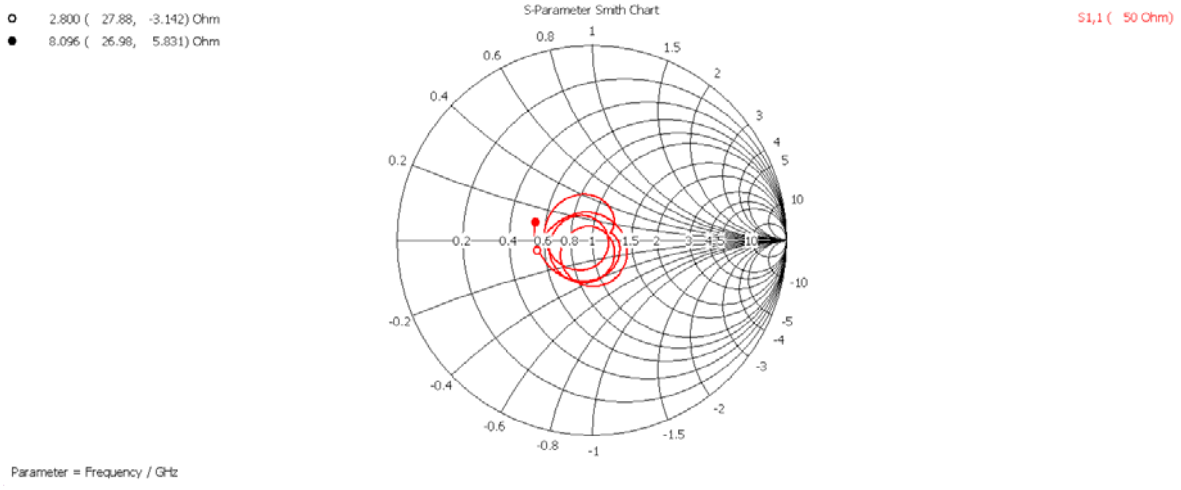

(b)

Fig.4.7. Simulated (a) return loss and (b) input impedance (normalized at 50 Ω).

The simulated return loss shows that the antenna geometry has good matching in its frequency bandwidth (Fig.4.7). In this figure it is shown that the antenna operates well between 2.75 GHZ and 8.2 GHz with return loss of better than -10 dB.

Also Fig.4.8 to 10 show the simulated directivity radiation patterns of the proposed antenna structure in its frequency bandwidth. The radiation patterns (antenna directivity) are simulated at frequencies of 3, 4, 5, 6, 7 and 8 GHz in H- and E-plane (Fig.4.9 and 4.10). The definition of H-plane and E-plane is shown in Fig.4.8.

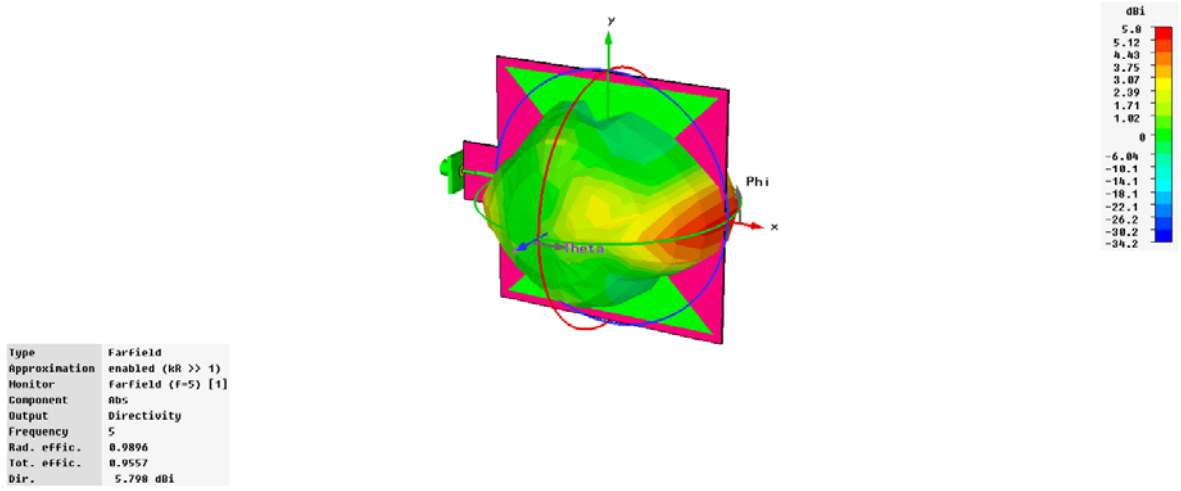

Fig.4.8. Definition of H-Plane (φ=0°) and E-Plane (φ=90°) and directivity radiation pattern is shown at f=5 GHz.

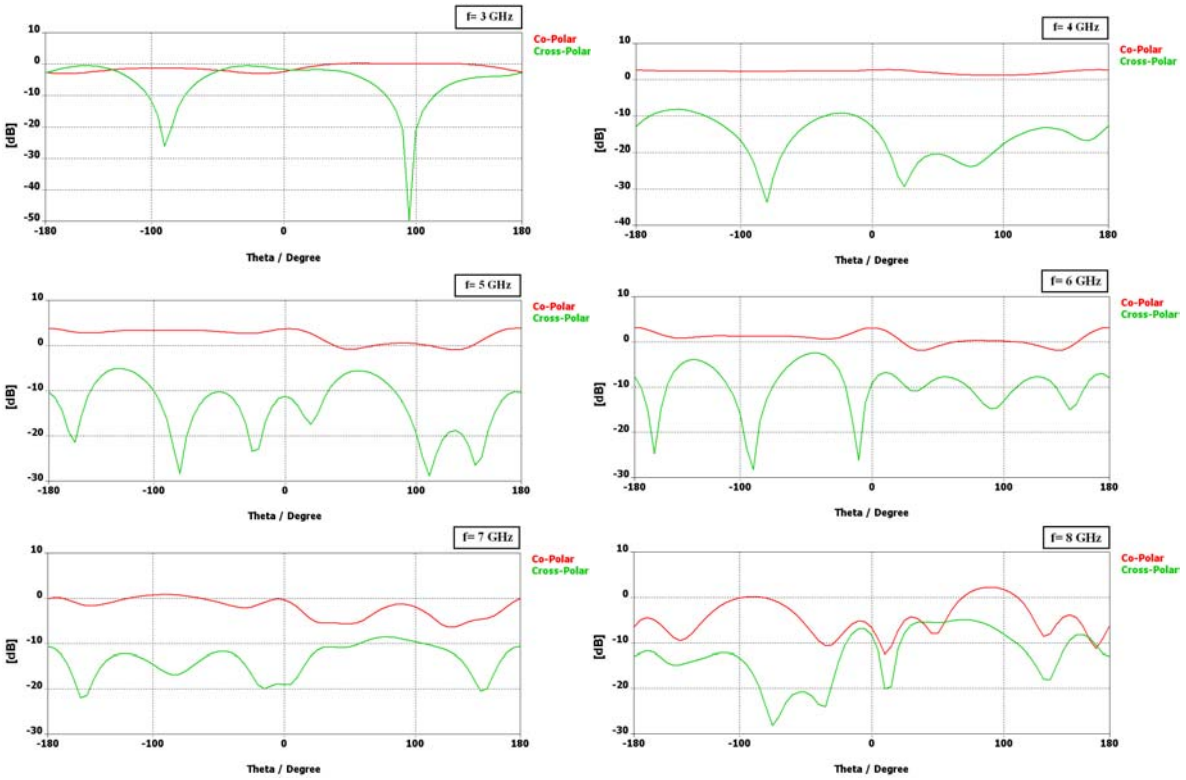

Fig.4.9. H-plane ($\phi = 0^{\circ}$) directivity radiation patterns at 3, 4, 5, 6, 7 and 8 GHz of the bow-tie antenna geometry in single polarization mode.

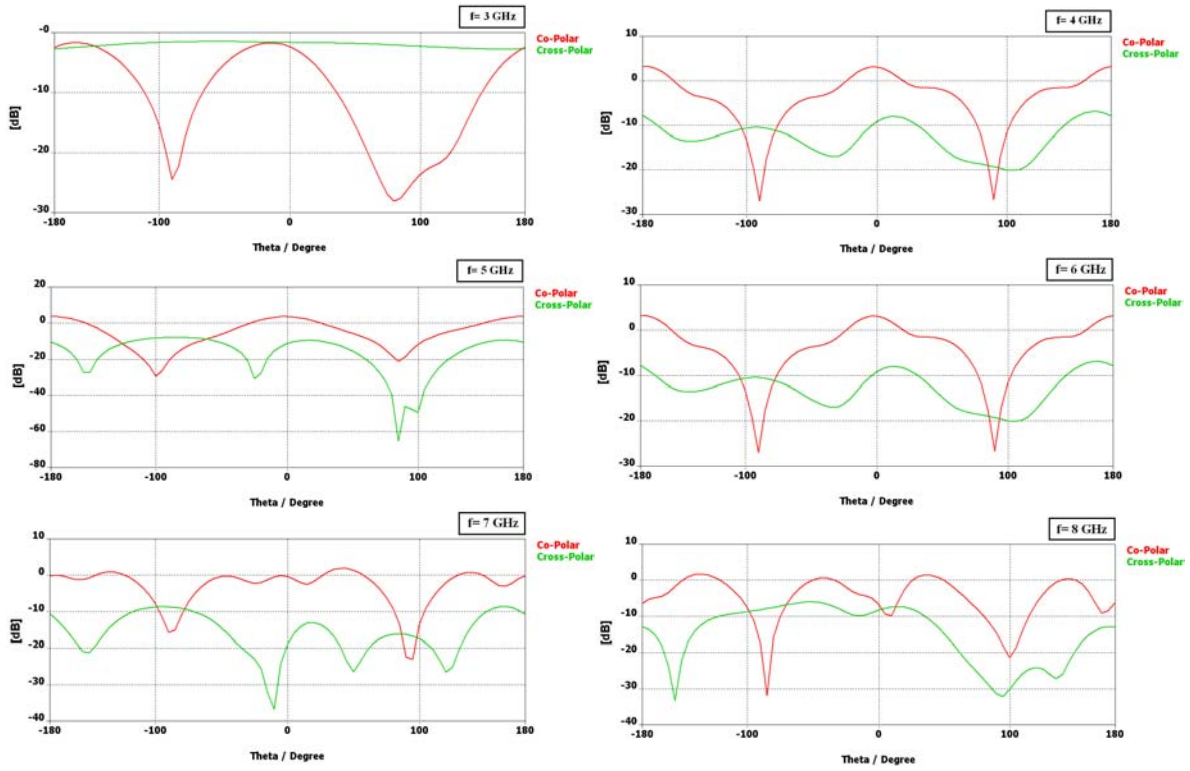

Fig.4.10. E-plane ($\phi = 90^{\circ}$) directivity radiation patterns at 3, 4, 5, 6, 7 and 8 GHz of the bow-tie antenna geometry in single polarization mode.

The directivity radiation patterns for E-plane are symmetric. In addition, the directivity radiation patterns show that the antenna has linear polarization characteristics and because of the existence of about 10 dB difference between co-polar and cross-polar components, the electric field at a point in space is always directed along a line. It shows that the radiation patterns of antenna connected to the balun have different behavior from the radiation patterns of bowtie without balun (simulated with a delta gap source: 4.2.2.3) and that's why this structure (antenna with balun) is directive (around θ= 90 ° in E-plane). Also, HPBW (Half-Power Beamwidth) is presented in H- and E-planes in Table II.

Table.II. HPBW in H- and E-planes for a single polarization bow-tie antenna.

Frequency (GHz)	HPBW H-Plane (°)	HPBW E-Plane (°)
3	90	36
4	90	35
5	84	61
6	111	33
7	54	31
8	54	42

Table.II shows that HPBW in E-plane has small variations (except in f=5 GHz). Also Table.II shows that HPBW in H-plane has small variations from 3 to 6 GHz (its average is about 90°), but for the frequencies higher than 6 GHz, HPBW decreases up to 53.55°.

Also the radiation patterns show that the bow-tie has omnidirectional dipole-type radiation pattern as we expected. The simulated gain of the antenna is shown in Fig.4.11. It shows that the gain of the bow-tie antenna oscillates from 3 to 6.1 dB between 3 and 8 GHz and the gain increases in the intervals of 3 to 5 GHz and 6 to 8 GHz.

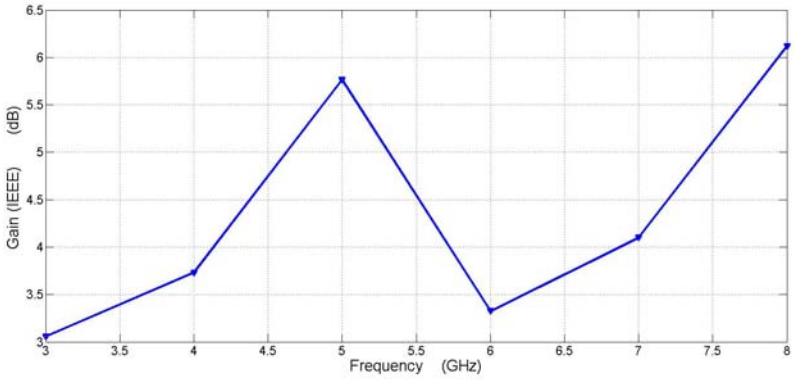

Fig.4.11. Simulated gain of the bow-tie antenna for single polarization.

Consideration of the parameters of return loss, radiation pattern and gain shows that the bow-tie antenna operates well in frequency band from 3 to 8 GHz and it is a good candidate for next stage to achieve a wideband dual polarization bow-tie antenna.

4.2.2.3.3 Dual Polarization Antenna Configuration Design

In this stage the desired structure is the dual polarized configuration. The idea is the implementation of two bow-tie antenna on the balun proposed in previous section on both sides of substrate with a 90° rotation. It seems that for obtaining good performance from this idea, we should implement the two planes of antenna on the two sides of a substrate without any connection between these two parts. In this case, it seems that the dual polarized antenna can operate well. But with 90 degree rotation of one bow-tie antenna and varying its position on the other side of substrate, there will be connections between each antenna plane and the ground plane of the other antenna. Also each CPS will have a ground plane and it turns consequently to other line type with other impedance characteristics.

Therefore we encounter two problems: firstly, the connection between each antenna and the other ground plane and secondly variation of microstrip-to-CPS to other kind of line with other impedance characteristics.

But for bow-tie antenna, the connection between each antenna plane and other ground plane balun is not important because the current surface on the bow-tie plane distributes on the sides of triangular not on the center part of antenna. In Fig.4.12, the current distribution for a simple polarization bow-tie antenna is shown. The simulated results show that the surface currents are placed only on the sides of the triangular especially on the right and left sides. Thus, if the ground plane of the second antenna connects to the first antenna plane, the distribution of the surface current will not change.

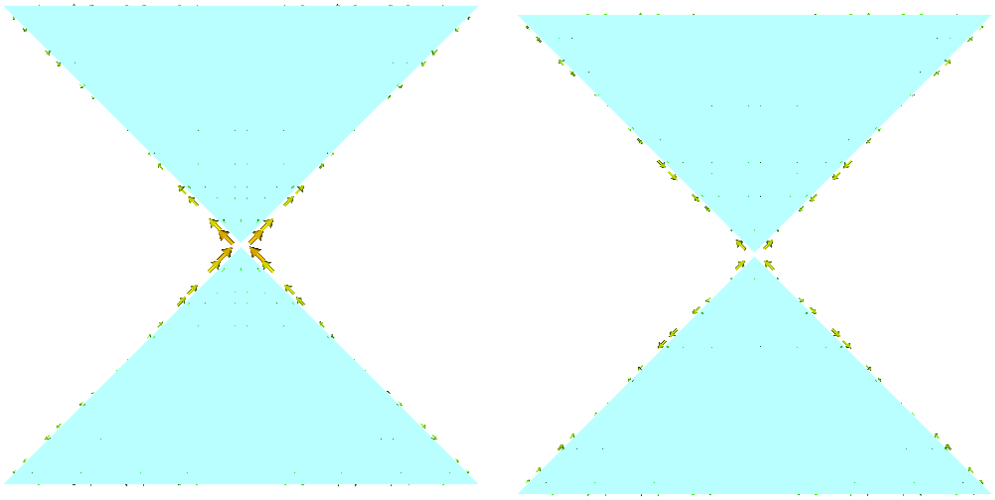

f=4 GHz f=5 GHz

Fig.4.12. Current surface distribution on the bow-tie antenna plane.

For solving the second problem the coplanar stripline geometry must be modified because now we have two strips with a finite ground plane. There are three parameters (strips width, the gap between strips and the strip length) which must be optimized to have impedance matching between microstrip and antenna parts.

Although good impedance matching can be obtained by changing the coplanar stripline, when two antennas are placed next to each other there is a huge coupling between the two systems (Fig.4.13). As it was indicated, it is due to the fact that the major surface current distribution is placed in left and right sides of bow-tie antennas. When these currents are placed next to each other it will produce a current coupling which changes the impedance matching and radiating patterns. For eliminating this destructive coupling the bow-tie antenna geometry must be changed in order to minimize the undesired coupling.

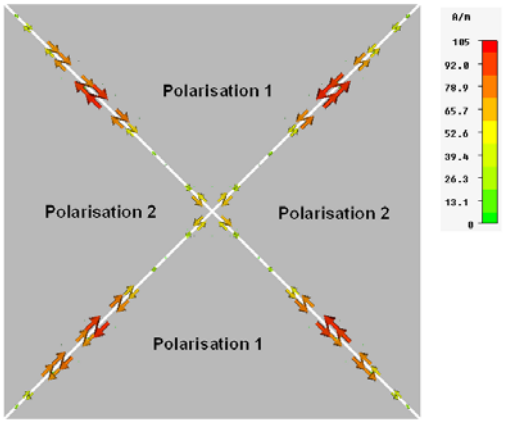

Fig.4.13. Coupling on the edge of the bow-tie antenna configuration in dual polarization mode.

In next section we will continue this procedure and we will propose a new quasi bow-tie to have a good dual polarized radiation.

4.2.2.3.4 Quasi bow-tie architecture instead of Bow-tie

To minimize the coupling between two antenna planes, the below configuration is proposed. First of all the two triangles of each bow-tie antenna are kept at a distance and it has been removed two sides of each triangle. Also as it is shown (Fig.4.14), the ending parts of our optimized triangle are eliminated and are replaced by a rectangular part. Now when the antenna planes with two polarizations are placed next to each other, the ending parts of each triangle will be far from each other. Then this geometry is optimized to have a good impedance matching. Table.III summarizes the quasi bow-tie antenna configuration parameters.

Note that with these changes in the geometry of the antenna, the input impedance was changed and the balun parameters were optimized again. Table.IV summarizes the balun configuration parameters.

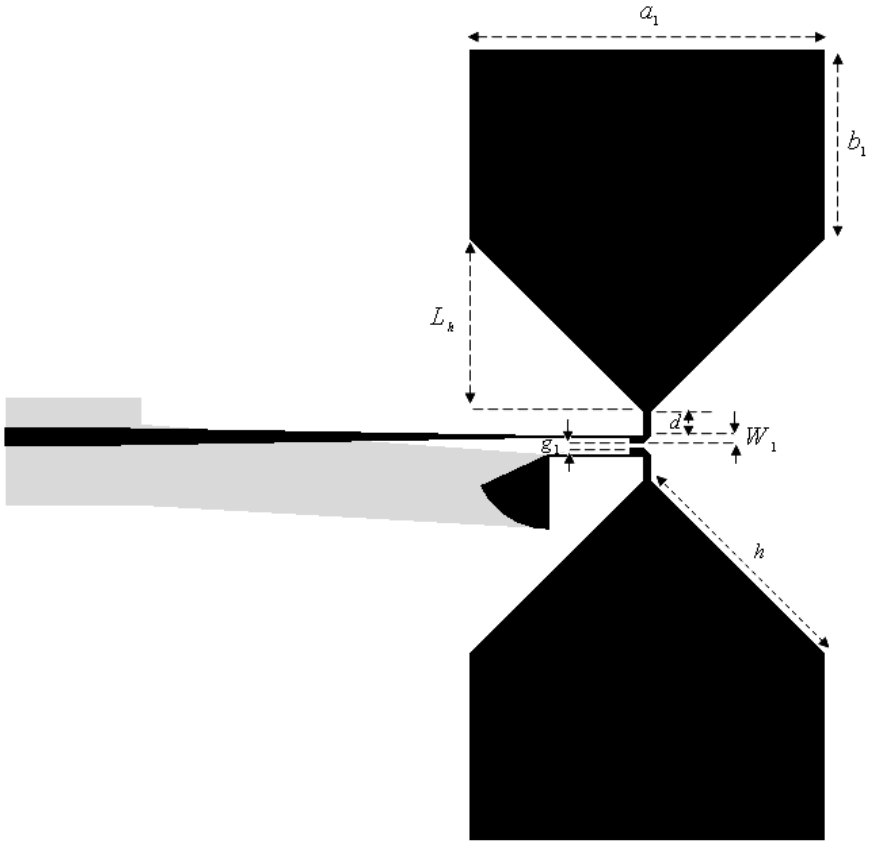

Fig.4.14. Quasi bow-tie antenna connected to the wideband balun configuration in single polarization mode.

Table III. Dimensions of the quasi bow-tie antenna in single polarization. (Unit: Millimeters)

L_1	L_m	L_{CPS}	L_h	W_{gnd}	W_{CPS}	W_m	h	R	θ_h	θ	d
10	40	14.6	38	8	1	1.3	53.74	5.5	90°	65°	1.61

Table IV. DIMENSIONS OF THE TRANSITIONS. (Units: Millimeters)

L_1	L_m	L_{CPS}	W_m	W_{gnd}	W_{CPS}	g	θ	R
10	40	5	1.3	8	0.3	1.275	65°	5.5

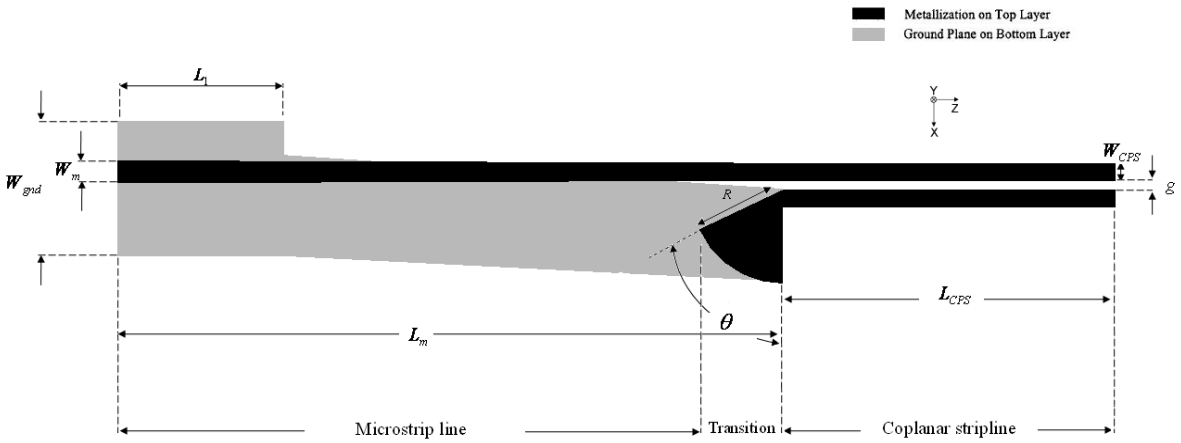

Fig.4.15. The microstrip-to-CPS architecture.

DiClad 880 is used as substrate with a dielectric constant of 2.17 and thickness of 0.762 mm. The simulated return loss of this proposed structure is shown in Fig.4.16. The quasi bow-tie antenna has a simulated bandwidth from 2.8 to 8.7 GHz for a return loss better than -10 dB.

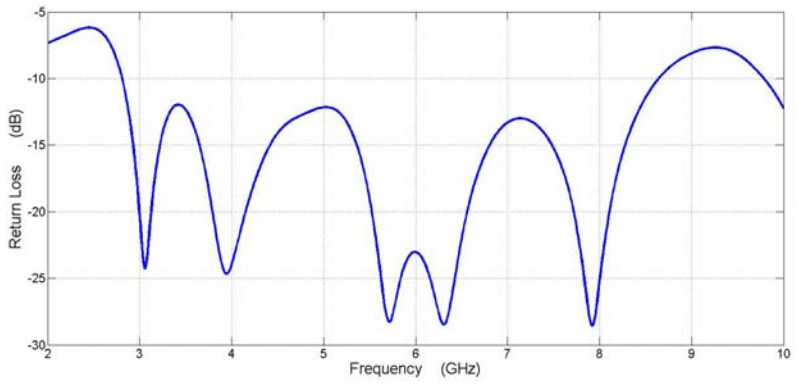

(a)

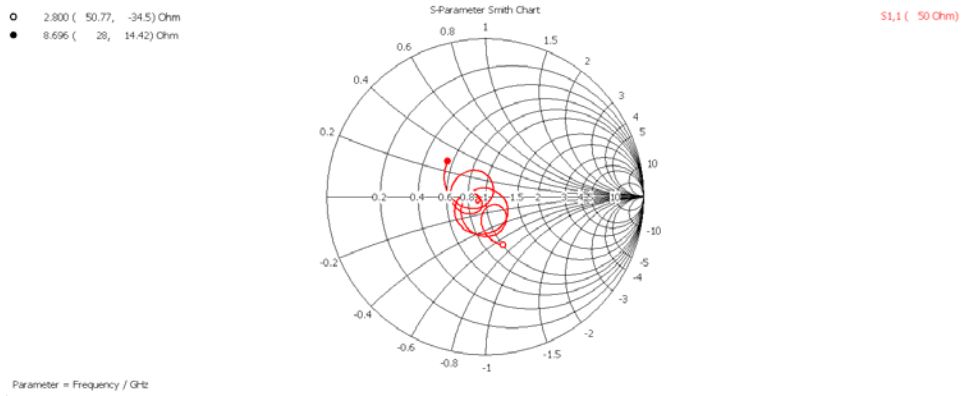

(b)

Fig.4.16. (continued) Simulated (a) return loss and (b) input impedance (normalized at 50 Ω) of the quasi bow-tie antenna.

The overall dimension of the proposed design is 6×6 cm^2 or $0.56\lambda_L \times 0.56\lambda_L \times 0.008\lambda_L$ where λ_L is the wavelength at low frequency (f_L=2.8 GHz). The modification of the bow-tie structure leads to the reduction of dimensions (comparing to $0.8\lambda_L \times 0.7\lambda_L$).

The simulated results shows the surface current distribution for f= 3, 4, 5, 6, 7 and 8 GHz of the quasi bow-tie antenna geometry (Fig.4.17).

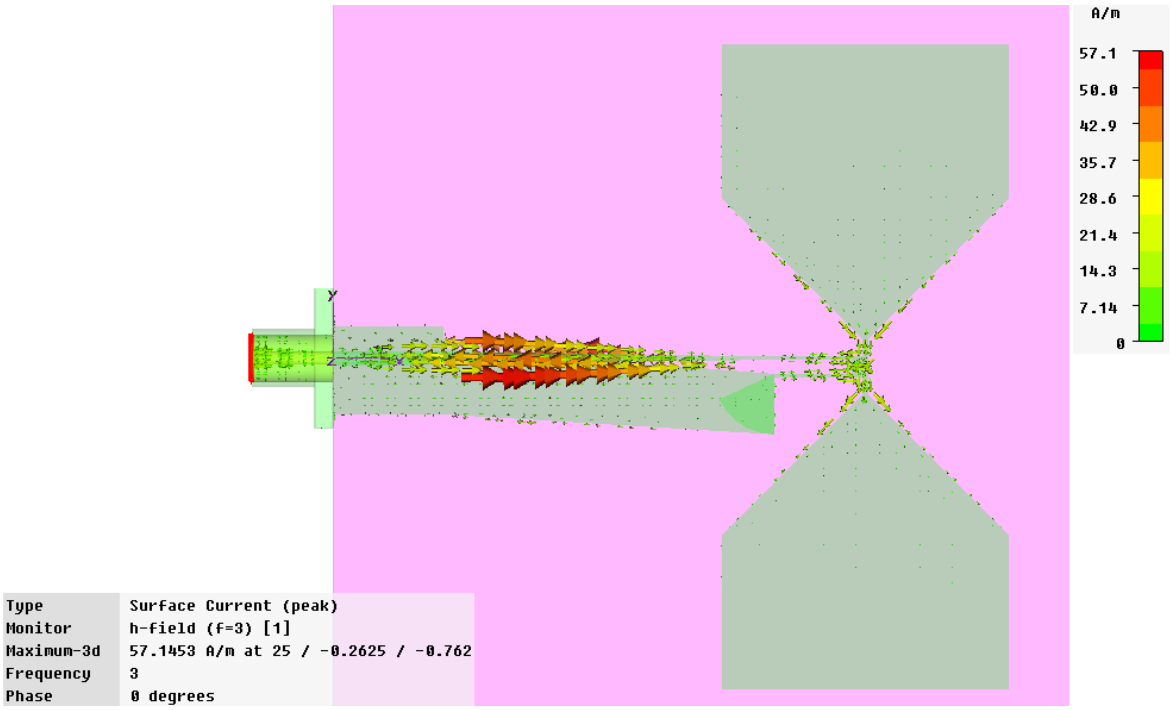

Fig.4.17. Surface Current distribution at 3, 4, 5, 6, 7 and 8 GHz of the quasi bow-tie antenna geometry in single polarization mode.

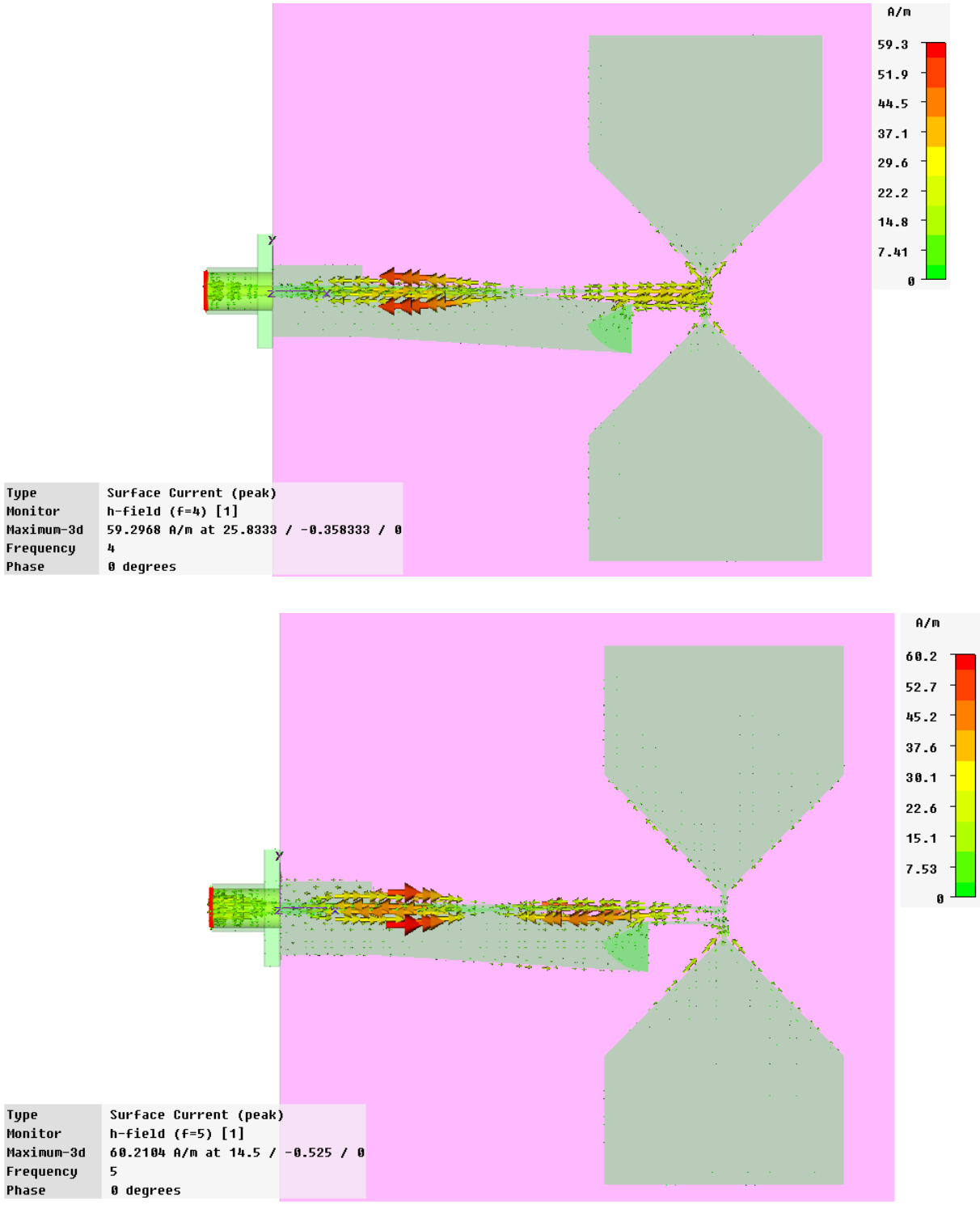

Fig.4.17. (continued) Surface Current distribution at 3, 4, 5, 6, 7 and 8 GHz of the quasi bow-tie antenna geometry in single polarization mode.

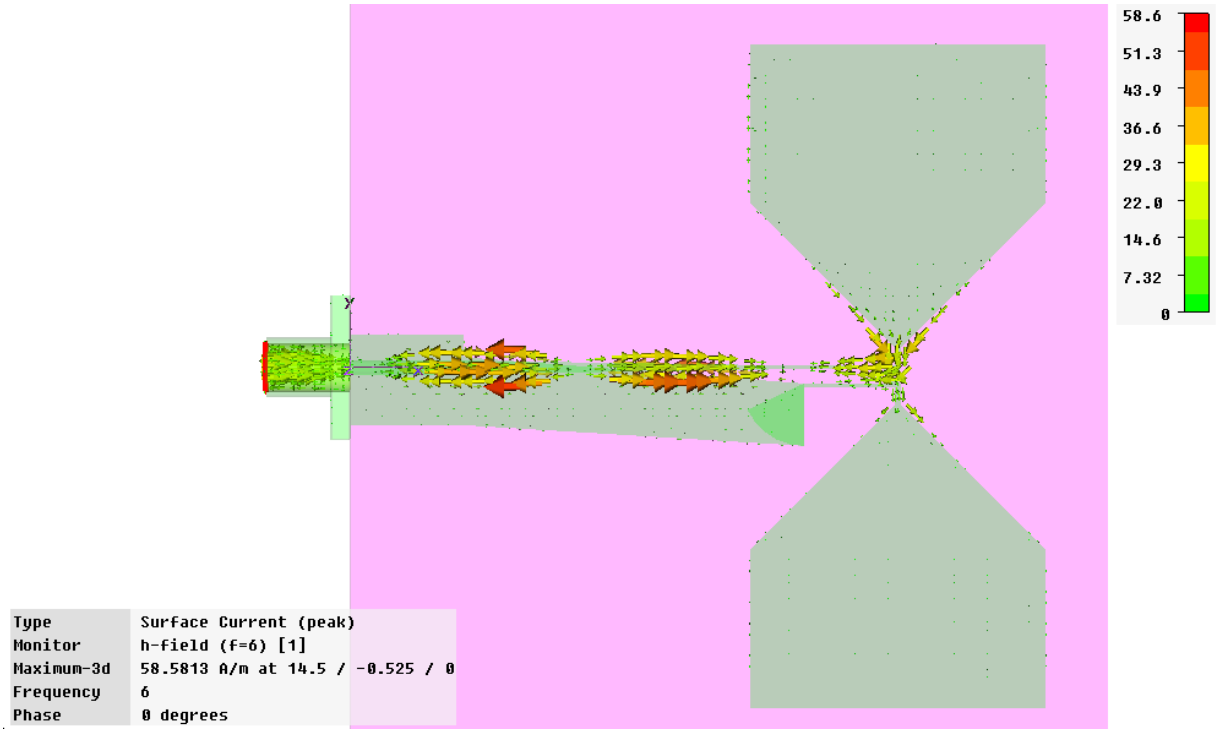

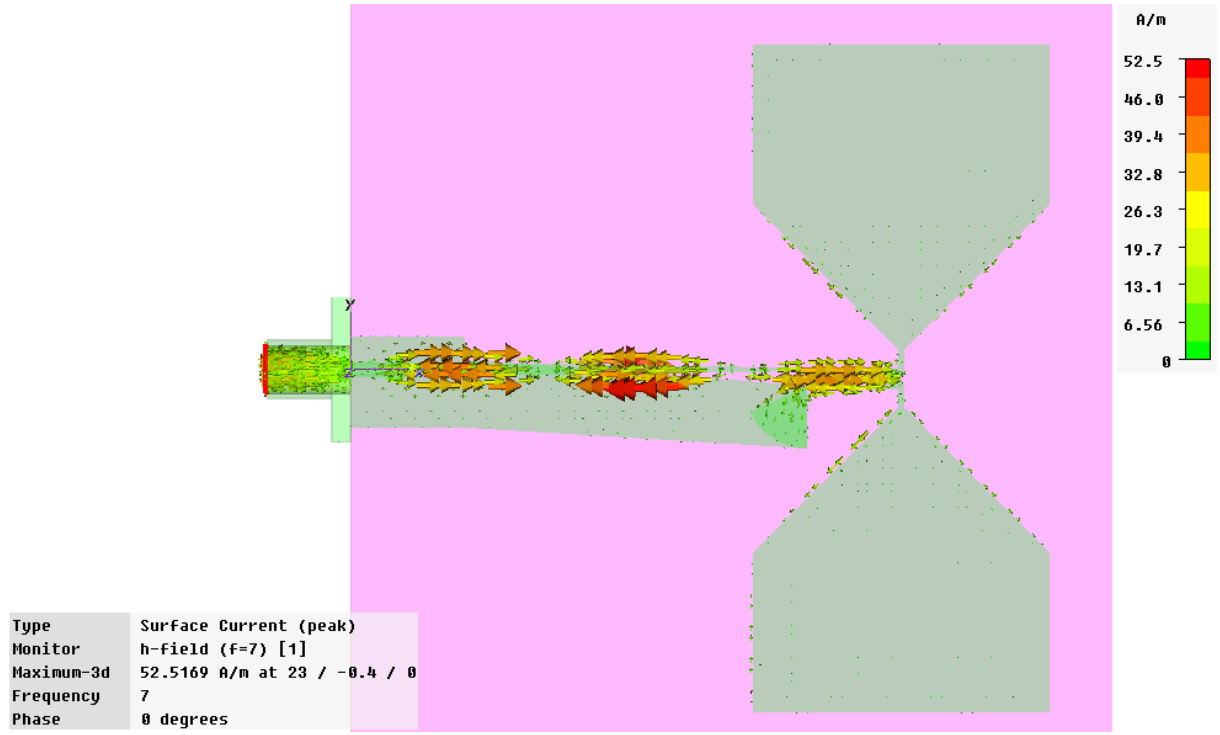

Fig.4.17. (continued) Surface Current distribution at 3, 4, 5, 6, 7 and 8 GHz of the quasi bow-tie antenna geometry in single polarization mode.

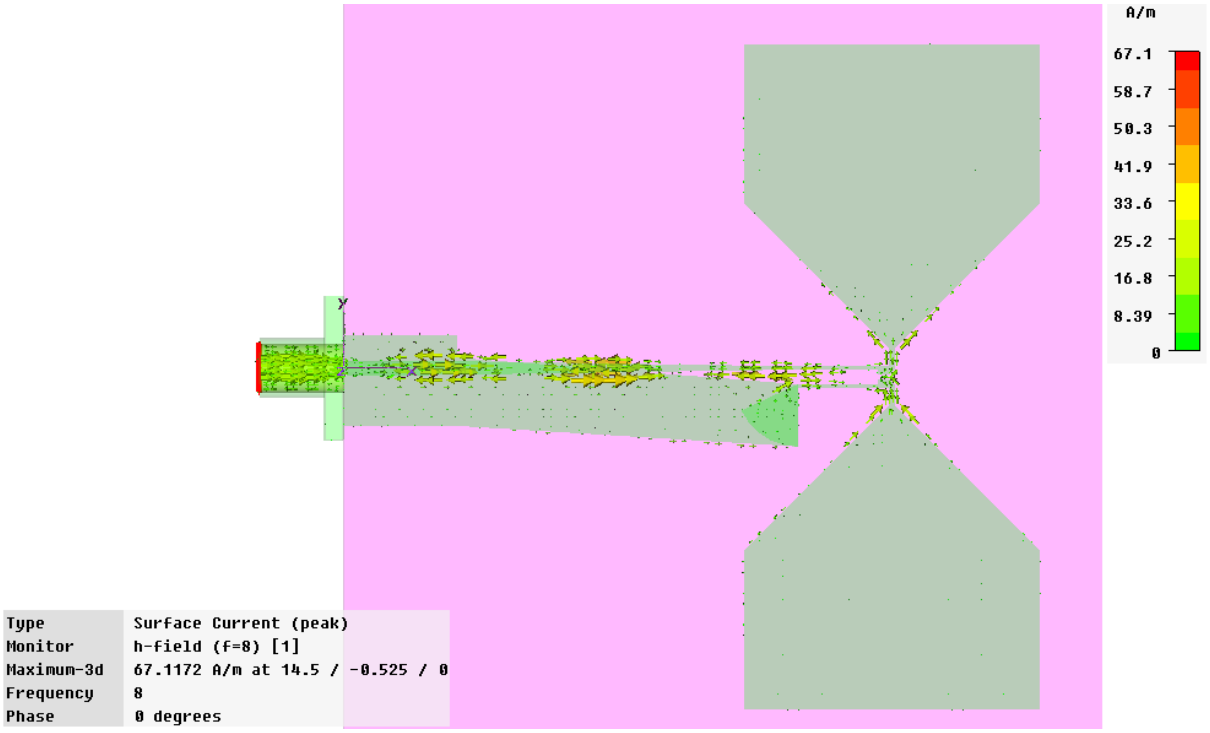

Fig.4.17. (continued) Surface Current distribution at 3, 4, 5, 6, 7 and 8 GHz of the quasi bow-tie antenna geometry in single polarization mode.

- ***Interpretation of the results:***

1. The distributions of surface current on bow-tie regions (two triangles) are almost symmetrical for the antenna frequency bandwidth.

2. As it is expected, the surface currents are placed on the sides of the triangular especially on the right and left sides.

3. The current distributions show the balun feed well in field matching between the coaxial transmission line (unbalanced current distribution) and a balanced bow-tie antenna. As it is shown in these figures, the CPS balun provide the two symmetrical feed points on the balance bow-tie antenna. So the balanced feed in the antenna input port can produce a symmetrical radiation pattern for bow-tie antenna. Fig.4.18 and 4.19 show the simulated directivity radiation patterns of the proposed quasi bow-tie antenna design in its frequency bandwidth for H- and E-plane. The definition of H-plane and E-plane is shown in Fig.4.8.

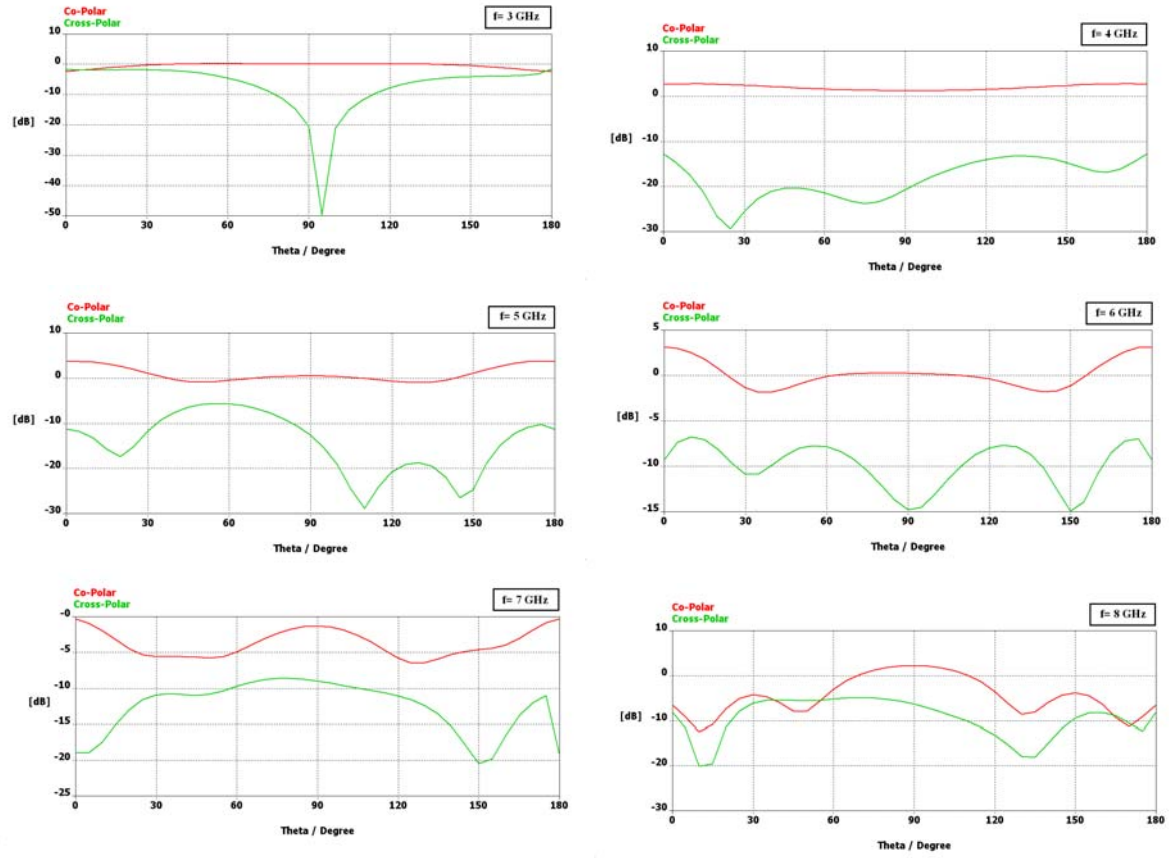

Fig.4.18. H-plane ($\phi = 0^{\circ}$) directivity radiation patterns at 3, 4, 5, 6, 7 and 8 GHz of the quasi bow-tie antenna geometry in single polarization mode.

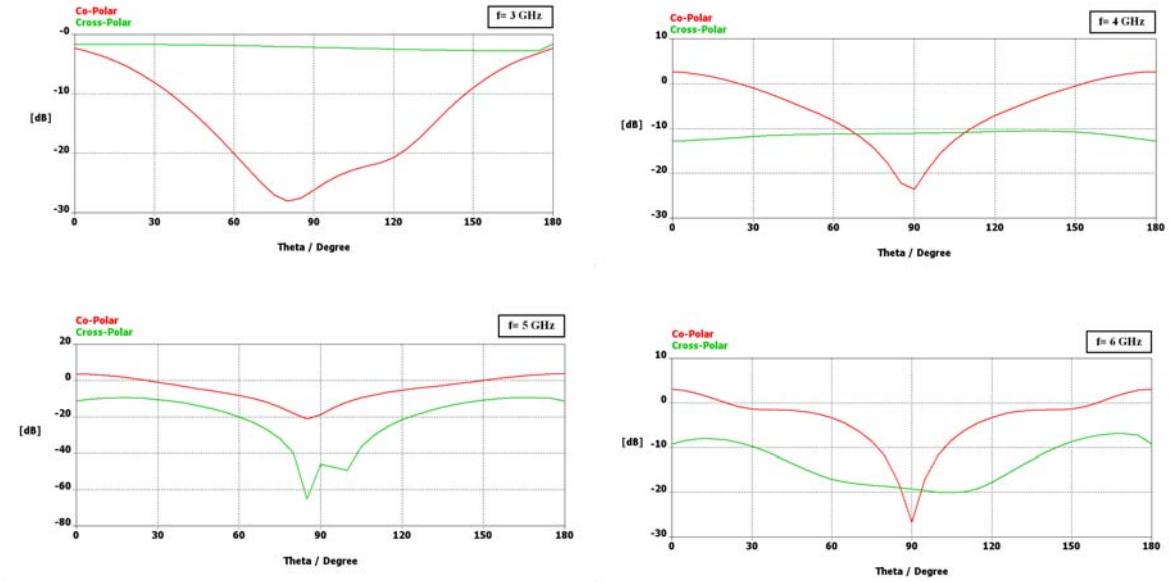

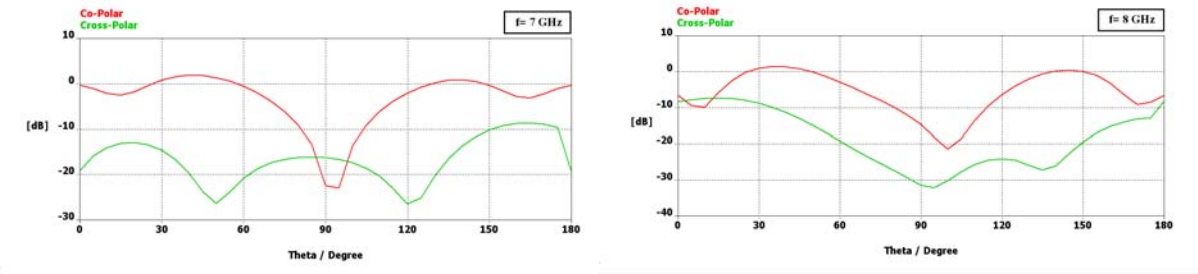

Fig.4.19. E-plane ($\phi = 90^{\circ}$) directivity radiation patterns at 3, 4, 5, 6, 7 and 8 GHz of the quasi bow-tie antenna geometry in single polarization mode.

As it is shown in Fig.4.18 and Fig.4.19, H-plane and E-plane radiation patterns are symmetrical. Also there are differences of at least 10 dB between co-polar and cross polar component except in 3 GHz (for H- and E-plane) where the difference between the two components is less than 10 dB around 0° (and 180°) and in 8 GHz (for H-plane) where the difference between the two component is less than 10 dB around 30° and 60° (and 180°). Also, HPBW (Half-Power Beamwidth) in H- and E-planes are presented in Table.V. Also the radiation patterns show that the bow-tie has quasi omnidirectional dipole-type patterns.

Table.V. HPBW in H- and E-planes for a single polarization quasi bow-tie antenna.

Frequency (GHz)	HPBW H-Plane (°)	HPBW E-Plane (°)
3	30	20
4	60	28
5	30	24
6	24	21
7	50	41
8	48	33

Table.V shows that HPBW in H- and E-planes has some small variations.

The simulated antenna gain has been shown in Fig.4.20. The quasi bow-tie antenna gain shows that the gain oscillates from 2.1 to 4.5 dB between 3 GHz and 8 GHz. Also Fig.4.20 shows that the quasi antenna gain has a peak in its curve in 5 GHz like the classic bow-tie antenna (Fig.4.11).

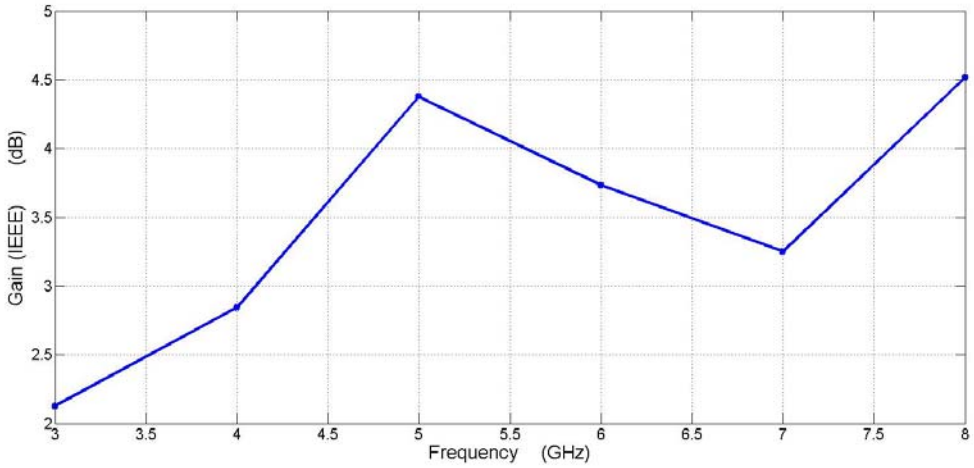

Fig.4.20. Simulated gain of the quasi bow-tie antenna in single polarization.

Consideration of the parameters of return loss, radiation pattern and gain shows that the bow-tie antenna operates well in frequency band from 2.8 to 8.7 GHz and it is a good candidate for next stage to achieve a wideband dual polarization bow-tie antenna.

4.2.2.3.5 Dual polarized bow-tie antenna configuration

The single polarized quasi bow-tie antenna was proposed in previous section. Now we present a dual polarized antenna configuration which is composed of two simple polarized quasi bow-tie antennas with a 90 degree difference on two sides of one substrate. The antenna design is illustrated in Fig.4.21.

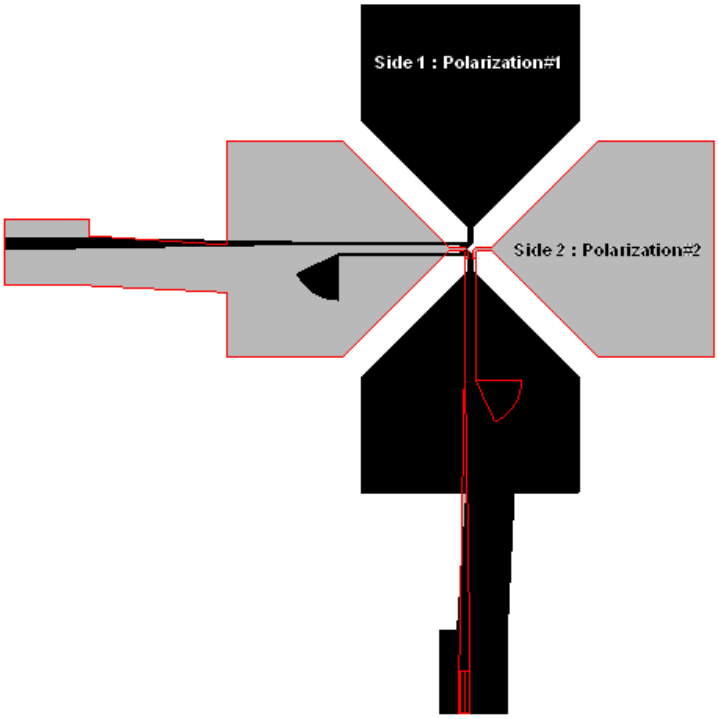

Fig.4.21. Quasi bow-tie antenna connected to the wideband balun configuration in dual polarization mode.

The top, bottom and perspective views of the fabricated antenna are shown in Fig.4.22.

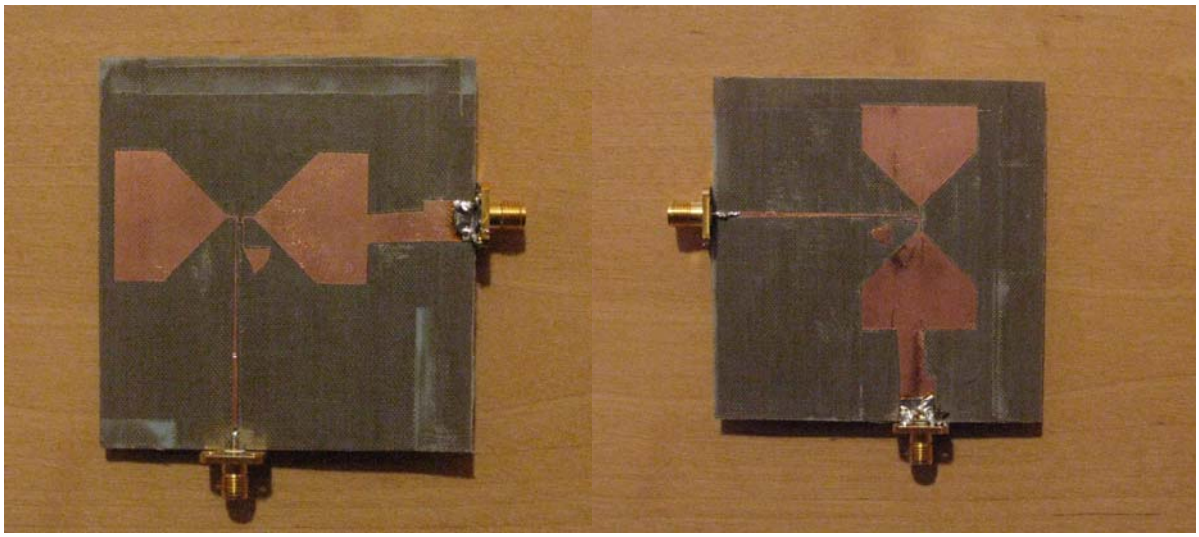

(a)

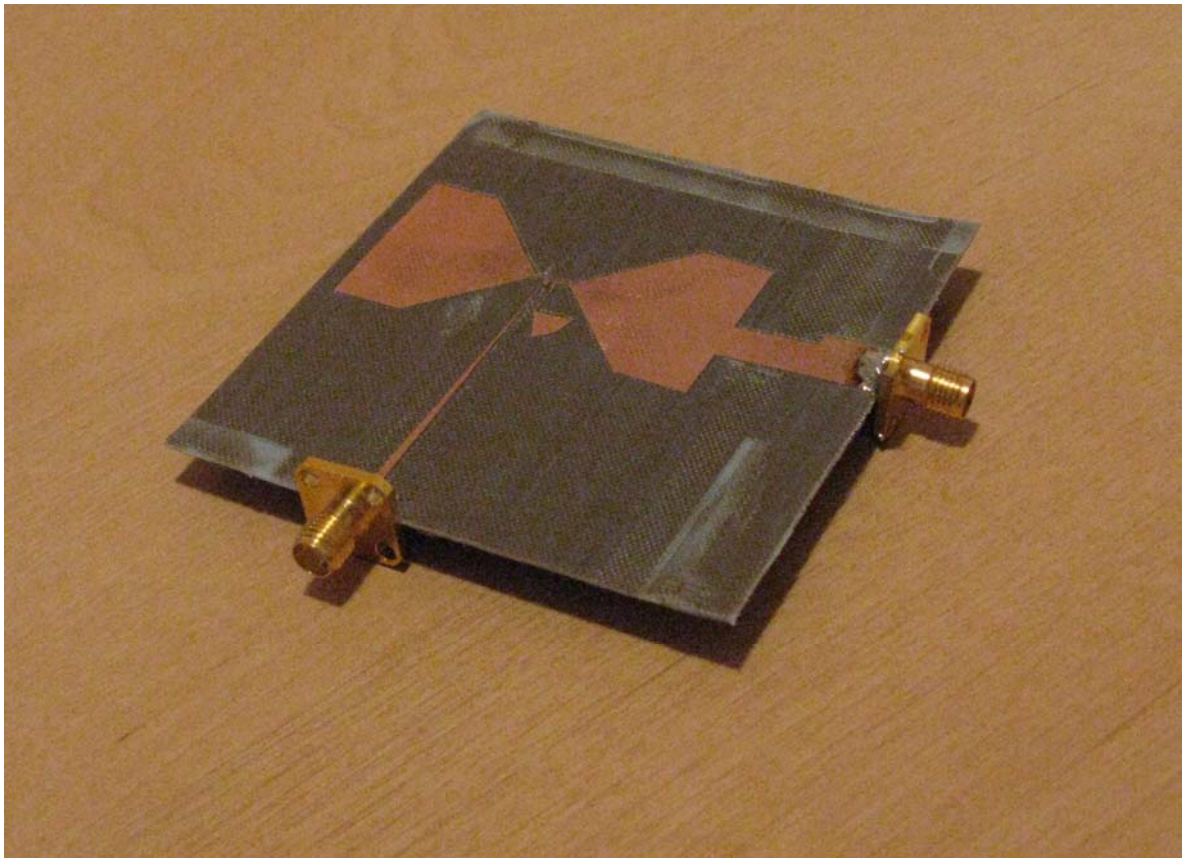

(b)

Fig.4.22. (a) Top and bottom and (b) perspective views of dual polarized quasi bow-tie antenna.

DiClad 880 is used as the substrate with a dielectric constant of 2.17 and thickness of 0.762 mm. The measured and simulation return losses of this proposed structure is shown in Fig.4.23 and Fig.4.24. As it is shown in Fig.4.23 (a), a -10 dB measured return loss bandwidth from 5.4 GHz to 12 GHz is obtained (BW=6.6 GHz) and the agreement between the measurement and simulation is good.

Also it is shown that the measured and simulation insertion losses (S_{21}) is inferior to 10 dB from 2.3 GHz (measurement) in Fig.4.23 (b). The insertion loss shows the decoupling between two structures in the frequency bandwidth.

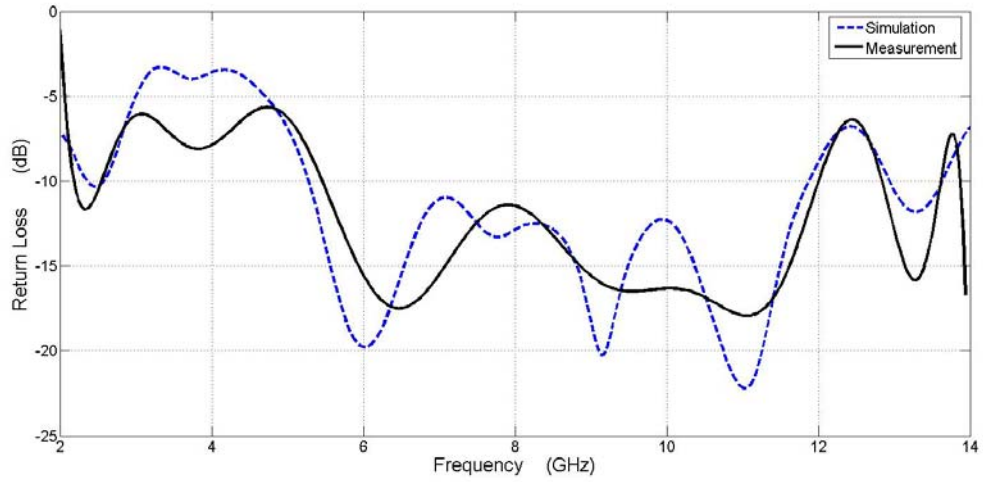

(a)

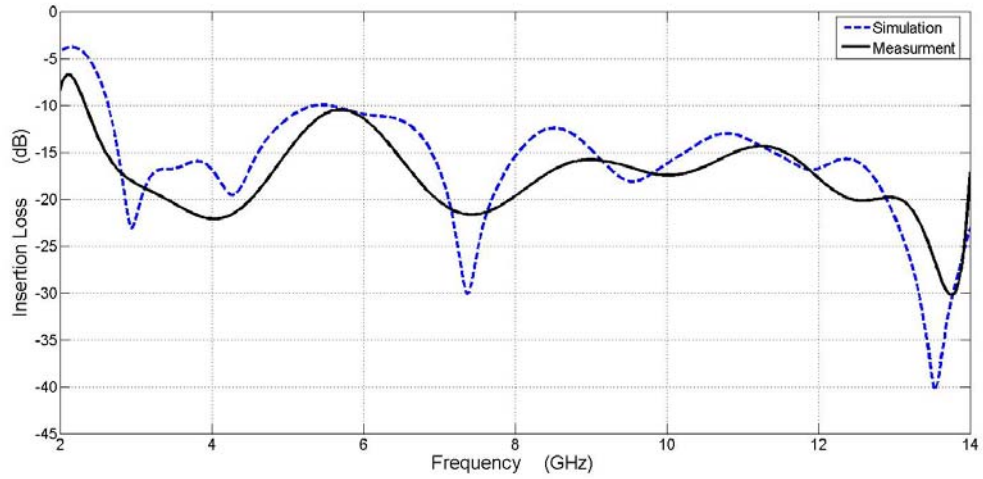

(b)

Fig.4.23. Measured and simulated (a) return loss and (b) insertion loss of the dual polarized quasi bow-tie antenna (normalized at 50 Ω).

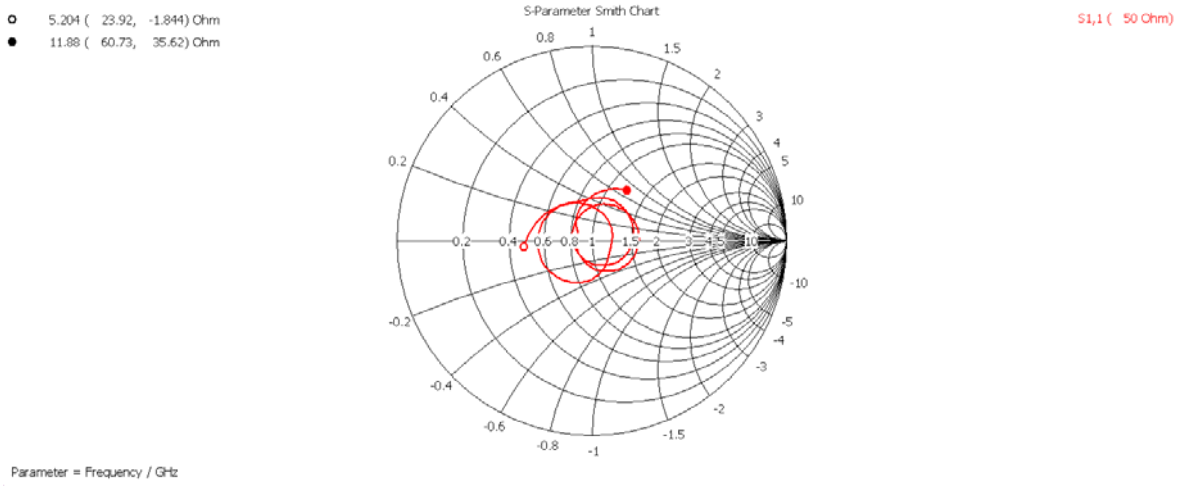

Fig.4.24. Simulated input impedance of the dual polarized quasi bow-tie antenna (normalized at 50 Ω).

The whole dual polarized system is implemented on just one substrate with dimensions 6×6 cm^2 or $1.1\lambda_L \times 1.1\lambda_L \times 0.015\lambda_L$ where λ_L is the wavelength at low frequency (f_L=5.2 GHz). Fig.4.24 and Fig.4.25 show the simulated directivity radiation patterns for H- and E-planes of the dual polarized structure at 5, 6, 7, 8, 9, 10 and 11 GHz, respectively. The definition of H-plane and E-plane was shown in Fig.4.8.

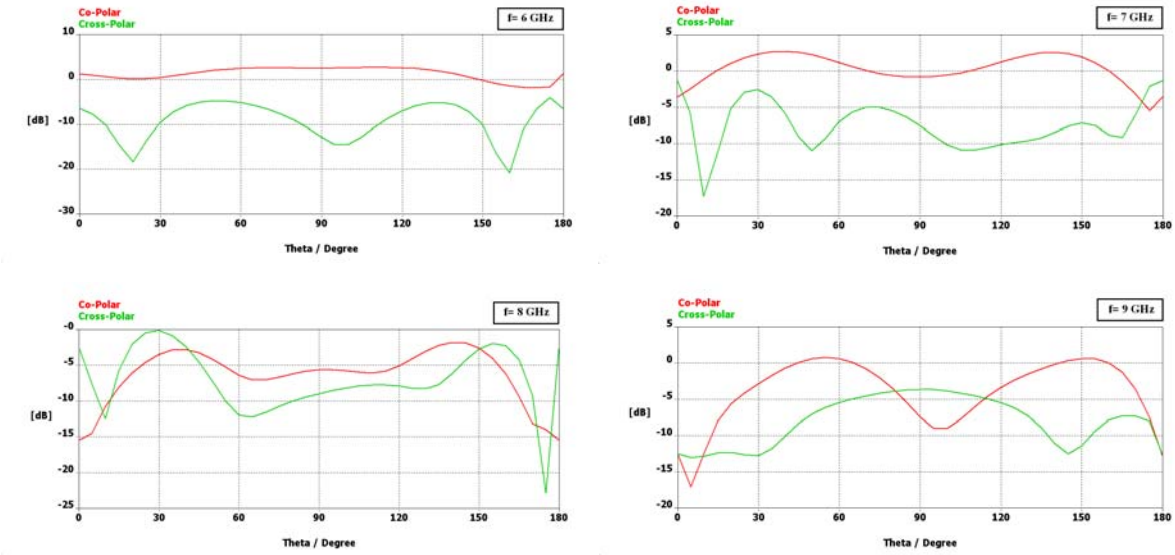

Fig.4.25. H-plane ($\phi = 0^\circ$) directivity radiation patterns at 6, 7, 8, 9, 10 and 11 GHz of the quasi bow-tie antenna geometry in dual polarization (Polarization1).

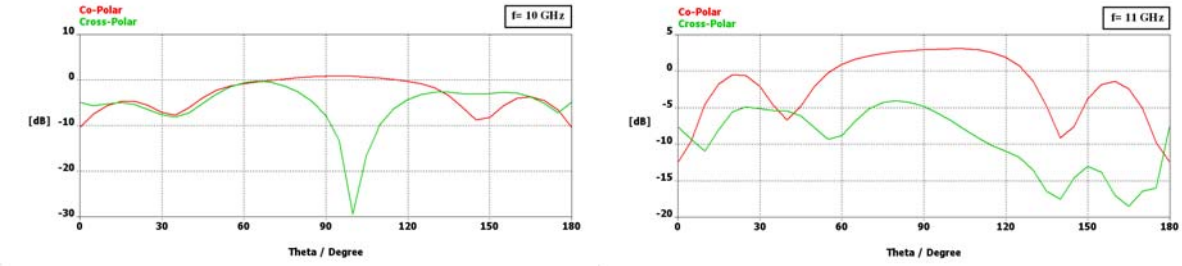

Fig.4.25. (continued) H-plane ($\phi = 0^{\circ}$) directivity radiation patterns at 6, 7, 8, 9, 10 and 11 GHz of the quasi bow-tie antenna geometry in dual polarization (Polarization1).

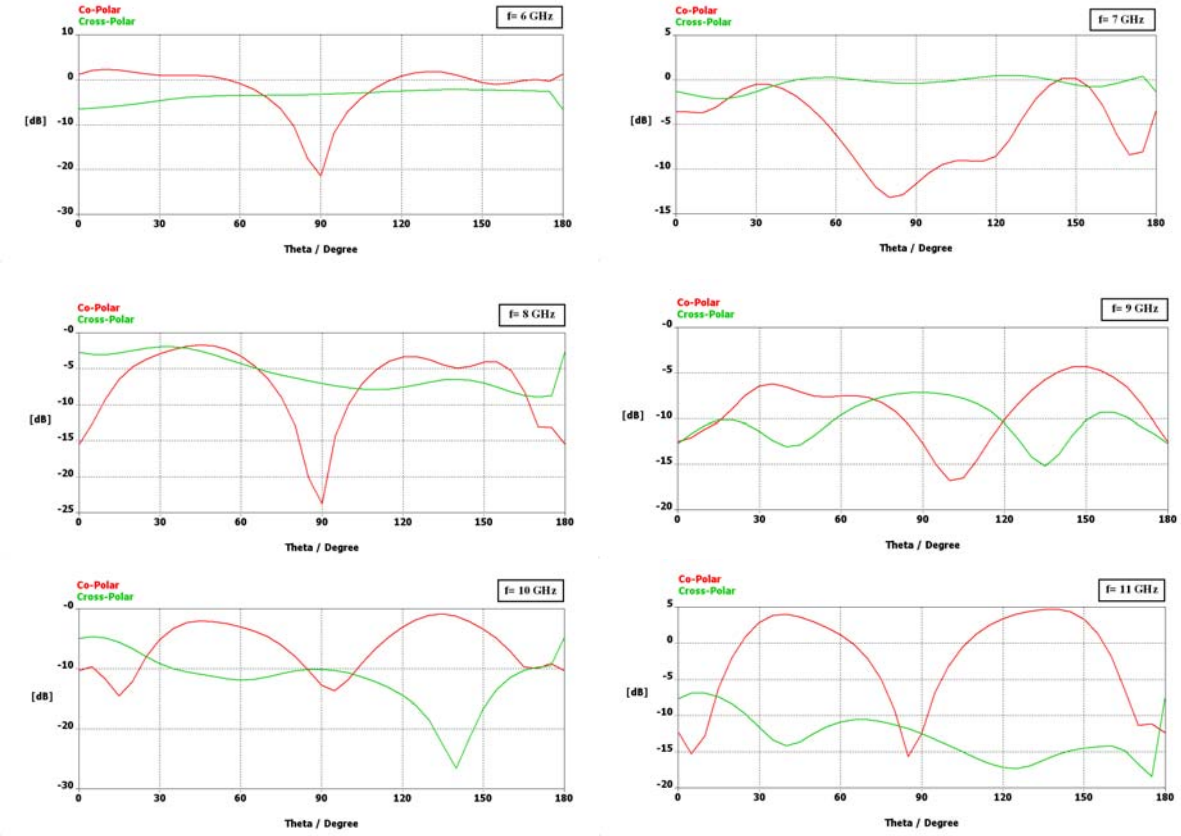

Fig.4.26. E-plane ($\phi = 90^{\circ}$) directivity radiation patterns at 6, 7, 8, 9, 10 and 11 GHz of the quasi bow-tie antenna geometry in dual polarization (Polarization1).

As it is shown in Fig.4.25 and Fig.4.26, H-plane and E-plane radiation patterns are about symmetric. It shows that the new quasi bow-tie antenna has dual polarization characteristics. These figures show only the simulation results of the first port (polarization 1) and the other one has identical characteristics. The antenna HPBW (Half-Power Beamwidth) values in H- and E-planes are presented in Table.VI.

Table.VI. HPBW in H- and E-planes for a dual polarization quasi bow-tie antenna.

Frequency (GHz)	HPBW H-Plane (°)	HPBW E-Plane (°)
6	128	66
7	72	33
8	37.5	46
9	40.5	40
10	76	36
11	70	43.5

In f=6 GHz, HPBW for H-plane is 128 ° and the directivity radiation pattern for dual polarization bow-tie is wide and it is not so interesting but, for f > 6 GHZ, Table.VI shows that HPBW in H-plane has almost small variations. Also it can be observed that HPBW in E-plane has small variations in its frequency band entire. Unfortunately the radiation patterns have not been validated experimentally because of the lack of time. The simulated antenna gain is shown in Fig.4.27. The quasi bow-tie antenna gain shows that the gain oscillates from 4.7 to 7 dB between 5 GHz and 11 GHz.

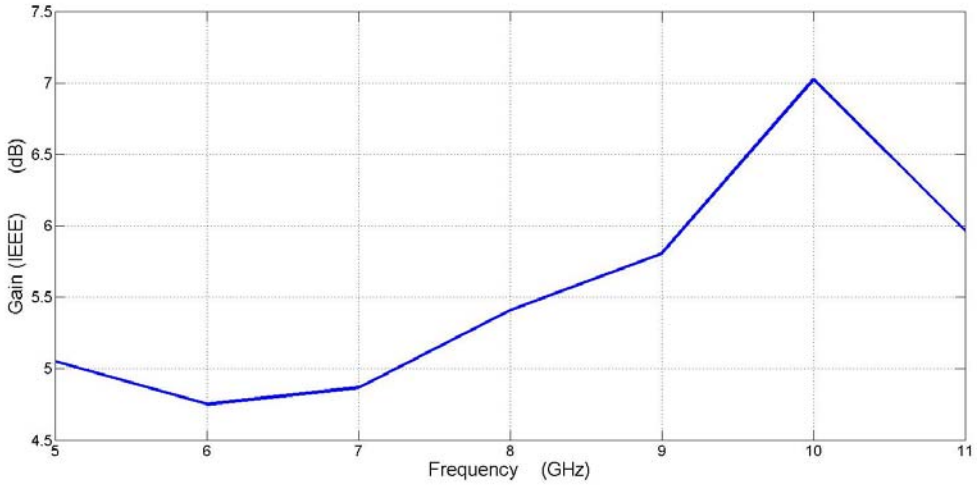

Fig.4.27. Simulated gain of the quasi bow-tie antenna in dual polarization.

4.2.4 Conclusion

In this section a UWB dual polarized quasi bow-tie antenna has been designed and fabricated in a compact geometry with overall dimensions of $1.1\lambda_L \times 1.1\lambda_L \times 0.015\lambda_L$. The antenna configuration is integrated with a microstrip-to-CPS form with UWB characteristics. An investigation is carried out to find out a compact form with dual characteristic in wideband bandwidth without destructive coupling between the two structures.

Simulation and measurement results of the return loss were presented and a wideband bandwidth for bow-tie antenna was achieved in dual polarization. Also, in measured frequency bandwidth (5.4 GHz to 12 GHz), the directivity radiation patterns were almost symmetric in E- and H-plane and thus, the antenna radiates well in its frequency bandwidth.

4.3 A New Integrated CPS-fed Sinuous Dual Polarized Antenna

4.3.1 Introduction

In chapter 2, it was introduced a sinuous antenna configuration with simple polarization characteristics and for its feeding system, a microstrip balun was proposed and the antenna and balun planes were orthogonal.

It was explained that the sinuous geometry has wideband characteristic and it is a good candidate to use in UWB applications. Although that sinuous slot antenna had wideband characteristic, the structure was voluminous and the antenna had only simple polarization. Now in this chapter, an integrated antenna geometry with wideband and dual polarization characteristics is proposed.

Also we use the developed wideband balun (90° bended microstrip-to-CPS) proposed in chapter 3 to feed the sinuous antenna configuration.

4.3.2 Using Microstrip-to-CPS Balun as a Wideband Antenna Feeding System for Sinuous Antenna

4.3.2.1 Introduction

Using the balun integrated form to feed DuHamel's sinuous antenna (with 4 arms) is not possible because these antennas are in center-fed form and the feeding systems position always is orthogonal to the antenna plane.

The design idea in this section is to use a two arms form of sinuous antenna. But to have a dual polarization we have two planes very close to each other for each polarization (with a 90 degree rotation). Also for each sinuous antenna plane an integrated wideband balun must be designed separately.

3.2.2 Modeling of the Connection of Balun and Sinuous Antenna

A version of sinuous antenna with two arms (and not 4 arms sinuous antenna) was introduced in chapter 3. In this chapter we want to use the same configuration. Microstrip sinuous antennas have two metal arms and it can be a suitable geometry to be fed by a microstrip-to-CPS balun. In the other hand this type of balun has two balanced coplanar striplines and the microstrip form of sinuous antenna has two arms so they can simply connect to each other (Fig.4.28).

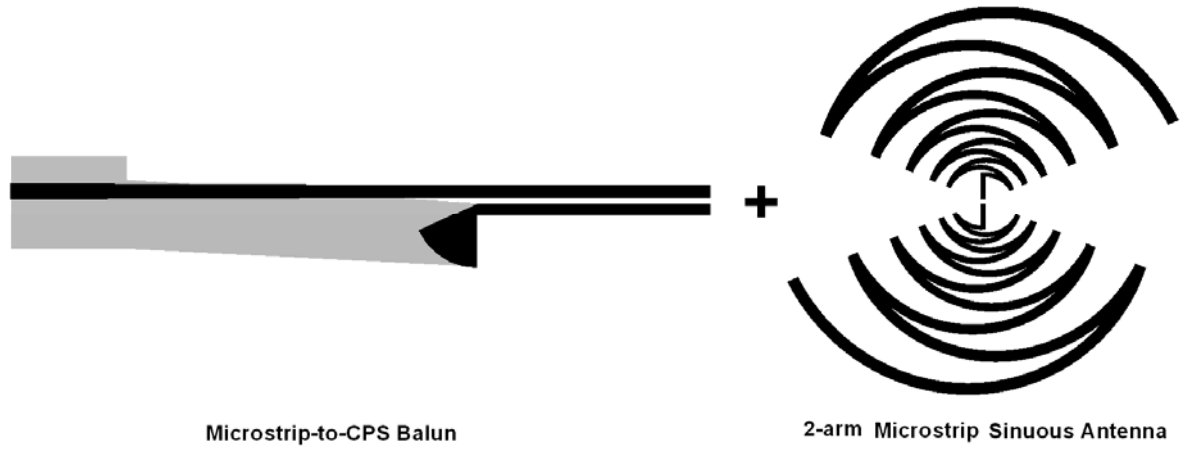

Fig.4.28. Modeling of the Connection of Balun and Sinuous Antenna.

To have a good antenna performance, first of all the sinuous antenna geometry should be optimized with the best wideband impedance matching. In next stage, a microstrip-to-CPS balun for impedance matching between 50 Ω and our desired antenna input impedance is optimized.

4.3.2.3 Optimization of a Microstrip Sinuous Antenna

The geometry of the microstrip sinuous antenna is shown in Fig.4.29, where each arm of sinuous antenna is contained in an area defined by α_0 . As it is indicated in chapter 2, it is done by rotating a single zigzag line clockwise and counterclockwise α_0 degrees about the origin and for a single polarized antenna there only two arms. The feeding region is constructed by two strips as it is shown in Fig.4.29.

The antenna geometry is optimized to obtain the best impedance matching. The antenna geometry parameters are the same as proposed in chapter 2 except the parameter g which is equal to 0.6 mm.

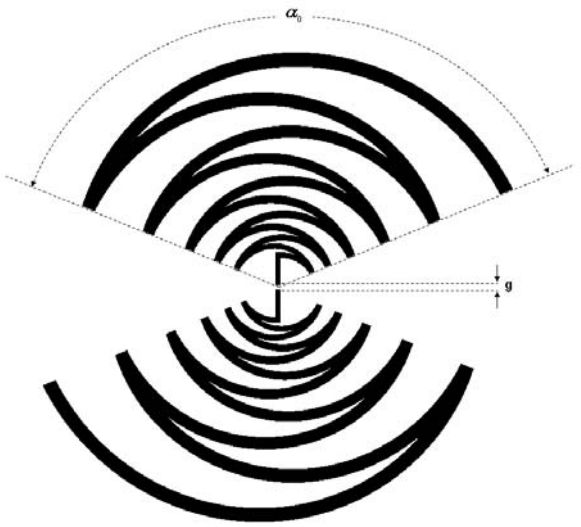

Fig.4.29. Sinuous antenna geometry.

For the simulation of this antenna structure, a delta gap voltage source is considered (discrete port in CST Studio suite) between two strips in antenna center. The simulated results of the return loss are illustrated in Fig.4.30 (in chapter 3, this simulation has been obtained in section 3.3.4.2). As it is shown a 10 dB return loss bandwidth from 2.2 GHz to 8.5 GHz is obtained. The return loss is normalized by R=160 Ohms and it means that the input impedance is considered close to R=160 Ohms in antenna frequency bandwidth.

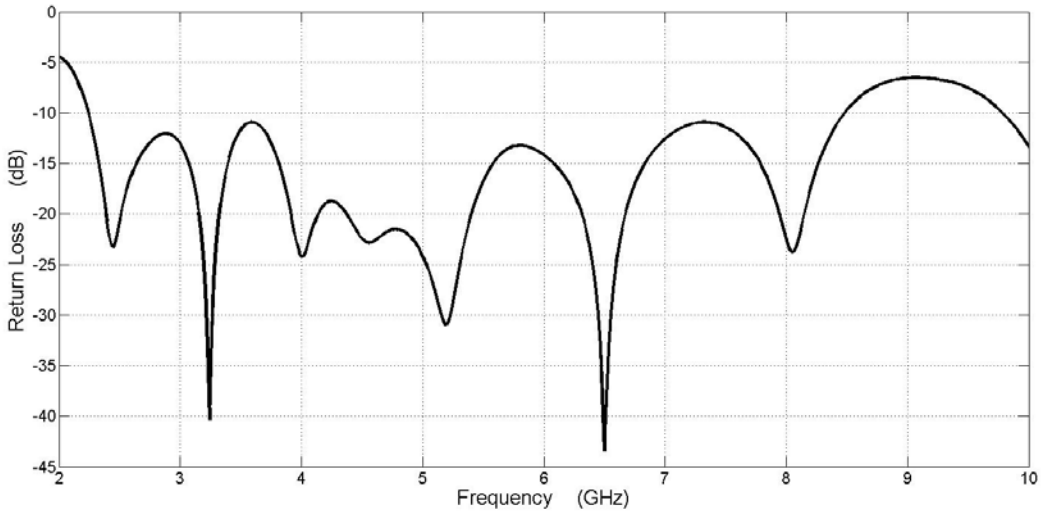

(a)

Fig.4.30. Simulated (a) return loss and (b) input impedance (normalized at 160 Ω).

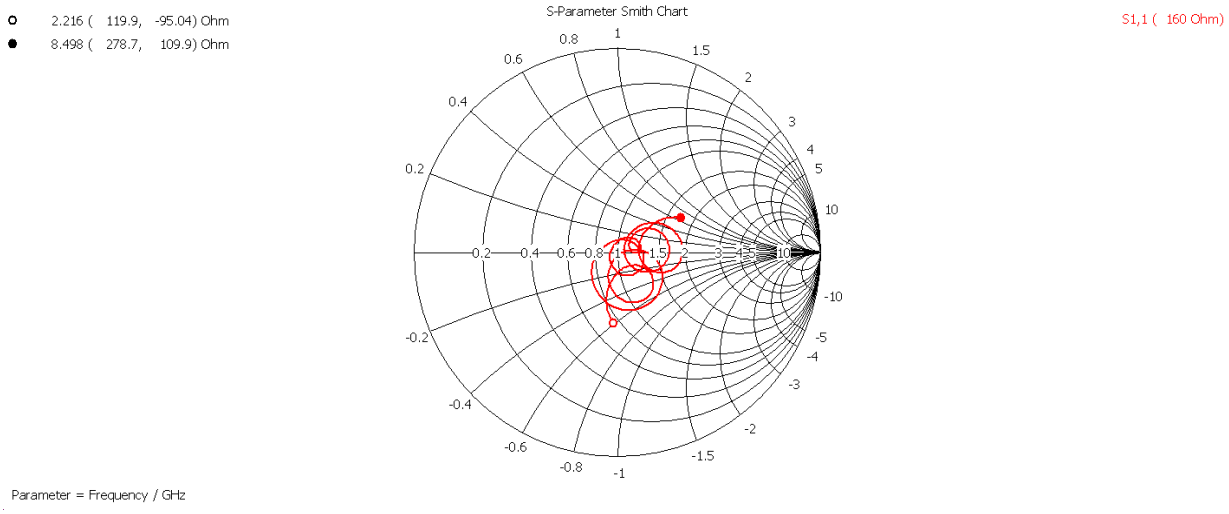

(b)

Fig.4.30. (continued) Simulated (a) return loss and (b) input impedance (normalized at 160 Ω).

Therefore, in the next step we design an integrated compact balun for wideband impedance transformation from 50 Ω to 160 Ω.

4.3.2.4 Microstrip-to-CPS Balun as a Wideband Antenna Feeding System for Sinuous Antenna

In section 3.3 (chapter 3) a new microstrip-to-CPS bended balun with wideband nature was proposed. Now this geometry is optimized in order to be used as a feeding system for microstrip sinuous antenna optimized in previous section. The antenna input impedance was 160 Ω and dimension of this balun is optimized to achieve an impedance transformation from 50 Ω to 160 Ω.

Fig.4.31 shows this transformer configuration and the Table.VII summarizes all parameters of the balun. The balun was fabricated on a DiClad 880 substrate. h is the thickness of the substrate (DiClad 880) and the substrate permittivity is 2.17 with tanδ=0.0009.

Table.VII. DIMENSIONS OF THE TRANSITIONS. (Unit : Millimeters)

L_1	L_2	L_3	L_{CPS}	W_{gnd}	W_m	W_{CPS}	g	R	θ
10	27.46	11.45	20	8	1.3	0.52	0.6	5.5	65°

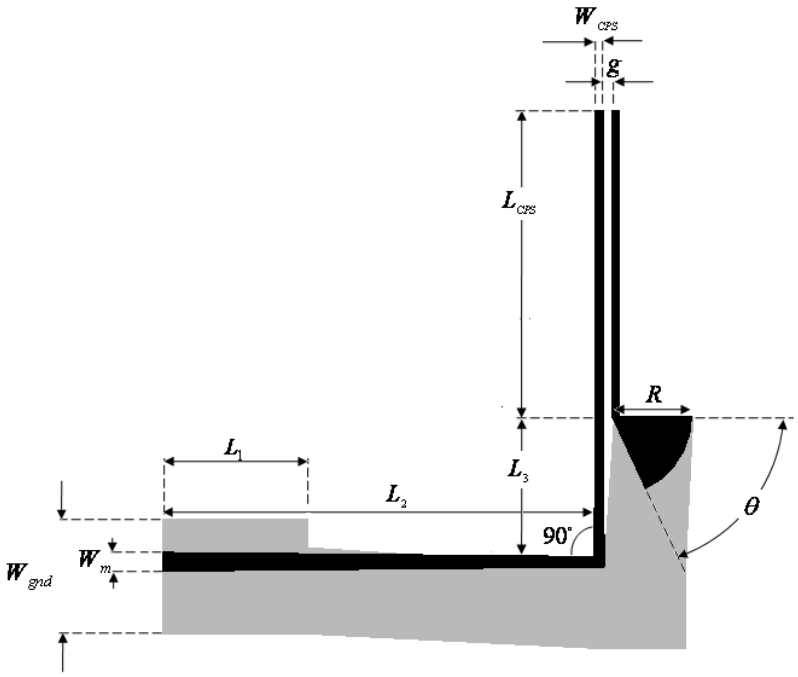

Fig.4.31. 90° bended microstrip-to-CPS balun configuration.

This balun has been simulated with a load of 160 Ω connected to the coplanar stripline. The other port has a 50 Ω SMA connector. The -10 dB simulated bandwidth is between 1.2 GHz and 18.4 GHz (Fig.4.32).

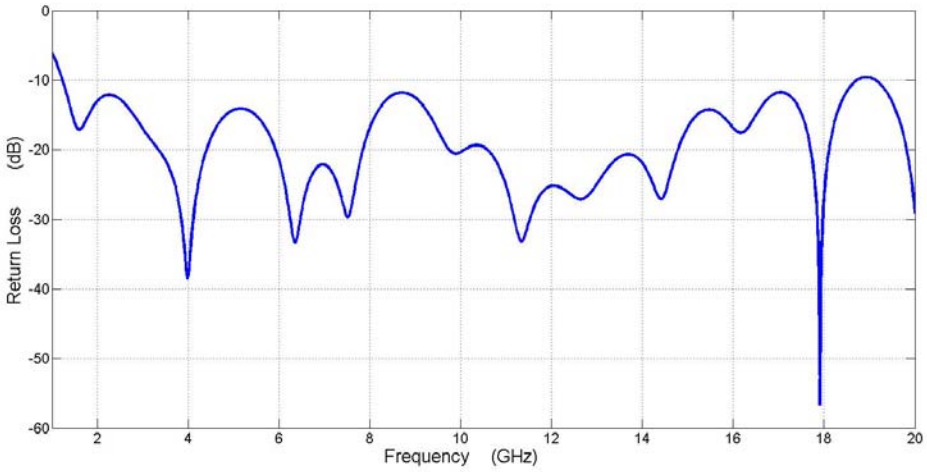

(a)

Fig.4.32. Simulated (a) return loss and (b) input impedance (normalized at 50 Ω).

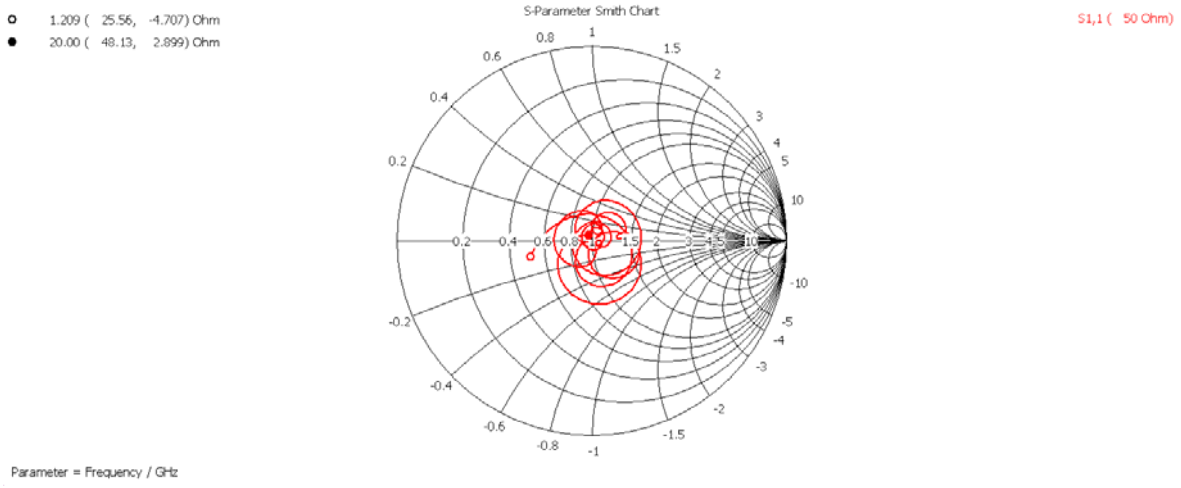

Fig.4.32. (continued) Simulated (a) return loss and (b) input impedance (normalized at 50 Ω).

As it was indicated in chapter 3, the balun designers are commonly interested in the study of back-to-back configurations because of several reasons: They can easily fabricate the balun and measure the return loss and insertion loss without the necessity of loads. Also it is possible to validate the convenience of the 180° phase difference.

The structure of back-to-back CPS-to-microstrip transition is illustrated in Fig.4.33.

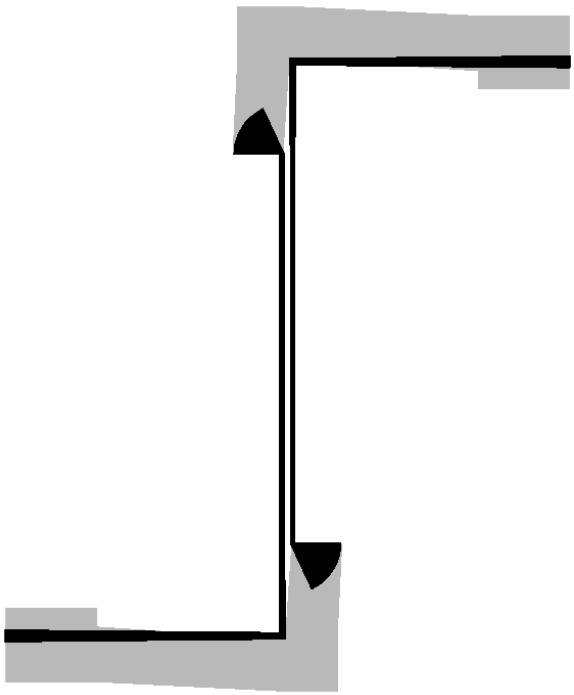

Fig.4.33. CPS balun in back-to-back configuration.

Simulated return loss and insertion loss (S_{11} and S_{21}) for the back-to-back configuration is shown in Fig.4.34. This Figure shows that the transmission property of this circuit is S_{21}>-2 dB for frequencies from 3.4 GHz to 8 GHz. The return loss is better than -10 dB for frequencies from 3.1 GHz to 10.7 GHz (Fig.4.34).

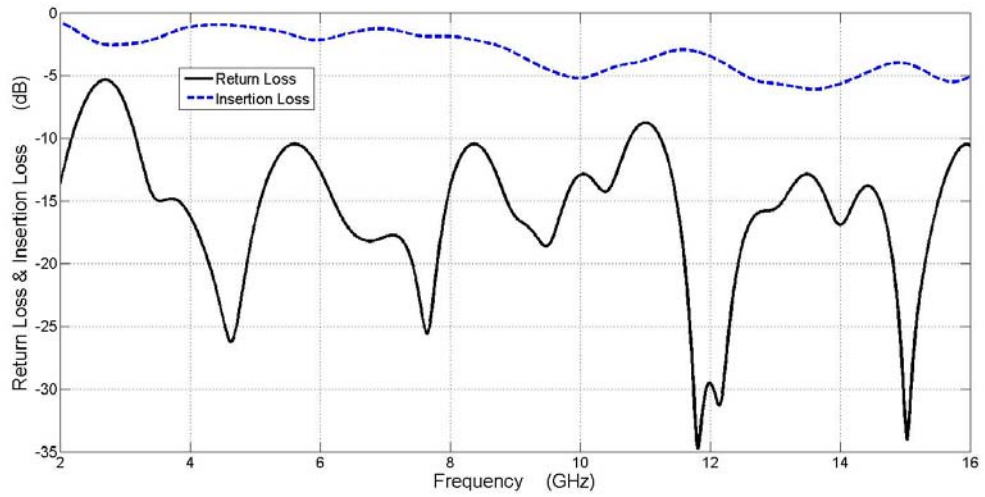

(a)

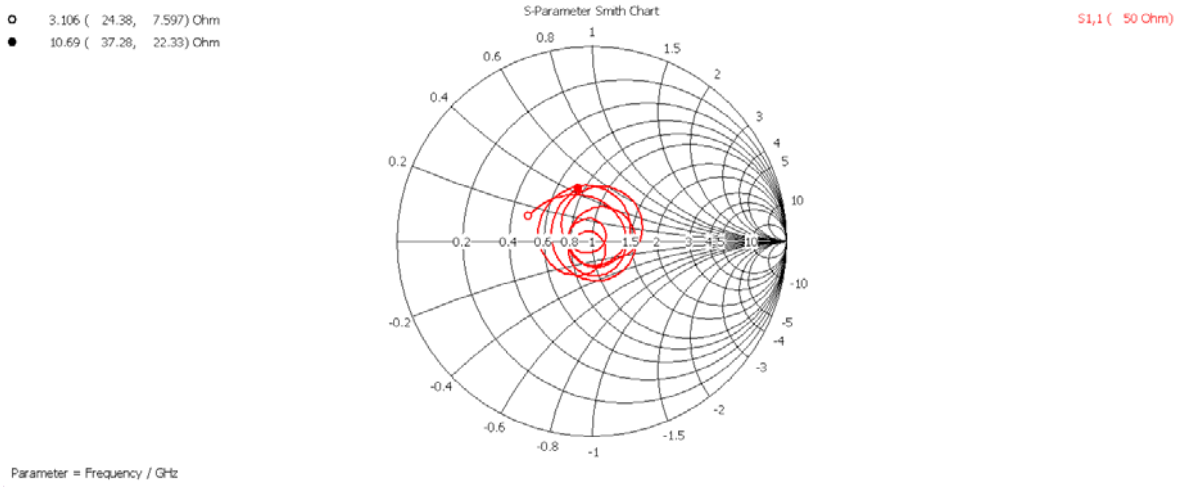

(b)

Fig.4.34. Simulated (a) return loss and insertion loss and (b) input impedance (normalized at 50 Ω).

Also for the convenience of the 180-degree phase difference function of the balun, the back-to-back transition configuration with the microstrip-line is studied. We placed two probes on the center of two coplanar striplines and we calculated the magnetic fields phase difference ($\vec{H}_1 - \vec{H}_2$) of these two points (Fig.4.35).

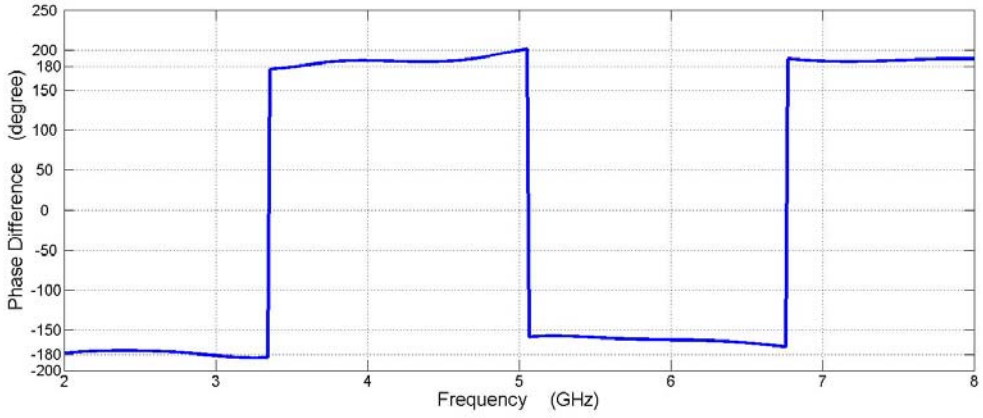

Fig.4.35. Phase difference of the central points of coplanar striplines in back-to-back configuration.

Fig.4.35 validates a 180-degree phase difference between these two points from 2 to 8 GHz with about 15 degree tolerance and thus, it is shown that the balun operates properly in field matching in this wideband frequency.

4.3.3 Sinuous Antenna in Compact CPS-fed Form

In this section, a 90° bended microstrip-to-CPS (which is designed in chapter 3) is employed to feed an optimized sinuous antenna as an integrated feeding system. This connection is illustrated in Fig.4.36.

To design an optimized a sinuous configuration, we have considered a wideband frequency between 2 and 10 GHz for antenna. It means f_L=2 GHz and f_H=10 GHz. In the other hand, the frequency bandwidth of sinuous antenna configuration has been used by below equation [26]:

$$R_{ex}.\alpha > \lambda_B/2 \quad (1)$$

$$R_{in} < 0.1\ \lambda_H \quad (2)$$

Thus, we arrive to α=135° with R_{in}=3 mm and R_{ex}=32.3 mm in optimization procedure. The antenna geometry parameters are the same as proposed in chapter 2 except the parameter g which is equal to 0.6 mm.

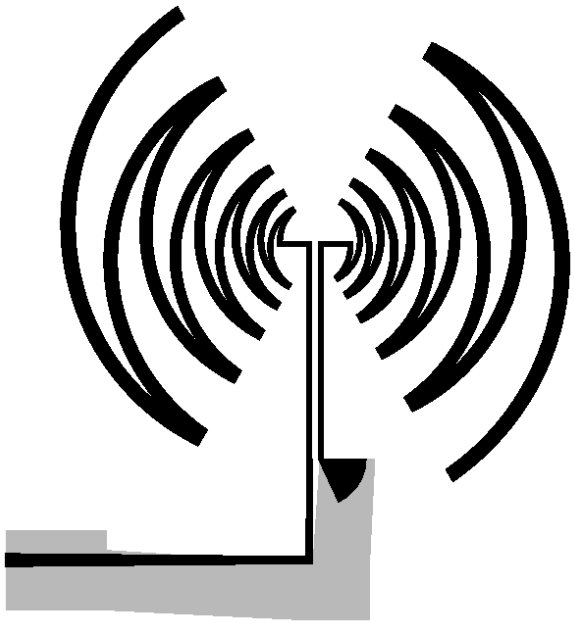

Fig.4.36. integrated sinuous antenna connected to the CPS balun geometry in single polarization mode.

The first attempt to simulate the antenna illustrates a field coupling between the CPS parts and discontinuities of the zigzag line (in sinuous antenna geometry) in connection region. In the other hand the metal parts of the two structures (antenna and balun) lead to a destructive coupling.

For decoupling, one method is to remove some metal part of antenna on the condition that any changes happen in the antenna radiation. In chapter 3, it is indicated that the antenna parameter $\alpha_0 = 135^\circ$. For this optimized antenna, an area defined by φ=45° is considered and this sector is removed (to decrease the coupling between antenna and balun) (Fig.4.37).

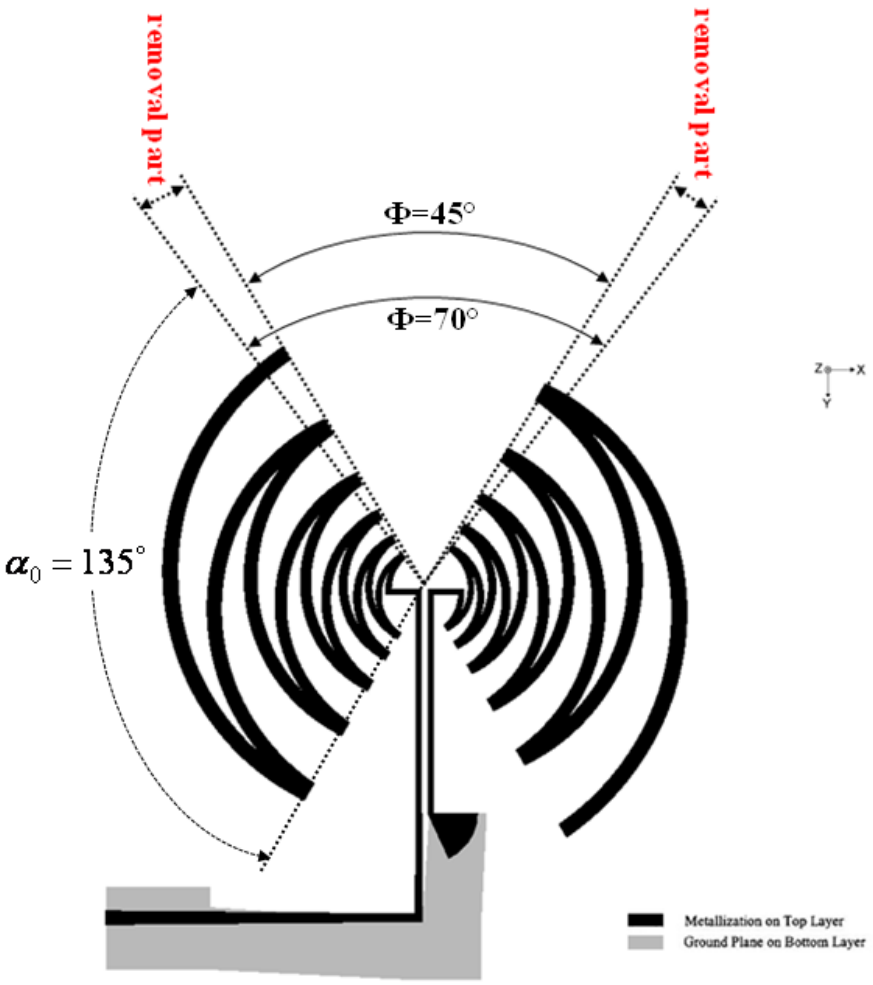

Fig.4.37. Sinuous antenna geometry with two different ϕ area.

The top and bottom views of the fabricated CPS-fed sinuous antenna are shown in Fig.4.38. Simulated and measured results for this CPS-fed sinuous antenna have performed. In fact the complete system consists of a coplanar stripline and an optimized sinuous antenna. The whole system has been realized on DiClad 880 substrate and the microstrip part of balun connected to a 50 Ω SMA connector. Fig.4.39 shows the simulated results for the return loss which normalizes to 50 Ω. It illustrates that the antenna has achieved a measured -10 dB bandwidth of 2.5 to 5.6 GHz and the comparison between measured and simulation return losses shows a good agreement..

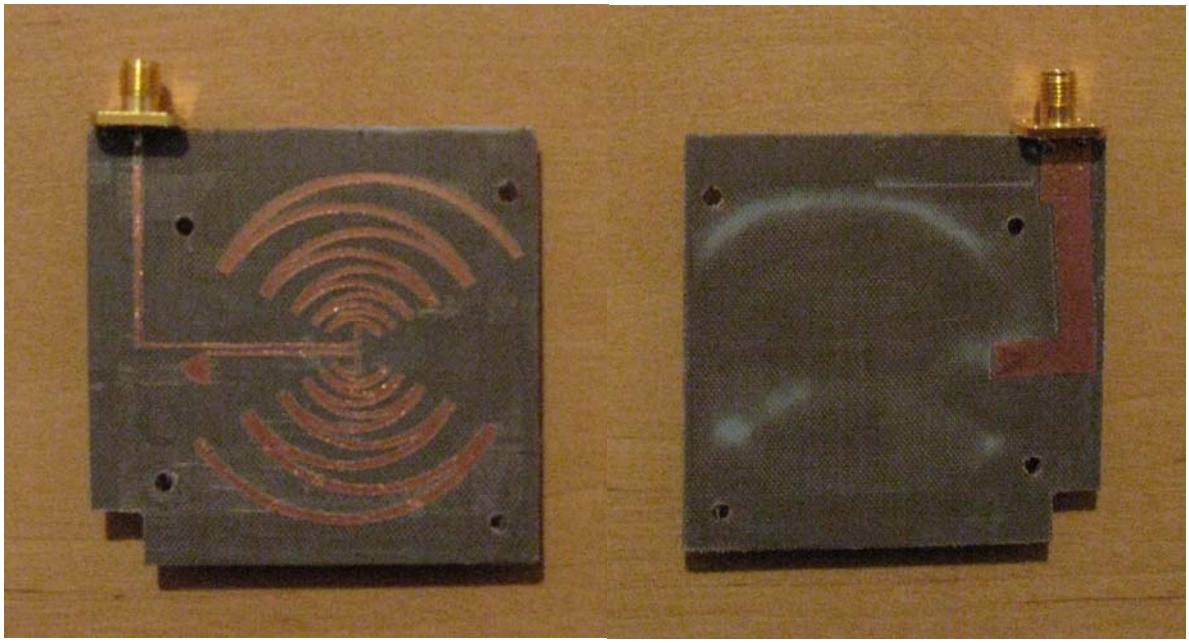

Fig.4.38. Top and bottom views of the fabricated CPS-fed sinuous antenna.

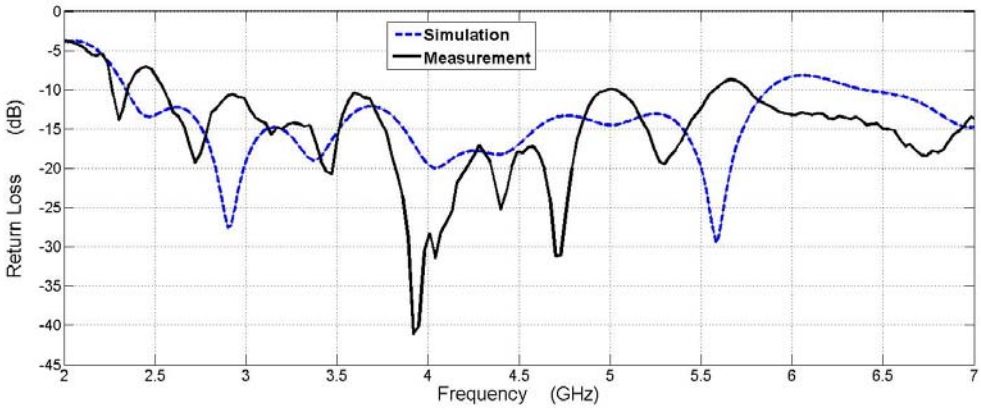

(a)

Fig.4.39. (a) Measured and Simulated return loss and (b) input impedance (normalized at 50 Ω).

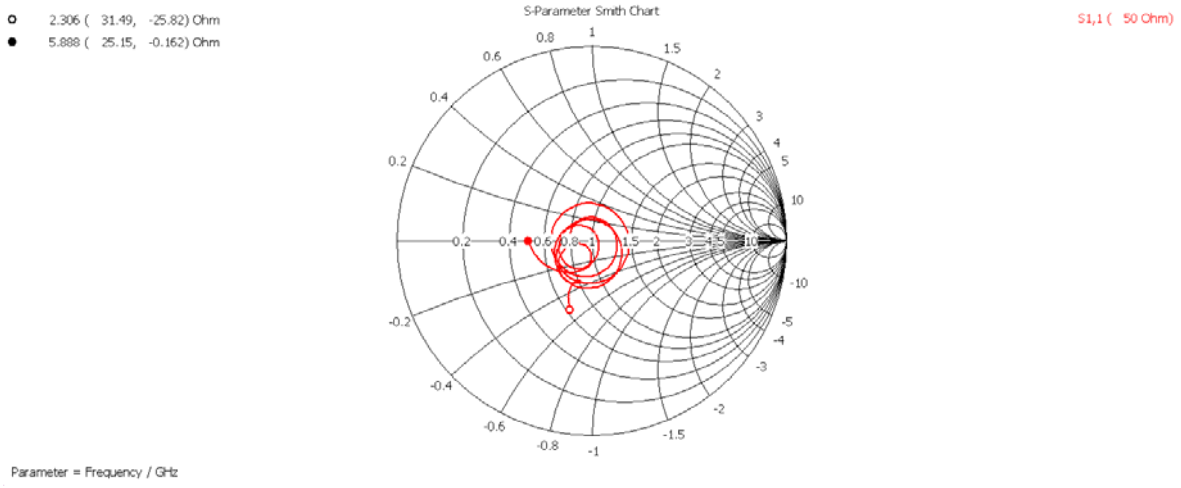

(b)

Fig.4.39. (continued) (a) Measured and Simulated return loss and (b) input impedance (normalized at 50 Ω).

The simulated results shows the surface current distribution for f= 3, 4 and 5 GHz of the sinuous antenna geometry (Fig.4.40).

- ***Interpretation of the results:***

1. The distributions of surface current on sinuous regions (two zigzag lines) are symmetrical for f=3 and 5 GHz and it has small distortion for f= 4 GHz.
2. For the higher frequency (f=5 GHz), the surface currents are placed on the interior lines (3 zigzag lines of the left and right arms), however for the lower frequency (f=3 GHz), the currents involve the exterior lines.
3. The current distributions show the balun feed almost well in field matching between the coaxial transmission line (unbalanced current distribution) and a balanced sinuous antenna. As it is shown in these figures, the CPS balun provide the two symmetrical feed points on the balance sinuous antenna. So the balanced feed in the antenna input port can produce a symmetrical radiation pattern for bow-tie antenna. The radiation patterns (antenna directivity) are simulated at frequencies of 3, 4, and 5 GHz in E- and H-plane (Fig.4.41 to 4.43). The definition of E-plane and H-plane is shown in Fig.4.41.

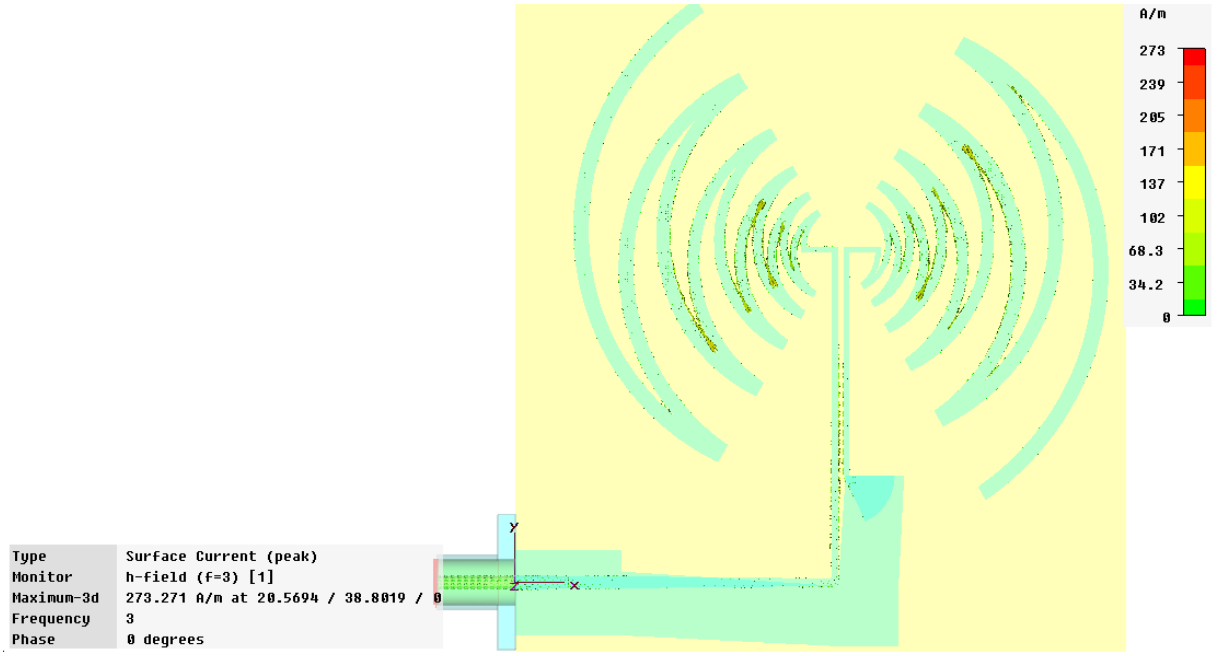

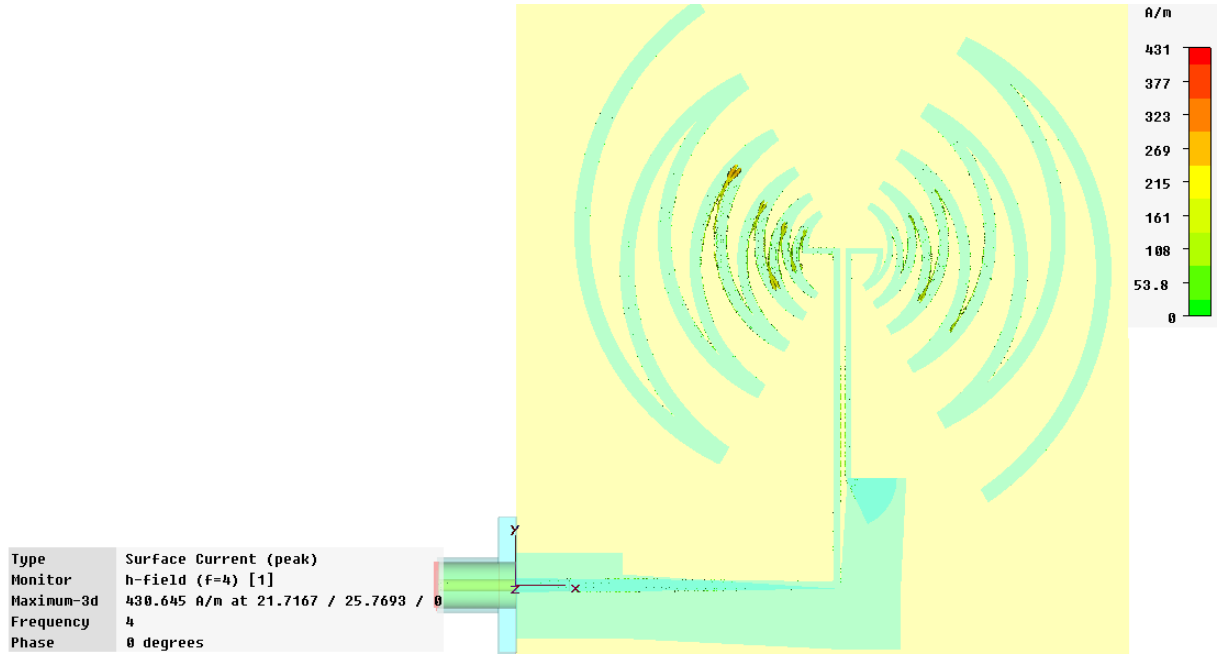

Fig.4.40. Surface Current distribution at 3, 4 and 5 GHz of the sinuous antenna geometry in single polarization mode.

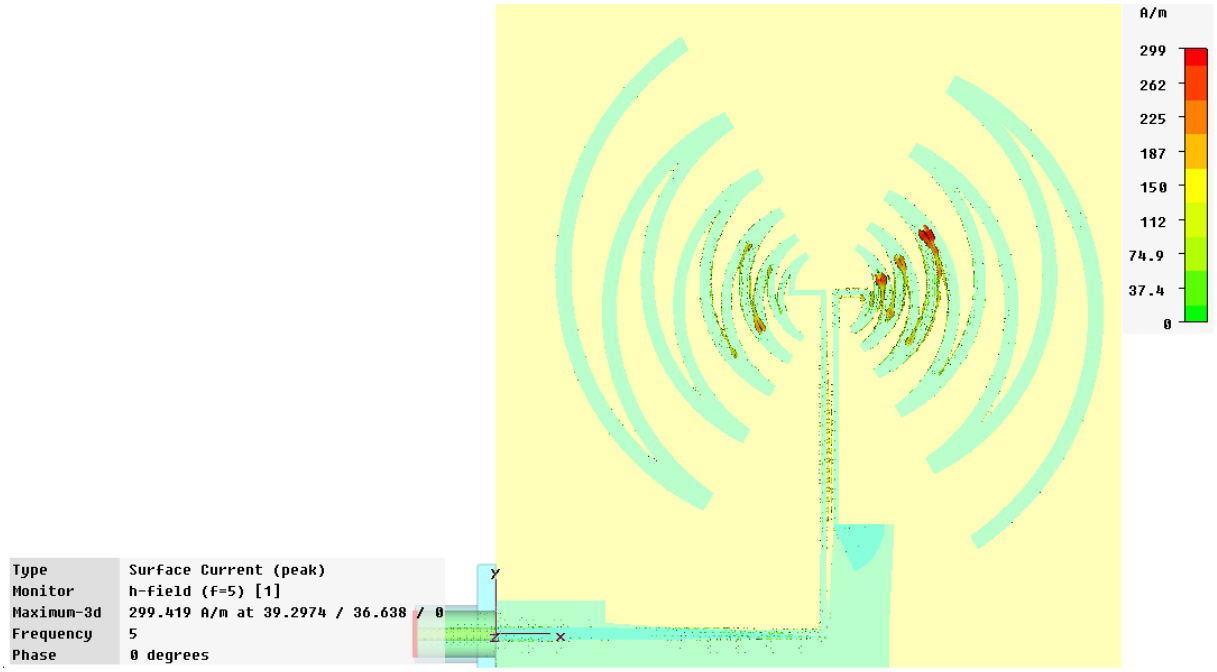

Fig.4.40 (continued) Surface Current distribution at 3, 4 and 5 GHz of the sinuous antenna geometry in single polarization mode.

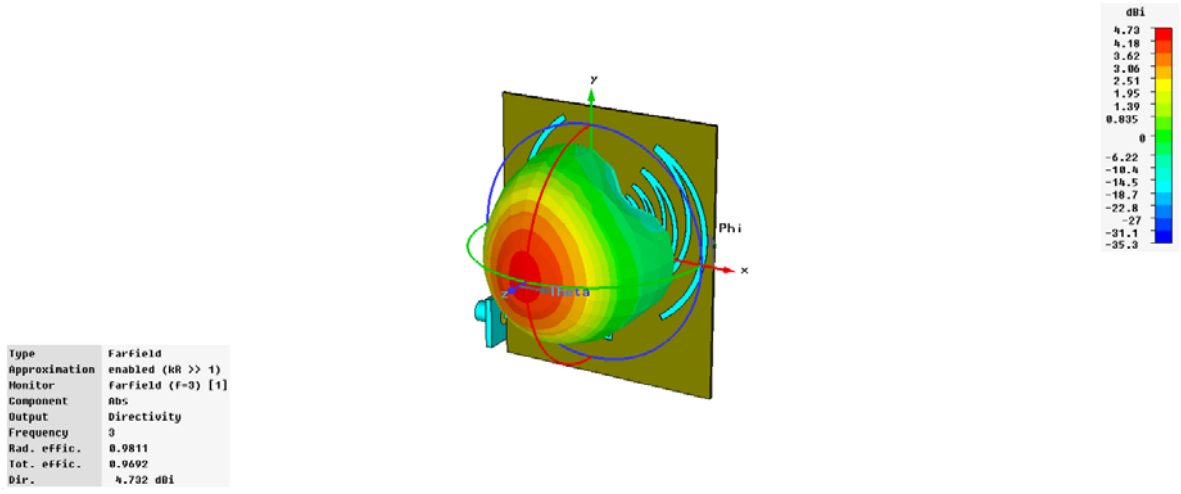

Fig.4.41. Directivity radiation patterns at 3 GHz of the sinuous antenna geometry and the definition of E-plane and H-plane.

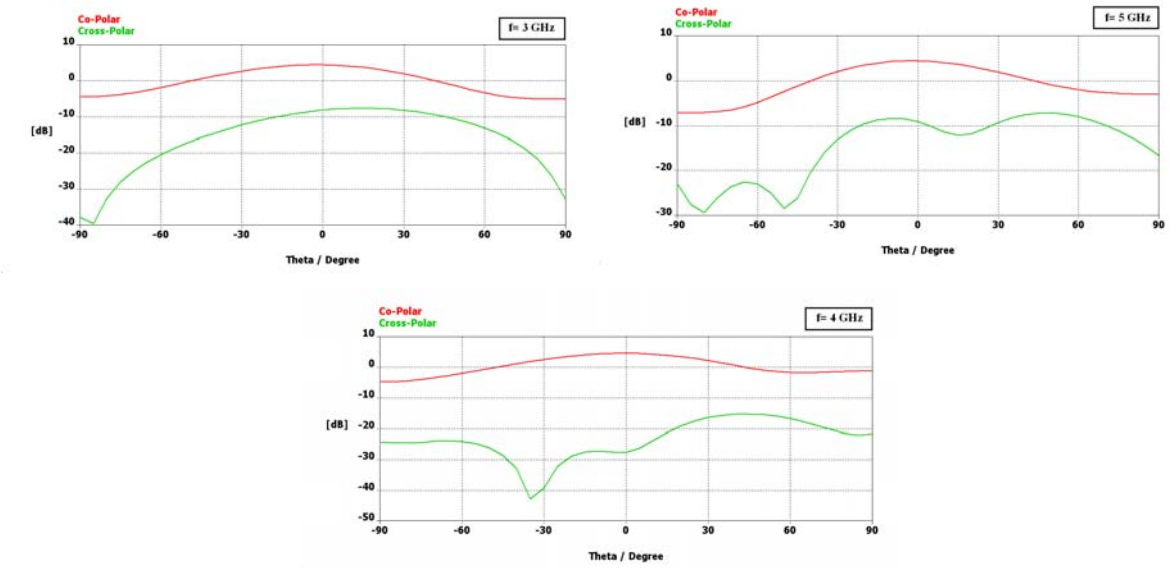

Fig.4.42. E-plane ($\phi = 0^{\circ}$) directivity radiation patterns at 3, 4, and 5 GHz of the CPS-fed antenna geometry in single polarization mode.

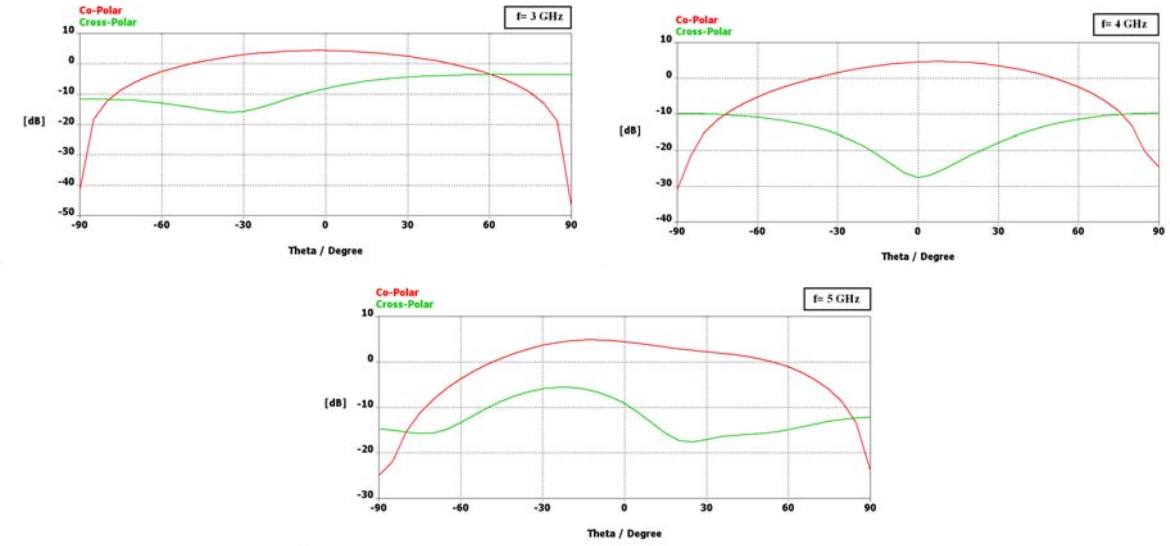

Fig.4.43. H-plane ($\phi = 90^{\circ}$) directivity radiation patterns at 3, 4, and 5 GHz of the CPS-fed antenna geometry in single polarization mode.

The radiation patterns were simulated at frequencies of 3, 4 and 5 GHz in E- and H-plane. As it is shown in Fig.4.42 and 4.43, E- and H-plane radiation patterns are symmetric around $\theta = 90°$. The antenna HPBW values in E- and H-planes are presented in Table.VIII.

Table.VIII. HPBW in E- and H-planes for a single polarization CPS-fed sinuous antenna.

Frequency (GHz)	HPBW E-Plane (°)	HPBW H-Plane (°)
3	70	75
4	70	72
5	66	73

It can be observed that HPBW in E- and H-plane has small variations in its frequency band entire. Unfortunately the radiation patterns have not been validated experimentally because of the lack of time.

Also there are differences at least about 13 dB between co-polar and cross polar component in its frequency bandwidth. It shows that the two arms of sinuous antenna are balanced (with a symmetric surface current distribution) and the feeding system work with good performance. Also the radiation pattern curves show antenna has linear polarization characteristic.

The simulated antenna gain is shown in Fig.4.44. This feature provides another important parameter that shows the antenna gain remains constant about 5 dB (up to 5.1 GHz).

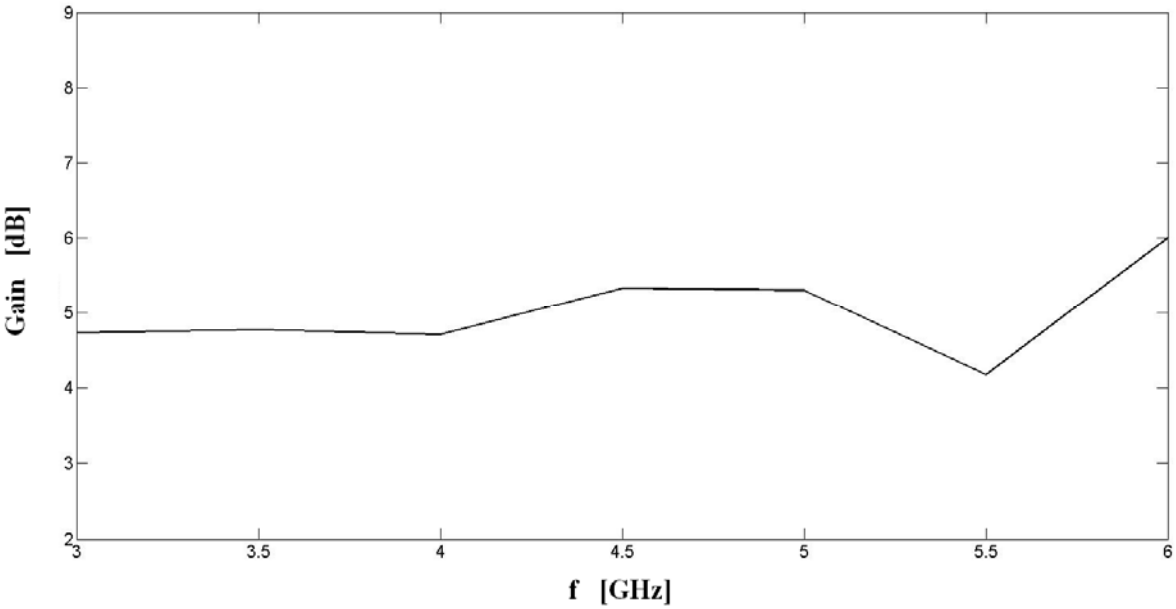

Fig.4.44. Simulated gain of the CPS-fed sinuous antenna in single polarization mode.

The overall size of the planar antenna is $5.7\times6.7\times0.0832\ cm^3$ or $0.475\lambda_L\times0.56\lambda_L\times0.007\lambda_L$ where λ_L is the wavelength at low frequency (f_L=2.5 GHz) which is very compact, low profile and can be integrated to other UWB devices. Finally with consideration the return loss and radiation pattern, it seems the CPS-fed

sinuous antenna operates well and it is a good candidate for next stage to arrive a wideband dual polarization antenna.

4.34. Implementation of the Bended Microstrip-to-CPS to the Dual Polarized Sinuous Antenna

In previous section we achieved a wideband sinuous antenna configuration with single linear polarization nature. Dual polarization capability can be obtained by using two orthogonal feeds in two different planes. In the other hand to reach a dual polarized sense we use two different antennas with balun connected to antenna with 90° rotation on two different planes. In this situation, each antenna plane radiate in a linear polarization mode and thus when two antennas works together, it will obtain two linear polarization orthogonal which have not any coupling.

If we want to utilize two antenna planes on just one substrate there will have an overlap between each antenna with other balun ground plane. The drawback is the connection between the last zigzag lines of each sinuous antenna and the other ground plane. The last lines produce the low frequency of the antenna bandwidth and this connection change the current surface distribution on the antenna plane. Therefore the frequency bandwidth will change and it is not desirable.

To overcome this problem, one solution is having two parallel substrates with a small distance. In this method we have two parallel identical antenna planes with a 90 degree rotation. It seems this two layer structure is capable of producing dual polarization radiation. Fig.4.45 illustrates this structure that it is used two identical CPS-fed sinuous antennas which proposed and optimized in previous section. The whole antenna and balun parameters are the same with antenna structure in 5.3 and the distance between two substrate planes is 2 mm (Fig.4.45).

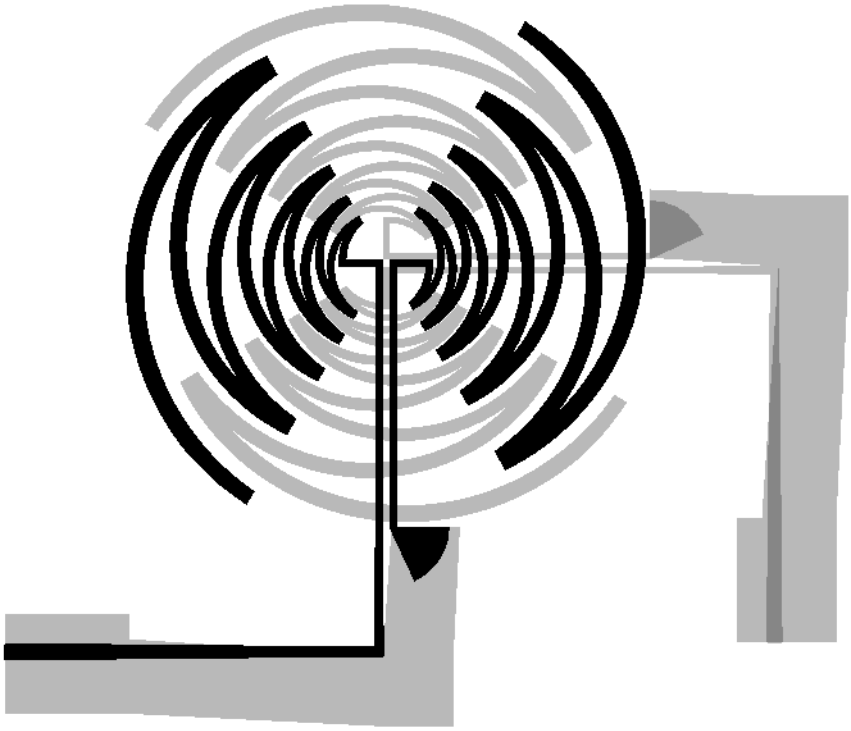

Fig.4.45. Integrated sinuous antenna connected to the CPS balun geometry in dual polarization configuration.

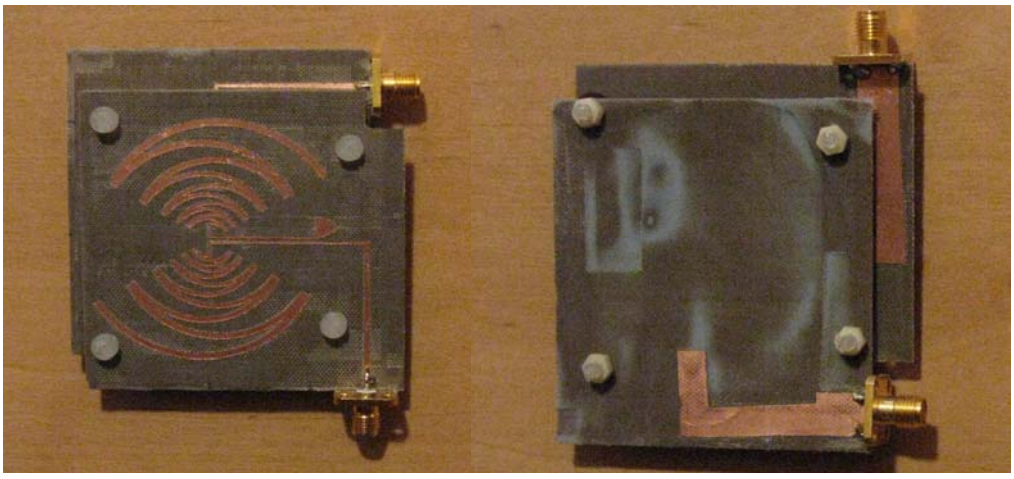

Fig.4.46. Top and bottom views of the dual polarized fabricated CPS-fed sinuous antenna.

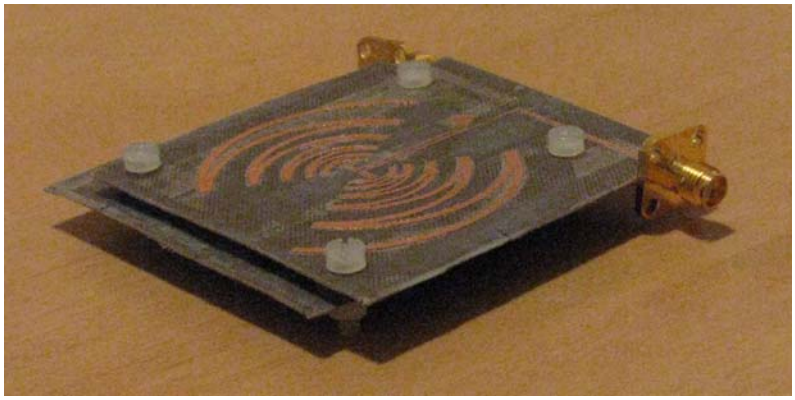

Fig.4.47. Perspective view of the fabricated dual polarized CPS-fed sinuous antenna.

Fig.48 and Fig.49 illustrate the simulated return loss and insertion loss of the CPS-fed dual polarized sinuous antenna. The results are shown just for the first antenna because for two polarizations they are the same. Fig.48 shows that the return loss is below -10 dB between 3.7 GHz and 7.3 GHz. The antenna bandwidth is about 4.1 GHz.

The insertion loss is below -12 dB in antenna frequency bandwidth. The insertion loss shows the decoupling between two structures in the frequency bandwidth between 3.2 GHz and 7.3 GHZ.

The comparison between the antenna return loss for the single and dual polarization shows that the impedance frequency band is almost changed and the bandwidth in dual polarized mode is increased.

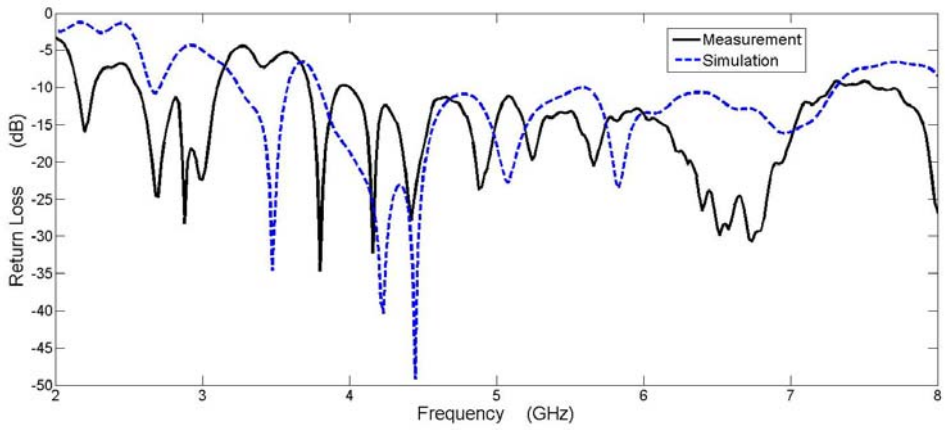

(a)

Fig.4.48. Measured and Simulated (a) return loss and (b) insertion loss for polarization 1(The input impedance is normalized at 50 Ω).

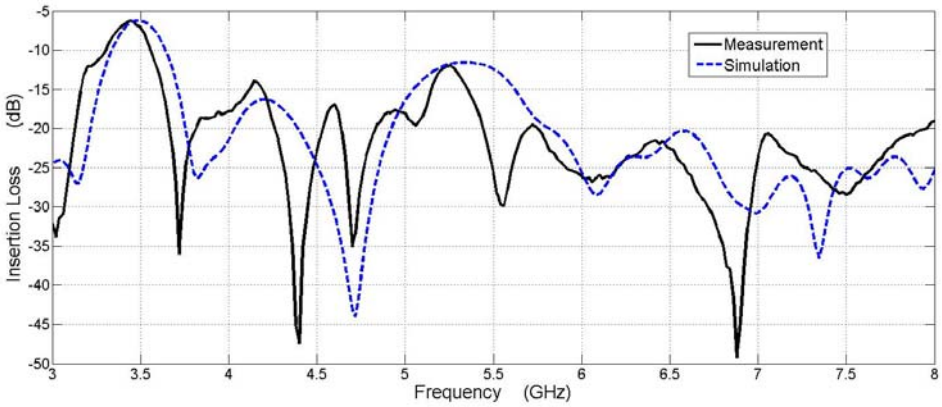

(b)

Fig.4.48. (continued) Measured and Simulated (a) return loss and (b) insertion loss for polarization 1(The input impedance is normalized at 50 Ω).

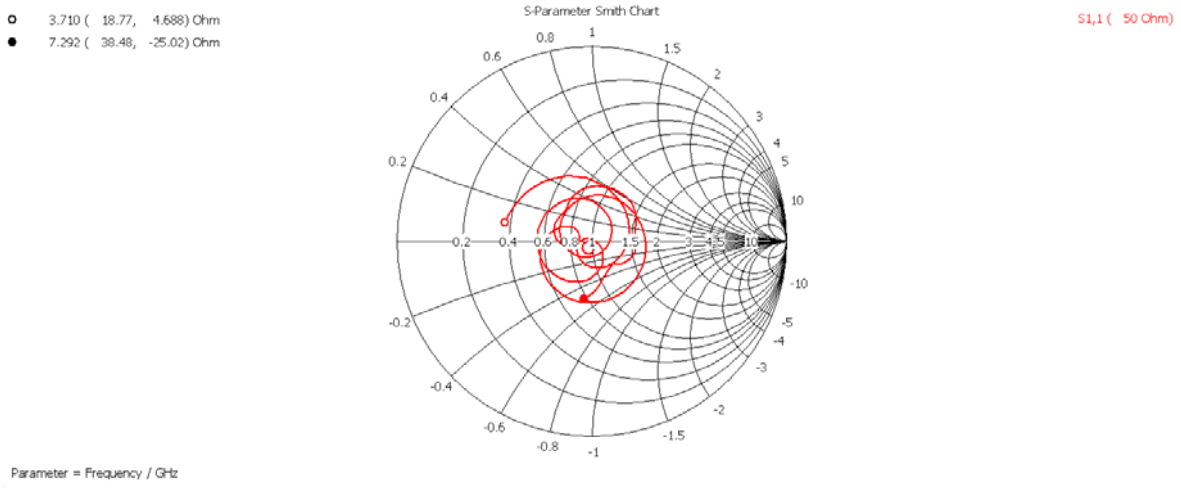

Fig.4.49. Simulated input impedance for polarization1 (normalized at 50 Ω).

The overall size of the planar antenna is $7.1\times6.7*0.3$ cm^3 or $0.87\lambda_L\times0.82\lambda_L\times0.04\lambda_L$ where λ_L is the wavelength at low frequency (f_L=3.7 GHz) which is very compact, low profile and can be integrated to other UWB devices. To study how antenna really radiate in dual polarization, we present the directivity radiation patterns at different frequencies 4, 5, 6 and 7 GHz in E and H-planes (Fig.4.50 and 4.51). It is just presented the directivity of polarization 1 because the two polarizations have had the same parameters.

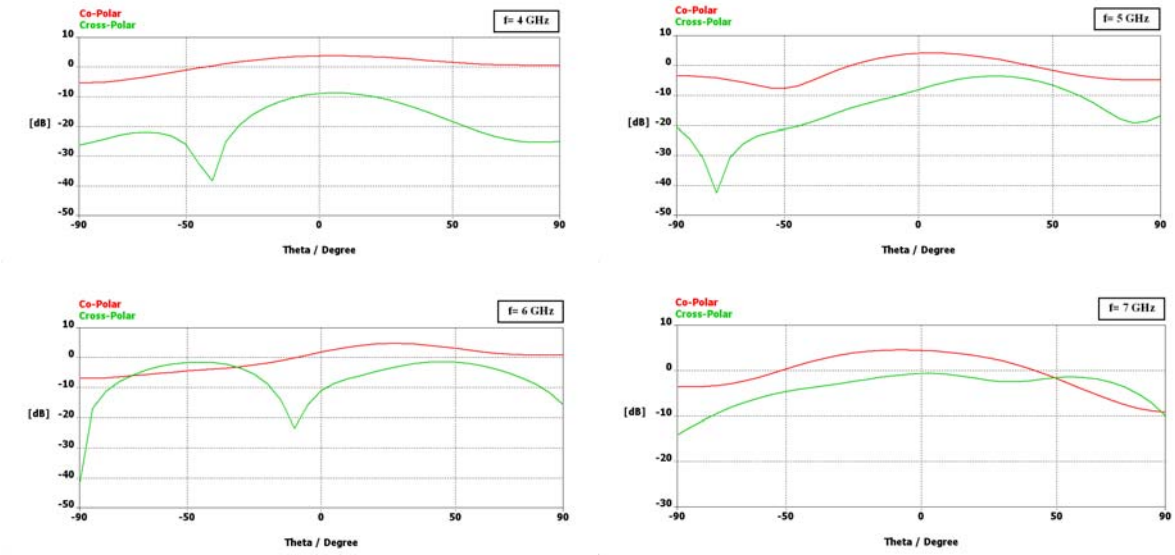

Fig.4.50. E-plane ($\phi = 0^{\circ}$) directivity radiation patterns at 4, 5, 6 and 7 GHz of the CPS-fed antenna geometry in dual polarization mode.

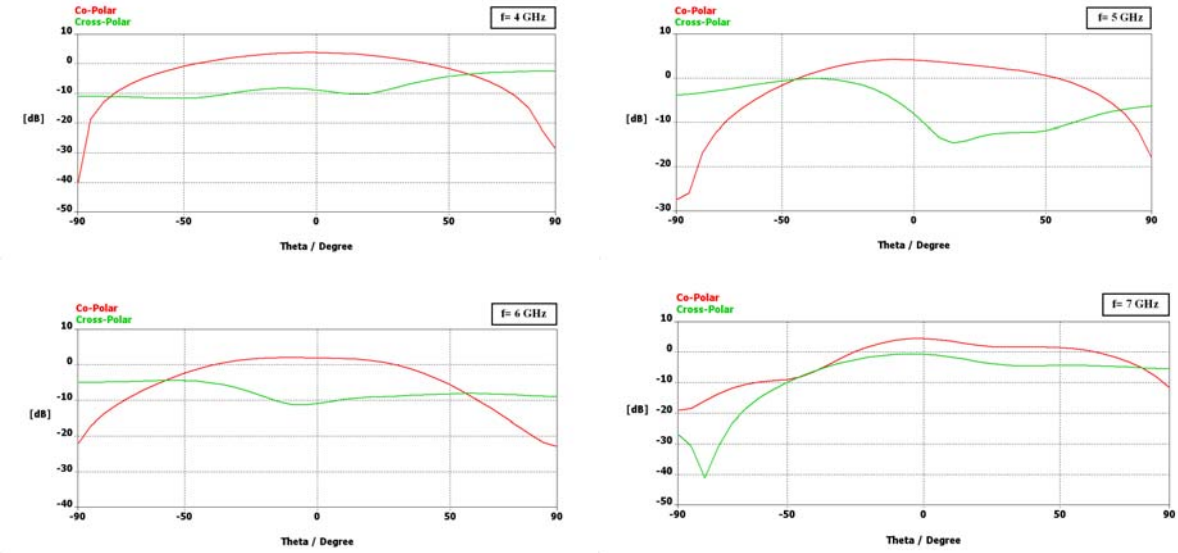

Fig.4.51. H-plane ($\phi = 90^{\circ}$) directivity radiation patterns at 4, 5, 6 and 7 GHz of the CPS-fed antenna geometry in dual polarization mode.

The radiation patterns in E- and H-planes show:

All the radiation patterns in E- and H-plane present an approximate symmetry behavior around $\theta = 0^{\circ}$ point except for H-plane at 7 GHz where small asymmetry is observed.

This point arises from the fact that the balun is well matched to the radiating part and its function to match the fields and impedance is acceptable.

The antenna HPBW values in E- and H-planes are presented in Table.IX.

Table.IX. HPBW in E- and H-planes for a dual polarization sinuous antenna.

Frequency (GHz)	HPBW E-Plane (°)	HPBW H-Plane (°)
4	87.5	76
5	52	78
6	65	75
7	74.5	67

It can be observed that HPBW in H-plane has small variations in its frequency band entire. The antenna gain is shown in Fig.4.52. This feature provides another important parameter that illustrates the antenna gain change between 4.3 to 5.8 dB from 3 to 7 GHz.

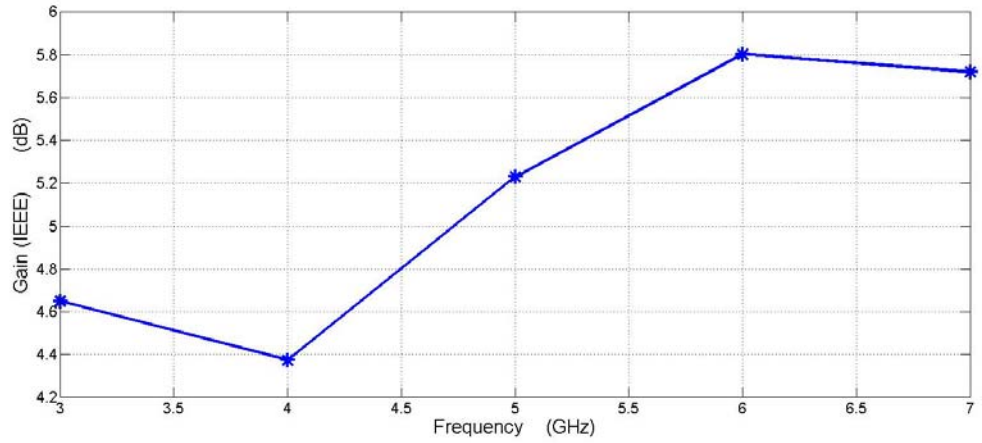

Fig.4.52. Simulated Gain of the CPS-fed sinuous antenna in single polarization mode.

The overall size of the planar antenna is 7.1×6.7×0.3 cm^3 which is very compact, low profile and can be integrated to other UWB devices.

4.3.5 Conclusion

A wideband CPS-fed sinuous antenna for single and dual polarization in compact form is developed. Sinuous antennas have two balanced arms and they are good candidate to use with coplanar stripline baluns. First of all a sinuous antenna with two arms optimized by a simulator tool (CST Studio Suite) with an input impedance around $160\,\Omega$. In the next step a microstrip-to-CPS balun as a wideband feeding system is designed to have a good transformation between 50 Ω (microstrip part) to 160 Ω (sinuous antenna input impedance).

Finally a developed wideband CPS-fed antenna configuration in integrated form was presented. In single polarization, a measured return loss better -10 dB from 2.5 GHz to 5.6 GHz was observed.

The radiation patterns show a good symmetrical directivity in E- and H-plane and the cross polarization level better than -10 dB in the frequency bandwidth.

Although for dual polarized sinuous geometry, an impedance bandwidth was reported bigger than single polarization, the radiation patterns were not symmetrical in entire frequency bandwidth and it is observed some small distortion.

4.4 Conclusion

In this chapter two geometries (sinuous and bow-tie) antenna were proposed. The quasi bow-tie structure has simple geometry to fabrication with ultra wideband impedance bandwidth but the radiation pattern directivity don't remain constant for the whole its frequency bandwidth. The sinuous antenna is more complicated to fabricate but it has wideband nature with radiation pattern approximate constant.

In addition, a new developed microstrip-to-CPS balun was presented and it has implemented on two lightweight and low cost antenna configuration (bow-tie and sinuous) in single and dual polarization. Finally we obtained a two integrated structure with good performance in impedance matching and radiation pattern. The overall size of the sinuous antenna is $0.87\lambda_L \times 0.82\lambda_L \times 0.04\lambda_L$ however the bow-tie geometry size is $1.1\lambda_L \times 1.1\lambda_L \times 0.015\lambda_L$ which they are compact, low profile and can be integrated to other UWB devices.

Also for dual polarization mode the sinuous antenna has a measured return loss better 10 dB from 3.2 GHz to 7.3 GHz. However the quasi bow-tie antenna has a measured return loss better 10 dB from 5.4 GHz to 12 GHz.

The other main conclusion is that our wideband coplanar balun can be used to feed dual polarized sinuous and bow-tie antennas in integration configuration.

4.5 References

[1] M.J. Ammann and Z.N. Chen, "Wideband Monopole Antennas for Multi-band Wireless Systems," *IEEE Antennas and Propagation Magazine*, 45 (2003), 146–150.

[2] S. W. Su, K. L. Wong, and C. L. Tang, "Ultra-Wideband Square Planar Monopole Antenna for IEEE 802.16a Operation in the 2-11 GHz Band," *Microwave and Optical Technology Letters*, vol. 42, no.6, pp. 463–466, Sep. 2004.

[3] X. H. Yang and W. X. Zhang, "Coplanar waveguide antenna arrays for MIC/MMIC at Millimeter wave frequencies," *Electronics Letters*, vol. 26, pp. 1464-1465, 1990.

[4] R.G. Vaughan, "Polarization Diversity in Mobile Communications," *IEEE Trans. Vehicular Technol.* 39, pp.177-186, August 1990.

[5] K. Hettak, G. Y. Delisle, M. G. Stubbs, "A Novel Variant of Dual Polarized CPW Fed Patch Antenna for Broadband Wireless Communications," *Antennas and Propagation Society International Symposium*, 2000. IEEE, vol.1, 2000.

[6] C.C.Y. Lee, "Polarization Diversity System for Mobile Radio," *IEEE Trans. Communications*, pp. 912-923, Oct. 1972.

[7] W. L. Stutzman and G.A. Thiele, *Antenna Theory and Design*, John Wiley & Sons Inc., 2nd edition, New York, 1998.

[8] Nasimuddin and Zhi Ning Chen, "Wideband Directional Microstrip Antennas fed by CPW-Loop Combination," *ICUWB 2007. IEEE International Conference*, pp. 700-702, 24-26 Sep. 2007.

[9] X. Ding and A. F. Jacob, "CPW-fed slot antenna with wide radiating apertures," *IEE Proc. Microwaves, Antennas and Propagation*, vol. 145, pp. 104-108, 2003.

[10] M. A. Saed, "Reconfigurable Broadband Microstrip Antenna Fed by a Coplanar Waveguide," *Progress In Electromagnetic Research*, Vol. 55, pp. 227–239, 2005.

[11] Y.-H. Suh and K. Chang, "A wideband coplanar stripline to microstrip transition," *IEEE Microw.Wireless Compon. Lett.*, vol. 11, no. 1, pp. 28–29, Jan. 2001.

[12] W.-H. Tu and K. Chang, "Wide-band Microstrip-to-Coplanar Stripline/Slotline Transitions," *IEEE Trans. Microw. Theory Tech.*,vol. 54, no. 3, pp. 1084–1089, March. 2006.

[13] Y-G. Kim, D-S Woo, K. W. Kim, Y-K. Cho, "A New Ultra-Wideband Microstrip-to-CPS Transition," *Microwave Symposium IEEE/MTT-S International*, pp. 1563-1566, 3-8 June 2007.

[14] M. C. Bailey, "Broad-Band Half-Wave Dipole," *IEEE Transactions on Antennas and Propagation*,

vol. AP-32, No. 4, pp. 410-412, April 1984.

[15] George H. Brown and O. M. Woodward Jr., "Experimentally Determined Radiation Characteristics of Conical and Triangular Antennas," *RCA review*, vol.13, pp.425-452, December 1952.

[16] R. C. Compton, R. C. Mcphedran, Z. Popovic, G. M. Rebeiz, P. P. Tong, and D. B. Rutledge, "Bow-tie Antennas on a Dielectric Half-space: Theory and Experimental," *IEEE Trans. Antennas Propag.*, vol. AP-35, no. 6, pp. 622–631, Jun. 1987.

[17] C. Waldschmidt, K. D. Plamer, "Loaded Wedge Bow-tie Antenna Using Linear Profile," *Electron. Lett.*, vol. 37, pp. 208–209, Feb. 2001.

[18] A. A. Lestari, A. G. Yarovoy, and L. P. Ligthart, "RC-loaded Bow-tie Antenna for Improved Pulse Radiation," *IEEE Trans. Antennas Propag.*, vol. 52, no. 10, pp. 2555–2563, Oct. 2004.

[19] Y, Mushiake, *Self Complementary Antennas: Principle of Self-complementary for Constant impedance,* Springer, 1996.

[20] G. Kumar and K. Ray, *Broadband Microstrip Antennas*, Artech House, 2003.

[21] K. Kiminami, A. Hirata, and T. Shiozawa, "Double-sided Printed Bow-tie Antenna for UWB Communications," *IEEE Antennas Wireless Propag. Lett.*, vol. 3, no. 1, pp. 152–153, Dec. 2004.

[22] K. Kiminami, A. Hirata, and T. Shiozawa, "Planar Bow-tie Antenna Embedded in Circular Aperture Within Conductive Frame," *IEEE Antennas and Wireless Propag. Lett.*, vol. 5, pp. 399-401, 2006.

[23] C. Balanis, *Antenna Theory; Analysis and Design,* John Wiley & Sons Inc., Third edition, 2005.

[24] Y. Qian and T. Itoh, "A Broad-band Uniplanar Microstrip-to-CPS transition," in *Proc. Asia–Pacific Microw. Conf.*, vol. 2, 1997, pp. 609–612.

[25] R. N. Simons, N. I. Dib, and L. P. B. Katehi, "Coplanar stripline to microstrip transition," *Electron. Lett.*, vol. 31, no. 20, pp. 1725–1726, Sep. 1995.

[26] R. C. Johnson, *Antenna Engineering Handbook*, Third Ed., McGraw Hill, 1993.

General Conclusion

This thesis has two main goals that are presented in 4 chapters:

- First of all the dissertation investigates the planar wideband feeding systems to implement on desired dual polarized antenna geometries. The objective of this part of thesis is to design a balun structure embracing these properties:

    - The ability of field matching between an unbalanced and a balanced structure in wide frequency bandwidth
    - The ability of impedance transforming between the coaxial cable with 50 Ω and a desired antenna input impedance in wide frequency bandwidth
    - Integrated form to connect simply to planar antenna structures with simple design for fabrication
    - The ability of obtaining the dual polarization properties

  We have developed two balun configurations as wide feeding system:

    - A wideband UWB tapered microstrip balun (chapter 2)
    - A new bended microstrip-to-CPS configuration balun (chapter 3,4)

- Moreover the thesis investigates planar, low-profile and wideband antenna which can be used in dual polarization modes. The objective of this part of thesis is to design an antenna structure with these properties:

    - Wide impedance frequency bandwidth with return loss better than -10 dB in UWB
    - Dual polarization radiation with cross polarization level better than -10 dB in the entire frequency bandwidth
    - Compact and integrated form useful for modern UWB application

Our investigations on compact wideband antenna show that in order to obtain a planar wideband antenna with dual polarization characteristics, the best candidates are:

- Sinuous antenna configuration
- Bow-tie antenna geometry

These antennas have two balanced arms and they need feeding system configurations which can obtain balanced surface current in the two arms.

In chapter 2 an optimized tapered balun was presented, connected to a slot sinuous antenna. Finally we presented a compact directive slot sinuous antenna which has a measured return loss better than -10 dB from 3.9 to 9.6 GHz but with single linear polarization. In this chapter we have arrived to all desired parameters except the dual polarization properties.

A wideband CPS-fed sinuous antenna for single and dual polarization in compact form were developed in chapter 3. The CPS-to-microstrip transition exhibits wideband performance from 3 GHz to 10 GHz with an insertion loss of less than 3 dB and a return loss of better than -10 dB for the back-to-back transition.

To validate the balun performance for field and impedance matching, a dual polarized antenna with wideband frequency in a 3-dimensional configuration was presented in chapter 3. In fact a sinuous antenna with microstrip-to-CPS balun which is perpendicular to the antenna plane was presented. The return loss is better than from 2.8 GHz to 9.2 GHz for polarization 1 and from 2.6 GHz to 8.3 GHz for polarization 2. Also the insertion losses show that the transmission property of this structure is almost in the impedance frequency band.

Chapter 4 presents two new configurations proposed for the first time to verify the wideband and dual polarization characteristics of our proposed feeding system. A developed quasi bow-tie antenna whose geometry consisted of a pair of bow-tie type antenna with 90° rotation on two sides of a substrate layer is proposed. The antenna configuration was integrated with a microstrip-to-CPS form with UWB characteristic. Measurement and simulation results of the return loss and simulated directivity radiation patterns of dual polarization show a wideband bandwidth from 5.4 GHz to 12 GHz. Also the comparison of measurement and simulation results show a good agreement .The whole size of the structure placed in a $1.1\lambda_L \times 1.1\lambda_L \times 0.015\lambda_L$ volume.

Also a bended microstrip-to-CPS balun was developed to connect a sinuous antenna in an integrated configuration. In single polarization mode a measured return loss better than -10 dB from 2.5 GHz to 5.6 GHz is observed. The radiation patterns show good symmetrical curves and the cross polarization level of better than -10 dB in the entire frequency bandwidth. Also for dual polarized mode we have achieved a

measured return loss better 10 dB from 3.7 GHz to 7.3 GHz. An agreement between measurement and simulation return losses and insertion losses were presented for single and dual polarization. The whole antenna structure is placed in a $1.1\lambda_L \times 1.1\lambda_L \times 0.015\lambda_L$ volume.

This work can be continued by two different ways:

First, it seems possible to present a new CPS-fed sinuous geometry in dual configuration which has implemented on one substrate (the same as dual polarized bow-tie structure in chapter 4). Now the problem is the connection between each balun ground plane (for vertical polarization) to other antenna plane (horizontal polarization). This connection changes the surface current distribution of the antenna (unlike the bow-tie antenna). If the size of ground plane is modified, it will be achieved to a more compact dual polarized sinuous structure without needing two planes four dual polarization. Table.1 summarizes the performance of the whole fabricated antenna configurations in this thesis (impedance bandwidth, volume).

Finally we propose a study of using metamaterials as antenna substrate to enhance antenna gain in wideband frequency. As it is indicated in chapter 2, there is a challenge between wideband characteristics and enhancement antenna gain by adding a ground plane. But it seems by adding metamaterial substrates to bow-tie and sinuous antenna is possible to achieve these advantages together.

Table.1. The comparison of performance of the whole fabricated antenna configurations in thesis.

Antenna-Balun	Impedance Bandwidth (GHz)	Bandwidth in ratio	Volume (λ_L)	Volume (cm^3)
Sinuous Slot (Single Pol., 3D) (Balun-1)	3.15 – 10	**3.2:1**	$0.52\lambda_L \times 0.52\lambda_L \times 0.52\lambda_L$	5×5×5
Directive Slot Sinuous (Single Pol., 3D), (Balun-1)	3.9 – 9.6	2.5 :1	$0.65\lambda_L \times 0.65\lambda_L \times 0.65\lambda_L$	5×5×4
Sinuous (Dual Pol., 3D) (Balun-2)	2.8 – 8.3	3:1	$0.65\lambda_L \times 0.65\lambda_L \times 0.37\lambda_L$	7×7×4
Sinuous (Single Pol., Integrated) (Balun-2)	2.5 – 5.6	2.2:1	$\mathbf{0.475\lambda_L \times 0.56\lambda_L \times 0.007\lambda_L}$	7.1×6.7×0.0832
Bow-tie (Single Pol., Integrated) (Balun-2)	2.8 – 7.8	2.8:1	$0.56\lambda_L \times 0.56\lambda_L \times 0.008\lambda_L$	6×6×0.0832
Sinuous (Dual Pol., Integrated) (Balun-2)	3.7 – 7.3	2:1	$0.87\lambda_L \times 0.82\lambda_L \times 0.04\lambda_L$	7.1×6.7×0.3
Bow-tie (Dual Pol., Integrated) (Balun-2)	5.4 – 12	2.2:1	$1.1\lambda_L \times 1.1\lambda_L \times 0.015\lambda_L$	6×6×0.0832

List of publications

1. M.Vahdani, X. Begaud, “A Directive Ultra Wideband Sinuous Slot Antenna,” *Eucap*, Nice, France, Nov. 2006.

2. M.Vahdani, X. Begaud, “Sinuous Antenna fed by a Microstrip-to-CPS Balun,” *Eucap*, Berlin, Germany, Mars 2009.

3. M.Vahdani, X. Begaud, “Wideband Integrated Feeding System for a Dual Polarization Sinuous Antenna”, *Submitted on IET Microwaves, Antenna and Propagation*, Sep. 2008.

4. M.Vahdani, X. Begaud, “Wideband Integrated CPS-fed Dual Polarized Quasi Bow-tie Antenna” *Submitted on Microwave and Optical Technology Letters*, Dec. 2008.

Résumé (Français)

Antennes et systèmes d'alimentations Ultra Large Bande, compacts et à double polarisation

Introduction Générale

L'objectif principal de cette thèse est de concevoir et d'analyser des antennes associées à des systèmes d'alimentations compacts à bande passante voisine ou supérieure à l'octave et à double polarisation. Cette étude a été effectuée au département COMELEC de TELECOM ParisTech sous la direction de Xavier Begaud.

Aujourd'hui dans les systèmes télécommunication sans fil, il y a trois demandes croissantes: Premièrement on a besoin d'émetteurs/récepteurs large bande pour augmenter le débit d'information. Deuxièmement pour des raisons d'esthétique et portabilité, il est nécessaire de concevoir des antennes très compactes et de faible-encombrement. Enfin dans les systèmes télécommunications sans fil notamment, les antennes de stations de base avec deux polarisations orthogonales peuvent aussi permettre d'augmenter la performance des systèmes.

On a donc besoin de systèmes d'alimentations avec ces trois caractéristiques : ultra-large bande, double polarisation et faible encombrement. Afin de valider les performances de ces systèmes d'alimentations, des antennes avec des caractéristiques compatibles ont été étudiées. Durant le déroulement de la thèse, on a parcouru les étapes suivantes : dans la première étape, un système d'alimentation ultra large bande à simple polarisation 3D a été réalisé. Dans la deuxième étape nous l'avons fait évoluer vers une structure à double polarisation. Finalement, une configuration intégrée à double polarisation a été conçue et réalisée. Cette dernière partie est le cœur de mon travail et les parties précédentes ont été conduites pour aboutir à cette configuration intégrée. Il faut noter que dans ce travail, l'expression « large bande ou ultra large bande (ULB ou UWB : Ultra Wide Band) » se réfère à une bande de fréquence voisine ou supérieure à une octave pour un module du coefficient réflexion inférieur à -10 dB.

J'ai présenté mon travail dans les quatre chapitres suivants: dans le chapitre 1, il y aura une présentation synthétique des antennes UWB et des deux antennes candidates qui seront ensuite utilisées pour étudier les systèmes d'alimentation. Dans le chapitre 2, un système d'alimentation UWB avec une antenne simple polarisation sera étudié. Puis dans le chapitre 3, un nouveau balun coplanaire intégré UWB sera proposé. Ensuite, ce système alimentera une antenne sinueuse à double polarisation dans une configuration volumique (3D). Finalement dans le

chapitre 4, ce type de balun coplanaire sera utilisé sur les deux antennes candidates pour conduire à une configuration intégrée. Une conclusion générale sur les performances des systèmes sera présentée.

Chapitre 1

Une présentation des antennes à Ultra Large Bande à double polarisation

Il y a plusieurs catégories d'antennes UWB. On a choisi deux types très connu: l'antenne biconique et l'antenne indépendante de la fréquence. L'antenne biconique est volumique avec une impédance d'entrée réelle. La version planaire de l'antenne biconique s'appelle Bow-Tie (papillon) et possède un diagramme de rayonnement omnidirectionnel comme un dipôle (Fig.1). L'avantage de ce modèle est sa géométrie simple.

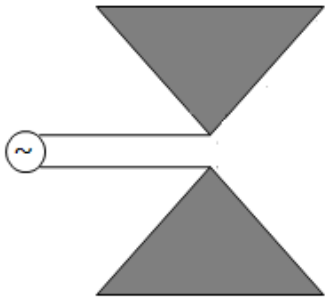

Fig.1. Géométrie de l'antenne Bow-Tie .

Fig.2. Géométrie de l'antenne sinueuse.

L'antenne spirale équiangulaire est une antenne indépendante de la fréquence avec un diagramme de rayonnement à polarisation circulaire et sa géométrie est auto-complémentaire. Son impédance d'entrée est donc égale à $60\pi\ \Omega$. L'antenne sinueuse (Fig.2) est une version alternative de ce type d'antenne et a été proposée par DuHamel en 1982 avec deux caractéristiques principales : double polarisation et compacité de la partie rayonnante.

Notre objectif dans cette étude est focalisé sur les antennes planaires compactes donc les antennes volumiques comme le cornet TEM, la spirale conique équiangulaire, … ont été éliminées. Notre choix s'est donc porté sur les antennes planaires sinueuse et Bow-Tie . L'antenne planaire sinueuse classique a les caractéristiques suivantes: UWB, double polarisation, directive avec une impédance d'entrée élevée. La deuxième candidate (Bow-Tie) a une géométrie simple et compacte avec une polarisation omnidirectionnelle. Pour une même

orientation des antennes, la polarisation de l'antenne Bow-Tie est perpendiculaire à celle de l'antenne sinueuse. Ces deux types d'antenne ont été choisis pour qu'on puisse évaluer nos baluns pour ces deux polarisations.

Chapitre 2

Systèmes d'alimentation pour antennes à Ultra Large Bande (à simple polarisation et à 3 dimensions)

Dans le chapitre 2 sera présenté l'état de l'art concernant les baluns ultra large bande, puis l'optimisation d'une antenne sinueuse simple polarisation à fente, le développement d'un balun UWB planaire, une antenne UWB directive et finalement la conclusion.

Les baluns utilisés pour faire une connexion appropriée entre les systèmes équilibrés et déséquilibrés dans la bande passant désirée pour qu'on puisse transférer le maximum d'énergie. Les antennes dipolaires doivent être alimentées aux points d'entrées par deux signaux de même-amplitude avec une différence de phase égale à π. Les baluns doivent en fait accomplir deux fonctions principales : l'adaptation des champs comme un symétriseur et aussi la transformation d'impédance.

Dans les années 1990, trois versions du balun à lignes bifilaire ont été présentés :

La version de M. Begaud alimente une antenne sinueuse à fente à double polarisation avec une impédance d'entrée voisine de 100Ω dans la bande 2 à 10 GHz. M. Sharaiha et son équipe ont présenté deux version alternatives pour alimenter une antenne sinueuse à double polarisation avec une bande passante supérieure à une octave. M. Kazemipour a employé un balun à ligne bifilaire optimisé pour calculer le couplage entre les antennes dipôles. Donc nous avons choisi de développer cette catégorie du balun UWB.

Tout d'abord afin de valider les performances du balun, on l'a testé avec une antenne sinueuse. Deux types d'antennes sinueuses sont étudiés. La version de Duhamel a impédance d'entrée voisine de 270 Ω qui a besoin d' un balun avec largeur de ligne microruban très fine et qui pose alors des problèmes de réalisation et de connexion. Donc il faut chercher une structure sinueuse à impédance basse. En 1996 M. Begaud a présenté une version à fente de l'antenne sinueuse (Fig.3) qui est la géométrie complémentaire de l'antenne sinueuse microruban. On peut ainsi montrer par le principe Babinet que l'impédance d'entrée de l'antenne sinueuse à fente est voisine de 100 Ω. Donc nous avons choisi ce type d'antenne sinueuse à simple polarisation dans cette partie. L'objectif est ici d'arriver à une adaptation d'impédance large bande de 2 à 10 GHz.

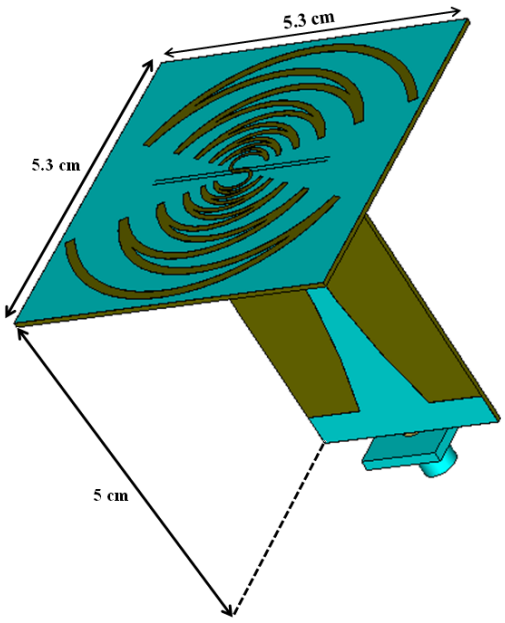

Fig.3. Géométrie de l'antenne sinueuse à fente (simple polarisation) connecté au balun optimisé.

En utilisant les équations de l'antenne sinueuse, on a définit l'ensemble des dimensions l'antenne désirée. Toutes les antennes étudiées durant la thèse ont été réalisées sur le matériau Diclad880 avec une permittivité de 2.17 et une épaisseur de 0.762 mm. Pour cette antenne, nous avons obtenu une impédance voisine de 70 Ω.

La figure suivante montre que notre balun est optimisé pour une transformation d'impédance de 50 à 70 Ω. Il y a un bon accord entre l'impédance mesurée et simulée entre 3.15 et 10 GHz.

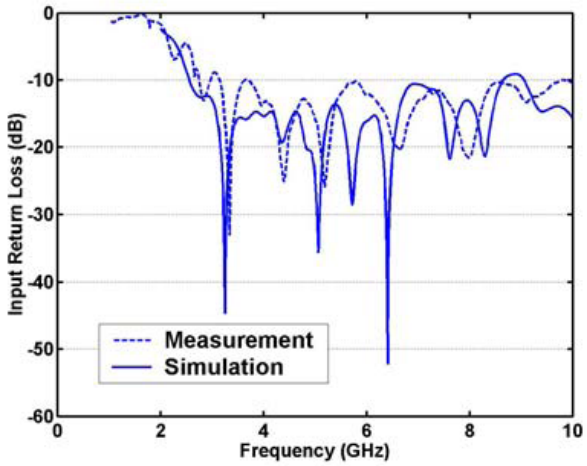

Fig.4. Coefficient de réflexion simulé et mesuré de l'antenne sinueuse à fente (normalisé à 50 Ω).

d

Nous avons validé ainsi la modélisation du balun UWB pour l'adaptation d'impédance. Il faut noter qu'on a utilisé la logiciel CST pour faire tous nos simulations.

Ensuite, une structure directive d'antenne sinueuse à fente est présentée. L'objectif est l'augmentation de la directivité d'une antenne UWB. Est-ce que le balun va modifier les caractéristiques de rayonnement de l'antenne si on ajoute un réflecteur ? Pour répondre à cette question, nous avons ajouté un réflecteur de façon parallèle au plan de l'antenne déjà réalisée dans la partie précédente, puis la distance entre deux plans a été optimisée à 3.75 cm.

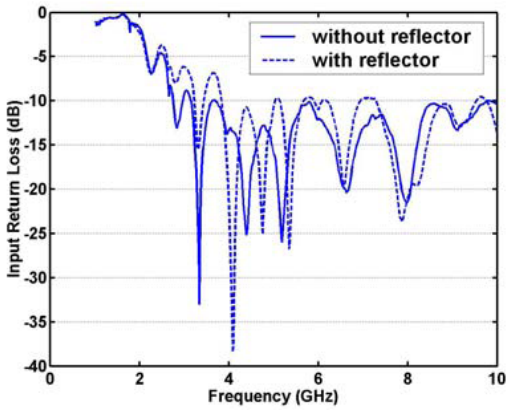

Fig.5. Comparaison des coefficients de réflexion mesurés des antennes sinueuses à fentes sans et avec le réflecteur (normalisé à 50 Ω).

Dans la Fig.5, on a présenté la comparaison des coefficients de réflexion mesurés des antennes sans et avec le réflecteur. Cette figure montre que la bande passante est supérieure à une octave.

En résumé dans le chapitre 2, nous avons obtenu un balun UWB bifilaire qui fonctionne bien entre 100MHz et 9.75 GHz. Nous avons utilisé ce balun planaire comme système d'alimentation de l'antenne sinueuse à fente simple polarisation et on a obtenu une bande passante supérieure à une octave. On a aussi présenté une version d'antenne sinueuse directive avec un réflecteur qui est adapté entre 3.9 à 9.6 GHZ et qui rayonne avec des diagrammes de rayonnement symétriques. Donc le balun peut alimenter une antenne UWB de manière équilibrée avec une transformation impédance de 50 à 70Ω.

Il faut donc considérer que ce type de balun est approprié pour la transformation d'une impédance basse vers une impédance de 50 Ohms. Dans le chapitre suivant, on va chercher un balun UWB avec une transformation impédance plus importante (impédance haute vers 50 ohms). Bien que les structures présentées soient compactes, elles ne sont pas planaires. Donc on va aussi proposer d'intégrer le balun dans les chapitres suivants.

Chapitre 3

Systèmes d'alimentation pour des antennes large bande à simple polarisation dans une configuration tridimensionnelle

L'objectif du chapitre 3 est d'arriver à un système d'alimentation avec les caractéristiques : large bande, intégré avec les circuits planaires, transformation d'impédances élevées, faible-encombrement et compatible avec une configuration à double polarisation. Parmi les baluns UWB compatible avec une utilisation en double polarisation comme celui proposé par M. Begaud (1996), il demeure trois principaux inconvénients: le système d'alimentation est volumique avec bande passante voisine de l'octave et il ne peut pas faire une transformation d'impédance haute. Donc dans cette partie on va présenter un balun coplanaire intégré avec les caractéristiques UWB et compatible avec la double polarisation.

Dans cette partie est présenté l'état de l'art des baluns coplanaire, la modélisation et la fabrication d'un nouveau système d'alimentation large bande et intégré, et la vérification des performances du balun sur une antenne sinueuse à double polarisation.

Généralement il y a un compromis à faire entre la bande passante et la compacité du balun. Il y a deux configurations alternatives de baluns UWB dans lesquelles la géométrie peut-être intégrée: Coplanaire Strip-line (CPS) et guide d'onde coplanaire (CPW). On a choisi la configuration CPS parce qu'elle a deux avantages particuliers: la transformation d'impédances hautes et aussi deux rubans avec des signaux équilibrés pour la connexion aux antennes symétriques comme le dipôle, la sinueuse, le Bow-Tie et etc.

Dans les années 90, plusieurs versions du balun coplanaire ont été présentées. Ce type du balun contient une partie microruban avec le CPS. En 1995, Dib a présenté une nouvelle transition uni-planaire avec une bande passante faible. Puis Qian en 1997 a proposé d'autres versions de ce type de balun avec une bande passante plus grande mais elle encore inferieure à l'octave. Ces baluns sont aussi compatible avec une impédance faible. En 2001, M. Suh et son équipe ont présenté une version performante d'un balun avec une transformation d'impédance haute voisine de 184 Ω dans une bande passante très large. Après quelques années, M. Tu a proposé un modèle multi-section qui a la capacité de réaliser une vaste quantité d'impédances d'entrée haute. Ce modèle nous permet d'optimiser la géométrie du balun pour arriver à l'impédance d'entrée des antennes désirées.

La Fig.6 montre la configuration de notre balun dont le principe vient des baluns proposés par Suh et Tu. Le balun contient trois parties : La région A-A' est une ligne microruban. Dans la modèle de Suh, cette partie est un ruban avec une largeur constante et dans la version Tu, elle est un transformateur d'impédance multi-section. On a modifié cette partie avec un ruban 'tapered'

pour un changement progressif de l'impédance caractéristique de ligne. Les champs électriques dans ligne microruban sont parallèle à l'axe 0x. La région C-C' est une ligne coplanaire classique dont l'impédance caractéristique peut être contrôlée par deux paramètres 'w_{CPS}' et 'g' et qui a les champs électriques parallèles d'axe 0z. Donc on a besoin d'un élément pour faire une rotation 90° des champs électriques. Le Stub radial fait cette rotation dans la partie transition B-B' et sur une large bande. En fait, le Stub radial fonctionne comme un court-circuit virtuel large bande. On optimise le rayon et l'angle de stub pour avoir un quart-longueur de d'onde à la fréquence centrale désirée. Après dans la région C-C', quand on supprime le plan de masse, on aura juste les champs parallèles de l'axe 0z entre les deux rubans et puis une rotation de 90° a été complètement effectuée par le Stub radial.

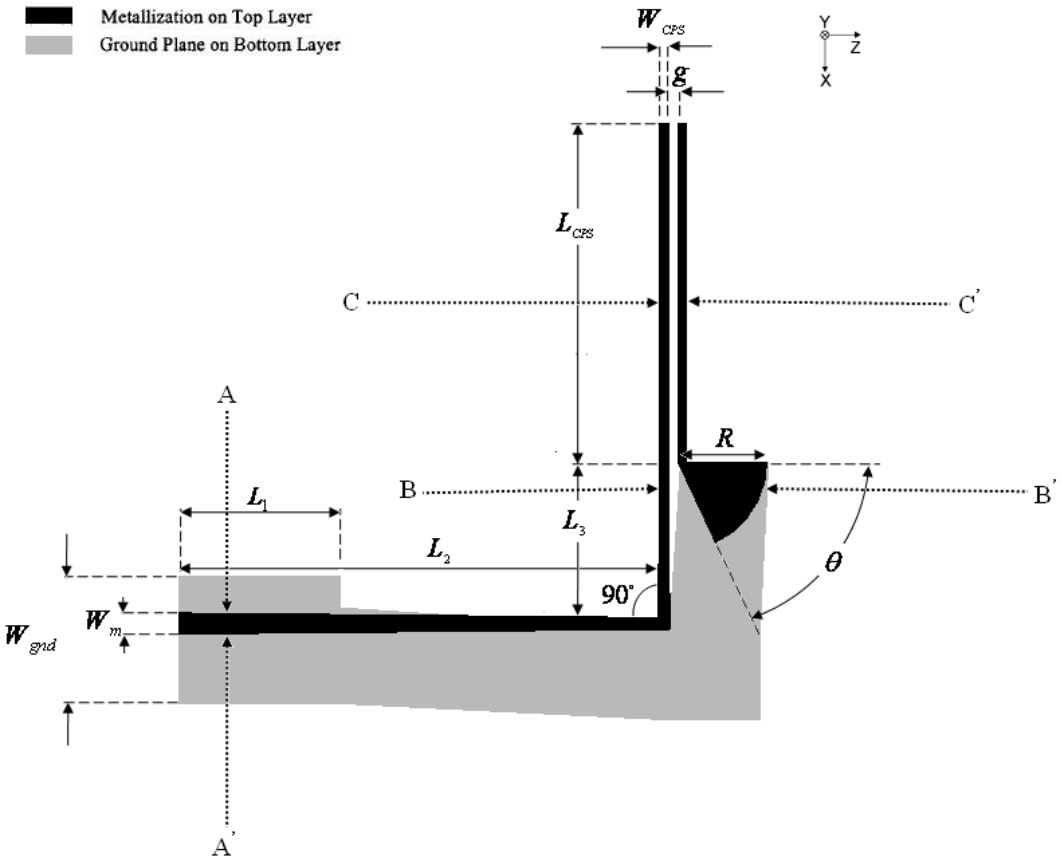

Fig.6. Configuration du Balun coplanaire coudé

On a aussi modifié le balun en ajoutant un coude à 90° dans la région microruban (A-A') pour diminuer la surface de balun de 50%.

Dans cette partie, on présente un balun coplanaire avec les paramètres optimisés. On a fabriqué une configuration back-to-back (Fig.7). La Fig.8 montre les courbes du coefficient de réflexion

et de transmission et traduisent le bon accord entre les coefficients mesuré et simulé. Il montre une bande passante supérieure à l'octave pour S_{11}.

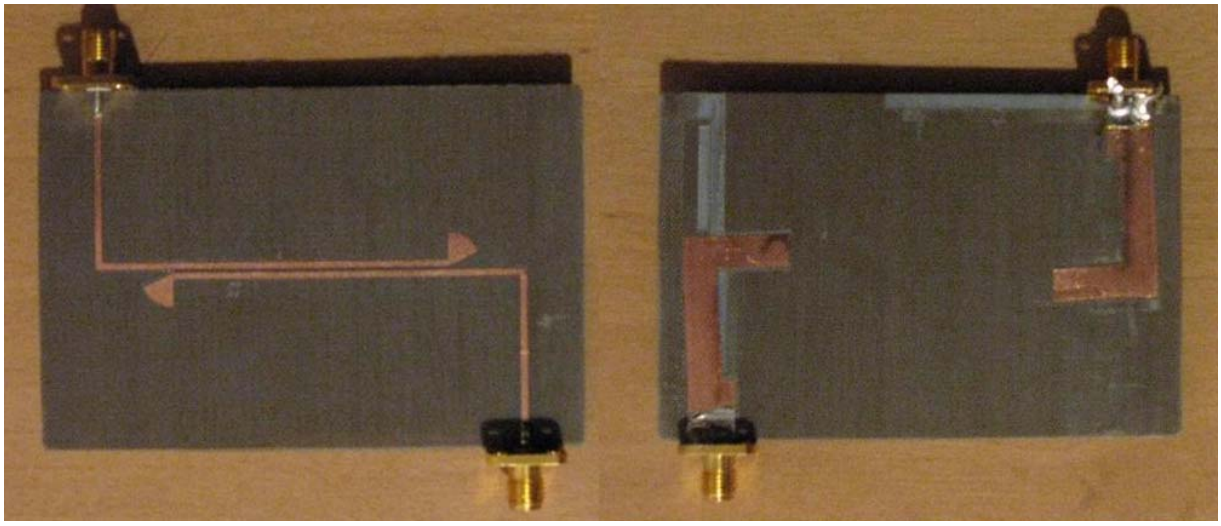

Fig.7 Les photos de la configuration fabriquée du balun back-to-back

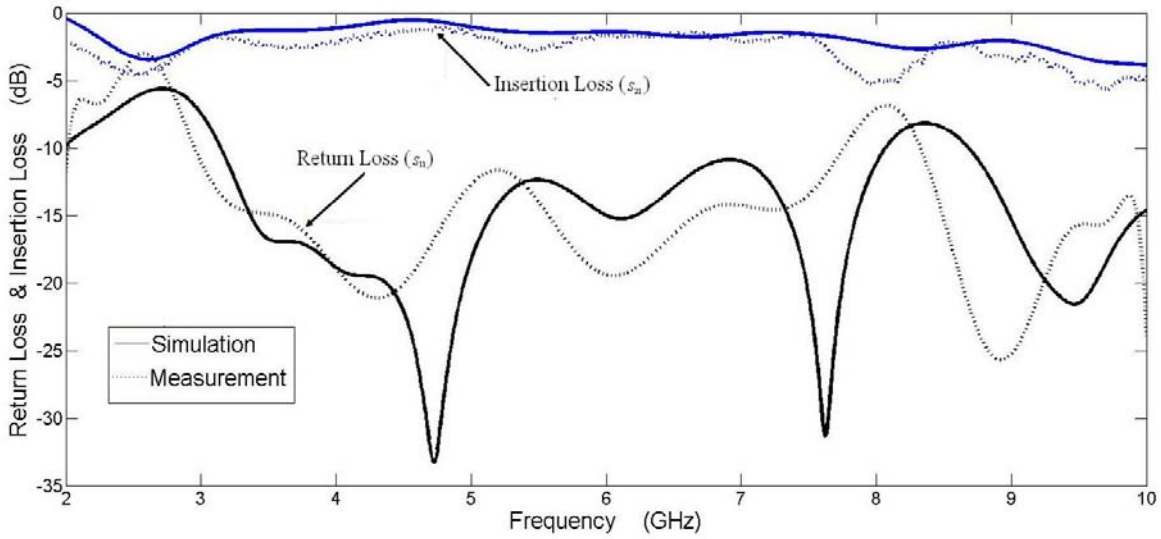

Fig.8. Coefficient de réflexion et de transmission simulé et mesuré du balun back-to-back (normalisé à 50 Ω).

On a aussi validé la différence de phase 180° attendue. Donc on constate que le balun a des caractéristiques de transformation d'impédance et de symétrie en large bande.

A la prochaine étape, on veut vérifier les caractéristiques du balun par une application sur une antenne sinueuse optimisée dans une configuration 3D (Fig.9). Bien que cette configuration 3D ne soit pas notre but principal, cette structure nous permet de vérifier les performances du balun UWB.

h

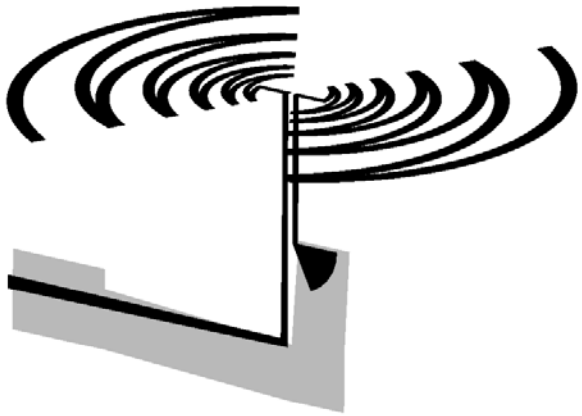

Fig.9. Géométrie de l'antenne sinueuse microruban (simple polarisation) connecté au balun coplanaire.

Il faut aussi noter qu'ici, on a appliqué une version microruban de l'antenne sinueuse et non pas à fente pour qu'elle puisse être connectée au balun. Dans le chapitre 2, on a utilisé une modèle à fente parce qu'on avait besoin d'une structure avec l'impédance d'entrée faible mais ici le balun peut facilement transformer l'impédance d'entrée haute de l'antenne microruban voisine de 160 Ω vers une impédance de 50 Ω.

Le coefficient réflexion mesuré montre une bande passante supérieure à une octave (Fig.10). La comparaison entre la mesure et simulation montre qu'il y a une différence entre ces quantités. Cette différence est liée à la réalisation de la soudure de la connexion antenne avec balun dans la région centrale de la sinueuse. Cette dernière remarque prouve que nous avons besoin d'une configuration intégrée pour une réalisation simple et fiable.

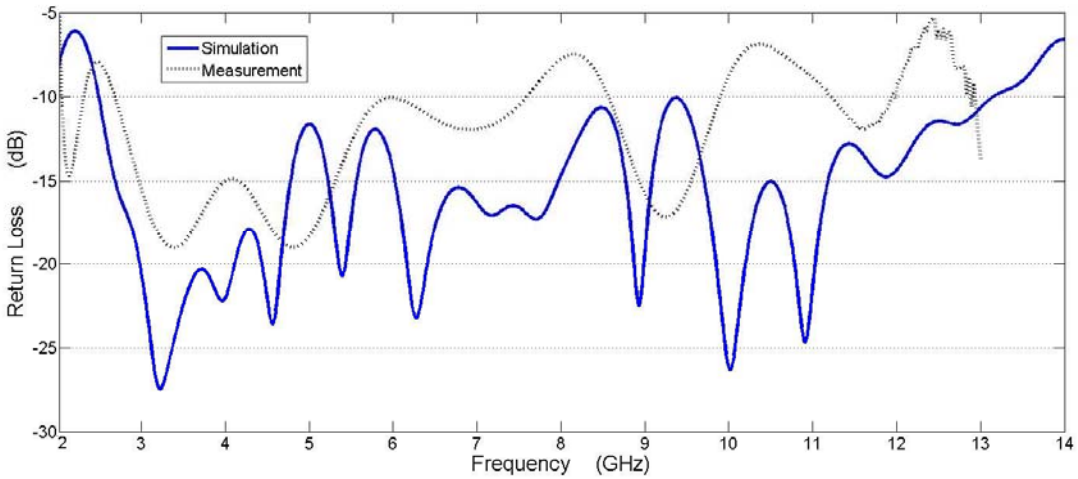

Fig.10. Coefficient de réflexion simulé et mesuré de l'antenne sinueuse microruban connectée au balun coplanaire (normalisé à 50 Ω).

Nous avons obtenu un balun coplanaire UWB qui fonctionne bien sur une bande de fréquence supérieure à une octave. Nous avons utilisé ce balun intégré comme un système d'alimentation de l'antenne sinueuse simple polarisation et on a obtenu une bande passante supérieure à une octave. Ces résultats sont validés par la mesure. On a aussi réalisé une antenne sinueuse à double polarisation adaptée dans une bande passante supérieure à une octave pour les deux polarisations. Cette application montre que ce type de balun coplanaire est approprié pour la transformation d'une impédance haute vers 50 Ohms. Dans le chapitre prochain, on va présenter deux types d'antennes large bande intégrées à double polarisation alimentées par le balun proposé.

Chapitre 4

Systèmes d'alimentation intégrés pour antennes large bande à double polarisation

L'objectif du quatrième chapitre de la thèse est d'arriver aux structures intégrées, large bande et à double polarisation. Il faut noter que cet objectif est le but principal de notre travail. En fait, nous avons appliqué le balun compact proposé dans le chapitre 3 sur les deux antennes sinueuse et Bow-Tie .

Dans cette partie sera présentée la conception et la fabrication d'une nouvelle structure Bow-Tie intégrée à double polarisation alimentée par un balun coplanaire, puis une nouvelle structure sinueuse intégrée à double polarisation alimentée par un balun coplanaire et finalement la conclusion.

D'abord on a optimisé une antenne Bow-Tie classique pour arriver à une grande bande passante. On doit indiquer que l'impédance d'entrée est fonction de θ_h (Fig.11). On aura uniquement une partie réelle de l'impédance d'entrée pour θ_h=90°, donc dans toute les versions Bow-Tie θ_h=90°. On a optimisé les dimensions de l'antenne et on est arrivé au modèle suivant :

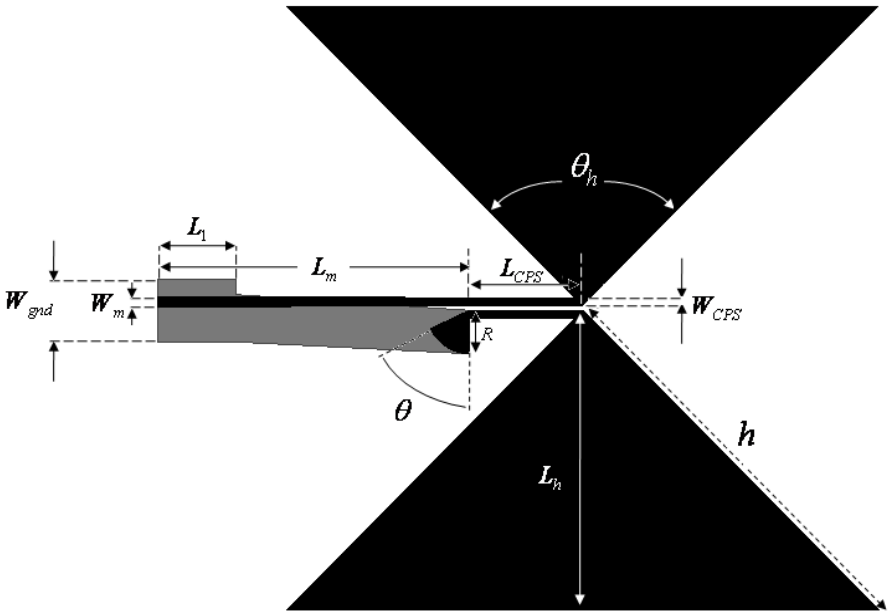

Fig.11. Géométrie de l'antenne Bow-Tie (simple polarisation) connecté au balun coplanaire.

L'adaptation de l'antenne montre que l'antenne Bow-Tie classique est ultra large bande.

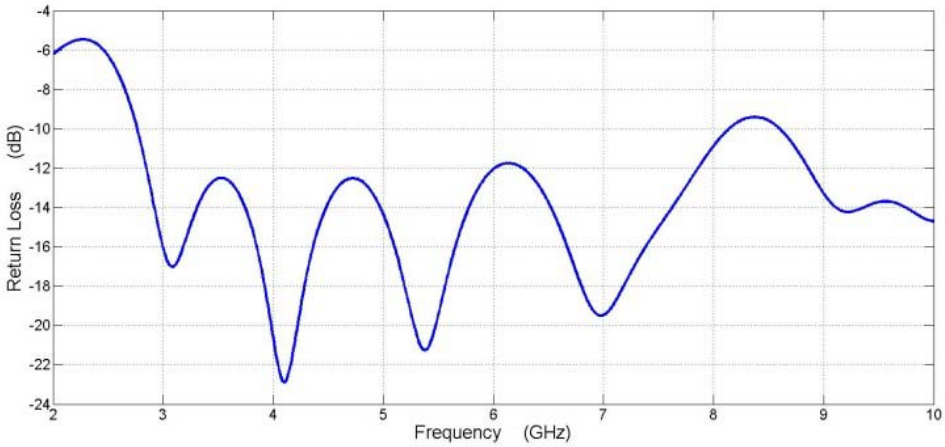

Fig.12. Coefficient de réflexion simulé de l'antenne Bow-Tie connecté au balun coplanaire (normalisé à 50 Ω).

Dans cette partie, on présente un Bow-Tie avec un balun optimisé dans une configuration intégrée à simple polarisation. La Fig.12 montre que la structure est adaptée entre 2.75 et 8.2 GHz avec une bande passante supérieure à une octave. L'antenne Bow-Tie est inscrite dans un plan de 9.2×9.2 cm^2.

Dans cette étape, on veut arriver à une structure Bow-Tie à double polarisation. L'idée est d'imprimer une antenne Bow-Tie de chaque coté d'un substrat avec une rotation 90° pour un des motifs pour réaliser deux polarisations orthogonales (Fig.13). Mais il y aura deux problèmes géométriques: il y aura une connexion électrique entre une partie rayonnante de l'antenne avec le plan de masse du système d'alimentation de l'autre. Ce problème n'est pas critique parce que les courants de surface de l'antenne Bow-Tie sont placés sur les bords des triangles (Fig.14). Cette figure montre un exemple des courants de surface d'un Bow-Tie simple polar. Donc cette connexion ne va pas influencer les performances de l'antenne et du balun.

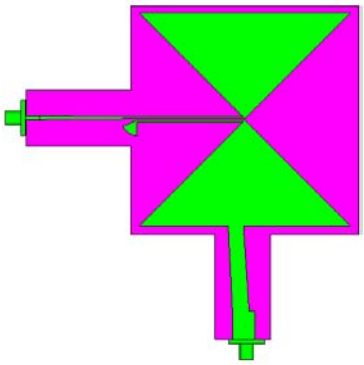

Fig.13. Géométrie de l'antenne Bow-Tie à double polarisation

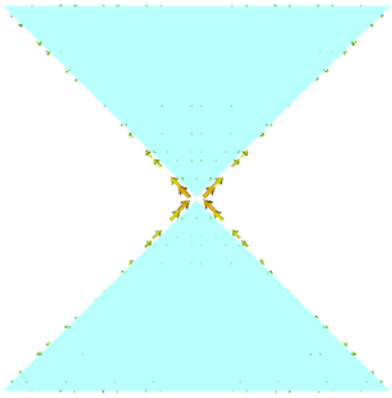

Fig.14. Les courants de surface de l'antenne Bow-Tie à simple polarisation.

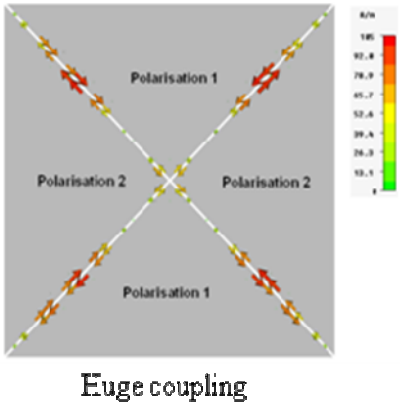

Fig.15. Les courants surface d'antenne Bow-Tie à double polarisation

Il y a un autre problème : la ligne CPS dans la structure à double polarisation a une plan de masse qui est le la partie rayonnante de l'autre polarisation. Ce plan change l'impédance caractéristique de la ligne. C'est-à-dire qu'on doit encore optimiser les dimensions de la ligne CPS.

On a tenté de faire l'optimisation de la structure à double polarisation mais en vain. Les courants de surface pour la configuration à double polarisation montrent qu'il y a un couplage destructif sur le Bow-Tie (Fig.15). On doit donc d'abord éliminer ce couplage destructif. C'est-à-dire que la géométrie de Bow-Tie doit être modifiée.

Ensuite, on a proposé une structure modifié de Bow-Tie intégré à simple polarisation: deux triangles sont espacés et deux rectangles ont été ajoutés sur la base du triangle (Fig.16). Puis la structure a été optimisée et on est arrivé à une bande passant supérieure à une octave (2.8-7.8 GHz) pour l'impédance d'entrée (Fig.17). Les diagrammes de rayonnement de l'antenne montrent un rayonnement symétrique pour les plans E et -H. L'antenne Bow-Tie est inscrite sur un plan plus petit que l'antenne Bow-Tie classique. Le gain de l'antenne varie entre 2.1 et 4.5 dB.

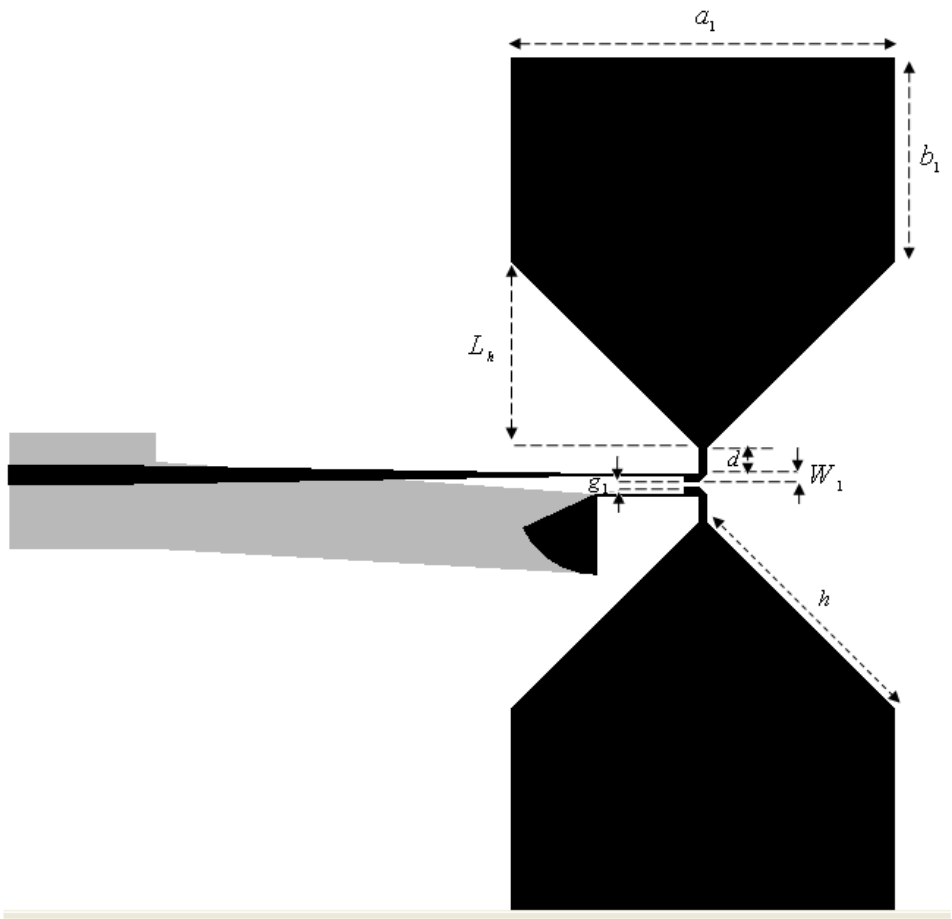

Fig.16. Géométrie de l'antenne quasi Bow-Tie à double polarisation.

m

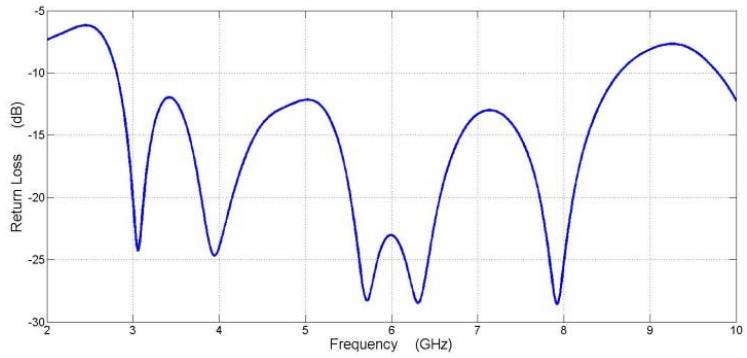

Fig.17. Coefficient de réflexion simulé de l'antenne quasi-Bow-Tie connectée au balun coplanaire (normalisé à 50 Ω).

Ensuite, on a proposé une structure modifiée de l'antenne Bow-Tie à double polarisation. La structure contient deux antennes Bow-Tie à simple polarisation imprimées de chaque coté d'un substrat avec une rotation 90° (Fig.18).

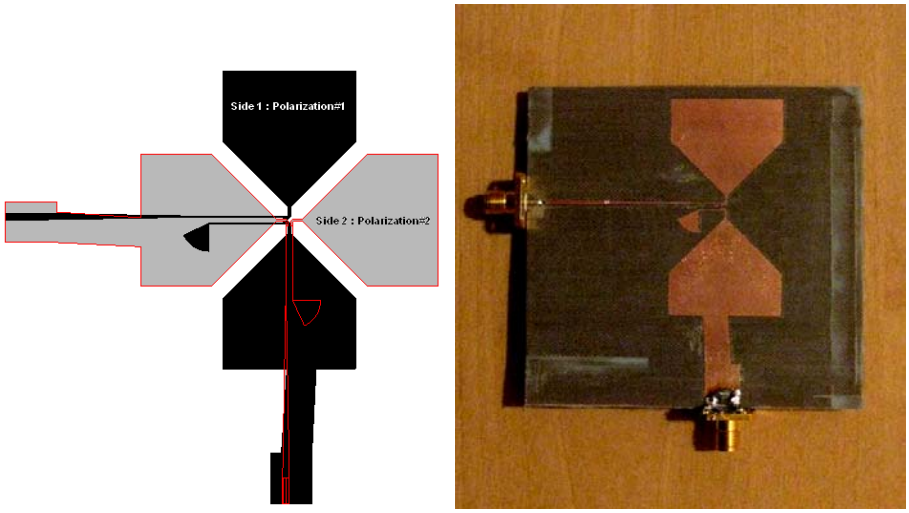

(a) (b)

Fig.18. (a) Géométrie de l'antenne quasi Bow-Tie à double polarisation et (b) photo de la configuration fabriquée.

La Fig.19 montre les coefficients de réflexion et de transmission mesuré et simulé de l'antenne Bow-Tie : la bande passante mesurée est très large et supérieure à une octave (5.4 – 12 GHz).

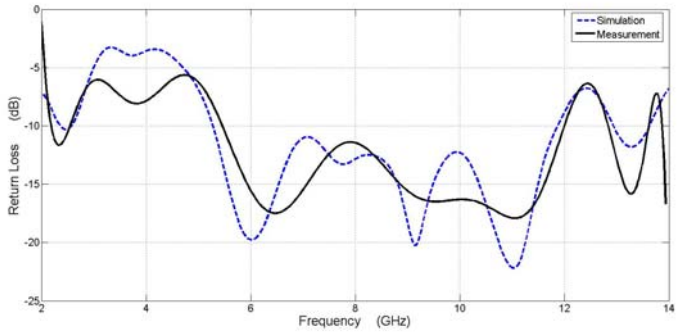

(a)

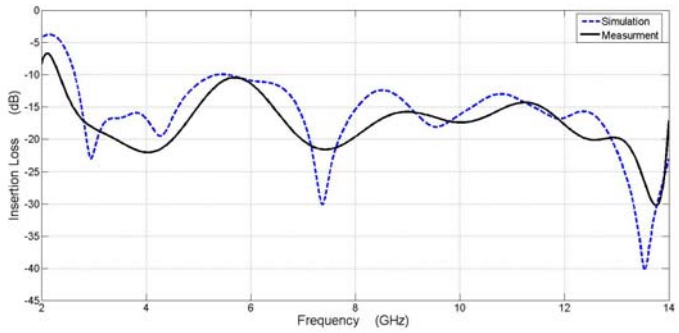

(b)

Fig.19. (a) Coefficient de réflexion et de (b) transmission simulé et mesuré de l'antenne quasi Bow-Tie à double polarisation (normalisé à 50 Ω).

Les diagrammes de rayonnement de l'antenne montrent un rayonnement symétrique pour les plans E et H et l'antenne rayonne bien les deux polarisations orthogonales. La Fig.20 montre que le gain d'antenne varie entre 4.7 et 7 dB avec un maximum à 10 GHz. La comparaison entre deux structures simple et double polarisation montre une augmentation de gain de l'antenne à double polarisation grâce à la présence d'un plan au dessous de chaque antenne comme réflecteur.

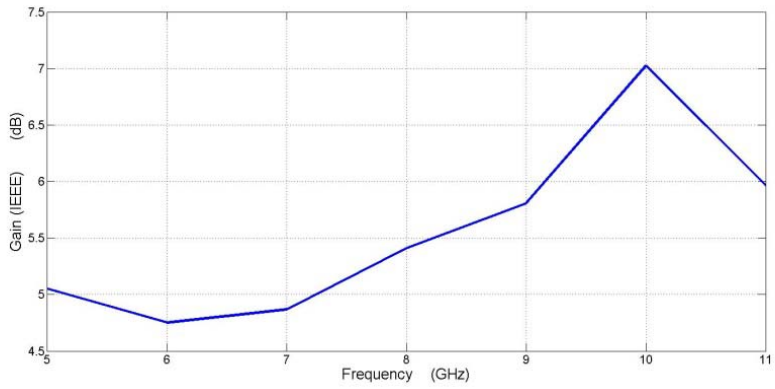

Fig.20. Gain de l'antenne quasi Bow-Tie à double polarisation.

o

Il montre que le balun coplanaire intégré peut être utilisé comme système d'alimentation d'antenne large bande à double polarisation.

Dans la partie suivante et pour la première fois, nous proposons une configuration intégrée de l'antenne sinueuse. Il est possible d'avoir une connexion planaire entre le balun coplanaire coudée et l'antenne sinueuse microruban.

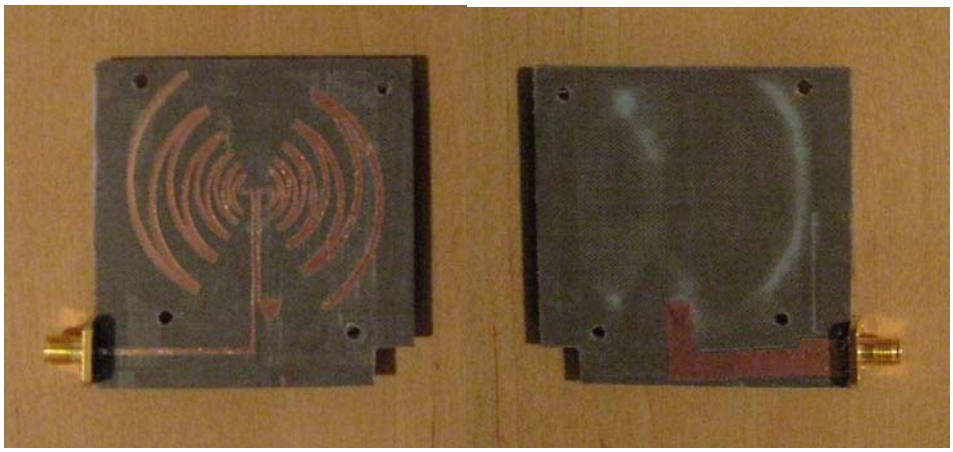

Fig.21. Photos de la configuration fabriquée de l'antenne sinueuse simple polarisation.

La Fig.21 montre la configuration de l'antenne sinueuse intégrée à simple polarisation. On a optimisé l'antenne sinueuse et le balun coplanaire séparément pour arriver une bande passante similaire et supérieure à une octave. La Fig.22 présente les coefficients de réflexion mesuré et simulé de l'antenne sinueuse et montre le bon accord avec une bande passante supérieure à une octave. L'antenne sinueuse intégrée et à faible-encombrement est imprimée sur un substrat et inscrite dans un rectangle de 5.7×6.7 cm^2.

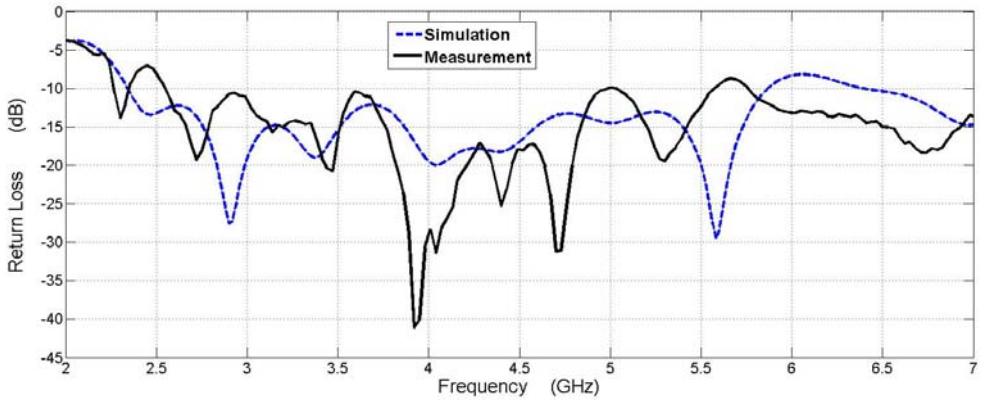

Fig.22. Coefficient de réflexion simulé et mesuré de l'antenne sinueuse simple polarisation (normalisé à 50 Ω).

Les diagrammes de rayonnement de cette structure sont symétriques et il y a une différence d'environ 13 dB entre les composantes coplanaire et croisée. Dans tableau.1 est présentée l'ouverture à 3dB entre 3 et 5 GHz pour les deux plane E et H et montrent les petites variations dans la bande passante. La Fig.23 présente la distribution des courants de surface symétrique de l'antenne sinueuse à simple polarisation à f=3 GHz. Ces résultats montrent que le balun intégré alimente bien les deux rubans équilibrés de la sinueuse.

Tableau.1

Frequency (GHz)	HPBW E-Plane (°)	HPBW H-Plane (°)
3	70	75
4	70	72
5	66	73

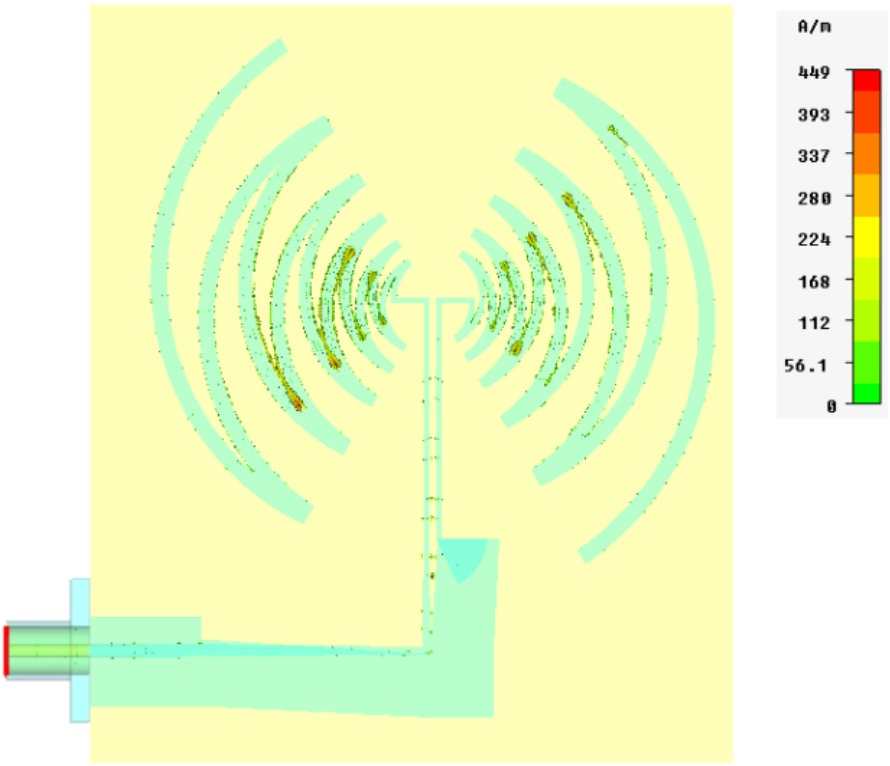

Fig.23. La distribution des courants surfaces de l'antenne sinueuse à simple polarisation à f=3 GHz.

Dans cette partie, on a proposé une structure compacte d'antenne sinueuse à double polarisation. La structure double polar contient deux antennes sinueuses optimisées à simple polar sur deux substrats parallèles avec une rotation 90° (Fig.24). On a optimisé la distance entre les deux substrats à d=2 mm.

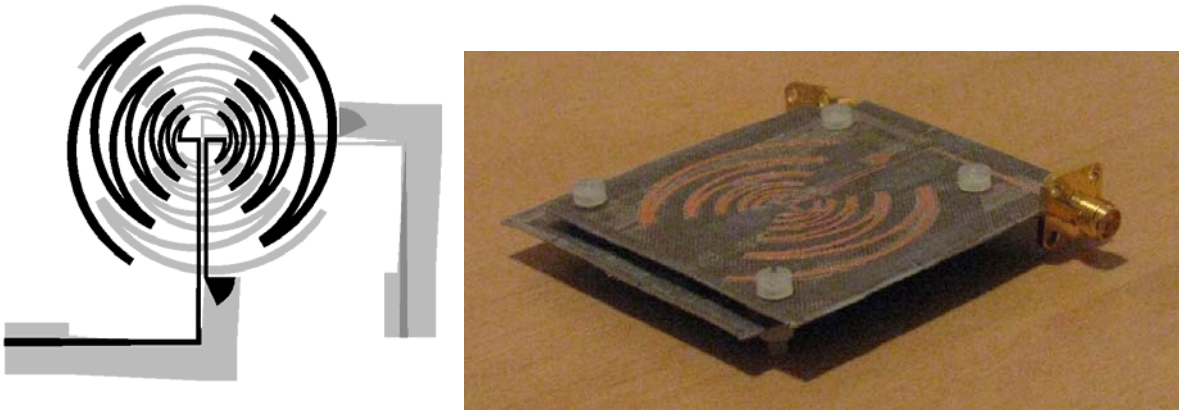

(a) (b)

Fig.24. (a) Géométrie de l'antenne sinueuse intégrée à double polarisation et (b) photo de la configuration fabriquée.

La Fig.25 montre les coefficients de réflexion et de transmission mesuré et simulé de l'antenne sinueuse à double polarisation. On obtient une bande passante mesurée voisine d'une octave (3.7 – 7.3 GHz). L'antenne sinueuse à faible-encombrement est inscrite dans un volume très compact $7.1\times6.7\times0.3$ cm^3 ($0.87\lambda_L\times0.82\lambda_L\times0.04\lambda_L$).

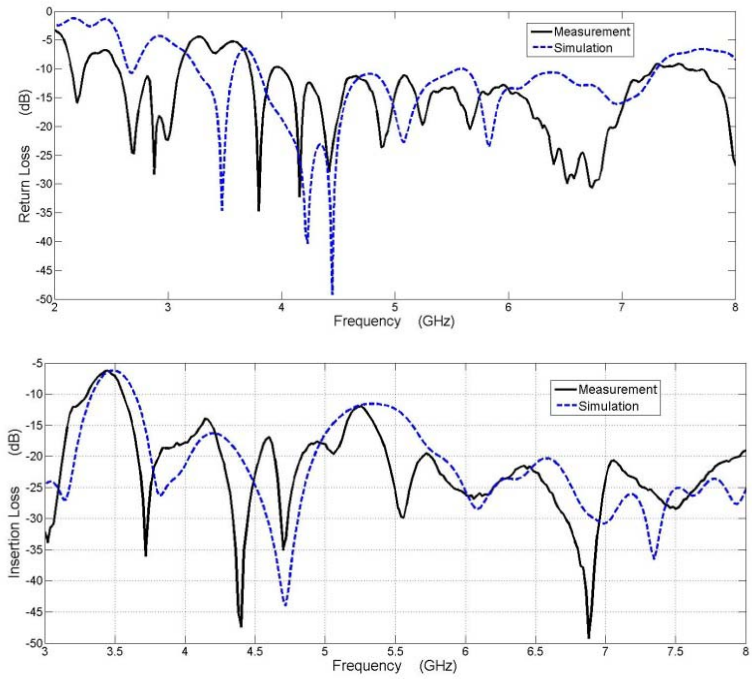

Fig.25. (a) Coefficient de réflexion et (b) de transmission simulé et mesuré de l'antenne sinueuse intégré à double polarisation (normalisé à 50 Ω).

Les diagrammes de rayonnement de cette structure sont presque symétriques. La Fig.26 montre que le gain de l'antenne sinueuse à double polarisation varie entre 4.3 et 5.8 dB.

r

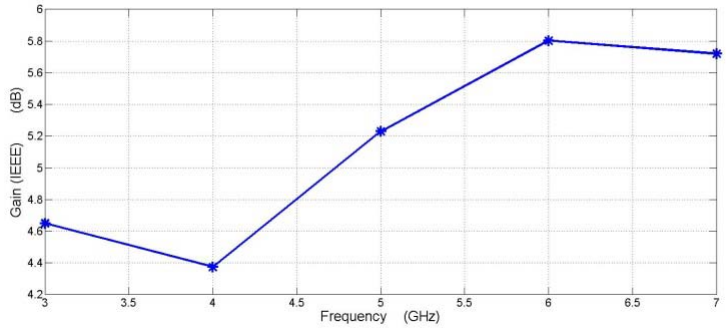

Fig.26. Gain de l'antenne sinueuse à double polarisation.

Ces résultats montrent que les deux balun intégrés fonctionnent correctement dans la bande passante de l'antenne et à double polarisation.

Conclusion Générale:

Deux différents types de systèmes d'alimentation large bande ont été proposé dans ce travail de thèse : symétriseur bifilaire à profil « taper » et le balun coplanaire. Ces deux baluns ont été intégrés sur deux antennes large bande : l'antenne sinueuse et l'antenne Bow-Tie. Pendant le déroulement de la thèse, on a parcouru les étapes de conception suivantes: une antenne sinueuse à fente à simple polarisation en configuration 3D, une antenne sinueuse microruban à double polarisation en configuration 3D et finalement deux antenne intégré à double polarisation en configuration Bow-Tie et sinueuse.

Dans le tableau suivant sont résumés tous les résultats importants des antennes étudiées :

Antenna-Balun	Impedance Bandwidth (GHz)	Bandwidth in ratio	Volume (λ_L)	Volume (cm^3)
Sinuous Slot (Single Pol., 3D) (Balun-1)	3.15 – 10	**3.2:1**	$0.52\lambda_L \times 0.52\lambda_L \times 0.52\lambda_L$	5×5×5
Directive Slot Sinuous (Single Pol., 3D), (Balun-1)	3.9 – 9.6	2.5 :1	$0.65\lambda_L \times 0.65\lambda_L \times 0.65\lambda_L$	5×5×4
Sinuous (Dual Pol., 3D) (Balun-2)	2.8 – 8.3	3:1	$0.65\lambda_L \times 0.65\lambda_L \times 0.37\lambda_L$	7×7×4
Sinuous (Single Pol., Integrated) (Balun-2)	2.5 – 5.6	2.2:1	$\mathbf{0.475\lambda_L \times 0.56\lambda_L \times 0.007\lambda_L}$	7.1×6.7×0.0832
Bow-tie (Single Pol., Integrated) (Balun-2)	2.8 – 7.8	2.8:1	$0.56\lambda_L \times 0.56\lambda_L \times 0.008\lambda_L$	6×6×0.0832
Sinuous (Dual Pol., Integrated) (Balun-2)	3.7 – 7.3	2:1	$0.87\lambda_L \times 0.82\lambda_L \times 0.04\lambda_L$	7.1×6.7×0.3
Bow-tie (Dual Pol., Integrated) (Balun-2)	5.4 – 12	2.2:1	$1.1\lambda_L \times 1.1\lambda_L \times 0.015\lambda_L$	6×6×0.0832

Toutes les antennes proposées ont de larges bandes passantes voisines ou supérieures à une octave. Les volumes occupés par chaque antenne montrent que les quatre dernières antennes sont intégrées et les deux dernières antennes accomplissent les objectifs de cette thèse.

Nous pouvons poursuivre ce travail de deux façons différentes :

Il faudrait continuer le travail sur l'antenne sinueuse à double polarisation pour trouver un plan de masse pour la balun compatible avec son intégration dans le motif de l'antenne sinueuse sans dégradation des performances du balun.

Enfin, il semble aujourd'hui possible de réaliser des réflecteurs à haute impédance (métamatériaux) et à large bande pour rendre les antennes directives et des travaux sur ce sujet sont en cours de réalisation à TELECOM ParisTech. L'idée est donc d'associer ces réflecteurs large bande aux antennes que nous avons conçus au cours de cette thèse pour les rendre très directives.